JSPS-CAS Core University Program Seminar on *Summary of 10-year Collaborations in Plasma and Nuclear Fusion Research Area* 9 – 11 March 2011, Okinawa, Japan

Edited by
Kazuo TOI and Kongjia WANG

Abstract

The JSPS-CAS Core University Program (CUP) seminar on "*Summary of 10-year Collaborations in Plasma and Nuclear Fusion Research Area"* was held from March 9 to March 11, 2011 in the *Okinawa Prefectural Art Museum*, Naha city, Okinawa, Japan. The collaboration program on plasma and nuclear fusion started from 2001 under the auspices of Japanese Society of Promotion of Science (JSPS) and Chinese Academy of Sciences (CAS). This year is the last year of the CUP.

This seminar was organized in the framework of the CUP. In the seminar, 29 oral talks were presented, having 14 Chinese and 30 Japanese participants. These presentations covered key topics related to the collaboration categories: (1) improvement of core plasma properties, (2) basic research on fusion reactor technologies, and (3) theory and numerical simulation. This seminar aims at summarizing the results obtained through the collaborations for 10 years, and discussing future prospects of China-Japan collaboration in plasma and nuclear fusion research areas.

Key words: Magnetically confined plasmas, Plasma wall interactions, Atomic and molecular processes, Plasma industrial applications, Laser produced dense plasmas, Fusion reactor technologies, Plasma theories and numerical simulations

Organizing Committee

Kazuo TOI (Chairperson, National Institute for Fusion Science, Japan)

Kongjia WANG (Chairperson, Institute of Plasma Physics, Chinese Academy of Science, China)

Program Committee

Japan

Kazuo TOI (National Institute for Fusion Science, Japan)

Shuichi YAMADA (National Institute for Fusion Science, Japan)

Shigeru MORITA (National Institute for Fusion Science, Japan)

Takeo MUROGA (National Institute for Fusion Science, Japan)

China

Kongjia WANG (Institute of Plasma Physics, Chinese Academy of Science, China)

Liqun HU (Institute of Plasma Physics, Chinese Academy of Science, China)

Xiang GAO (Institute of Plasma Physics, Chinese Academy of Science, China)

Conference Secretariats

Mayumi KATO (Secretary, National Institute for Fusion Science, Japan)

Shaohua DONG (Secretary, Institute of Plasma Physics, Chinese Academy of Science, China)

Preface

The JSPS-CAS Core University Program (CUP) seminar on "*Summary of 10-year Collaborations in Plasma and Nuclear Fusion Research Area"* was held from March 9 to March 11, 2011 in *the Okinawa Prefectural Art Museum*, Naha city, Okinawa, Japan. The collaboration program started from 2001 as a 10-year program under the auspices of Japanese Society of Promotion of Science (JSPS) and Chinese Academy of Sciences (CAS), focusing on the following three categories: (I) improvement of core plasma properties, (II) basic research on nuclear fusion reactor engineering, and (III) theory and simulation. This seminar was organized in the framework of the CUP in the field of plasma and nuclear fusion. This year is the final year of the CUP.

This seminar aims at summarizing results obtained through these collaborations for 10 years, and discussing future prospects of China-Japan collaborations in plasma and nuclear fusion research areas. In this seminar, 29 oral talks were presented, having 14 Chinese and 30 Japanese participants. The seminar consists of the following eight sessions: (1) Magnetically confined plasmas, (2) Plasma wall interactions, (3) Atomic and molecular processes, (4) Plasma industrial applications, (5) Laser produced dense plasmas, (6) Fusion reactor technologies, (7) Plasma theories and numerical simulations, and (8) Topical session. At the beginning of these sessions, the history of ASIPP-NIFS collaborations, and short summary of the former half of the CUP were presented by the coordinators and sub-coordinators in the former half of the CUP. In the sessions from (1) to (7), 15 key research topics in the above-mentioned categories (I)-(III) were summarized over 10 years, and recent research activities in each topic were also introduced. In the last topical session, three additional new topics were also presented.

The seminar was successfully carried out with a lot of collaboration results and fruitful discussions toward future collaborations. Finally, the organizing and program committees express the gratitude for all participants for their supports and cooperation to this seminar.

Kazuo TOI and Kongjia WANG
Chairpersons of Organizing Committee

Contents

11A: Development of Advanced Plasma Heating for High Performance Plasma Confinement-Summary and Topical Report

R.Kumazawa, X.GAO[1)] and L.YAN[2)]

National Institute for Fusion Science, Toki 509-5292, Japan

[1)]Institute of Plasma Physics, Academia Sinica, Hefei, CHINA

[2)]South West Institute of Plasma Physics, Chengdu, China

1.Introduction

In this report we summarize results of the collaboration between Japan and China about the advanced plasma heating for high performance plasma confinement (11A) during five years (2006~2010). Collaboration results and future proposals are reported from collaborations of Neutral Beam Injection (NBI), Electron Cyclotron Heating (ECH), Lower Hybrid Current Drive (LHCD) and Ion Cyclotron Heating (ICH) in the first part. In the second part the proposal toward an efficient ICRF heating on EAST is described as a topical report.

2. Summary and proposal

2-1. Neutral Beam Injection (NBI)

2-1-1 Personal exchange: 11 persons

Japan to China: 6 persons and China to Japan: 5 persons

2-1-2 Summary of collaborations

The NBI heating has been already carried out on HL-2A: 1.5MW/45keV for a few seconds with balanced injection. On the other hand it is planned that the NBI will be carried out at 2013 on EAST. For that purpose the NBI test stand is fabricated and an initial experiment has been recently started. One of the important issues for improving the efficient positive NBI is how high rate of the primary hydrogen or deuterium ions is produced, i.e., how to reduce the secondary and third hydrogen or deuterium ions. Measurement of ion fraction in the ion source was carried out at the NBI test stand in NIFS. These ratios were measured with a charge exchange spectroscopic method as seen in Fig.1 [1]. E_0, $E_0/2$ and $E_0/3$ indicate the primary ^{+}H, the secondary $^{+}H_2$ and third hydrogen $^{+}H_3$ ions, respectively. This measurement was carried out in various arcing power from 20kW to 100kW as seen in Fig.2. The fraction of the primary hydrogen ion was increased with the arcing power and reached to 88% at the arcing power of 100kW. The other key is a beam divergence. In general an acceleration grid has many holes with a diameter of 6~8mm and these acceleration hole positions at the several grids is determined by taking into account a beam trajectory. A beam width due to the beam divergence was measured with the spectroscopic measurement and a calorimetric measurement. The beam width, i.e., the beam divergence was a function of the beam perveance, which is assessed using the beam current and applied acceleration

voltage. The minimum beam width measured with the calorimetric measurement was found at the perveance of 25×10^{2}A/kV$^{3/2}$ as seen in Fig.3.

The experiment at the NBI test stand has been recently started in ASIPP. The ion source was mounted at the NBI test stand as seen in Fig.4. A DC power with 18V/5.5kA was supplied to the filament for 120 sec. as seen in Fig.5. In addition the arcing power source was tested at 180V/3.1kA for 30 sec. as seen in Fig.6.

A numerical calculation code was developed in NIFS to optimize the structure of the ion source. The electron trajectories are tracked in the presence of the applied electrostatic and magnetic fields. The typical calculation results are shown in Fig.7 and 8. The electron beam trajectories (with yellow lines) and the termination points of the electrons (with blue dots) in the designed ion source for EAST are plotted in Fig.7. Figure 8 shows them in the present ion source for HL-2A. It is expected that the optimized NBI system will be fabricated for EAST NBI using the numerical code.

Physics experiments about H-mode research, high T_i plasma, physics for high-energy ions and NBI current drive are proposed as candidates of a future collaboration using high power NBI heating on HL-2A and EAST.

2.2 Electron Cyclotron Heating (ECH)

2-2-1 Personal exchange: 13 persons

Japan to China: 8 persons and China to Japan: 5 persons

2-2-2 Summary of collaborations

The collaboration of ECH experiments has been carried out on HL-2A. Four Gyrotron systems were already installed and a power of 2MW is available to inject to the plasma on HL-2A. The groove mirror was designed by Japanese scientist, fabricated and installed to HL-2A as seen in Fig. 9 [2,3]. It has a capability to change the wave polarization, so the ordinary or the extra ordinary ECH heating becomes possible. Two typical experiment data using ECH are introduced: the one is the remarkable increase in the electron temperature as seen in Fig.10 and the other is a successful suppression of the neo-classical tearing mode (NTM) excited neat the magnetic surface of q=2 as seen in Fig.11. The time evolution of the electron temperature T_{e0} on the plasma axis measured with Thomson scattering is shown in Fig.10. The ECH pulse is applied from 600ms to 800ms and the T_{e0} is increased from 1.2keV to 5keV with P_{ECH}=1.5MW from four Gyrotorn systems. The NTM was often excited on HL-2A and degraded the plasma confinement. The second harmonics of the electron cyclotron resonance was located near the magnetic surface of q=2 and the EC wave with the X mode was excited with P_{ECH}=190kW aiming the q=2 surface shown in red lines in Fig.11. Then the NTM oscillation with m/n=2/1 could be suppressed as seen in Fig.11. After the suppression of the NTM the electron density was increased from $n_e=1\times10^{19}$m^{-3} to 2.2×10^{19}m^{-3}, then the gas puffing was ceased at 700ms. The plasma-stored energy was increased from 7kJ to 12kJ. On the other hand when the injected ECH power was focused at the q=1 surface shown in blue

lines, no suppression of the NTM and no improvement of the plasma parameters were observed.

Recently the new two Gyrotron systems with f=68GHz were installed on HL-2A and another two Gyrotron systems with f=140GHz will be installed soon. Japanese scientists proposed several method to increase the output power from Gyrotrons and improve the transmission efficiency in the transmission waveguide.

1. It is recommended that a He-Ne laser beam should be used for the alignment to acquire the efficient injection of HE_{11} mode from the matching Optics Unit (MOU) of the Gyrotrons.
2. Now aging Gyrotrons is carried out using a D.C. power from FW generator shared with HL-2A experiment. The time interval is so long, i.e., in every several minutes. Therefore it is recommended that another D.C. power source supplied to the collector of Gyrotron should be fabricated for quickly aging Gyrotrons.
3. A new switching device to change the ECH power to the antenna on HL-2A or the dummy load.
4. Design and fabrication of new antenna with variable injection angle using NIFS code [4].
5. Development of analysis on electro-magnetic wave pattern in corrugate waveguide.

2.3 Lower Hybrid Current Drive (LHCD)

2-3-1 Personal exchange: 2 persons

China to Japan: 2 persons

2-3-2 Summary of collaborations

The lower hybrid current drive (LHCD) is carried out on HL-2A [5] and EAST [6]. Specifications of the LHCD system on EAST are as follows. The applied frequency is 2.45GHz, and the maximum output power is 2MW with 20 Klystrons of 100kW for steady-state operation. The LHCD antenna consists of 8 multi-junctions with water-cooled as shown in Fig.12. The refractive index of launching wave in the toroidal direction, i.e., $N_{//}$ can be changed $1.6 < N_{//} < 2.2$. A fully non-inductive plasma discharge with Ip=250kA and $n_e=1\times10^{19}m^{-3}$ has been achieved for 8 seconds with P_{LHCD}=1MW in both DN (double null) and SN (single null) configurations as shown in Fig.13. The radial profile of the electron temperature in this plasma discharge is shown in Fig.14. The electron temperature on the axis was increased to 1.6keV from 0.8keV at the Ohmic plasma. Specially the long pulse plasma of Ip=250kA was sustained for 30 seconds with P_{LHCD}=0.6MW in both DN (double null) and SN (single null) configurations as shown in Fig.15. In 2011 another LHCD system with f=2.45GHz will be installed and a non-inductive discharge with a larger plasma current will be tried. In addition a new system with a higher frequency of 4.6GHz will be installed as seen in Fig.16. Its specification is f=4.6GHz, P_{LHCD}=6MW for 1,000 seconds. The refractive index of the launched wave, i.e., $N_{//}$ has a range of $1.79 < N_{//} < 2.23$ in 2013.

The future experiments are proposed as follows.

1) The non-inductive discharge with a higher plasma current of I_P=1MA at $n_e=4\times10^{19}m^{-3}$ will be the next target. The q value at the edge, i.e., q_{95}=4.2.

2) The long pulse discharge of 1,000 seconds.

3) Increase in the current drive efficiency η : At present $\eta = 0.9 \times 10^{19} A/Wm^2$.

η obtained on Alcator C-Mod: $\eta = 2 \sim 2.5 \times 10^{19} A/Wm^2$.

4) Trial to a higher density: ω_{LH}/ω=1/3, e.g., ω_{LH}/ω=1/3 on Alcator C-Mod.

Definition of the normalized density limit is expressed as $\omega_{LH}/\omega = \omega_{pi}/\omega \cdot \{1 + (\omega_{pe}/\omega_{ce})^2\}^{-1/2}$.

At present n_e=1x$10^{19}$$m^{-3}$ => ω_{LH}/ω=1/9.

2.4 Ion Cyclotron Range of Frequency (ICRF) Heating

2-4-1 Personal exchange: 19 persons

Japan to China: 11 persons and China to Japan: 8 persons

2-4-2 Summary of collaborations

In these five years new three RF generators were fabricated as seen in Fig.17. They consist of three stages of amplifier, i.e., 5kW, 100kW and 1.5MW in each stage. The structure of the amplifier is very similar to that of the NIFS RF power sources. The specifications of the RF generator are as follows: the frequency range of 25MHz < f < 70MHz and the RF output power of P_{RF}=1.5MW for 10 seconds and P_{RF}=1.0MW for steady-state. This year a liquid dummy load will be installed, and then the high RF power operation for steady-state will be tested [7].

Three impedance matching systems with a liquid stub tuner are employed as seen in Fig.18. Each impedance matching systems consists of three liquid stub tuners so as to acquire the impedance matching in the wide frequency range such as 25MHz < f < 70MHz. These liquid stub tuner systems will be useful for the ICRF heating applied to the long pulse plasma discharge. This has been already verified with the real-time feedback control of the liquid height [8]. These impedance matching systems were used in the EAST and in the HT-7 ICRF heating experiments. Therefore they are located near the HT-7 device and are far from the EAST, e.g., the distance of 80~100m to the EAST ICRF heating antenna. As described later, this long length between the impedance matching system and the EAST ICRF heating antenna reduces the ICRF wave injection efficiency.

An ICRF heating antenna system as seen in Fig.19 with two straps (shown in Fig.20) is installed. The RF power is supplied to the antenna from two RF generators. A typical shot of the plasma discharge with the ICRF heating of 500kW for 0.5~0.7second is shown in Fig.21. The employed frequency was f=27MHz. The minority heating in D(H) plasma was carried out with 10% of the minority ratio of H. During the ICRF heating the plasma-stored energy was increased by 10kJ, the electron temperature increase was 0.25keV and the large increase in the neutron flux was observed as also shown in Fig.21 [9]. The H-mode was sustained for 4 seconds with simultaneous heating of LHCD and ICRF heating, i.e., P_{LHCD}=0.6MW and P_{ICH}=0.9MW as seen in Fig.22.

On the other hand in the 14th experiment cycle (2010) in LHD a new one pair of ICRF heating antennas was installed: This pair consists of two antennas arrayed in the toloidal direction and has a

controllability of the wave number along the magnetic field line $k_{//}$ with changing the phase difference between them. When two antennas are seen from the plasma axis, they look like to handshake each other and so it is called HAS (Handshake) antenna as seen in Fig.23 [10]. The first experiment using the HAS antenna was carried out in this cycle. The frequency was employed as 38.47 MHz to excite the ICRF fast wave and heat the plasma using a minority heating method in the condition of the magnetic field strength of 2.75 T at 3.6 m of the magnetic axis. The target plasma consisted of the helium plasma as the majority with the hydrogen minority. Several experiment results were obtained and compared with those obtained using the previous poloidal (PA) arrayed antenna (no ability of changing $k_{//}$). The fast wave with a large $k_{//}$ is excited with (0, π) phasing between two antennas, and a small wave number of $k_{//}$ with (0, 0) phasing. The plasma loading resistance in (0, π) was found to be smaller than that of (0, 0) phasing. It is understood that the fast wave with the large $k_{//}$ can not propagate in the low density, because the R-cutoff occurs at $ck_{//}/\omega \sim (\omega_{pi}/\omega_{ci})^2/2$. Therefore the HAS antenna was put close to 6~7cm from the lost closed plasma surface when injecting the high RF power with a reasonable RF voltage: The distance was 10cm in the case of the PA arrayed antennas. The plasma heating efficiency was measured with an RF power modulation using an RF power modulation system fabricated by Chinese scientist as shown in Fig.24. A time evolution of the plasma stored energy and the modulated ICRF heating power with 4Hz is shown in Fig.25. The heating efficiency was measured with the phase difference between the applied ICRF heating power and the plasma-stored energy. In (0, π) phasing the heating efficiency was much better than that in (0, 0) phasing as shown in Fig.26.

Another important issue is a realization of the real-time feedback control to always reduce the reflected RF power from the ICRF heating antenna during the long pulse operation [8]. The reflected RF power was increased with the change of the emissivity of the liquid due to the temperature increase and the change in the characteristic impedance of the transmission line. The test of the real-time feedback control was carried out using a low RF power less than 1W. The RF power was supplied from the cavity of the final amplifier of the RF power source in NIFS as shown in Fig.27. The impedance matching system with three liquid stub tuners was employed for that. The flow chart of the real-time feedback control is shown in Fig.28. A directional coupler measured the forward and the reflected RF powers, and the phase differencer between the forward and the reflected RF powers. Then the computer analyzed the impedance matching solution using above three data. The each liquid surface height of three liquid stub tuners was changed with cylinder pump in accordance with the solutions. This process was repeated several times until the reflected RF power fraction becomes less than 1%. The test of the real-time feedback control was started at the initial reflected RF power fraction of 18% as seen in Fig.29. It took a few seconds in the one cycle in the flow chart as seen in Fig.28. The reflected RF power fraction could be reduced to less than 1% within 5 seconds. Finally it became the order of 0.001% as seen in Fig.29.

3.Topical Report-Toward Efficient ICRF Heating

3-1. RF generator

The specifications of the RF generator (seen in Fig.17) in ASIPP are as follows: the frequency range of 25MHz < f < 70MHz and the RF output power of P_{RF}=1.5MW for 10 seconds and P_{RF}=1.0MW for steady-state. This year a liquid dummy load will be installed [7], and then the high RF power operation with a long pulse will be tested. A vacuum tetrode tube of TH-525A was employed in the final amplifier stage for the RF generator for EAST. Two different vacuum tetrode tubes are employed in the NIFS RF generators, i.e., 4CM2,500kG (EIMAC, USA) and TH-525A (THALES, EU). The long pulse operation with high RF power of 1.6MW for 5,000 seconds was achieved at f=50MHz [11] using 4CM2,500kG. Several parameters of these tubes during the operation with about 1MW are very similar. There is not different between them except for the RF conversion efficiency: It is a little better in 4CM2,500kG than in TH-525A. The long pulse operation of 0.5MW for 1,000 sec was achieved in both vacuum tetrode tubes in NIFS.

3-2. Real-time feedback control for impedance matching

The importance of the real-time feedback control for impedance matching was already described in the previous section. The test was carried out in the lower RF power level and the initial reflected RF power fraction of about 20% could be reduced to less than 1% within several seconds as seen in Fig.29. In the long pulse ICRF heating on the LHD the real-time feedback control for impedance matching was achieved as shown in Fig.30. In this discharge the plasma duration time was more than 30 minutes. The data acquisition time for the measurement of the reflected RF power fraction is up to 120 seconds as seen in Fig.30. In this plasma discharge, 4 antennas, i.e., 3.5U, 3.5L, 7.5U and 7.5L antennas were used to launch the fast wave to the plasma. The initial reflected RF power fraction of 7.5L was about 50%, but it was reduce to less than a few % within 40seconds [8].

3-3. ICRF heating during H-mode

The H-mode was achieved with P_{ICH}=0.7MW and P_{LHCD}=0.8MW on EAST as shown in Fig.31. But the reflected RF power was almost constant, i.e., 20~30kW for the forward power of 200kW during ELM as seen in Fig.31. The reflected RF power fraction changed little, e.g., 3% to 4%. As reported with the ICRF heating during the H-L transition on JET, the reflected RF power was observed to quickly change by 30~40% [12]. It was also reported that the plasma loading resistance in the H- and L-modes changed from 2Ω to 8Ω. It is thought that the plasma loading resistance should change at least by factor 2 during the H-L transition on EAST. It was thought that the RF power was lost in the transmission line between the ICRF heating antenna and the stub tuner, because the standing wave with the high RF voltage was excited and the RF Ohmic loss occurred there. When the launched wave power from the antenna is much smaller than the RF Ohmic loss power, the loading resistance during the ICRF heating does not change so much during the H-L transition. This may be the reason why the reflected RF power fraction did not change so much as seen in Fig.31.

3-4. Injection efficiency

The injection efficiency is defined with the ratio of $R_p/(R_p+R_v)$. Here R_p and R_v are the plasma loading resistance and the vacuum loading resistance, respectively. R_v is measured with injected RF power P_v and the maximum RF voltage standing there V_{rfv} without plasma using the following equation,

$$R_v = 2P_v(Z_0/V_{rfv})^2$$

Here Z_0 is the characteristic impedance of the transmission line. Then R_v+R_p is measured with injected RF power P_p and the maximum RF voltage standing there V_{rfp} during plasma,

$$R_v + R_p = 2P_p(Z_0/V_{rfp})^2$$

The net power P_p injected from the antenna can be assessed using the following equation,

$$P_p = 1/2R_p(V_{rfp}/Z_0)^2 = P_p - 1/2R_v(V_{rfp}/Z_0)^2$$

The injection efficiency is the ratio of $R_p/(R_p+R_v)$. At present the length between impedance matching and antenna on EAST is about 100m as shown in Fig.32. A simple estimation of the RF Ohmic resistance can be assessed as $R_v>1\Omega$, using the RF skin depth and the resistance of the aluminum material. To measure the RF voltage of the standing wave many RF probes are allayed along the transmission line on EAST as shown in Fig.33, and R_v and R_p are calculated using the above equations.

3-5. Reduction of standing RF voltage to increase in injection efficiency using pre-stub tuner

The Ohmic loss is proportional to the standing RF voltage. So if the standing RF voltage can be reduced, the Ohmic loss becomes much smaller, which results in the reduction of the vacuum resistance R_v. When the stub tuner (referred to as pre-stub tuner) is installed between the antenna and the impedance matching device as shown in Fig.34, the standing RF voltage can be reduced with the optimum selection of A_{Ap} and A_p as seen in Fig.34. Here A_{Ap} is the normalized length between the pre-stub tuner and the antenna, and A_p is the normalized length of the pre-stub tuner. The standing RF voltage V_L (the RF current I_L) between the pre-stub tuner and the impedance matching device is calculated using the following equation.

$$\begin{pmatrix} V_L \\ I_L \end{pmatrix} = \begin{pmatrix} \cos(2\pi A_L) & jZ_0\sin(2\pi A_L) \\ j/Z_0\sin(2\pi A_L) & \cos(2\pi A_L) \end{pmatrix} \begin{pmatrix} 1 & 0 \\ j/Z_0/\tan(2\pi A_P) & 1 \end{pmatrix} \begin{pmatrix} \cos(2\pi A_{AP}) & jZ_0\sin(2\pi A_{AP}) \\ j/Z_0\sin(2\pi A_{AP}) & \cos(2\pi A_{AP}) \end{pmatrix} \begin{pmatrix} V_A \\ I_A \end{pmatrix}$$

Here A_L shows the normalized length of the arbitrary position measured from the pre-stub tuner. V_A and I_A are the RF voltage and the current at the RF antenna, respectively. The ratio of V_A to I_A is the loading resistance, i.e., R_v or R_p. The maximum V_L as V_{max} is compared with the maximum standing RF voltage V_{max0} between the pre-stub tuner and the RF antenna. The effect of the pre-stub tuner is shown with the contour lines as seen in Fig.35; the abscissa is the A_p and the ordinate is A_{AP}. When A_{AP}=0.445 and A_p=0.05, the reduction rate becomes 0.1. The minimized reduction ratio is available in the case of $A_{AP}+A_P$=0.5 as seen in Fig.35 [13]. The measurement of the standing RF voltages in various positions along the transmission line was carried out at NIFS, and they are shown with and without the effect of the

pre-stub tuner as seen in Fig.36 and 37. The reduction of the RF voltage is realized to one third. When the pre-stub tuner is installed at the optimized position, the Ohmic loss can be reduced with the square of the reduction voltage ratio. Then the better injection efficiency can be expected.

3-6. Reduction of the reflected RF power during H-L transition

As previously described, a large RF power should have been reflected during H- to L-mode transition, i.e., ~30~40%. In this case the reduction of P_p may not lead to H-mode again. Several ideas have been proposed for that. Here two challenging methods are proposed. One is a method of the frequency feedback control using twin stub tuner as seen in Fig.38 and the other is a complex conjugate antenna system as seen in Fig.39.

1) Frequency feedback control using twin stub tuner.

In this method a double stub tuner system is employed as an impedance matching system. The double stub system consists of two stub tuners. When the distance between two stub tuners is employed a quarter of the RF wavelength, and the double stub tuner system is located at the particular position, the reflected RF power can be reduced with only changing the length of the stub tuner at the RF generator side in changing the plasma loading resistance. But this change is so rapid as less than 1ms, and the time response is not enough. An innovative twin stub tuner is installed with replacing the conventional stub tuner. When the frequency is changed, the twin stub tuner equivalently works as changing the length of the stub tuner of A_L as seen in Fig.38. The typical example is shown in Fig.40. When the plasma loading is changed from 2Ω to 8Ω as measure on JET, the reflected RF power fraction would have increase to 50%. But the reflected RF power fraction can be reduced to < 1% with 0.1% of Δf/f of the frequency modulation [14].

2) Complex conjugate antenna system

The RF power is supplied to two identical antennas after divided into two transmission lines at the T-junction as seen in Fig.39. When selecting A_{AC1} and A_{AC2} as $A_{AC1}+A_{AC2}=0.5$, the imaginary part of the impedance at the T-junction becomes to zero. This is the reason why this system is referred to as the complex conjugate antenna system. When the plasma loading resistances are known in the H- and L-mode as R_H and R_L, the A_{AC1} is determined in the following equation,

$$R_H R_L = Z_0^2 \tan^2(2\pi A_{AC1})$$

Then the impedance at the T-junction becomes the same in the different R, i.e., R_H and R_L. When the impedance matching is obtained at R_H using the single stub tuner system located the RF generator side as seen in Fig.39, the reflected RF power fraction becomes to zero again at R_L. The typical example is shown in Fig.41. When plasma loading is changed from 2Ω to 8Ω, a reflected RF power fraction would have increase to 50%. But the reflected RF power fraction is reduced to ~1% with a complex conjugate antenna system [15].

4.Acknoledgement

This report is based on 11A of the five years collaborations in CUP program. During the period of 2006~2010 many scientists were exchanged. The authors appreciated the fruitful discussions with Profs. K.Tsumori (NIFS), G.Lei (SWIP), C.Hu (ASIPP), Z.Liu (ASIPP), S.Kubo (NIFS), K.Nagasaki (Kyoto U.), X.Ding (SWIP), J.Zhou (SWIP), S.Ide (JAEA), J.Shan (ASIPP), F.Liu (SIPP), Y,Zhao (ASIPP), X.Zhang (ASIPP) and B.Wang(ASIPP). The authors appreciated Profs. T.Watari (the former Japanese coordinator), K.Toi (the Japanese coordinator), and K.Wan (the Chinese coordinator). They also appreciated Profs. O.Motojima (former Director-general of NIFS) and A.Komori (Director-general of NIFS) as the Japanese representative and Prof. J.Li (Director-general o ASIPP) as the Chinese representative. The authors expect that another intimate collaboration will continue between China and Japan.

References

[1] Y. Li-Ming, L. Guang-Jiu, C. Jian-Yong et al, 2010, *Chinese Phys. Lett.* **27**:042901.

[2] G.Zhang, K.Nagasaki et al., Plasma and Fusion Research, Volume 3, 020 (2008).

[3] G.Zhang, K.Nagasaki et al., Plasma Sci. Technol. 11 (2009) 619-624.

[4] S.Kubo et.al., Fusion Eng. And Design, 26(1995) 319.

[5] L.Yan et al., in Fusion Energy 2010 (Proc. 23rd Int. Conf. Geneva, 2010) (Vienna: IAEA) CD ROM file OV/4-5

[6] J.Li et al., in Fusion Energy 2010 (Proc. 23rd Int. Conf. Geneva, 2010) (Vienna: IAEA) CD ROM file OV/1-2

[7] Y.Zhao, private communication.

[8] K.Saito et al., Fusion Engineering and Design, 81 (2006) pp.2834-2842.

[9] X.Zhang, private communication.

[10] H.Kasahara, et al., J. Plasma Fusion Res., Vol. 5, S2090 (2010).

[11] T.Seki et al., Fusion Technology, Vol.40, No.3(2001), pp.253-264.

[12] I.Monakhov et al., 15th Topical Conf. of RF Power in Plasmas 2003, AIP Conf. Proc. 694, pp.146-149.

[13] R.Kumazawa et. al., Journal of Plasma and Fusion Research, Vol.75, No.7(1999), pp.842-853.

[14] R.Kumazawa et al., Nuclear Fusion, **48**(2008), 115002.

[15] R.Kumazawa et al., to be published in Nuclear Fusion.

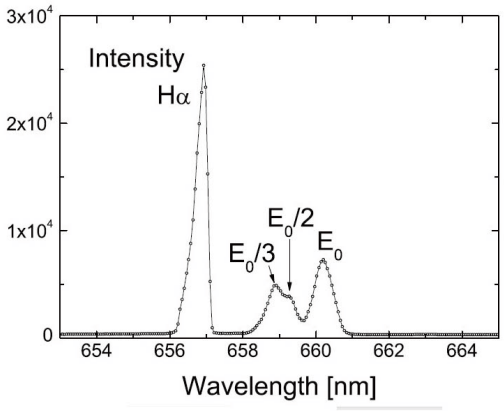

Fig.1 Spectroscopic measurement of E_0, $E_0/2$, $E_0/3$

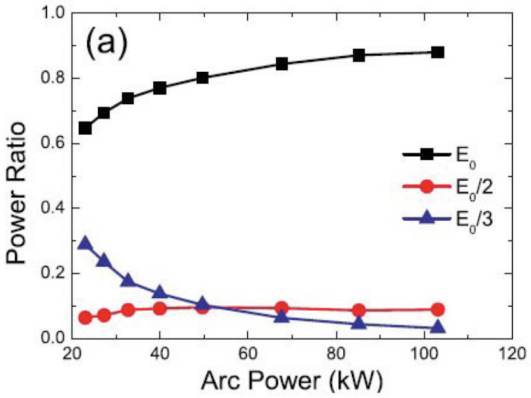

Fig.2 Dependence of E_0, $E_0/2$, $E_0/3$ on arc power

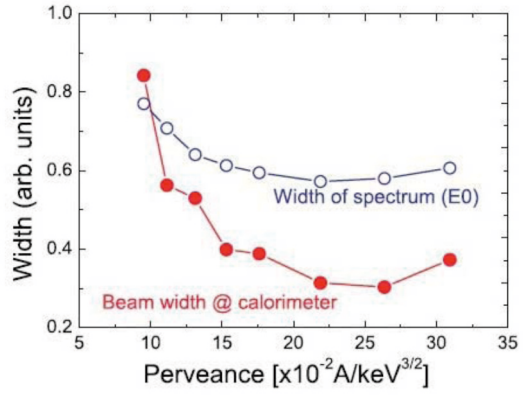

Fig.3 Beam divergence vs. perveance

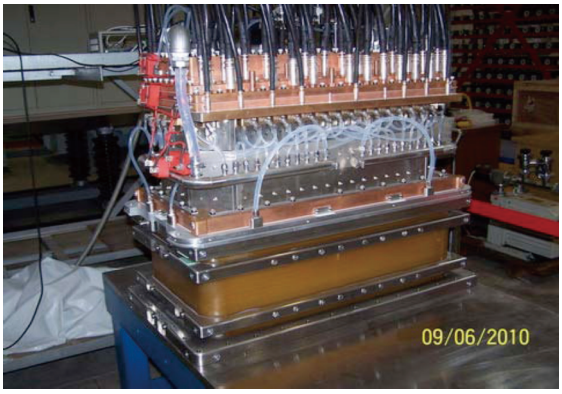

Fig.4 Ion source of NBI in ASIPP

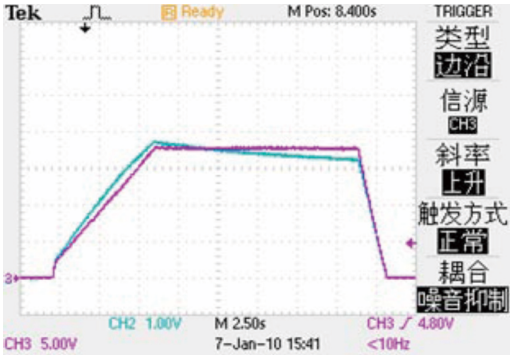

Fig.5 Filament power test: 18V/5.5kA/120s

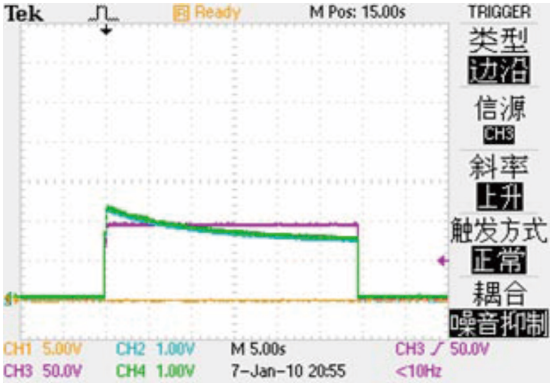

Fig.6 Arc power test: 180V/3.1kA/30s

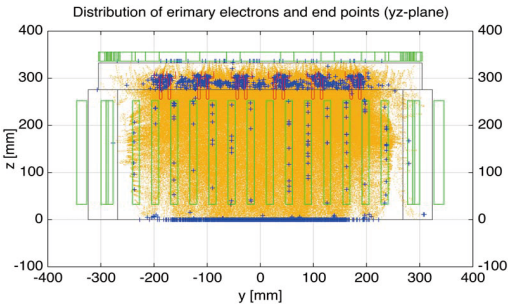

Fig.7 Electron trajectories on EAST ion source

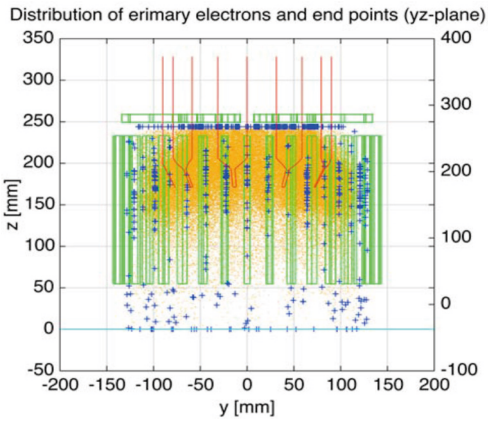

Fig.8 Electron trajectories on SWIP ion source

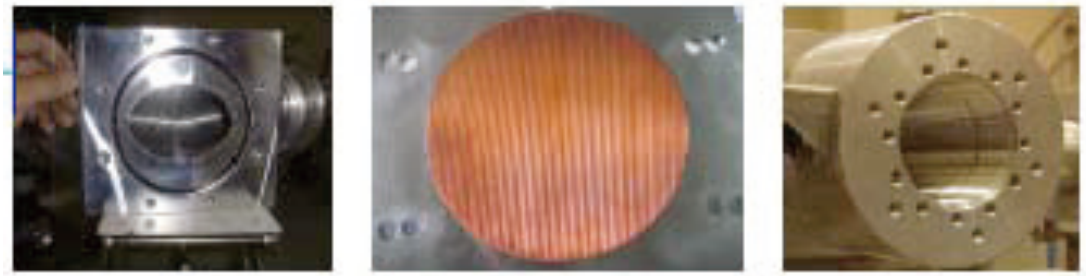

Fig.9 Groove mirror system

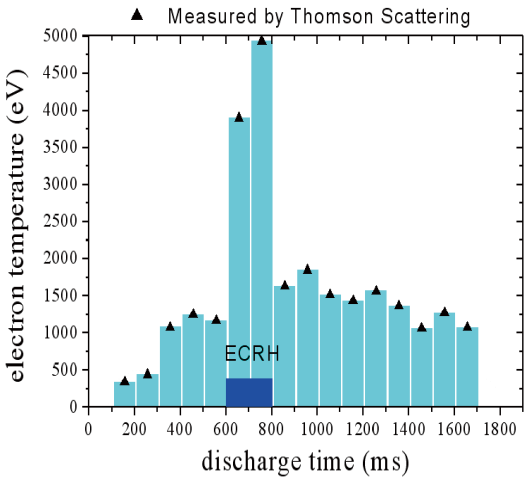

Fig.10 Increase in electron temperature with ECH

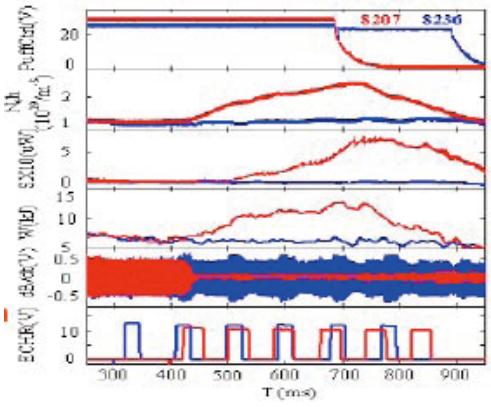

Fig.11 Suppression of NTM with X2 at q=2

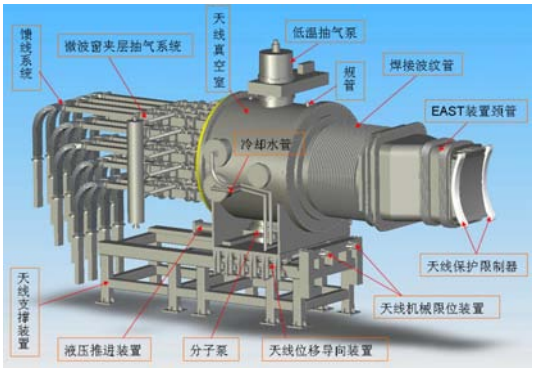

Fig.12 LHCD system on EAST

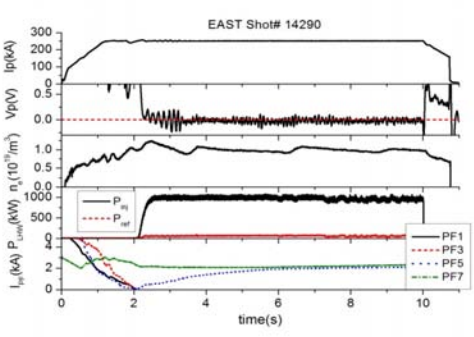

Fig.13 Fully non-inductive plasma current with LHCD

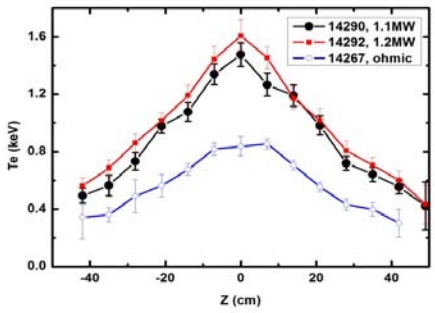

Fig.14 Radial profile of electron temperature during Ohmic and LHCD phases

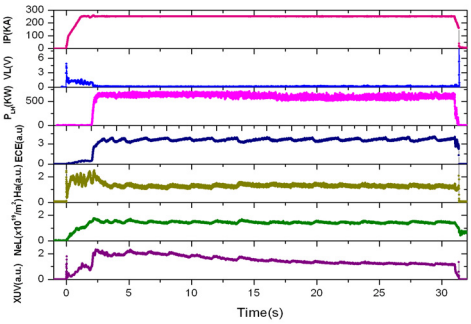

Fig.15 Long pulse plasma discharge with LHCD

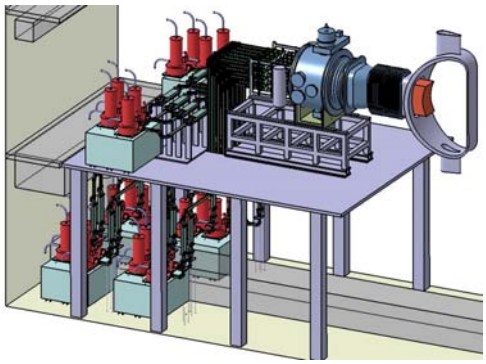

Fig.16 New LHCD system with f=4.6GHz installed on EAST

Fig.17 RF generators for ICRF heating at ASIPP

Fig.18 Impedance matching system with three Liquid stub tuners

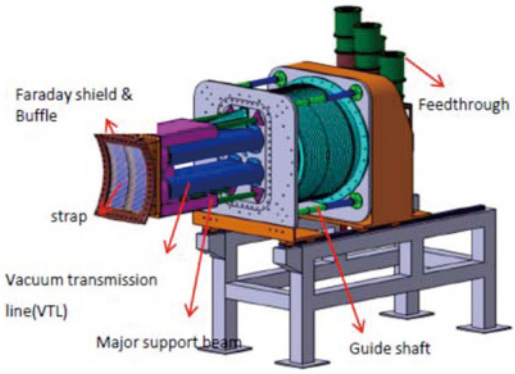

Fig.19 ICRF heating antenna system

Fig.20 ICRF heating antenna with two straps

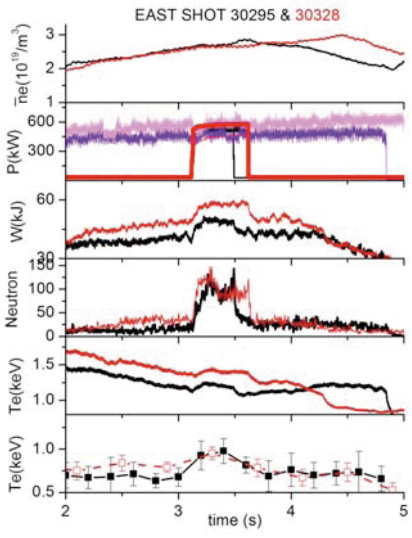

Fig.21 Time evolutions of plasma parameters during minority ICRF heating

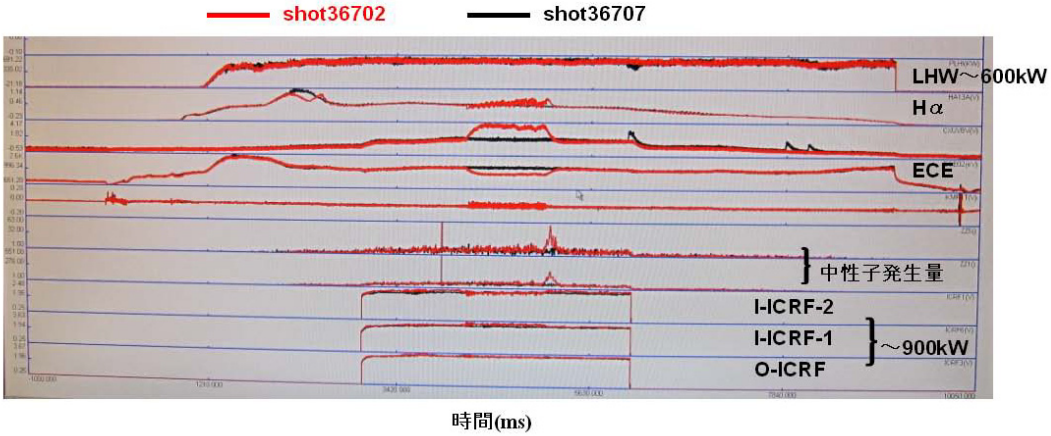

Fig.22 Observation of H-mode during LHCD and minority ICRF heating

Fig.23 ICRF heating power modulation system

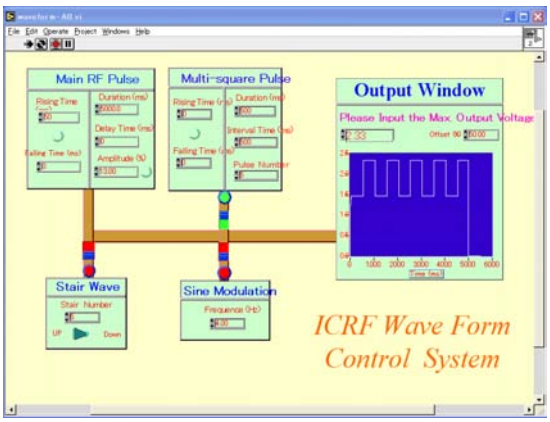

Fig.24 New antennas installed on LHD

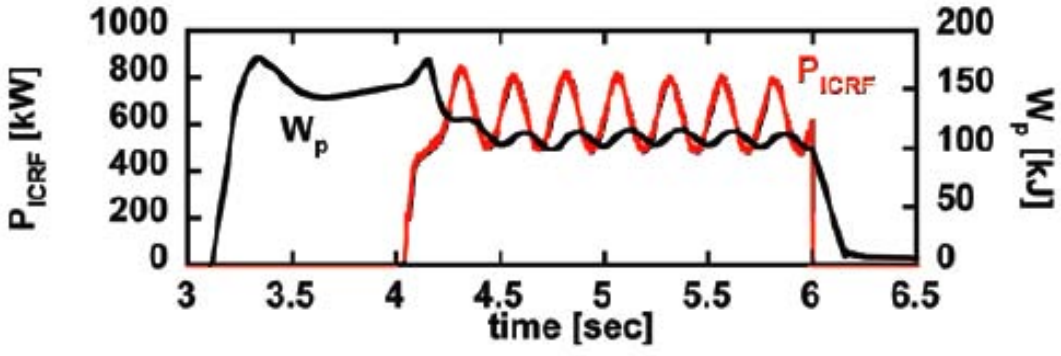

Fig.25 Time evolutions of plasma stored energy and modulated ICRF heating power

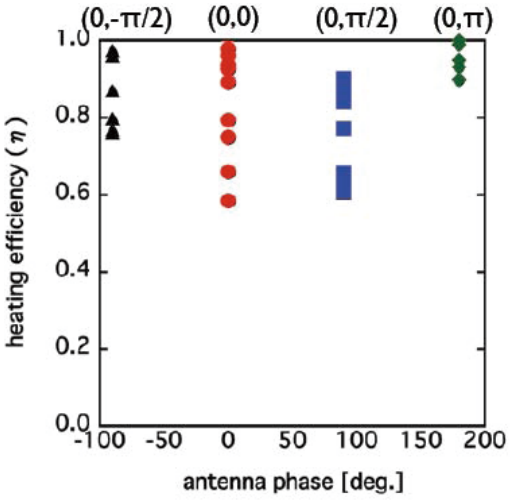

Fig.26 ICRF heating efficiency against antenna phase

Fig.27 Low RF power supplied from cavity of final amplifier

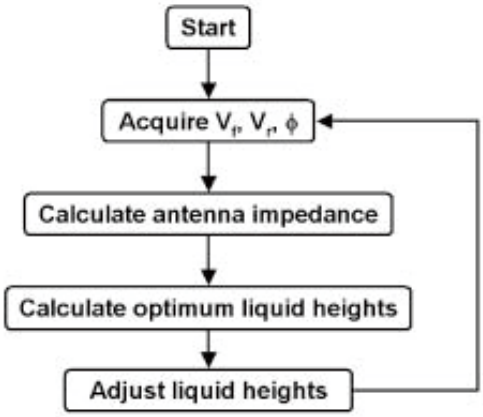

Fig.28 Flow chart of feedback control for impedance matching

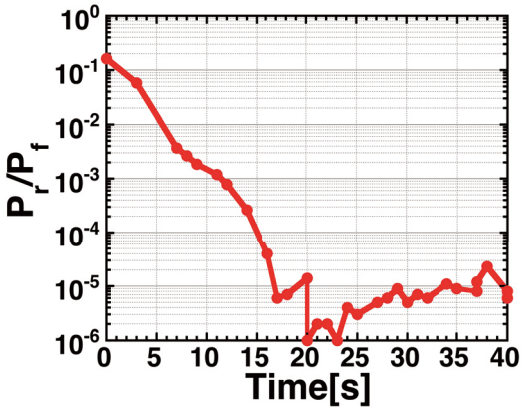

Fig.29 Time evolution of reflected RF power fraction with real-time feedback control

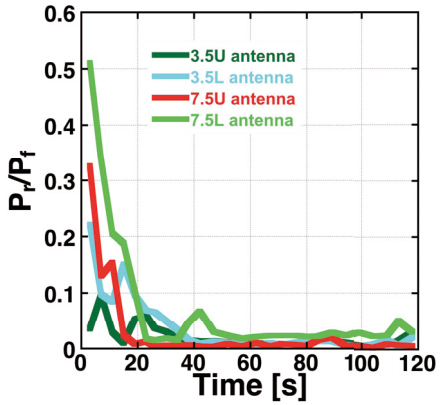

Fig.30 Real-time impedance matching on LHD

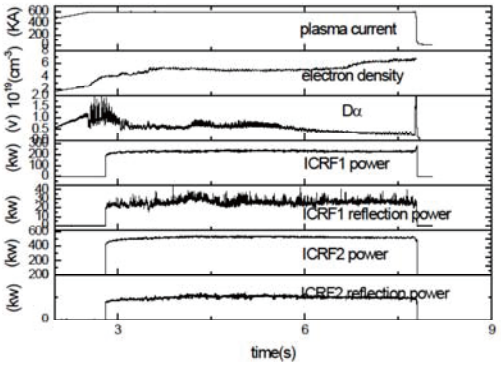

Fig.31 H-mode plasma on EAST

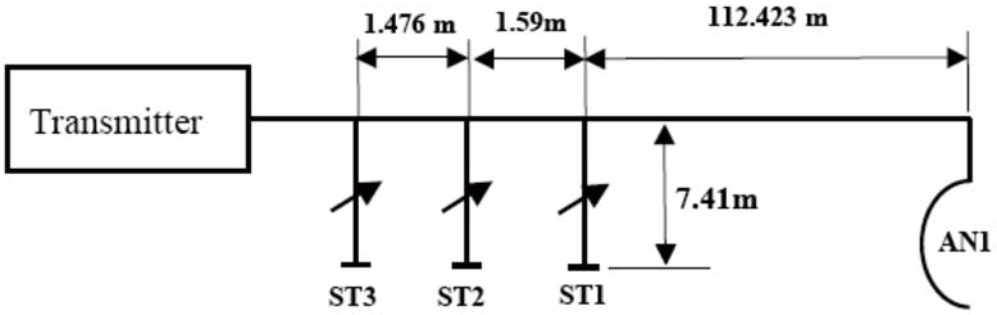

Fig.32 Impedance matching system with three liquid stub tuner for ICRF heating on EAST

Fig.33 RF prove array on EAST

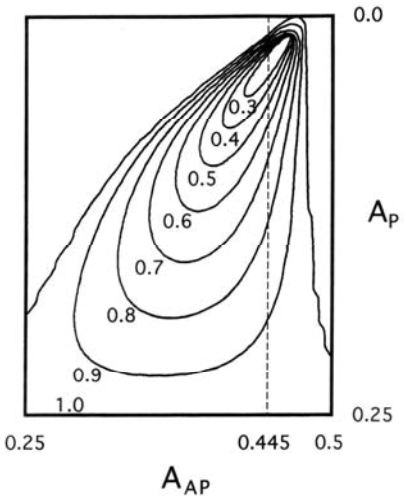

Fig.35 Contour map of reduction of RF voltage

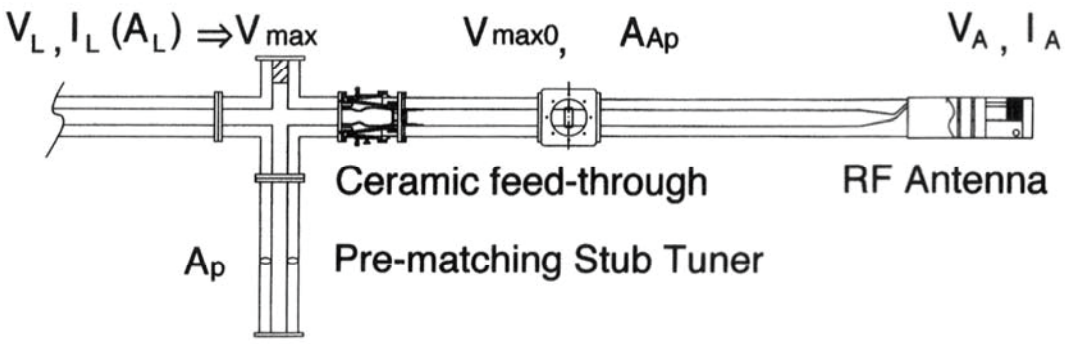

Fig.34 Pre-matching stub tuner system

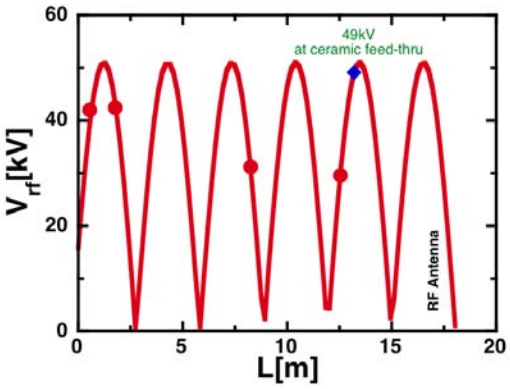

Fig.36 Distribution of standing RF voltage without pre-stub tuner

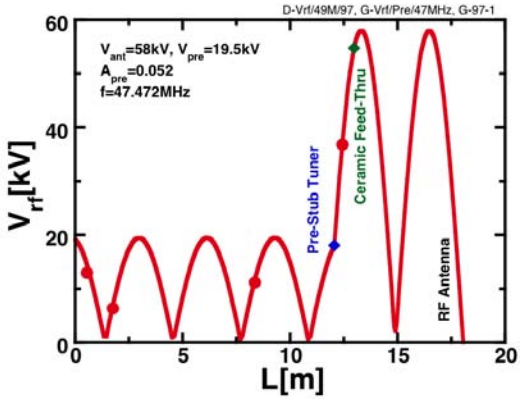

Fig.37 Distribution of standing RF voltage with pre-stub tuner

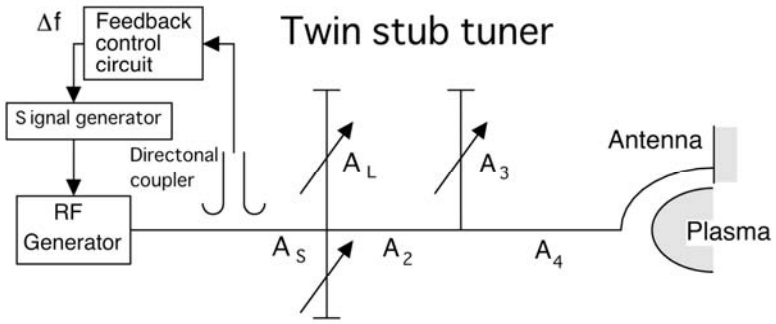

Fig.38 Frequency feedback control impedance matching system with twin stub tuner

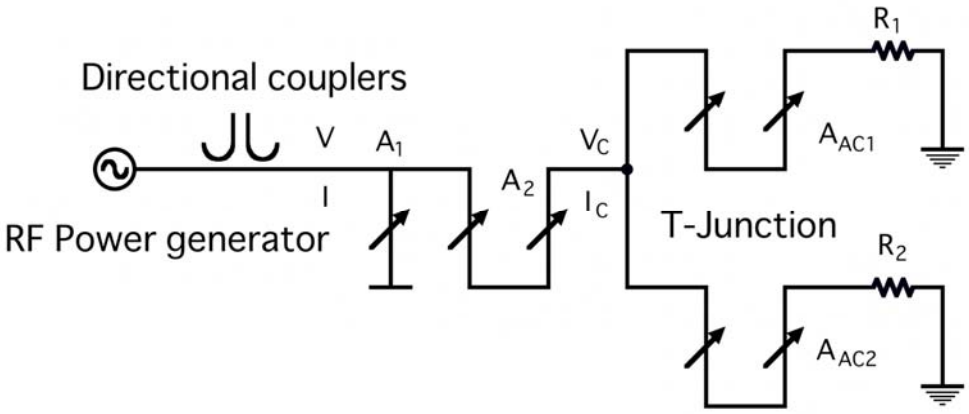

Fig.39 Impedance matching system with complex-conjugate antennas

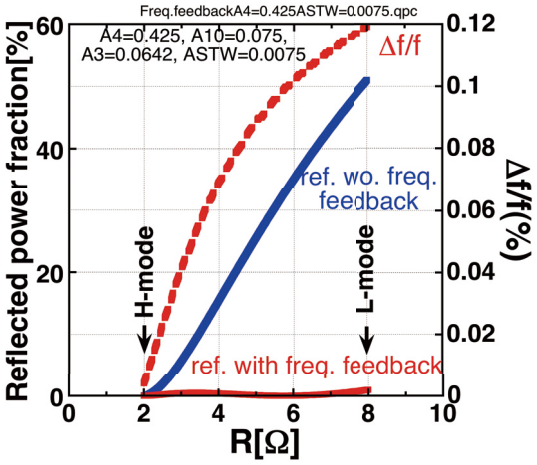

Fig.40 Reduction of Reflected power fraction using frequency feedback control with twin stub tuner

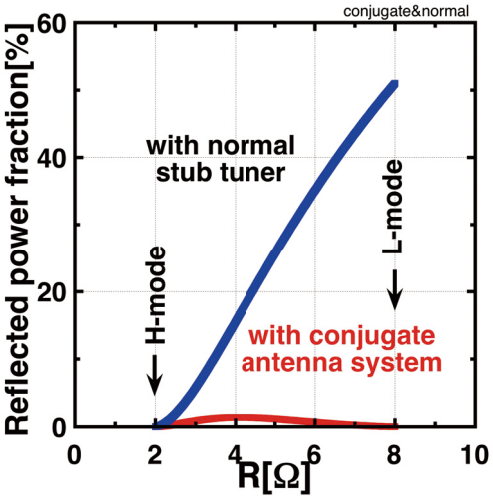

Fig.41 Reduction of Reflected power fraction using complex-conjugate antennas

Summary of Research Activities on 11B during Past Five Years And Future Prospect

S.Morita, X.Gao[1], K.Hanada[2], S.Ide[3] and L.W.Yan[4]

National Institute for Fusion Science, Toki 509-5292, Gifu, Japan
[1]Institute of Plasma Physics, Chinese Academy of Sciences, P.O.Box 1126, Hefei, Anhui 230031, China
[2]Research Institute for Applied Mechanics, Kyushu University, Kasuga 816-8580, Fukuoka, Japan
[3]Japan Atomic Energy Agency, Naka 311-0193, Ibaraki, Japan
[4]Southwestern Institute of Physics, P.O.Box 432, Chengdu 610041, Sichuan, China

1. Introduction

Collaborative study has been made on "Development of Diagnostic and Control methods for high-performance Plasma Confinement" at a category of 11B in magnetic confinement fusion experiment. Production and control of high performance plasmas are crucial issues for realizing an advanced nuclear fusion reactor in addition to developments of advanced plasma diagnostics. The collaboration has been done along the issues with many tokamak and helical devices in both countries of Japan and China, i.e., LHD (NIFS), JT-60U (JAEA), QUEST, CPD, TRIAM-1M (Kyushu Univ.), LATE (Kyoto Univ.), Heliotron-J (Kyoto Univ.), EAST, HT-7 (ASIPP), HL-2A (SWIP), J-TEXT (HUST) and SUNIST (Tsinghua Univ.). Many scientists (15-20 persons per year) including young researchers joined in the collaboration of 11B category as personal exchange programmed by key persons of Profs. X.Gao (ASIPP), L.W.Yan (SWIP), S.Morita (NIFS), S.Idei (JAEA) and K.Hanada (Kyushu Univ.). In addition, two seminars (Lijiang, 2008 and Guilin, 2010) with participation of many Chinese and Japanese PHD students were held to make fruitful discussions on the present status and future plan, which certainly lead to further productive collaboration. Two Chinese PHD students graduated from SOKENDAI and four Chinese PHD students in SOKENDAI are now studying in LHD with one Chinese PD-student based on NIFS COE program. Japanese PHD students also joined in the EAST experiment.

Many fruitful results have been obtained through the collaboration during past five years in both countries. In particular, high-density plasmas with super-dense core were studied in LHD and discussed with operational range in tokamaks including EAST.

The blob, which is known as an anomalous cross-field transport in SOL with an intermittent density pulse event, was analyzed in QUEST and the result was compared with HL-2A experiment. MHD events in EAST LHCD discharges and HL-2A NB-heated discharges were analyzed in relation to MHD modes driven by energetic electrons and ions, respectively. The results were discussed with beam-ion-driven MHD modes appeared in LHD. Edge impurity behavior was studied in HL-2A discharges with tokamak SOL characterized by short magnetic field connection length. The result was compared to LHD discharges with ergodic layer characterized by long magnetic field connection length in terms of the impurity screening (EXD/6-5Ra, 23rd IAEA Fusion Energy Conference, 2010, Korea).

The research activities obtained at the 11B category during past five years are presented in this proceeding.

2. Typical results of CUP collaboration during past five years

2-1 Fast ion confinement [1,2]

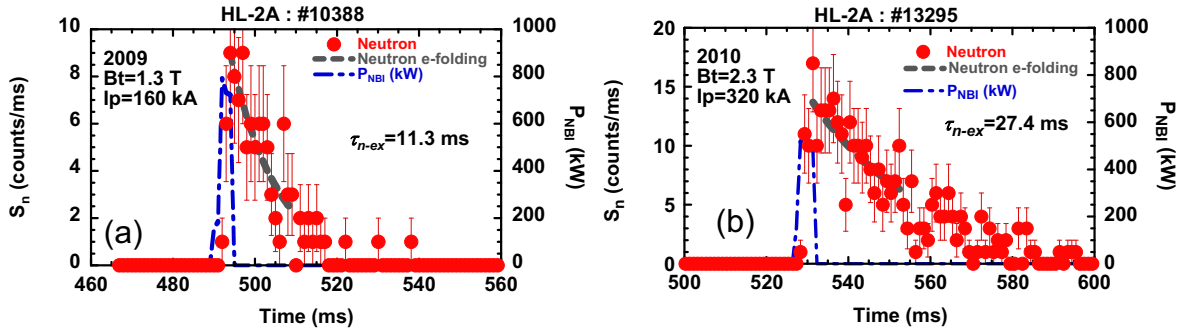

Fig.1 Typical time behaviors of D-D (2.45MeV) neutron emission rate after short pulse NB injection in HL-2A tokamak at (a) B_t=1.3T and (b) 2.3T.

Time traces of the d-d neutron emission rate, S_n, and short pulse NBI (blip), P_{nb}, in HL-2A are shown in Fig.1. The deuterium NB blip is injected during 5ms in the MHD-quiescent deuterium ohmic discharge for two different Bt of 1.3T and 2.3T. The d-d neutrons in HL-2A are basically produced by the beam-plasma reaction, since the E_b of 30 keV is much higher than ion (≡deuteron) temperature, T_i, in ohmic discharges. The effective T_i evaluated from a perpendicular NPA typically ranges around 1 keV. The d-d fusion reaction rates, $\langle\sigma v\rangle_b$ in $D(d,n)^3He$ for monoenergetic beam deuterium are shown in Fig.2 as a parameter of T_i. The neutron yield, S_n, rapidly goes up after turning on the NB, as shown in Fig.1, and the S_n starts to decay exponentially after

turning off the NB. The decay rate in S_n is determined by the energy decay of the NB as a function of time. Here, the beam deuteron energy of 30 keV is decelerated through Coulomb collisions with background electrons in the classical theory. In order to deduce the birth deposition rate of the NB, the peak counts of the d-d neutrons are measured at the end of the blip NB for several discharges with different n_e. The result is plotted in Fig.3 as a function of n_e. Although the data points are somewhat scattered due to the weak neutron emission, the S_n tends to increase with n_e. The calculation of the NB deposition rate, plotted with dashed line, is in fairly good agreement with the experimental data, indicating that the birth deposition rate of the NB increases with n_e.

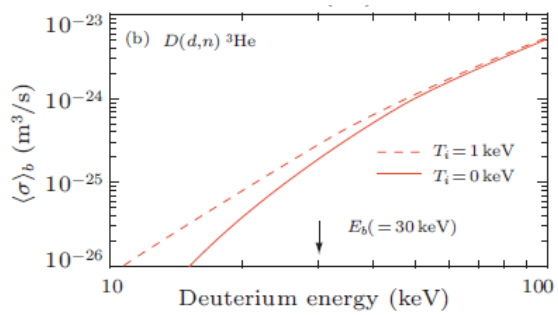

Fig.2 Fusion reactivities of (D, n)^{3}He as a function of deuterium energy for plasmas with T_i=0 (solid line)) and 1keV (dashed line).

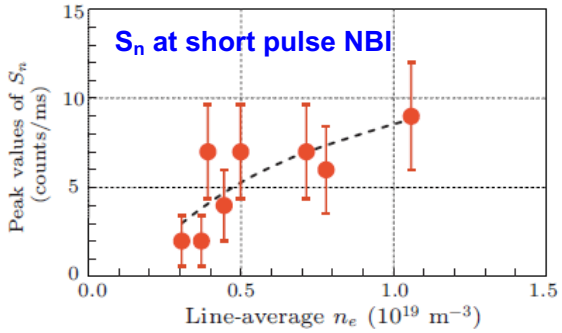

Fig.3 Neutron emission rate at the end of short pulse NB injection with width of Δt=5ms.

Figure 4(a) shows typical radial profiles of n_e measured with multi-channel HCN interferometer and T_e measured with Thomson scattering system, which are used for the present analysis. The radial profile of the theoretical $\tau_{n\text{-}th}$ is thus obtained as shown in Fig.4 (b), assuming that $T_i(r/a)$ is equal to $T_e(r/a)$. In the figure the $\tau_{n\text{-}th}$ is smaller in the peripheral region, since the $\tau_{n\text{-}th}$ becomes small with decrease in T_e. The experimental neutron decay rate, $\tau_{n\text{-}ex}$, is determined to be 11.3 ms in discharges with

the NB blip for Bt=1.3T case. It is also plotted with a dashed line in Fig. 4(b). The result shows an excellent agreement with the experimental value in the core region of r/a<0.4. This means that the tangentially injected beam ions are well confined in the plasma core according to the classical theory, depositing their energies to electrons.

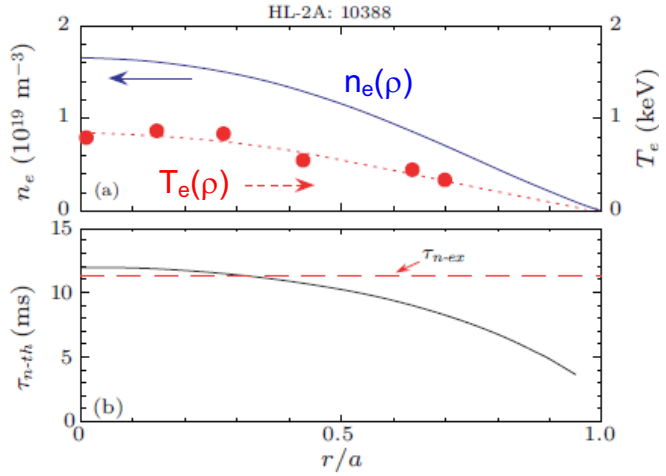

Fig.4 (a) Radial profiles of electron density (solid line) and temperature (dotted line) and (b) radial profile of theoretically predicted D-D neutron decay time (solid line). Experimentally measured neutron decay time is shown with dashed line.

2-2 Energetic particle driven MHD [3,4]

The fishbone instabilities have an m/n = 1/1 structure by the Mirnov signals and soft x-ray emission on HL-2A, as shown in Fig.5. Higher poloidal harmonics with m > 1 are also observed, while the Mirnov signals are usually dominated by m = 3 or m = 4 modes. However, this is not surprising since the m = 1 internal kink modes have very small amplitudes on the edge, where the magnetic coils are located. Three kinds of ion fishbones have been identified during NBI. They are hybrid sawtooth–fishbone, classical fishbone and run-on fishbone.

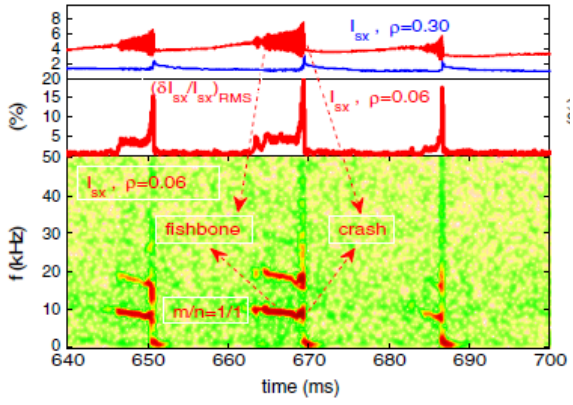

Fig.5 Ion fishbone (sawtooth hybrid fishbone instability) identified during NBI discharge in HL-2A tokamak.

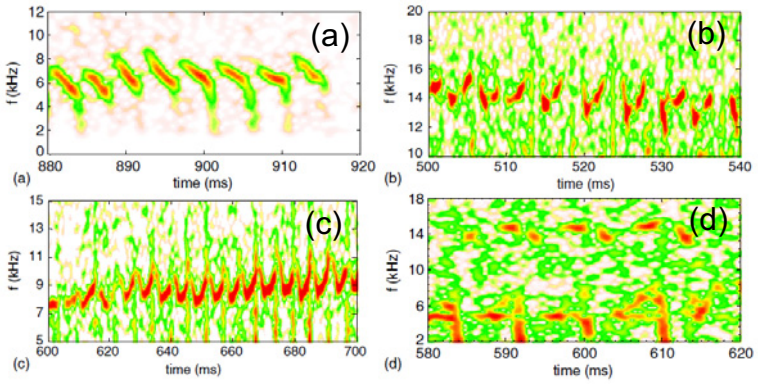

Fig.6 Frequency behaviors of electron fishbone identified during ECH discharges in HL-2A tokamak; (a) chirping down, (b) chirping down and chirping up, (c) V-front-style sweeping and (d) frequency jumps.

The e-fishbone has been also identified and investigated during low power ECH on HL-2A, but the previous experiments did not present frequency-chirping behaviors of e-fishbone. However, when the ECH power exceeds 0.7MW, the features of e-fishbone are novel and complex. Numerous experimental results indicate that e-fishbone frequencies are higher and provided with up- and down-chirping behaviors; sometimes, also with V-font-style sweeping. Periodic mode frequency jumps have been detected for the first time during large-power ECH on HL-2A. Figure 6(a) shows that the mode frequencies (f = 5–8 kHz) are only chirping down between two sawtooth crashes. Figure 6(b) shows that the mode frequencies (f = 11–16 kHz) are chirping down after a sawtooth crash, and then chirping up before the next sawtooth crash, and the two chirping processes are discontinuous. Figure 6(c) shows that the mode frequencies (f = 7–11 kHz) are V-font-style sweeping between two sawtooth crashes, namely the chirping-down and chirping-up processes are continuous. Figure 6(d) gives the periodic mode frequency jumps of e-fishbone activity. It can be found that one mode (f ≈ 5 kHz) appears around 585–589 ms, and another mode (f ≈ 15 kHz) develops at 589–592 ms. A sawtooth crash occurs at 592 ms and a chirping mode appears around 592–594 ms, and then it starts the next cycle. As in the case of low ECH power, the modes can be excited by ECH deposited on both the LFS and HFS, and the modes occur much more easily during off-axis heating. The chirping modes propagate in the electron diamagnetic drift direction in the laboratory frame of reference. The mode excitation is correlated with the energetic electrons. The counts of hard x-ray photos increase substantially during ECH, and the chirping modes are excited when the counts increase to a higher level. It is clear that the mode frequency increases along with increasing counts.

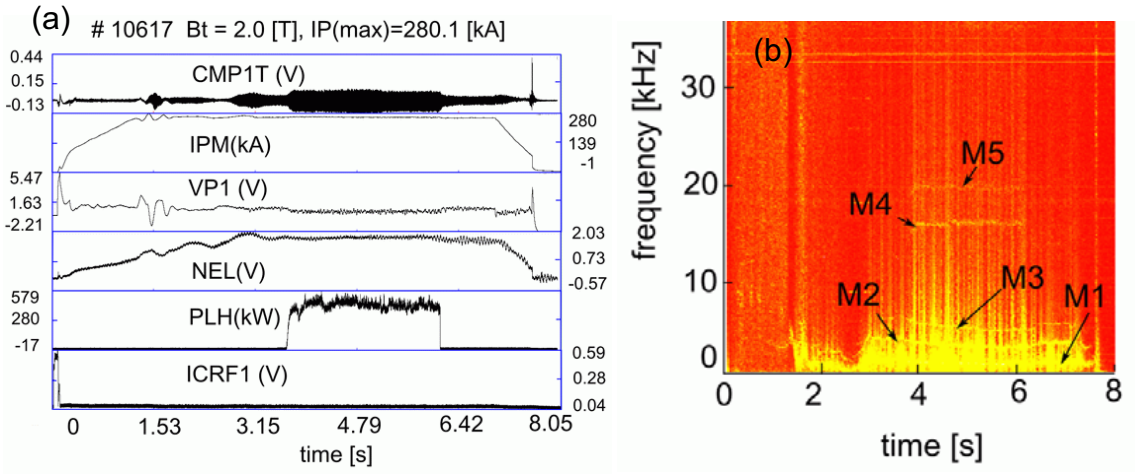

Fig.7 (a) Typical waveform of LHCD discharge in EAST and (b) Magnetic fluctuation spectrum analyzed from magnetic probe at inboard mid plane.

Typical discharge waveform of LHCD plasma in EAST is shown in Fig.7(a). The toroidal magnetic field, plasma current and electron density are 2T, 280kA and $2x10^{13}cm^{-3}$, respectively. In this discharge several specific frequencies of 2kHz, 4kHz, 6kHz, 17kHz and 20kHz are identified from poloidal magnetic probe analysis, which are named M1, M2, M3, M4 and M5, respectively. The M1 mode is frequently observed in ohmic discharges. The M2 and M3 are higher harmonic modes of the M1. The M1 mode is analyzed using the poloidal magnetic probe array. The result indicates m=2 poloidal mode number, suggesting tearing mode. However, the toroidal mode number has not been obtained because of the absence of the toroidal magnetic probe. When the time behavior of the M4 and M5 modes is examined, it is observed that the modes are quickly saturated after switching on the LHCD and quickly disappeared after switching off the LHCD. The excitation of the modes is probably brought by a change in the density profile or safety factor. These modes are not observed in ohmic discharges and heating mode of the LHCD. Therefore, it may be related to the energetic electrons accelerated LH waves.

2-3 Development of TV Thomson scattering system [5]

TV Thomson scattering system has been developed in EAST, as shown in Fig.8(a). The spectrometer is designed such that the whole image intensifier area, 25 mm in diameter, can be used in sufficient image quality. In order to check the coupling quality of the C-mount lens, the CCD camera is located at a place where the object plane of the CCD is on the back focal point of the spectrograph. Note that in the actual situation, the back focal point of the spectrograph is placed at the front surface of the image intensifier

(multi-channel plate: MCP), and the object plain is located at the back surface (phosphor screen), so that the position of the CCD goes slightly behind by the thickness of the I.I. In order to couple the aperture of the I.I. with 25 mm in diameter with the CCD area 8 mm in dimension the magnification M = 1/3 is required.

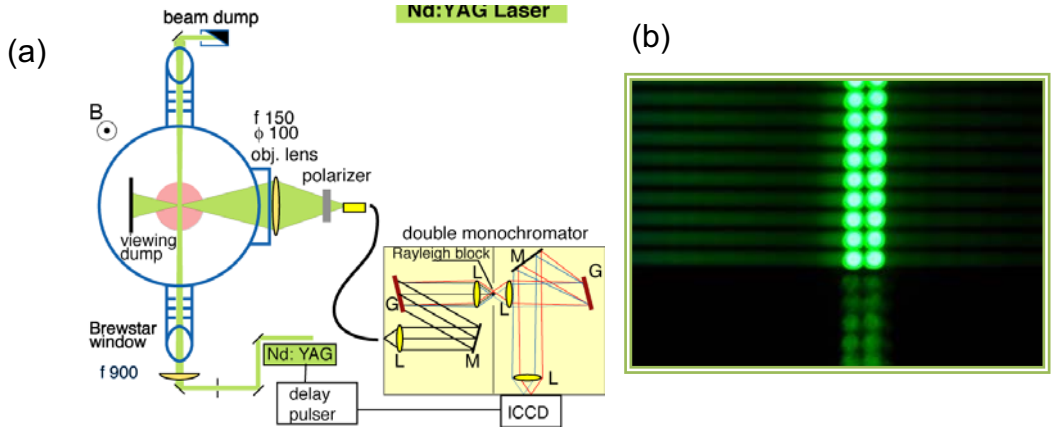

Fig.8 (a) TV Thomson scattering system in EAST and (b) optical fiber array image at ICCD detector.

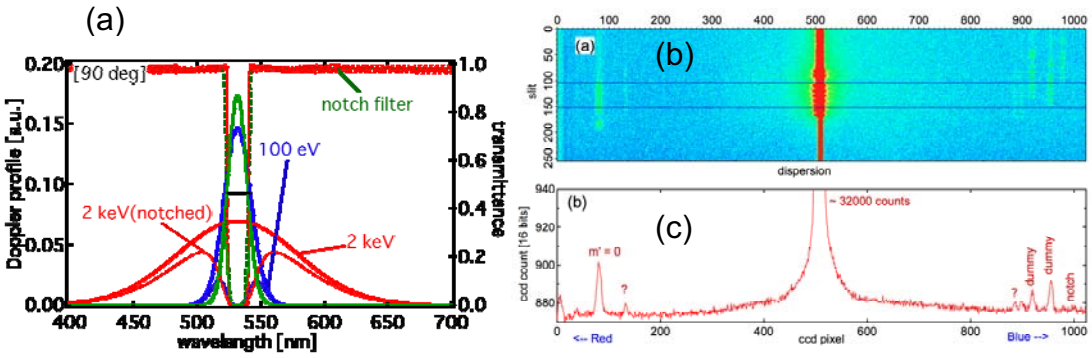

Fig.9 (a) Calculation of visible spectrum to be observed by Czerny-Turner f=85mm spectrometer, (b) visible image from HgI (5460.7Å) recorded with ICCD and (c) visible spectrum.

A transmission grating is used instead of usually used reflection grating in the visible spectrometer to increase the throughput. However, ghost spectra are appeared when the transmission grating is used. In order to examine multi-reflection ghost (MRG,) an experiment is done with a simple optical arrangement. Photographic lens (Nikon f135 F/2.8, i.e. D = 48mm, NA=0.18) both for collimator and camera optics and a 600 grooves/mm (d=1.67 x 10^{-6} m) grating 50 x 50 mm^2 in dimension are adopted. Dispersed spectra are recorded using Nikon D90 digital camera in 8-bits JPEG format. The angle at which the first order light coincides with the MRG is measured by rotating

the grating mount. The results for H I (656.285 nm) and Hg I (546.073 nm) are shown in Fig. Fig.8(b).

The visible spectra of the YAG laser scattered from electrons in plasmas to be measured by the visible spectrometer are calculated, as shown in Fig.9(a). It indicates the the present system can measure the electron temperature in range of 0.1 to 2keV. In the actual situation, the MRG can occur at every optical component, though the refection could be a small part of the incident light. There are several ways to mitigate the disturbance caused by the MRG. Firstly, if a strong component crucially superposes the emission line of interest with small intensity, the location of MRG at the wavelength spectra can be shifted by rotating the grating in the dispersion direction, unless m' = 0. Secondly, the MRG can be shifted to the slit direction by inclining the grating towards perpendicular to the dispersion direction. As mentioned above, the reflection at the surface of the input fiber array produces the brightest MRG because of the mirror-like perfect reflection, the inside surface of the entrance slit of the spectrograph is blackened. The spectrograph in the present work adopts these functions. Figure 9(b) shows the MRGs observed by intentionally inputting the strong light at 532 nm close to the saturation level of the 16-bits CCD detector (ANDOR Newton 26 μm/pixel, 1024 x 512 pixels). The intensity of the MRG due to the partial reflectance is approximately 1/1600 to the 1st order light. This does not probably bring a serious effect in the analysis, even if the grating is inclined.

2-4 Blob phenomena [6]

The blob size in HL-2A has been measured by an electrostatic probe array with 8 radial tips and 10 poloidal tips. Minimum and maximum separations of two probes are 0.4 cm and 3.6 cm, respectively, while maximum radial and toroidal separations are 2.8 cm and 80 cm. The radial size of blob turbulence for two discharges with different densities is presented in Fig 10. The blob duration at high density discharge shown in Fig.10(b) is longer than that at low density discharge shown in Fig.10(a). The corresponding speed of the blob in high-density case is slower compared to the low density case. Typical radial size is 1-2 cm in HL-2A. At the vicinity of the separatrix, the total particle loss rate is estimated to be $dN/dt = 1.6\times10^{22}s^{-1}$. The number of particles in one blob is estimated as, $Nb \sim nb\pi rb^2L = 6.6\times10^{16}$, using the blob density $n_b \sim 2.5\times10^{12}$ cm^{-3}, connection length L=21 m and the blob size $\delta r = 2.0$ cm. Therefore, the blob generation rate is estimated to be $F_b = (dN/dt)/Nb \sim 2.4\times10^5 s^{-1}$. If the poloidal length of the blob-generation region is assumed to be a quarter of circumference at the separatrix, i.e. $l \approx 60cm$, the effective blob rate (f_b) produced by plasma turbulence is

estimated to be $f_b = F_b \times (\delta r/l) = 8.0 \times 10^3 s^{-1}$. This frequency is the range of drift wave frequency, suggesting that the drift wave to be a possible candidate mechanism for blob ion. The radial profiles of poloidal velocities of plasma blobs (V_θ) are measured from a time delay between the probes, as plotted in Fig.10(c). The E×B drift velocity is estimated with $V_{E\times B}=(-\nabla_r V_p)/B_t$, and the diamagnetic drift velocity (V_{de}) is estimated from plasma parameters. In the SOL, the poloidal velocity is 0.7-2.0 km/s along the ion–diamagnetic drift direction. However, the turbulence structures inside the LCFS may have larger velocity and propagate in the electron–diamagnetic drift direction. The change of the propagation direction across the separatrix implies the different characteristics of turbulence, which is correlated with the magnetic field line transition from close to open one. This result suggests that the poloidal movement of blobs is dominated by the E×B drift.

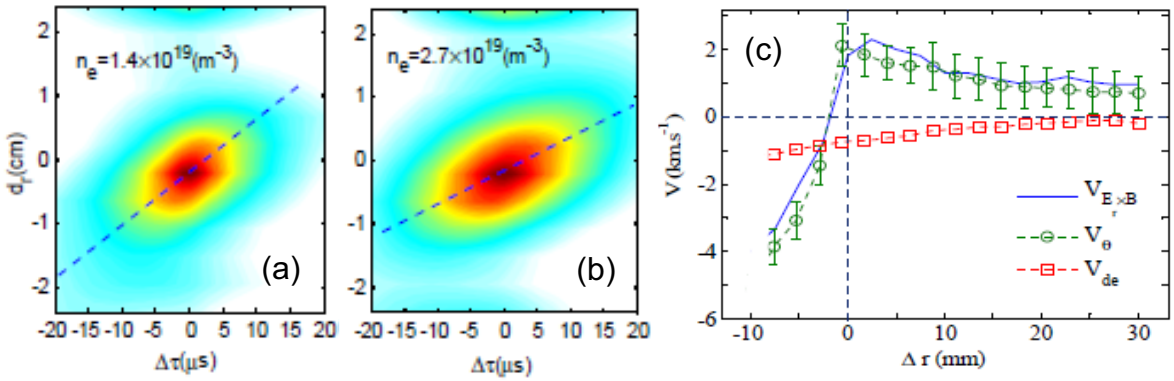

Fig.10 (a) Blob size at ne=1.4x10^{13}cm^{-3}, (b) blob size at ne=2.7x10^{13}cm^{-3} and (c) poloidal rotation of blob (measurements: open circles, calculation by ExB force and calculation diamagnetic drift)

In QUEST, the blob-like structures with intermittent and frequent bursts are simultaneously observed using the combination of Langmuir probe and a fast camera in the edge plasma. The features and the radial motion of the observed blob-like structures are studied. The framing rate of the high speed camera is typically set at three operation modes, i.e., 40,000 FPS (frames per second) with 192 × 144 pixels, 20,000 FPS with 288 × 240 pixels and 10,000 FPS with 320 × 240 pixels. For comparing the blob-like events with the probe, the maximum framing rate of 40,000 FPS with 192 × 144 pixels is selected in the experiment with viewing area of half plasma space. Although no filter is used in the measurement, the observed visible image seems to be attributed to Hα emission. The Langmuir probe array consists of five tungsten pins, which have a diameter of 1 mm and length of 1 mm, being separated

by ~ 7 mm in toroidal and poloidal directions. The pin interval is radially separated by ~ 5 mm. Two methods are applied to measure the probe signals with sampling rate of 1 MHz. The distance between the probe head and the first wall is about 25 cm.

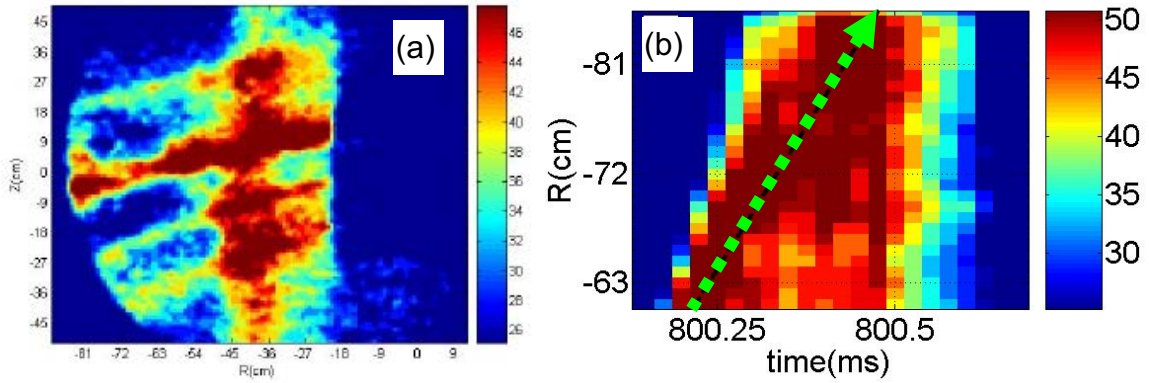

Fig.11 (a) High-speed camera image in QUEST and (b) radial propagation of blob-like event.

Figure 11(a) shows the light intensity distribution measured by the fast camera through the midplane. Each blob-like structure clearly moves along a magnetic field line. Typical frequency of the intermittent blob-like structures ranges in 0.7-4 kHz with central value of 1.4 kHz. The propagation of the blob-like structure is also shown in Fig.11(b). From the figure the velocity of the blob-like events is evaluated as 0.9 km/s. When the velocity of the blob-like events is compared with that measured at different radial positions, one can understand that the blob-like events is accelerated along a path. The average radial velocity of the blob-like events is about 1 km/s at the probe position. The radial velocity of blob-like structures is smaller than 1 km/s in the region near the plasma source, and it is larger than 1 km/s in the region near the first wall. Typical electron density and temperature of bulk plasma are $n_e = 6 \times 10^{10}$ cm^{-3} and $T_e = 4.5$ eV. A radial particle flux caused by the blob-like events is estimated to be 1.2×10^{16} cm^{-2}s^{-1}, while the average particle flux is expected to be much lower.

2-5 Mode structure analysis of ELM [7,8]

The ELM bursts have been studied in HL-2A using poloidal magnetic probe array. The analysis is done with Singular Value Decomposition (SVD) method. The method can be divided into three parts of the amplitude of the magnetic probe signal during the ELM event, ie., [A] = [U] × [W] × [V]. It means [Magnetic probe data] = [Space structure] × [Singular values] × [Time series]. Here, the probe signal is resolved in eight components. The result is plotted in Figs.12 (a)-(e). The summation of the eight components analyzed with SVD method is shown in Fig.12 (e). The summation

of three components and five components are shown in Figs.12 (c) and (d), respectively. The time behaviors of the two plots are compared with ion saturation current, I_{is}, measured with electrostatic probe, as shown in Fig.12 (b). The time behavior of the three components selected from the eight components is very similar to that of I_{is}. The result is also compared with the Ha signal during the ELM event as shown in Figs. 12(f) and (g). The time behavior between two signals is considerably different.

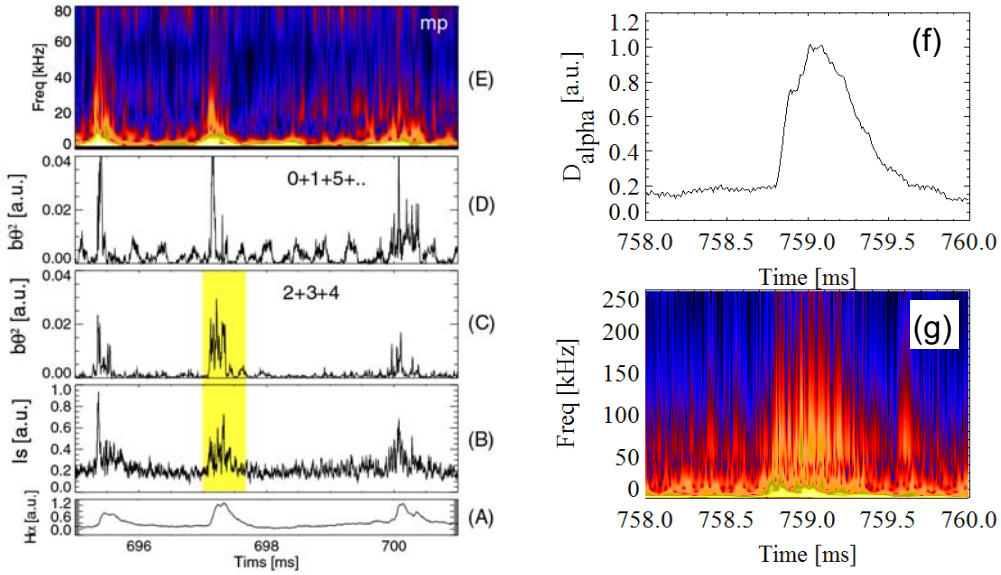

Fig.12 (a) Hα, (b) Iis, (c) 3 components from SVD analysis, (d) 5 components from SVD analysis, (e) frequency analysis of magnetic probe signal, (f) Hα during ELM and (g) frequency analysis during ELM.

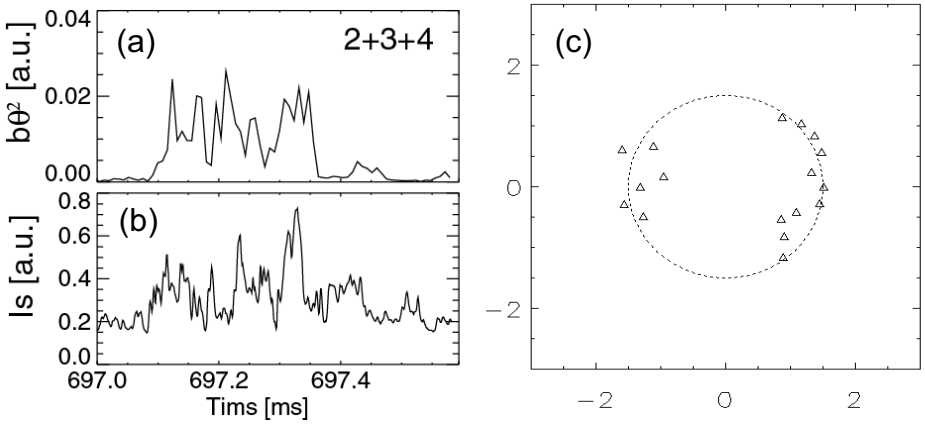

Fig.13 (a) Time behaviors of selected 3 components, (b) time behaviors of I_{is} and (c) poloidal mode number.

The summation of three components is compared with the I_{is} in detailed in Figs.13 (a) and (b). We can understand that the both signals are quite similar and it looks like

an intermittent event similar to the blob. The present analysis with the SVD method seems to be applicable to the mode analysis study of the ELM event using the magnetic probe signal. A typical result of the mode analysis on the ELM event is shown in Fig.13 (c). It indicates the presence of m=8 poloidal mode during the ELM event. At present, the toroidal mode analysis is difficult.

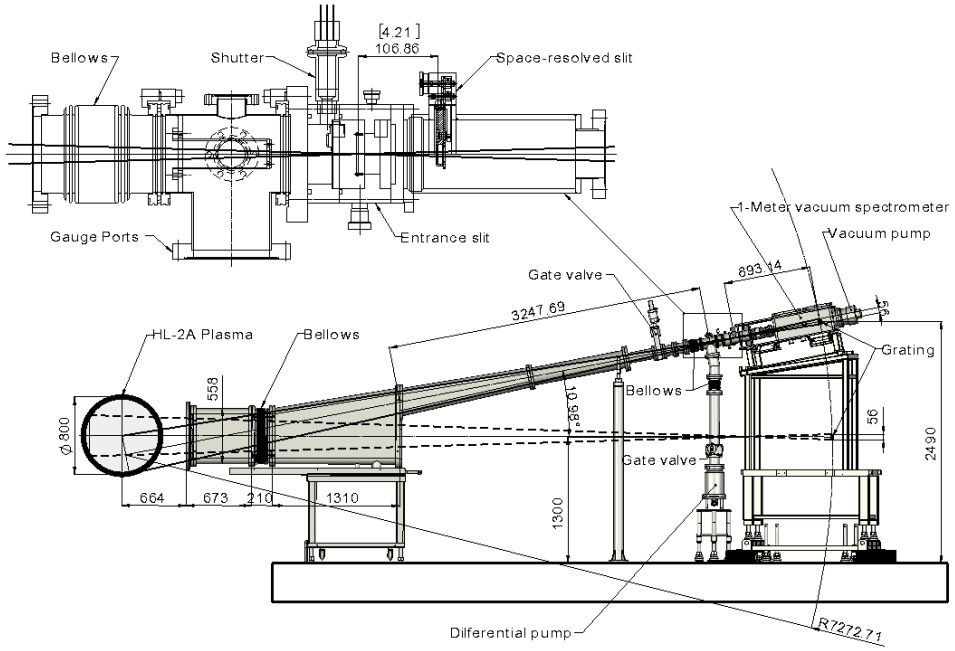

Fig.14 Space-resolved 1m normal incidence VUV spectrometer system and poloidal cross section of HL-2A plasma.

2-6 Development of space-resolved VUV spectrometer [9-15]

Space-resolved VUV spectrometer system has been developed in HL-2A to observe edge radial profiles of impurity, ion and electron temperatures and poloidal rotation velocity. A schematic view of the VUV spectrometer installed at midplane diagnostic port with aperture of 600 mm in diameter is shown in Fig.14. The 1 m normal incidence spectrometer equipped with two manually interchangeable 1200 grooves / mm gratings (800 Å blaze with Pt coating and 1500 Å blaze with Al-MgF_2 coating in rectangular size of 56 × 96 mm^2) is located at a distance of 6.3 m away from the plasma center. The sight line of the spectrometer is tilted by an angle of $\phi = 10.98^0$ vertical to the horizontal plane. A racetrack 673 mm long vacuum tube and a 210 mm long bellow flange with horizontal aperture of 100 mm and vertical aperture of 400 mm are directly connected to the diagnostic port. A further distance is added between the bellow flange and the spectrometer by a vacuum extension chamber with the length of

about 4.7 m to obtain high magnification of the CCD image and to observe at least half of the full vertical image of HL-2A plasma. The vacuum of the spectrometer is isolated from the main vacuum chamber of HL-2A tokamak by an automatically controlled vacuum gate valve placed in front of the spectrometer. The space between the gate valve and the entrance slit of the spectrometer is by a 620 l/s turbo molecular pump as differential pumping system. The spectrometer itself is evacuated by another turbo molecular pump with pumping speed of 350 l/s. The two pumping systems perform a good vacuum isolation for the spectrometer and the CCD, which can be independent on the HL-2A vacuum condition.

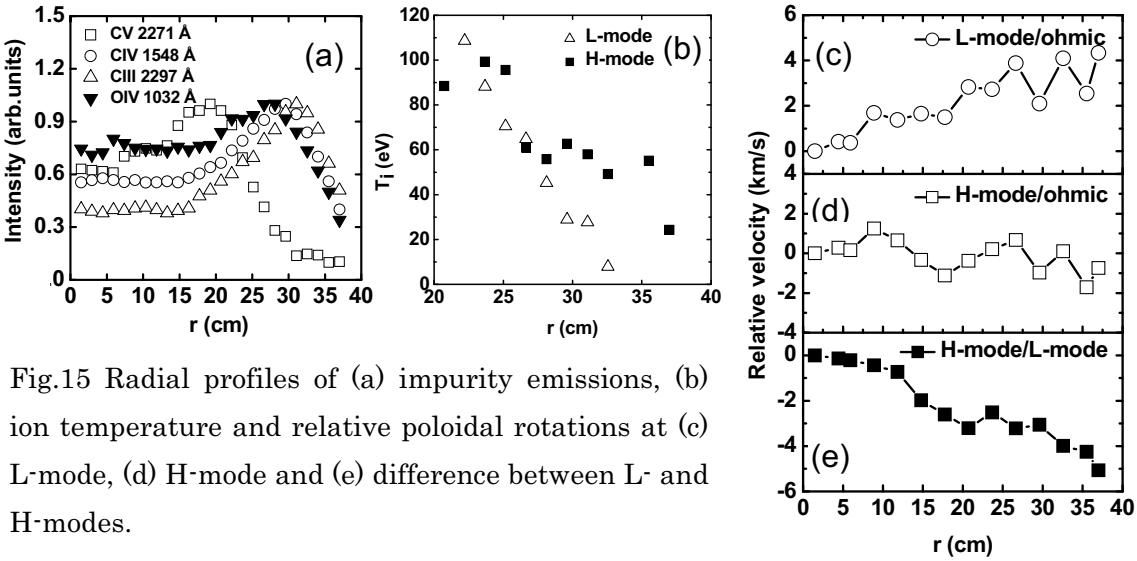

Fig.15 Radial profiles of (a) impurity emissions, (b) ion temperature and relative poloidal rotations at (c) L-mode, (d) H-mode and (e) difference between L- and H-modes.

The radial profiles of CIII (977 Å), CIV (1548 Å) and OIV (1032 Å) are compared with CV (2271 Å) in Fig. 15(a). In the figure each profile is normalized at the maximum value for the comparison, although four different discharges with similar plasma parameters are selected for the plot. Since the charge state of impurities changes according to T_e, the impurity ions having lower or higher ionization energy, E_i, exist in outer or inner region of plasmas, respectively. Therefore, the radial profiles in Fig. 15(a) indicate that the impurity ions are located in certain radial position according to the ionization energy, i.e., CV (E_i = 392 eV) at r = 20 cm, OIV (E_i = 77 eV) at r = 27 cm, CIV (E_i = 64 eV) at r = 29.5 cm and CIII (E_i = 48 eV) at r = 32 cm. Radial profiles of the ion temperature measured from CV are plotted in Fig. 15(b). The entrance slit width of 120 μm and the space–resolved slit width of 100 μm are used for the measurement. The profiles are compared between L- and H-mode discharges. In the discharge with I_p = 160 kA and B_t = 1.3 T the electron density is maintained to be $n_e = 2.0 \times 10^{13}$ cm^{-3}. The expansion of the profile during the H-mode clearly indicates the

increment of the edge ion temperature suggesting one of typical H-mode characteristics. The poloidal rotation measurement is attempted using the CV emission during the L- and H-mode phases. Identical discharges are used for the measurement. The spectral shape of CV is fitted by the Gaussian profile in order to define the profile center. The radial profile of the CV central wavelength is clearly changed in different plasma performances, such as the L-mode and H-mode. The astigmatism of the normal incidence spectrometer can also cause the shift of the CV central wavelength based on the deformation of the focal image at the CCD position. However, the deformed CV image on the CCD does not change even if the wavelength is scanned many times. The relative change of the line shift can be therefore affected by the plasma rotation after the system is fully set up. The relative change of the poloidal rotation is analyzed by comparing two profiles of the line shift between H- and L-modes. The result is shown in Figs. 12(c)-(e). The relative poloidal rotation speed increases up to 5 km/s at the plasma edge in the direction of the electron diamagnetic drift for the H-mode case. The result is in good agreement with one from other tokamak. The uncertainty in the present result is relatively large because of the low signal quality of CV. The error typically takes 40% as the maximum value. However, the significant change is clearly seen in the poloidal rotation before and after the L-H transition.

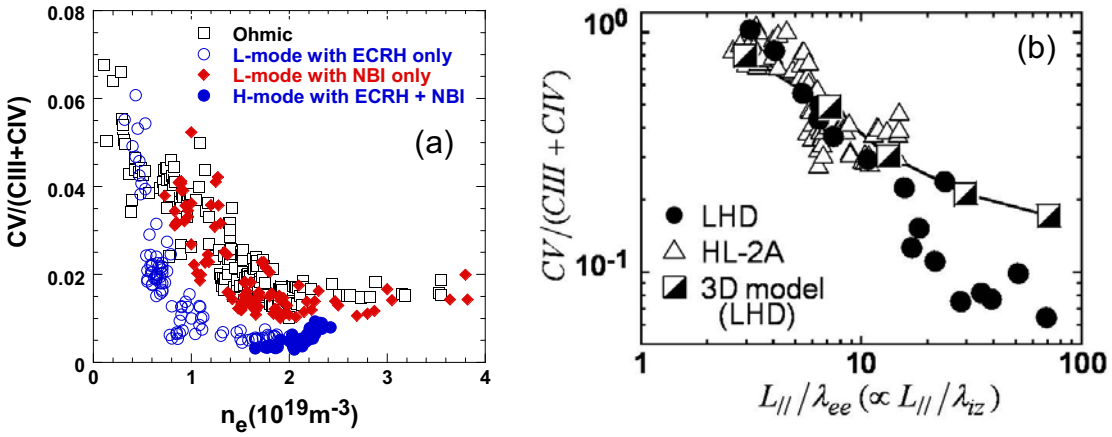

Fig.16 (a) Edge impurity screening at L- and H-modes in HL-2A and comparison of edge impurity screening between LHD and HL-2A.

The ratio of CV/(CIII+CIV) as a typical indicator of the impurity screening has been studied for the H-mode regime, which is achieved by simultaneous heating based on the ECH and NB pulses. The ratios obtained in the present study are summarized in Fig.16(a) as a function of n_e including different plasma discharge conditions, i.e., ohmic discharge, L-mode with ECH (or NBI), L-mode with ECH+NBI and H-mode with

ECH+NBI. The ohmic discharges indicate the smooth density dependence of the ratio because the reproducibility among the discharges is quite good. The impurity screening is clearly seen at $n_e < 2\times10^{19}m^{-3}$. Behaviors of the ratios in the case of L-mode with NBI are also very similar to the ohmic case. However, the ratios behave very differently when the ECH pulse is applied. The density dependence of the ratio is extremely large in ECH discharges at $n_e < 1\times10^{19}m^{-3}$ and the ratio takes very small values less than 0.005 at $n_e = 1\times10^{19}m^{-3}$. This tendency is also similar to the case of L-mode with ECH+NBI. The lowest ratio is obtained in the H-mode discharges at relatively high-density range of $1.5 \leq n_e \leq 2.5\times10^{19}m^{-3}$ suggesting a sudden change of the edge impurity transport. These experiments show that the two heating regimes seem to have significantly different effects on the edge impurity transport.

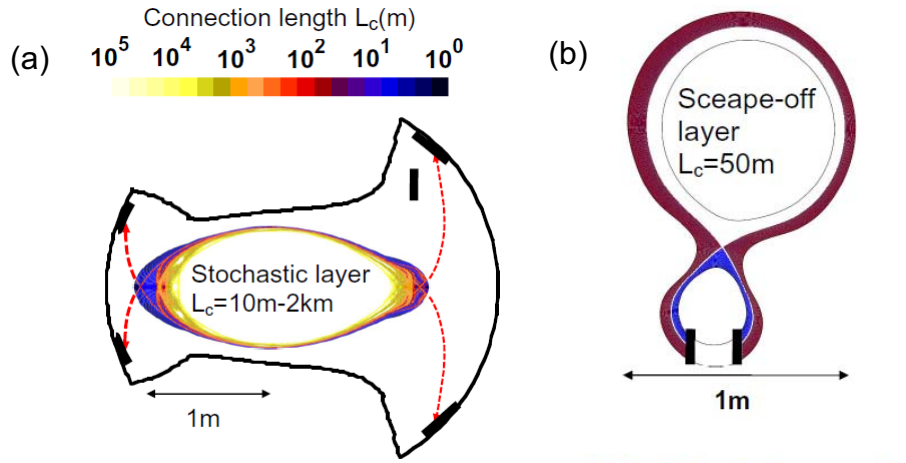

Fig.17 Magnetic field connection lengths of (a) stochastic layer in LHD and scrape-off layer in HL-2A.

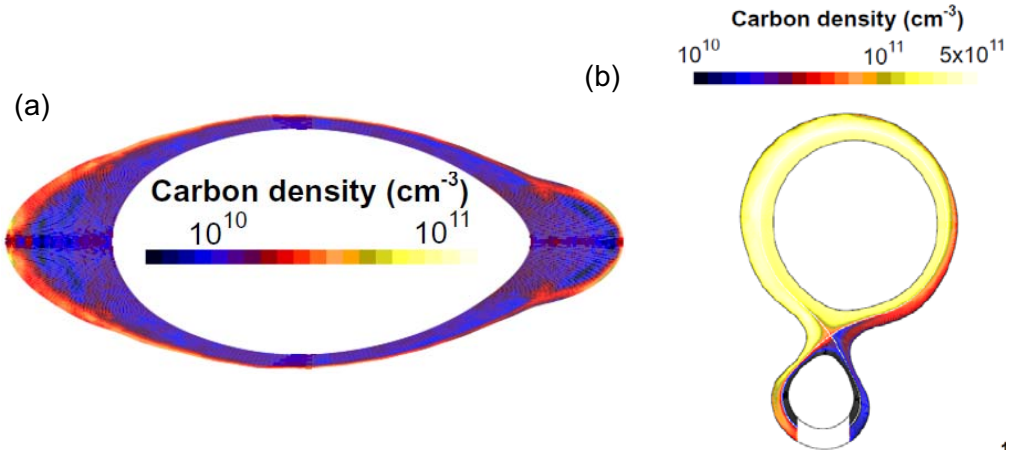

Fig.18 Carbon densities of (a) stochastic layer in LHD and scrape-off layer in HL-2A.

The ratios of CV/(CIII+CIV) from HL-2A are compared with those from LHD, as shown in Fig.16(b). A result from edge three dimensional simulation is also plotted in the figure. The horizontal axis means the collision frequency during the travel along field lines in the SOL of HL-2A and ergodic layer of LHD. The experimental result shows a good agreement with the simulation in low collision frequency range, whereas there is a clear discrepancy between them at high collision frequency range. The both results in the experiments and simulation, however, indicate the edge impurity screening can be enhanced when the collision frequency increased. The magnetic field connection length at the ergodic layer of LHD and the SOL of HL-2A is shown in Figs. 17(a) and (b), respectively. It is clear that the connection length in the ergodic layer of LHD has much longer that in the SOL of HL-2A. It should be noticed that the connection length of HL-2A is relatively long only in the private region near the X-point. The carbon density is calculated with the simulation code. The results are shown in Fig.18. In LHD the carbon density of the ergodic layer is small due to the enhanced impurity screening based on the long connection length (see Fig.18(a)). In HL-2A, on the contrary, the carbon impurity density in the SOL is considerably high except for the private region. The short connection length of the SOL makes high ion temperature gradient along the magnetic filed line. The higher gradient of the ion temperature can increase the upstream flow of the impurity. However, the long connection length makes large density gradient along the magnetic field. The large density gradient can increase the downstream flow of the impurity, which means the impurity screening.

2-7 Others

Z_{eff} profile measurement has been done in LHD as a part of the CUP collaboration [16-21]. It is found that the Z_{eff} profiles are radially flat in most of the LHD discharges, indicating a spatially constant partial impurity pressure. A space-resolved EUV spectrometer has been also studied in LHD to observe the impurity profile at plasma core in addition to plasma edge [12]. The edge impurity radial transport, in particular in the ergodic layer, is examined using the impurity profiles. It is certificated that the diffusion coefficient is enhanced in the ergodic layer due to the stochastic magnetic filed structure [22-23]. Non-inductive lower hybrid current drive (LHCD) plasmas have been studied in TRIAM-1M and HT-7 superconducting tokamaks [24]. In TRIAM-1M tokamak the plasma current is directly controlled by lower hybrid wave, but in HT-7 tokamak the plasma current is controlled with ohmic heating. The result shows that both methods are all feasible in steady-state plasma operation. The current startup has

been also studied in QUEST tokamak using non-thermal electrons produced by ECH [25]. A smooth startup achieved in the QUEST can lead to a constant non-inductive discharge operation with 100kA plasma current. The cross-field transport at plasma edge is studied in JT-60U tokamak based on B2.5 Eirene edge plasma simulation code [26]. The profiles of anomalous particle transport coefficient D, anomalous electron and ion heat transport coefficients, χ_e and χ_i, have been obtained by modeling the plasma experiments and fitting the experimental data from L-mode and H-mode in JT-60U tokamak with NBI and ohmic heating. ICRF (ion cyclotron resonance frequency) wall conditioning has been studied in EAST superconducting tokamak, including ICRF cleaning in-between shots, boronization associated with ICRF plasmas and ICRF oxidation with an ITER-relevant full metallic wall material [27]. The LHCD and ion Bernstein wave (IBW) heating have been significantly studied in HT-7 tokamak [28]. A long pulse discharge up to 400 s is obtained with LHCD when high power lower hybrid wave (P_{LHW}=800 kW at 2.45 GHz) is launched. The current drive efficiency is studied at different P_{LHW}. The vibrational distributions of hydrogen and deuterium molecules in low temperatures are studied based on the quasi-steady state and quasi-stationary approximation [29, 30] Newest cross section data in the literature are applied while the unavailable data are calculated by applying Gryzinski-method. The modeling shows that the initial absolute slopes of the vibrational distribution curves are increasing functions of the electron temperature when the electron temperature is less than 10 eV. However, this dependence can not be verified by the experiment performed in MAP-II linear plasma device.

3. Summary

Many fruitful results were published through the CUP collaboration in the 11B category during past five years. Those are, of course, obtained from all the fusion devices in Japan and China. A lot of papers were also published to Journal of Plasma Science and Technology (PST) in the seminars held at Lijiang and Guilin in China, although we could not introduce them at all in the present report due to the page limitation. The paper publication in PST was really effective to know what we did in detail in the 11B category.

This is a final scientific report on the 11B category in the CUP collaboration. However, some of the collaborations are being still progressed at present. In addition, new plans are also proposed for the future collaboration between Japan and China. Further progress on the CUP collaboration is undoubtedly promising. We strongly believe that the activity in the 11B category of the CUP collaboration during the past five years could contribute to not only the scientific collaboration but also the friendship between Japan and China. Finally, we have to say, we wish further productive and interesting results will be also obtained in the future collaboration.

Acknowledgements

We also wish to express our great acknowledgements to all the collaborators for their sincere efforts, who joined in the 11B category collaboration including the seminars. This work has been partially supported by the National Natural Science Foundation of China under No. 10975048 and by the JSPS-CAS Core University Program in the Field of Plasma and

References

[1] M.Isobe, Y.Liu, J.W.Yang, W.Chen et al., Chin.Phys.Lett. **26** (2009) 105201.
[2] M.Isobe, Y.Liu et al., to be published in PFR.
[3] W.Chen, X.T.Ding, Y.Liu, M.Isobe, et al. Nucl.Fusion **50** (2010) 084008.
[5] K.Ogawa, et al., scientific report in the CUP collaboration, 2010.
[5] X.Q.Xi, J.Y.Zhao, S.Kado, X.Gao et al., submitted to PST
[6] L.W.Yan et al., scientific report in the CUP collaboration, 2010.
[7] S.Ohdachi, Y.Liu et al., presented in International Toki Conf. March 2010.
[8] .F.Ming, S.Ohdachi, Y.suzuki, submitted to PFR.
[9] Z.Y.Cui, P.Sun, J.Dong, S.Morita et al., PST, **10** (2008) 298.
[10] Z.Y.Cui, S.Morita, B.Z.Fu, Y.Huang, P.Sun, et al., RSI, **81** (2010) 043503.
[11] Z.Y.Cui, S.Morita, Y.D.Gao, P.Sun et al., 37th EPS Conf. Dublin, 2010, P2.124.
[12] C.F.Dong, S.Morita, et al., RSI, **81** (2010) 033107.
[13] M.Kobayashi, S.Morita, Z.Y.Cui et al., 23rd IAEA, Korea, 2010, EXD/6-5Ra.
[14] M.Kobayashi, S.Morita, Z.Y.Cui et al., submitted to Nucl.Fusion.
[15] S.Morita, C.F.Dong, M.Kobayashi, Z.Y.Cui, X.Gao et al., PFR, **5** (2010) S2004.
[16] H.Y.Zhou, S.Morita, et al., RSI, **79** (2008) 10F536.
[17] H.Y.Zhou, S.Morita, et al., PFR, **5** (2010) S1021.
[18] H.Y.Zhou, S.Morita, et al., JAP, **107** (2010) 053306.
[19] H.Y.Zhou, S.Morita, et al., RSI, **81** (2010) 10D706.
[20] H.Y.Zhou, S.Morita, et al., JJAP, **49** (2010) 106103.
[21] S.Morita, M.Goto, Z.Y.Cui, C.F.Dong, X.Gao, L.W.Yan, H.Y.Zhou et al., presented in 11th APPC, Shanghai, 2010.
[22] C.F.Dong, S.Morita, et al., to be published in PFR.
[23] C.F.Dong, S.Morita, et al., to be published in PST.
[24] H.D.Xu, K.Hanada, M.Hasegawa, M.Wang et al., Fusion Eng. Des. **83** (2008) 211.
[25] X.Gao et al., Scientific report in the CUP collaboration, 2010.
[26] Y.P.Chen, H.Kawashima, X.Gao, N.Asakura, et al., J.Nucl.Mater. **390** (2009) 452.
[27] X.Gao, J.S.Hu, Y.P.Zhao, S.Morita et al., J.Nucl.Mater. **390** (2009) 864.
[28] X.Gao, Y.P.Zhao, K.Toi, S.Morita et al., Plasma Sci. Tech. **11** (2009) 381.
[29] B.J.Xiao, S.Kado et al., J.Nucl.Mater. **337-339** (2005) 1082.
[30] B.J.Xiao, S.Kado, M.He, J.Plasma Fus. Res. SERIES, **7** (2006) 59.

Recent results on EAST

X.Gao and EAST Team

Institute of Plasma Physics, Chinese Academy of Sciences,

P.O.Box 1126, Hefei, Anhui 230031, China

e-mail: xgao@ipp.ac.cn

Abstract

The significant progress has been achieved on EAST since the 23rd IAEA Fusion Energy Conference in 2010. The ELMy H mode plasma has been achieved by LHCD and ICRF heating on EAST. The ICRF power is 0.5-0.7 MW at 27 MHz, and LHCD power is 0.5-1 MW at 2.45 GHz. The toroidal field is 1.8-2 T, and the plasma current is 0.6-0.8 MA. Lithium wall condition was performed for H mode experiment. The ratio of H/(H+D) is about 5-7% after wall condition. By means of Lithium dropping technology in current ramp up phase, an ELMy H mode was obtained with lower threshold power of 1 MW by LHCD on EAST.

Discharge with a plasma current of 1 MA was realized on EAST in 2010. The key issues to achieve the discharge with 1 MA plasma current include both early shaping and LHCD assistance during start-up phase to extend the voltage margin of poloidal field (PF) coils for easier plasma control, an optimization of the control methodology for PF coils to avoid over-current fault and a very good wall condition.

Towards steady state operation and relative PSI issue study, long pulse diverted plasma discharges (up to 100 s) were also obtained by LHCD on EAST recently.

Keywords: EAST tokamak, H mode plasma, 1 MA plasma current, long pulse

1. Introduction

One of the basic requirements for future fusion reactors is steady-state operation [1]. The Experimental Advanced Superconducting Tokamak (EAST) is a non-circular advanced steady-state experimental device. It was built at the Institute of Plasma Physics (ASIPP), Chinese Academy of Sciences, beginning in 1998. The first plasma discharge was achieved successfully in EAST in 2006 [2-5]. The scientific mission of the EAST project is to study the physical issues involved in steady-state advanced tokamak devices. The engineering mission of the EAST project is to establish the technology basis of fully superconducting tokamaks in support of future reactors. The use of full superconducting poloidal field coils on EAST is the first trial in the world for the International Thermonuclear Experimental Reactor (ITER).

The significant progress has been achieved on EAST in 2010. Technique achievement has been made related to experimental investigation on plasma control for plasma breakdown and startup within the safe margin of the full superconducting magnets. Repeatable plasma breakdown and perfect plasma current startup have been performed with higher initial active currents. High frequency glow discharge can be employed to guarantee repeatable plasma breakdown. Low loop voltage breakdown with aid of LHW has been fulfilled successfully, which is necessary for future large size tokamak. Control of the shaping rate of LCFS in non-circular configuration has been successfully performed in the plasma startup stage. Also with the aid of LHW, control of LCFS in non-circular configuration has been gained perfectly. Progress has been made to optimize the divertor configuration, especially, the control of X points, based on study of the control strategy. All of these successful experiments should lay a solid foundation for high parameters plasma experiments within the safe margin of the full superconducting magnets. The impurities and hydrogen content could be continuously lowered due to the accumulation of lithium in the vacuum vessel of EAST by using lithium conditioning. Great progress has been made based on the above studies and well plasma wall conditioning.

The ELMy H mode plasma was achieved by LHCD and ICRF heating on EAST. Discharge with a plasma current of 1 MA was realized on EAST in 2010. Long

pulse diverted plasma discharges (up to 100 s) were also obtained by LHCD on EAST recently.

2. Experimental setup

The EAST device, formerly known as HT-7U, is the first full superconducting tokamak with advanced configuration. The design parameters of EAST are major radius R=1.75 m, minor radius a=0.45 m, toroidal field BT =3.5 T, plasma current Ip =1 MA [6].

It is equipped with twelve independently powered poloidal field coils and a pair of water-cooled fast-response copper coils (IC1 and IC2) inside the vacuum vessel. Both IC1 and IC2 in an anti-parallel connection are driven by a fast-response power supply and used to stabilize vertical displacement instability for highly elongated plasma. Flexible configurations with an elongation k from 1 to 1.9 and a triangularity δ of up to 0.65 in double-null or single-null plasma can be easily obtained by the PF system. The D-shape vacuum vessel is of a continuously welded structure with low toroidal resistance. Inside the vacuum vessel plasma facing components (PFCs) and supporting structures, several sets of magnetic probes and flux loops for device-operation and plasma control, divertor cryopump, baking system and thermal coupler, etc are integrated.

Both lower hybrid current drive (LHCD) system of 2 MW and ion cyclotron resonant heating (ICRH) system of 6 MW were applied routinely for current drive and heating. About forty diagnostics were used for physics study [7].

3. Experimental results

The first H-mode plasma was achieved by LHW alone on November 7, with the plasma current, Ip = 0.6 MA, line averaged density, <ne> = 2xE19 m-3, and toroidal magnetic field, BT = 1.35 T. The LHCD power of 1 MW (source power) was applied in EAST, producing the ELM-free H-mode plasma. The transition of H-mode to L-mode was mainly due to increased radiation and LHW reflection during the H-mode phase. Further efforts were made to reduce the radiation and improve the

performance of the target plasma, including intensive lithium evaporation, suppressing run-away electrons during plasma current ramp-up and early shaping of the plasma into divertor configuration to reduce plasma radiation, localized gas puffing at the LH launcher to improve LHW coupling, high field side gas fuelling, etc. These reduced the L-H transition power threshold, allowing to achieve reproducible ELMy H-mode plasmas with LHW alone. ELMy H-modes have also successfully been achieved with the combination of LHW and ICRF heating. Stationary H-mode plasmas have been achieved on EAST during the present H-mode campaign by either LHW alone or combination of ICRF and LHW.

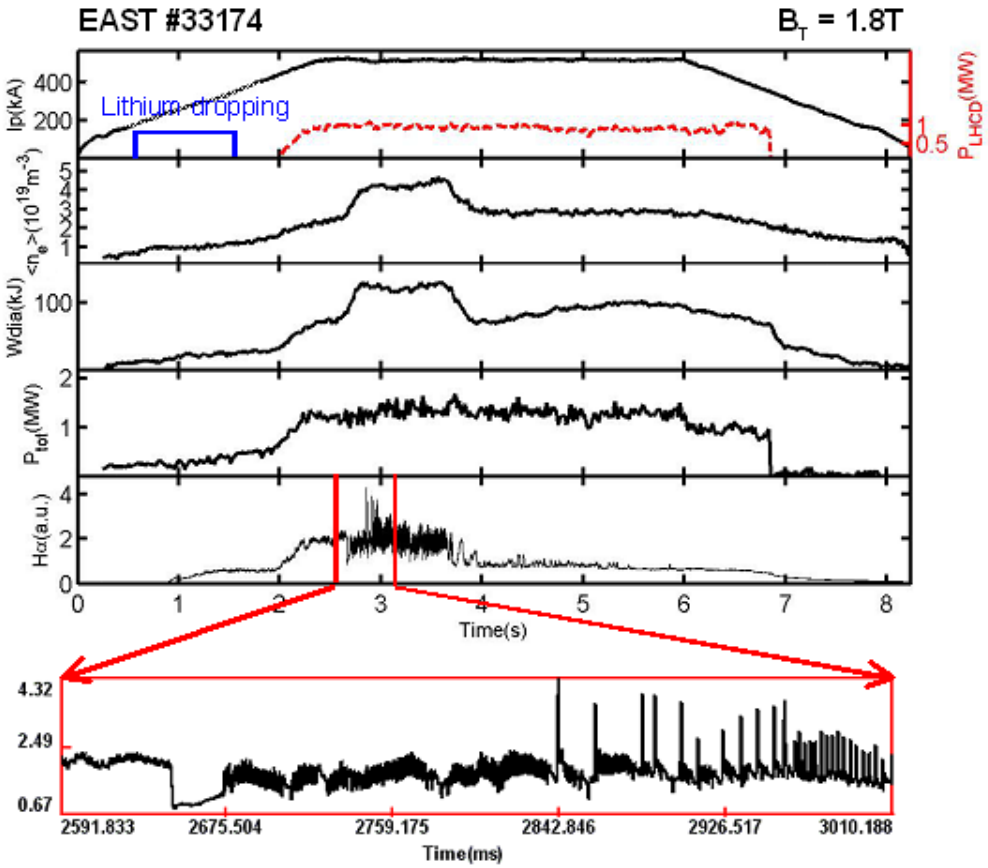

Fig.1 A typical ELMy H mode by LHCD on EAST

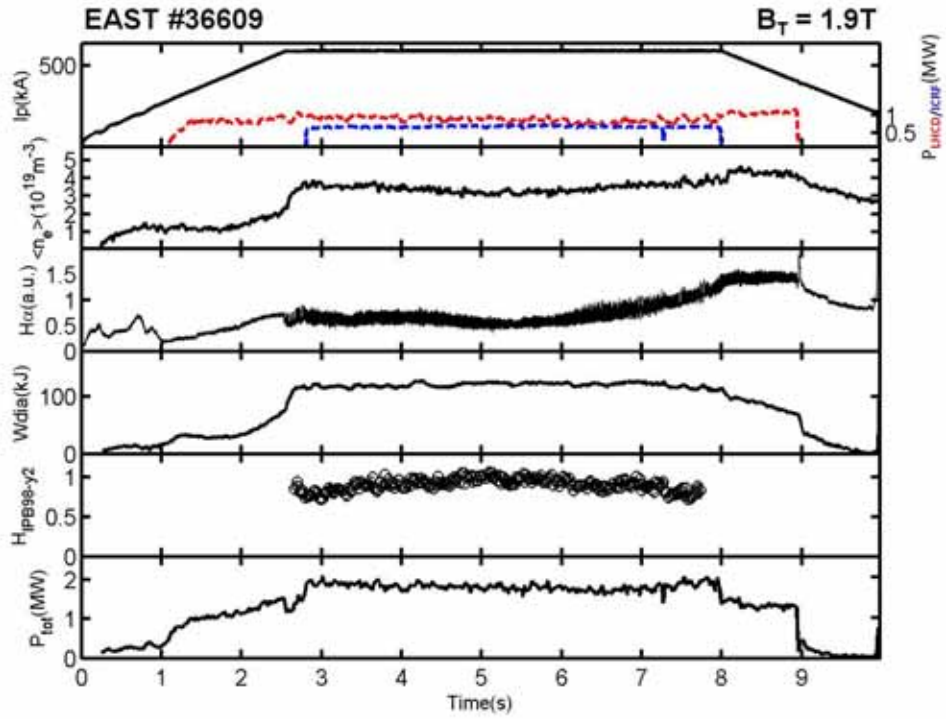

Fig.2 Stationary H mode plasma produced by LHCD and ICRF heating on EAST

Fig.1 shows a discharge of ELMy H mode by LHCD on EAST tokamak. Fig.2 shows the stationary H mode plasma produced by LHCD and ICRF heating. The ELMy H mode plasma has been achieved by LHCD and ICRF heating on EAST. The ICRF power is 0.5-0.7 MW at 27 MHz, and LHCD power is 0.5-1 MW at 2.45 GHz. The toroidal field is 1.8-2 T, and the plasma current is 0.6-0.8 MA. Lithium wall condition was performed for H mode experiment. The ratio of H/(H+D) is about 5-7% after wall condition.

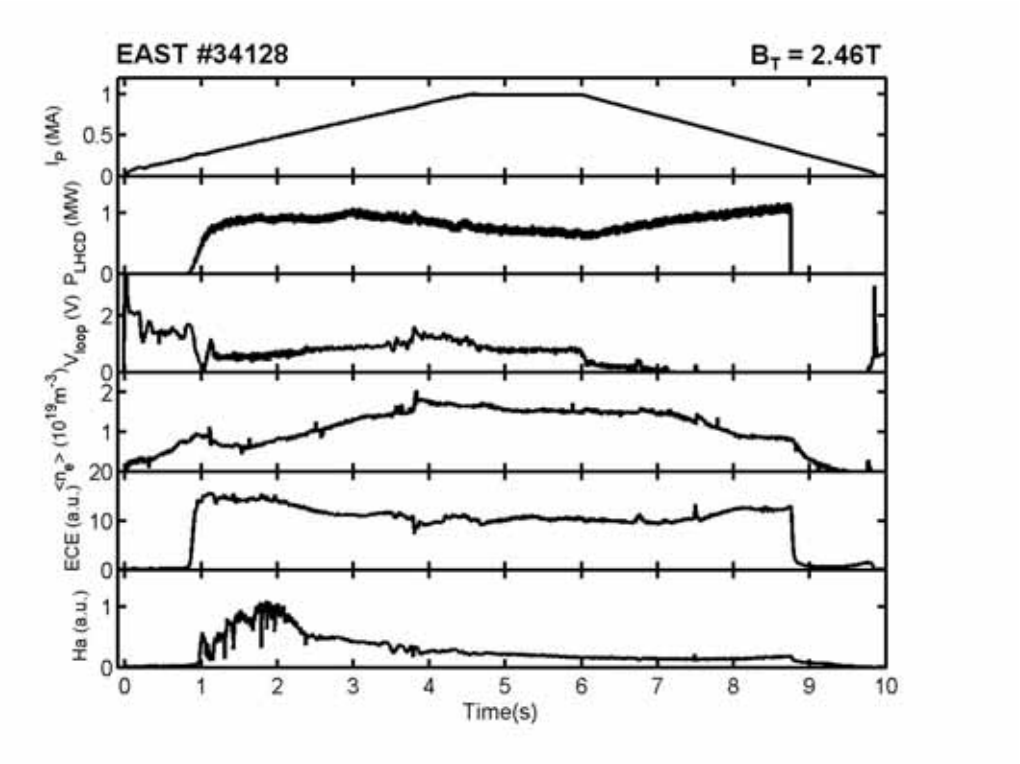

Fig.3 Discharge with a plasma current of 1 MA on EAST

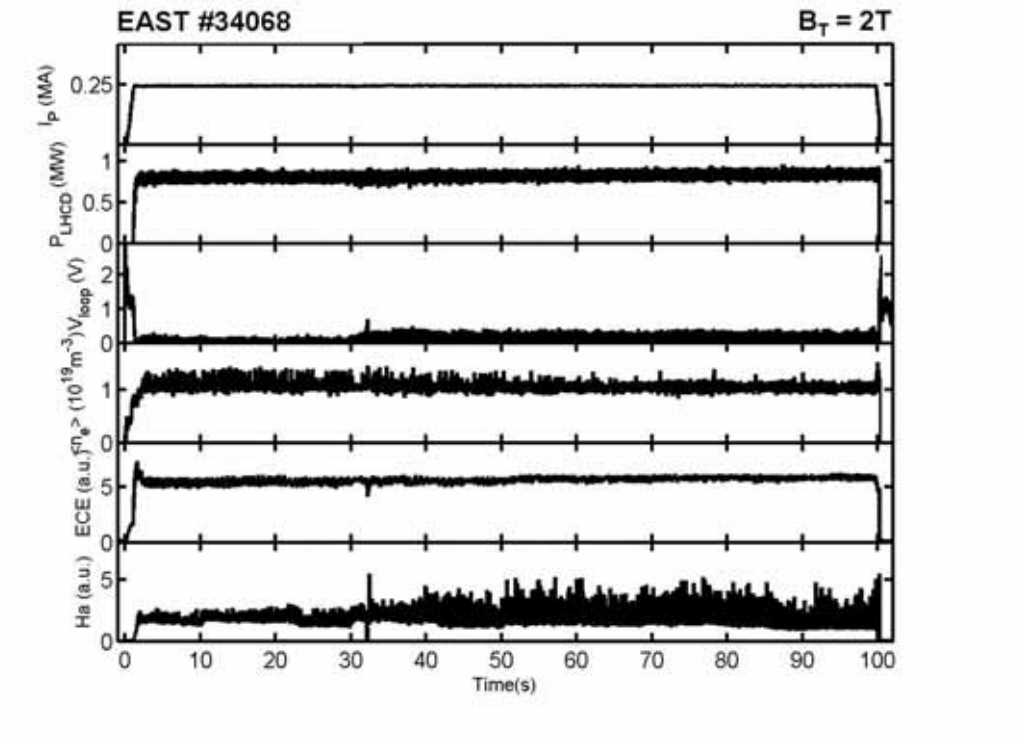

Fig.4 Long pulse plasma (t > 100 s) which is obtained and sustained by LHCD on EAST

Discharge with a plasma current of 1 MA was realized on EAST in 2010 [6]. The key issues to achieve the discharge with 1 MA plasma current include both early shaping and LHCD assistance during start-up phase to extend the voltage margin of poloidal field (PF) coils for easier plasma control, an optimization of the control methodology for PF coils to avoid over-current fault and a very good wall condition. Towards steady state operation and relative PSI issue study, long pulse diverted plasma discharges (up to 100 s) were also obtained by LHCD on EAST recently. Fig.3 shows the discharge with 1 MA plasma current on EAST. Fig.4 shows long pulse plasma ($t > 100$ s) which is obtained and sustained by LHCD on EAST.

4. Summary

The significant progress has been achieved on EAST in 2010. The ELMy H mode plasma was achieved by LHCD and ICRF heating on EAST. Discharge with a plasma current of 1 MA was realized on EAST. Long pulse diverted plasma discharges (up to 100 s) were also obtained by LHCD on EAST recently.

5. Acknowledgements

Thanks to international collaborators from USA (GA, PPPL, MIT, FRC), France (CEA), Japan (NIFS, JAEA), Korea (NFRI), Germany (IPP). This paper has been supported by National Magnetic Confinement Fusion Science Program (Code number 2010GB106000, and 2010GB106001). This work was partially supported by the JSPS-CAS Core-University program in the field of ‘Plasma and Nuclear Fusion’.

References

[1] Y.X.Wan et al., “Overview of steady state operation of HT-7 and present status of the HT-7U project”, Nuclear Fusion, Vol.40, 2000 (1057).

[2] Y.X.Wan et al., 2006, "Overview progress and future plan of EAST Project". Presented at the Proc. of the 21st Int. Conf. on Fusion Energy (Chengdu, China, Oct., 2006) International Atomic Energy Agency, Vienna. CD-ROM file OV/1-1.

[3] X.Gao et al., “Diagnostics for first plasma study on EAST tokamak”, Phys. Lett. A, Vol.372, 2008 (2286).

[4] J.G.Li et al., 2010, "Wall conditioning towards the utilization in ITER". Presented at the 19th Plasma Surface Interaction (PSI) Conference (San Diego, USA, May 24, 2010) R-3.

[5] B.N.Wan et al., 2010, "Recent progress in high power heating and long pulse experiments on EAST". Presented at the 23rd IAEA Fusion Energy Conference (Daejeon, Korea, October 11, 2010) International Atomic Energy Agency, Vienna. OV1-2.

[6] J.P.Qian et al., “Operation with 1 MA Plasma Current in EAST”, Plasma Science and Technology, Vol.13, 2011 (1).

[7] L.Q.Hu et al., “Present Status of the EAST Diagnostics”, Plasma Science and Technology, Vol.13, 2011 (125).

The JT-60SA project and its plasma regimes

S. Ide[1] and the JT-60SA team

[1]*JT-60SA JA-Home Team, 801-1 Mukoyama, Naka, Ibaraki, 311-0193 Japan*

1. Introduction

The JT-60SA project has been pursued under the Broader Approach Satellite Tokamak Programme jointly implemented by Europe and Japan, and under the Japanese national program. The objective of the project is to support researches on ITER and develop physics and engineering basis towards DEMO reactor. Towards realization of a steady-state tokamak DEMO reactor, establishing a plasma operational scenario of high normalized beta (β_N) and high bootstrap current fraction (f_{BS}) is indispensable. This is one of the major objectives of the JT-60SA project. For understanding of plasma physics in DEMO relevant regimes, operation at the higher plasma current is also important. Towards these issues, several operational domains are considered in JT-60SA. The plasma current (I_p) up to 5.5 MA is expected both in a double null and a single null configurations. The high β_N operation is expected at I_p of above 2 MA. An important feature of the JT-60SA device is its flexible heating and current derive system inherited from JT-60U. Especially, the tangential N-NB (Negative-ion based Neutral Beam) system as a strong current driver. In this paper, brief over view of plasma variation in JT-60SA and what freedom, especially in terms of the current profile, can be expected are presented.

2. Tokamak and heating and current drive systems

JT-60SA (Super Advanced) is a superconducting tokamak updated from JT-60U [1]. Both 18 toroidal field coils, 4 central solenoid modules and 6 poloidal field coils are superconducting coils and newly designed. The maximum toroidal field at the plasma center of a typical equilibrium is about 2.3 T. Also the vacuum vessel and the cryostat are renewed or newly installed. The major radius is about 3 m and the minor radius is about 1.2 m.

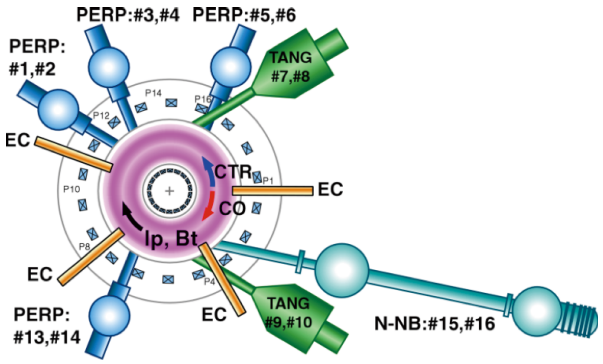

Fig.1: Schematic view of the JT-60SA heating and current drive system.

The heating and current drive system (Fig.1) is succeeded from JT-60U maintaining their large capability and flexibility in heating, current-drive, and momentum- input. The total heating power is 41 MW and consists of 34 MW of neutral particle beam (NB) injection and 7 MW of ECRF powers. The positive ion source

based neutral beams (P-NBs) at 85 keV consist of 2 units of co-tangential beams (4 MW), 2 units of counter-tangential beams (4 MW), and 8 units of near perpendicular beams (16 MW). The total power of the P-NB system is 24 MW. The negative ion source based neutral beam (N-NB) system provides 10 MW/500 keV co-tangential injection. The N-NB injection trajectory is off-axis for optimization of the weak / negative magnetic shear plasmas. The ECRF system composed of 110 GHz gyrotrons provides 7 MW and is capable of a real time control of the deposition location by steerable mirrors with high frequency modulation capability (>5 kHz).

3. Plasma configurations and tools for analysis

As mentioned, I_p up to 5.5 MA is expected. To reach this high current with keeping q_{95} > ~3, the plasma bore should be maximized even at the highest toroidal magnetic field (B_t) of ~2.2 T. Such a plasma can be obtained either in a double null or single null configuration. For ITER contribution, a plasma cross section as close as possible to that of ITER would be desired. Since the optimum aspect ratio is determined from the engineering geometry, it is around 2.5, matching to the ITER aspect ratio (3) is practically difficult. Also due to the lower divertor design which is aligned to higher triangularity (δ), the lower triangularity in JT-60SA tends to larger than that of ITER. Therefore, a configuration that has the same up and down averaged triangularity and elongation as those of ITER standard scenario is taken as an ITER-like configuration. Due to smaller cross-section, the maximum I_p for this configuration with q_{95}~3 at the maximum B_t would be ~4.6 MA. A higher β_N configuration should be cope with the high δ lower divertor. These configurations are illustrated in Fig.2. Several reference plasmas have been designed from assumed performance and conditions for each domains. That is, the confinement enhancement ($H_{98(y,2)}$), the density normalized to the Greenwald density (f_{GW}), q_{95} non-inductive current drive requirement and so on. These reference plasmas have been used for engineering design and assessment. At the same time, validation of these plasmas in view of physics is under way, with updated knowledge and codes.

In order to analyze characteristic of these plasmas, various codes are utilized. TOSCA and

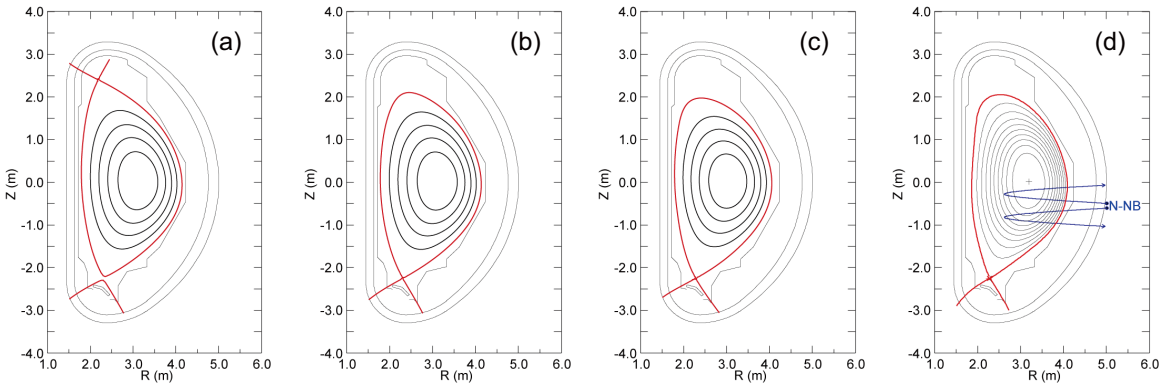

Fig.2: Typical plasma configurations. (a) Full bore double null, (b) full bore single null, (c) ITER-like and (d) high triangularity.

ACCOME[2] for solving equilibrium. ACCOME is also used to evaluate current profiles, ohmic, bootstrap, NB and EC driven currents. TOPICS[3] is used for transport analysis. And MARG2D[4] is used for ideal MHD stability in both the core and the pedestal regions. SONIC[5] is used to evaluate the divertor heat and particle handling capability. These codes have been developed at JAEA.

4. Plasmas in high β_N domain

As mentioned a reference scenario for the high β_N domain was designed from assumed performance and conditions. Full non-inductive current drive capability is also added towards steady-state DEMO. A reference plasma in this domain is shown in Fig.3, I_p=2.3 MA at B_t=1.7 T. In Fig.3 (a) plotted are assumed density (n_e) and electron and ion temperature (T_e and T_i) profiles. The pedestal is defined so as to maximize the performance with constraint on the pedestal height and the width and the MHD stability. The MHD stability was confirmed by MARG2D code. The core profiles are chosen to meet f_{GW} = 0.85, $H_{98(y,2)}$ = 1.3 with the injected power of 37 MW (N-NB: 10 MW, P-NB: 20 MW and ECRF: 7 MW) and full non-inductive current drive condition (the ohmic current is zero everywhere in the plasma). The bootstrap current fraction is 68%. Fig.3 (b) shows breakdown of the total current (NBCD, Boot Strap and ECCD) and the safety factor (q). It is noted that this plasma is confirmedt to be stable by MARG2D against ideal kink-ballooning mode up to n = 4 with an ideal wall. Another evaluation at lower I_p of 2.1 MA, even higher f_{BS} of about 0.8 can be achieved with a slightly higher $H_{98(y,2)}$ of 1.4 and density f_{GW} = 1.

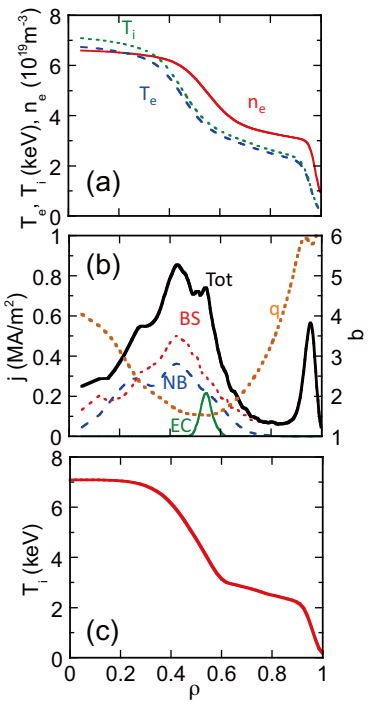

Fig.3: A reference plasma profile for high β_N full non-inductive CD. (a) Density (solid), ion (dotted) and electron (dashed) temperatures, (b) break down of driven currents and q, (c) electron temperature profile from TOPICS + CDBM simulation

Though the profiles in Fig.3 (a) are prescribed from the JT-60U experience with reasonable $H_{98(y,2)}$, it is necessary to assess confinement characteristics. For that a transport model "CDBM (Current Diffusive Ballooning Mode)"[4] model is used. The T_e profile evaluated by TOPICS + CDBM is shown in Fig.3 (c). Here, the q and n_e profiles and the pedestal T_e and T_i are prescribed from the reference. As shown in the figure, the simulation indicates better confinement that expected. The enhancement factor reached ~1.5 in the simulation. Full simulation including the evolutions of the current and the density profiles will be carried out as the next step.

As the current profile plays an important role in such a reversed shear plasma, capability of the current profile modification is one of the key issues. The JT-60SA N-NB system has two ion sources. These sources can be injected separately. In Fig.4 (a). the N-NB driven current profiles using the upper (solid line) or the lower unit (dashed line) respectively. The target plasma is similar to that shown in Fig.3 but with lower density (f_{GW} = 0.7) but higher temperature to keep near full non-inductive CD condition. Suppose that the back ground plasma does not change, resultant safety factor profiles varies largely as shown in Fig.4 (b). By modulating power of each unit, intermediate j_{BD} can be produced. Though, the background plasma should not stay unchanged in reality, the results would give an idea how widely the current (safety factor) profile can be modified. It should be noted that with higher confinement ($H_{98(y,2)}$~1.5), f_{BS} ~ 0.7-0.8 in these cases. Even though, small fraction of NBCD can give these changes.

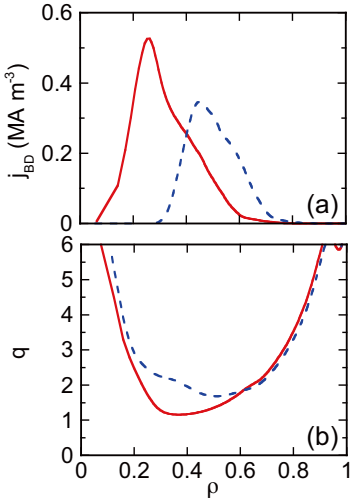

Fig.4: (a) N-NB driven current profile, upper beam line (solid), lower one (dashed), and (b) resultant q profiles.

5. Handling of heat and particle by divertor

Demonstration of high heat and particle fluxes with maintaining high core performance is one of the most important missions of JT-60SA. JT-60SA is equipped with an ITER-like lower divertor, W-shaped with a V-corner. The divertor target consists of the CFC monoblock. The divertor performance was evaluated by SONIC. The results indicate that the peak heat flux (q_{peak}) is suppressed within the monoblock capability (nominally 15 MW/m^2, desirably 10 MW/m^2) by gas puffing for a 5.5 MA plasma of f_{GW} = 0.8 even with 41 MW injection. Increasing the separatrix density (n_e^{sep}) enhances radiation to reduce q_{peak}. On the other hand, as the absolute density at the separatrix is smaller for a lower I_p plasma such as high β_N plasmas, it would be difficult to reduce the q_{peak} only by gas puffing for such a plasma. SONIC results also indicate that n_e^{sep} to keep q_{peak}

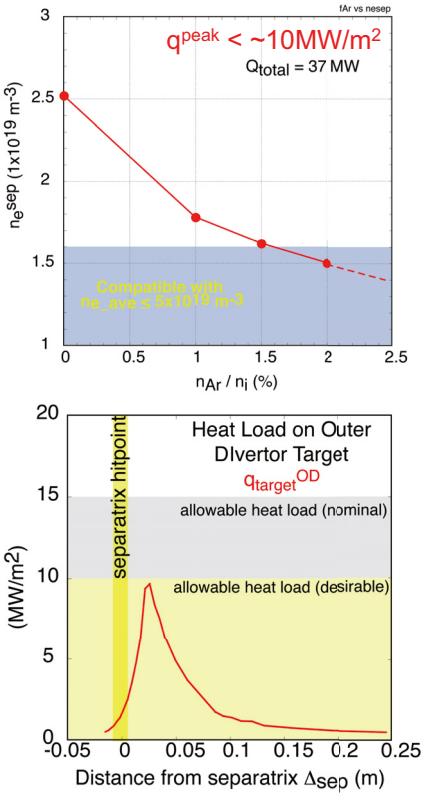

Fig.5: (a) N-NB driven current profile, upper beam line (solid), lower one (dashed), and (b) resultant q profiles.

$\leq$ ~10 MW/m^2 decreases as more Ar seeded at the divertor (Fig.5) and can be low enough to be compatible with a 2.3 MA plasma.

6. Summary

Assessment of plasmas foreseen in JT-60SA is in progress. Various codes, such as TOSCA, ACCOME, TOPICS, MARG2D and SONIC, are used for the assessment. Based on a modeled and MHD stable pedestal, high β_N full-CD plasma capabilities have been evaluated. It is shown that a 2.3 MA plasma with prescribed profiles can reach $\beta_N = 4.3$ and $f_{BS} = 0.68$ with a full-CD condition and is stable against ideal kink-ballooning up to $n = 4$ with an ideal wall. A predictive modeling with TOPICS using the CDBM transport model indicates that this plasma can have better confinement of $H_{98(y,2)} = 1.5$ than assumed to evaluate the above performance. It was shown that by combining two N-NB units, the q profile in such a high β_N plasma can be modified largely. The divertor modeling code, SONIC, showed that even with a lower absolute density in these high β_N plasmas the peak heat load to the divertor can be suppressed within the monoblock capability by impurity seeding.

Reference

[1] S. Ishida et al., in press, Fusion Eng. and Design.

[2] K. Tani and M. Azumi, 1992 J. Comp. Phys **98** 332 (1992).

[3] H. Shirai, et. al., Plasma Phys. Control. Fusion **42** 1193 (2000).

[4] S. Tokuda and T. Watanabe, Phys. Plasmas **6**, 3012 (1999).

[5] K. Shimizu, et. al., J. of Nucl. Mater. **363–365** 426 (2007).

[6] A. Fukuyama, et. al., Plasma Phys. Control. Fusion **37** 611 (1995).

Overall activities on plasma wall interactions (12A) since 2006 and collaboration researches conducted at Hokkaido University

T. Hino[1*], N. Ashikawa[2] and N. Noda[2]

[1]Laboratory of Plasma Physics and Engineering, Hokkaido University, Sapporo, Japan

[2]National Institute for Fusion Science, Oroshi-cho, Toki, Gifu, Japan

1. Introduction

Japan and China have aggressively and continuously carried our numerous researches on plasma wall interactions in order to contribute to the present large fusion devices (LHD, EAST, HT-7), International Thermonuclear Fusion Experimental Reactor (ITER) and demonstration reactors so far, under the JSPS-CAS CUP Program. Every year, 4-6 persons visited from Japan to China. Major institutes are Institute of Plasma Physics and Southwestern Institute of Physics. From China to Japan, every year, 7-8 persons visited to National Institute for Fusion Science (NIFS), Hokkaido University, Shizuoka University and University of Toyama. The averages of stay period of Chinese and Japanese visitors are 6-7 days and 15-23 days, respectively.

In these exchanges, numerous researches were conducted mainly using the unique experimental devices in both countries. The development of the wall conditionings and analyses of the plasma wall interactions in the fusion devices using material probes were successfully conducted in LHD (NIFS), HT-7 and EAST (IPP). The tritium absorption and desorption behavior was investigated using the Tritium Facility at University of Toyama. The fuel hydrogen behavior in the plasma facing materials such as boron, tungsten and carbon was investigated using ion source and surface analysis devices at Shizuoka University. The helium retention behavior in the plasma facing materials and the tritium inventory in tritium breeding materials used for blanket in ITER and demonstration reactor were investigated using ion source and surface analysis devices at Hokkaido University. These results were summarized by many academic papers published.

In addition to the exchange of every year, China-Japan CUP-CAS Symposium on PWI/PFC and Fusion Technologies was organized by J. Chen and T. Hino, and held at Huangshan in 2008. The number of participants was 48, and the topics covered plasma wall interaction, advanced fusion material and blanket technology. These important issues were very fruitfully and globally discussed toward a fusion reactor.

In the present, it is quite important to conduct the researches toward fusion reactors. For example, the performance of tungsten as the plasma facing material has to be clarified. In addition, the blanket module has to be developed. The experimental studies with respect to these issues have been carried out as the Japan-China collaboration researches. These activities are introduced in the followings.

*Corresponding author: T. Hino, tomhino @qe.eng.hokudai.ac.jp

2. Deuterium retention and thermal desorption behaviors in tungsten

Tungsten is regarded as the plasma facing material of fusion reactors owing to its high melting point, high sputtering threshold energy, low tritium retention and relatively low activation induced by fusion neutron irradiation. Tungsten is selected as the plasma facing material in both ITER and demonstration reactor. Therefore, the compatibility of tungsten with fusion plasmas has been investigated widely in the world. In the collaboration research between SWIP (Prof. X. Liu) and Hokkaido University (T. Hino), retention behavior of fuel hydrogen was investigated using ECR ion source at Hokkaido University for tungsten materials fabricated in SWIP, namely tungsten alloy doped by TiC particles (W-TiC alloy) and pure polycrystalline tungsten made by the powder sintering technology (PCW). There may be a possibility that the addition of TiC into tungsten changes the ductile-brittle transition temperature.

Testing samples were pure polycrystalline tungsten with purity of 99.95% and W-TiC alloy with TiC content of 0.1 wt.% (about 1 at. %). The test sample size was $50\times10\times1$ mm^3. The test sample was polished mechanically. Before deuterium ion irradiation, the testing sample was degassed in vacuum by 30 min at 1273K, then installed in ECR ion source for deuterium ion irradiation, after that the irradiated sample was transferred to thermal desorption spectroscopy (TDS) facility for the analysis of thermal desorption spectra.

The deuterium ion energy was 1.7 keV and ion flux about 1×10^{14} D/cm^{2}s, and the sample was irradiated with the fluences of 0.5×10^{18}, 1×10^{18} and 2×10^{18} D/cm^2. After the irradiation, the amount of retained deuterium was measured using TDS facility. Here, the sample was heated to 1273K with a heating rate of 0.5 K/s, and then kept at 1273K for 20 min. During the heating, the released gas was measured by QMS. For W and W-TiC alloy irradiated by deuterium ions, the release gases were HD, D_2 and D_2O, however, the amount of the latter gas (D_2O) was too small compared with the others. The desorption rates of HD and D_2 from PCW and W+TiC alloy are shown in Figs. 1 and 2, respectively. It is seen that the main desorption peaks of HD and D_2 both for W and W+TiC alloy appeared at the temperature of approximately 573K. The amount of retained deuterium was obtained by integrating the desorption rate with heating time. The amounts of retained deuterium in PCW and W+TiC alloy are plotted against the deuterium ion fluence in Fig.3. The amount of retained deuterium was comparable in these materials. The amount of retained deuterium saturated at the fluence regime higher than 1×10^{18} D/cm^2 in these two materials.

From the present results, we confirmed that the tungsten material (PCW) has the fuel hydrogen retention a few times smaller than that of graphite and the desorption temperature (573K) is very lower than that of graphite (1073K). These advantages are conserved for the TiC doped tungsten

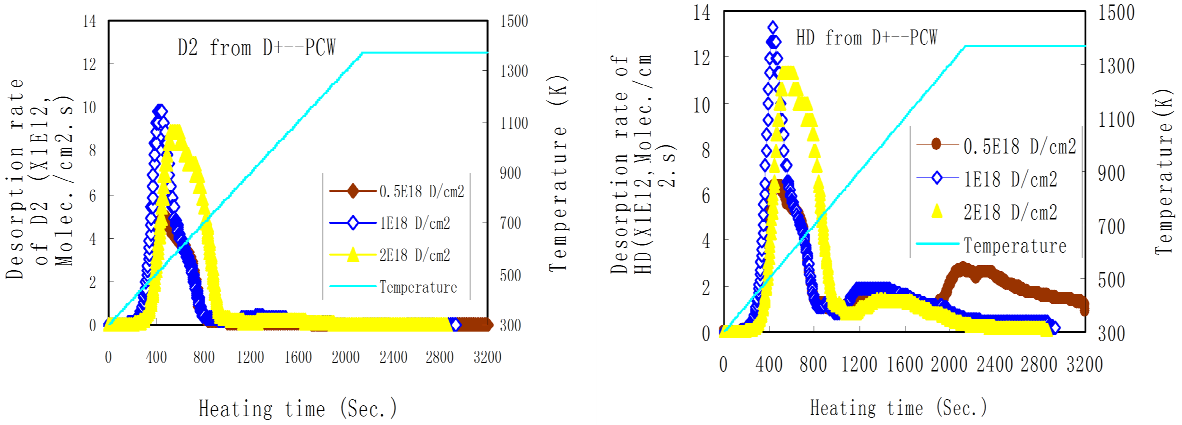

Fig.1 Desorption rate of HD and D_2 from PCW.

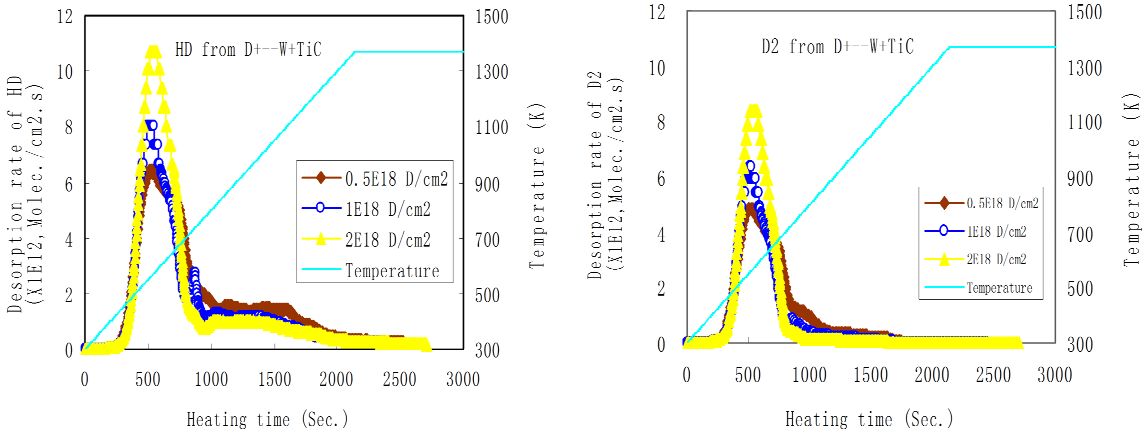

Fig.2 Desorption rates of HD and D_2 from W-TiC alloy.

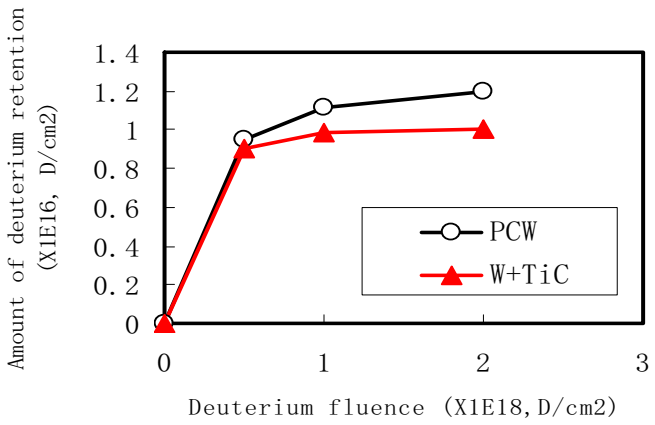

Fig.3 Amount of retained deuterium versus deuterium ion fluence.

3. Deuterium retention and desorption behavior of tritium breeding material, lithium titanate

Lithium titanate (Li_2TiO_3) is candidate as the tritium breeding material of solid tritium breeding blanket of fusion reactors. Japan and China, as the ITER participant members, have developed the TBM (test blanket module) for ITER. The tritium inventory of the blanket in fusion reactor has to be low from a view point of safety. Therefore, it is important to study the tritium retention and desorption behavior in this breeding material. The deuterium retention in the lithium titanate was investigated as the Japan-China collaboration study (Prof. X. Liu and Prof. T. Hino) in order to evaluate the tritium inventory. In the present experiment, Li_2TiO_3 pebbles prepared by SWIP were irradiated by 1.7keV deuterium ions using an ECR facility at Hokkaido University. The deuterium retention and release behavior was measured by using a technique of thermal desorption spectroscopy (TDS).

Before deuterium ion irradiation, the testing sample was preheated at 973 K for 1h in a vacuum chamber with base pressure of 10^{-7} Pa, and then it was transferred into ECR ion source for deuterium ion irradiation. Fig.4 is the sketch drawing of ECR irradiation apparatus, and the new design sample holder was also shown in this figure. The size of Li_2TiO_3 was 5 × 5 mm^2. The sample was irradiated with different fluences, 0.5 × 10^{18} D/cm^2, 1 × 10^{18} D/cm^2, 3 × 10^{18} D/cm^2, 5 × 10^{18} D/cm^2 and 7 × 10^{18} D/cm^2. After ion irradiation the sample was transferred to the other vacuum chamber for TDS measurement. The irradiated sample was heated by an infrared furnace from RT to 973 K with a heat rate of 10 K/min. When the sample temperature reached to 973 K, the the temperature was kept for 1 h. The released gases were measured by using QMS.

The deuterium retained in the lithium titanate desorbed in forms of HD, D_2, HDO and D_2O. Fig.5 shows the desorption spectra of released gases with temperature at different deuterium ion fluences. Two groups of desorption peaks were found in these figures. The first peak appeared at about 500 K, and the second peak 650-700 K. The first peak is due to the de-trapping of Li-D bond (or Li-OD bond), and the second peak the de-tapping of Ti-D bond (or Ti-OD bond).

The amount of retained deuterium was obtained by integrated the desorption rate of all released gases containing deuterium with respect to time. The amount of retained deuterium as a function of deuterium ion fluence is shown in Fig. 6. The amount of deuterium trapped by lithium or titanium is obtained by integrating the first or second peak profile, respectively. The ratios of deuterium trapped by lithium and titanium versus ion fluence are shown in Fig. 7. The amount of retained deuterium saturated for the fluence higher than 1×10^{18} D/cm^2 and the saturated amount was about 1×10^{17} D/cm^2. The ratio of the deuterium trapped by Ti is higher than that by Li.

We now consider the tritium inventory of the blanket module based upon the present experimental results. The temperature of the tritium breeding material region is 900K. From Fig.5, there is a small amount of deuterium in the regime higher than 900K. This amount corresponds to the tritium inventory of the blanket module. In the case of ITER, this amount is very small, lower than 1gram. But, in the fusion reactor, this amount becomes several grams, so that the total inventory of all blanket modules becomes several hundred grams. In the case of fusion reactor, the temperature profile in the blanket module has to be adjusted for the tritium inventory to be small.

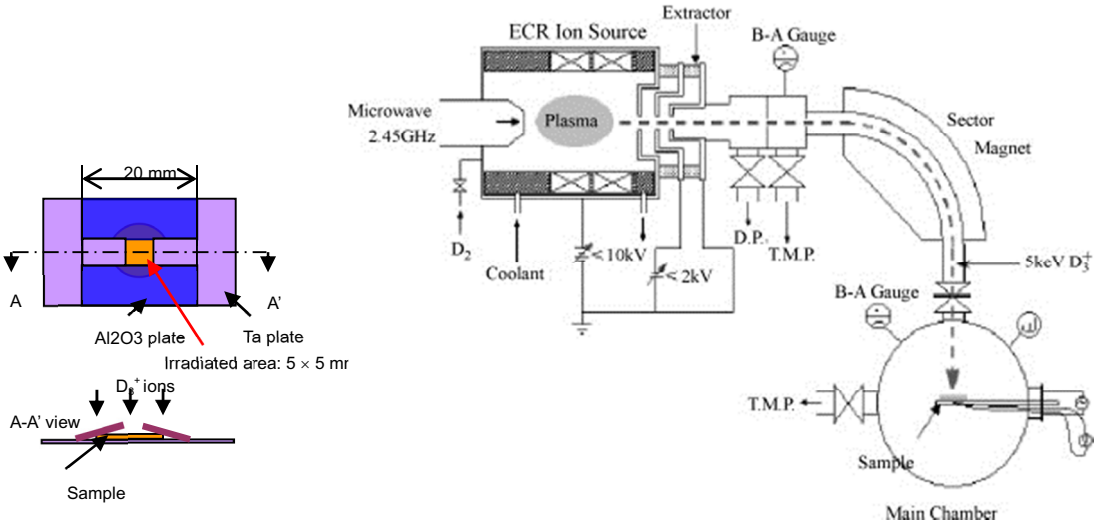

Fig.4 ECR ion irradiation apparatus and the sample geometry.

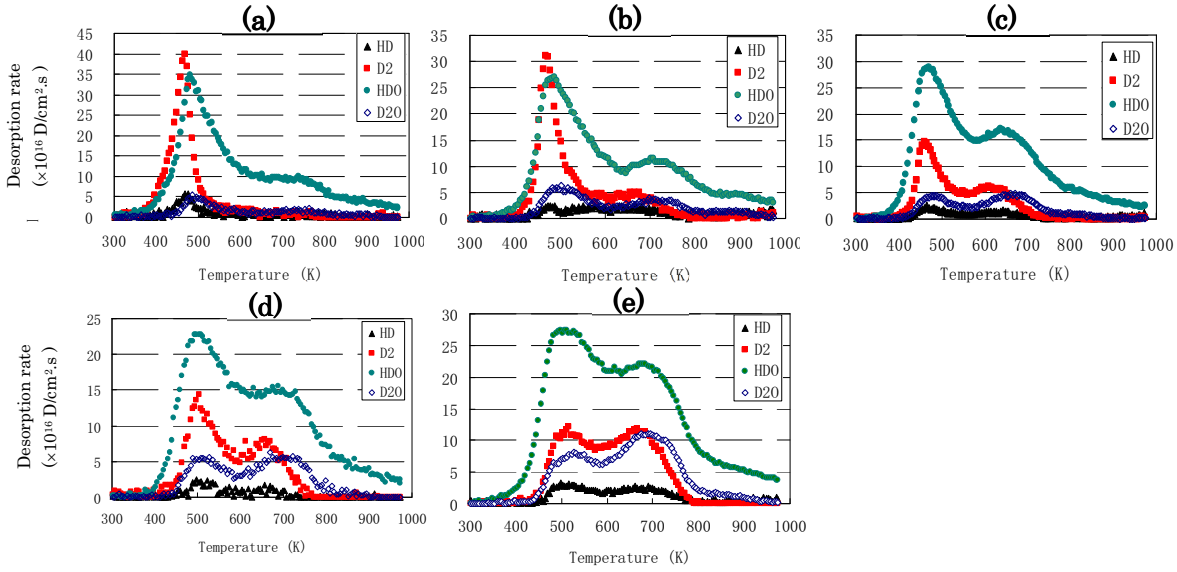

Fig. 5 Thermal desorption spectra of gases containing deuterium for lithium titanate at different fluences. (a) 0.5×10^{18} D/cm^2, (b) 1×10^{18} D/cm^2, (c) 3×10^{18} D/cm^2, (d) 5×10^{18} D/cm^2, (e) 7×10^{18} D/cm^2.

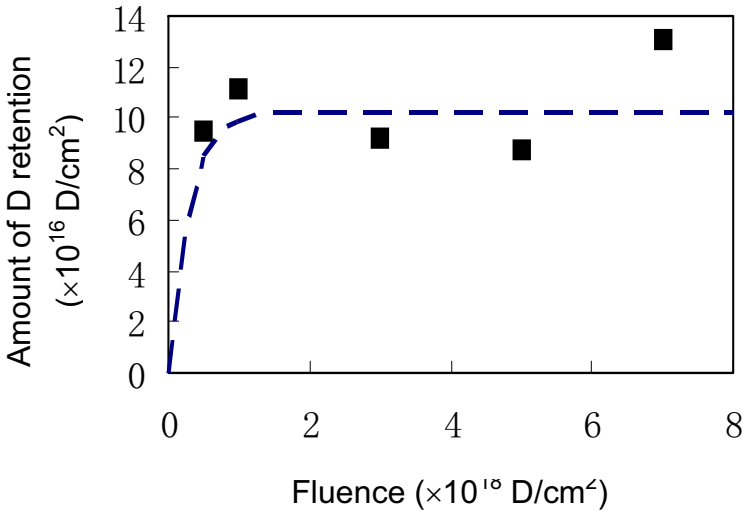

Fig. 6 Amount of retained deuterium as a function of deuterium ion.

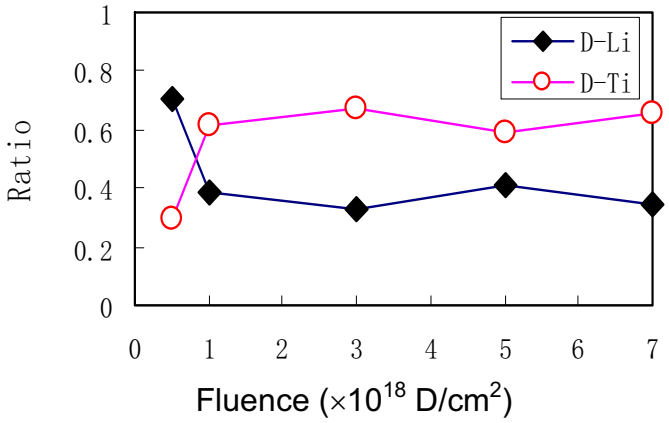

Fig. 7 Ratios of implanted deuterium trapped by lithium and titanium.

Summary of 12A since 2006 from China side

J.L. Chen[1], J.G. Li[1], Q.G. Guo[2], Z.J. Zhou[3], T.Hino[4], N. Ashikawa[5]

(1) Institute of Plasma Physics, Chinese Academy of Sciences, Hefei 230031, P.R. China
(2) Institute of Coal Chemistry, Chinese Academy of Sciences, Taiyuan 030001, P.R. China
(3) School of Materials Science and Engineering, USTB, Beijing 100083, P.R. China
(4) Fusion Engineering Department, Hokkaido University, Kita-13, Nishi-8, Kita-ku, Sapporo, 060-8628 Japan
(5) National Institute for Fusion Science, 322-6 Oroshi-cho, Toki-shi 509-5292, Japan

Collaborations between China and Japan in fusion research have been rapidly enhanced by the supports of JSPS-CAS Core-University Program on Plasma and Nuclear Fusion. Since 2006, both Chinese and Japanese scientists have conducted plenty of collaboration researches and communications in the field of 12A: Plasma Surface Interactions (PSI) and Plasma Facing Materials (PFM). Fruitful and impressive results have been achieved from both sides. Many institutes and universities are involved in the collaboration research programme of PSI and PFM. They are Institute of Plasma Physics, Chinese Academy of Sciences (ASIPP), Southwestern Institute of Physics (SWIP), Institute of Coal Chemistry, Chinese Academy of Sciences (ASICC), Shanghai Institute of Ceramics, Chinese Academy of Sciences (ASSIC) and Northwest Institute for Nonferrous Metal Research (NINMR) from China, and National Institute for Fusion Science (NIFS), Hokkaido University, Shizuoka University, Kyushu University, University of Toyama, Tokushima University and Japan Atomic Energy Agency (JAEA) from Japan. Both sides benefit well from the frequent exchange of people and working together. Large numbers of high-level scientific papers by authors from both sides have been published in the mainstream fusion relevant journals. Many young researchers were involved in the programme.

In addition to several CUP key person / task leader meetings, the China-Japan CUP-CAS Symposium on PWI/PFC and Fusion Technologies was held at Huangshan, Anhui, China in October 2008. The symposium has broad topics including plasma wall interaction, plasma facing materials and components, core plasma behavior, blanket, tritium, superconductor, ITER related R&D and theory. Thorough discussions and exchange of ideas and results were carried out during the symposium. There were 45 participants (18 from Japan and 27 from China) with 39 papers presented. Finally, 29 papers were published in a special issue of NIFS proceedings: NIFS-PROC-76 (2009).

The studies of Plasma Surface Interactions (PSI) and Plasma Facing Materials (PFM) are critical issues in fusion research. The interaction of plasma with surrounding surfaces will have a considerable impact on the performance of fusion plasmas, the lifetime of plasma facing components (PFC), and the tritium retention in next-step burning plasma experimental devices, such as ITER. The major topics of collaboration research between each other are in these areas: erosion and deposition, tungsten coatings, fuel retention in plasma facing materials, wall conidtionings and fuel removal, blanket breeding materials, dust etc. Here the main achievements from China side is summarized.

1. Erosion and deposition

The erosion of PFM in fusion devices can seriously limit the life time of PFCs, while the impurity deposition on the PFM can affect the properties on PFCs. Furthermore, the codepositon of fuel and impurities will lead to serious safety problems. The erosion and deposition studies of different

materials were carried out in HT-7 and EAST tokamaks. The erosion and deposition of present PFM for HT-7 and EAST, multi-element doped graphite with thick SiC gradient coatings [1], has been studied in detail [2]. Different material analysis methods, such as Scanning Electron Microscopy (SEM), X-ray Photoelectron Spectroscopy (XPS), Energy Dispersive Spectrometer (EDS), Atomic Force Microscopy (AFM), Auger electron spectroscopy (AES) and Thermal Desorption Spectroscopy (TDS) have been used for analysis. Quite a number of measurements were made in different Japanese universities with the aid of Japanese collegues. In addition to experimental studies, collaborations on computer simulations were also performed. The erosion and deposition behavior of the SiC coating on plasma facing components were simulated by the modified Erosion and Deposition based on DYnamic model (EDDY code), using typical edge plasma parameters for the Experimental Advanced Superconducting Tokamak (EAST) [3]. Compared to non-doped graphite, less deposition and erosion were observed on the SiC coating. Simulation results showed that, the carbon deposition rate decreased as the electron temperature increased at low plasma density, while increased with the electron temperature at high plasma density.

2. Tungsten coatings

Tungsten (W) and its alloys have been considered as candidate PFMs ITER and future DEMO reactors, due to their favourable properties. It is also planned to use the tungsten coatings as the PFCs for EAST tokamak [4]. W coatings on copper (Cu) substrate have been developed by means of vacuum plasma spraying (VPS) method employing a Cu/W gradient interlayer so as to alleviate mismatch of the physical properties between Cu and W. VPS-W/Cu PFCs with built-in cooling channels were prepared and mounted into the HT-7 acting as a directly-cooled movable limiter for materials evaluation, which showed a good integrity [5]. Directly-cooled VPS-W/Cu plasma-facing component (PFC) can withstand e-beam high heat flux (HHF) irradiation of 20 cycles, 100 s/cycle, and heat loads of 9.6 MW/m^2. Furthermore, VPS-W coatings on CuCrZr with W/Cu interlayer and powder metallurgic W/Cu functionally graded material (FGM) were tested under high heat flux with active cooling and plasma irradiation in the HT-7 device [6]. Results showed that after 10 MW/m^2 thermal shock experiment, exfoliation and crack appeared, however, the interface was not damaged except a few pores. VPS-W can withstand 150 cycles for 100s pulses under 6 MW/m^2. VPS-W coatings on CuCrZr with W/Cu interlayer have good thermal performance, and W/Cu interlayer was a better alternative compliant layer which can realize reliable W/CuCrZr joint, and the pore microstructure of VPS-W coating is helpful to inhibit the bubble formation.

3. Fuel retention in plasma facing materials

Due to safety considerations, the investigation of hydrogen isotope retention in present tokamaks is of crucial importance for understanding underlying mechanisms and for assessing the impact of tritium retention on design and operation of next step devices. The fuel retention and behaviour in different materials for PFCs in HT-7 and EAST were deeply studied. Particle balance analysis was used to study deuterium retention during long pulse discharge on HT-7 [7]. Basically more than 90% of the input D_2 molecules are retained at the end of the discharges. More retention happens in longer pulse. About 60 % of the puffed gas is retained relatively permanently. Pumping speed is not a decisive factor for D_2 retention control. D_2^+ implantation experiments have been performed in Shizuoka university to study deuterium retention. For VPS-W coatings, the chemical states of tungsten coatings were not changed after D_2^+ implantation [8]. The desorption phenomenon of D_2 in tungsten coatings occurred in two temperature ranges of 300–700 K and 800–1150 K. The retention behavior of deuterium in tungsten coatings was greatly different from that of bulk tungsten, which was related to the existence of oxygen. Similar experiments were also carried out for the SiC coated doped graphite. At R.T, two D_2 desorption peaks were observed from the TDS spectra at a peak temperature of around 850K and 1050K, which correspond to the desorption of D bond to Si and C,

respectively. Deuterium was preferentially trapped by C in the initial D_2^+ implantation. At ion fluence of 1.5×10^{22} D^+m^{-2}, the trapping of D was almost saturated. Only the desorption peak of D bond to C can be seen in the case of samples implanted at 900K, which indicates that most of D bond to Si was quickly re-emitted by thermal annealing effect. VPS-W coatings boronized by an ICRF discharge in HT-7 were also investigated [9]. Two broad desorption peaks of D_2 were observed: The first peak from about 500 K to 650 K at low temperature range and the second one about 830 K to 950 K at high temperature range corresponding to the desorption of D bound to B and the bridge bonds B–O–D and B–C–D due to O and C incorporation into the boron film respectively. In University of Toyama, Different tritium exposed samples , including doped graphite, SiC coated graphite, VPS-W coatings and polycrystalline tungsten, were examined by β-ray-induced X-ray spectrometry (BIXS) in an argon atmosphere [10]. The results indicated that the SiC coated graphite absorbed the most tritium and the polycrystalline tungsten the least.

4. Wall conidtionings and fuel removal

Wall conditioning is essential for fusion device to achieve high plasma performance. Different techniques such as glow discharge cleaning (GDC), Electron cyclotron resonance (ECR) discharge cleaning and ion cyclotron resonant (ICR) discharge cleaning have been used. ECR discharge cleaning is conducted on HT-7 with Radio frequency (RF) waves of 2.45 GHz under toroidal field of 0.088–0.066 T [11]. Toroidally symmetric ECR plasmas were obtained, and the resonance layers were scanned by toroidal field. It was observed that RF powers made little difference, and higher neutral pressure resulted in higher cleaning efficiency, and working gas D_2 had higher removal rates than that of He. Removal rate of hydrogen in ECR discharge cleaning was 5–10 times lower than that in ICR. The differences between ICR cleanings with various working gases, He-ICR, D_2-ICR, O-ICR and He/O-ICR, were investigated after long deuterium plasma operation in the HT-7 machine on hot walls with a temperature of 402–470 K [12]. For each working gas, ICR cleanings with high power and/or high pressure promoted H release. Both the pure O-ICR and D_2-ICR cleanings had a higher removal rate for hydrogen than that in He-ICR cleanings by a factor of 4–6. The O-ICR cleaning had a much higher deposits removal rate than the He-ICR and D_2-ICR cleanings by a factor of a few tens. Plasma recovery under various events, such as after shutdown, boronization, oxidation and air leak, were systematically studied [13]. After boronization, plasma recoveries would depend on the procedures of the boronization ($C_2B_{10}H_{12}$). After oxidation, boronization would effectively suppress impurities and would be beneficial for plasma recovery. ICRF cleanings in various working gases, such as He and D_2, would be useful for impurities and hydrogen removal. He–ICR cleanings were also successfully carried out on full metallic walls in EAST [14]. The removal efficiency for H during 20 kW 4.5×10^{-3} Pa He–ICR cleaning was same as that in He–GDC cleaning (2 Pa, 4A). Highest H removal rate in EAST with full metallic material walls, 1.7×10^{22} H/h in 20 kW 3×10^{-2} Pa He–ICR, was higher by a factor of four than that in HT-7 with carbon limiter configuration.

Oxidation treatment is one of promising methods for amorphous tritiated carbon layers removal. A series of experiments of oxidation wall conditioning, including thermo-oxidation, glow discharge (O-GDC) and radio frequency wave associated oxidation (O-ICR) have been performed in HT-7 and EAST [15, 16]. The results showed that O-GDC appeared to be the most efficient on HT-7. However, O-ICR was almost as good and could be applied with the magnetic field in ITER. Comparisons of O-ICR on both EAST and HT-7 also revealed that power density, working pressure, plasma facing area and materials, pumping speed and wall temperatures were main possible factors influencing the deposits removal of the O-ICR. High power, low oxygen pressure and He in O-ICR are beneficial for reducing oxygen retention [17].

5. Blanket breeding materials

Testing TBM (Test Blanket Modules) is one of important engineering test objectives in ITER project. Lithium titanate and Lithium silicate were considered as the tritium breeding materials for solid tritium breeding blanket of fusion reactors. Therefore, it is very important to study the tritium retention and desorption behavior in these breeding materials since this investigation will supply the necessary database for TBM design and optimization. Li_2TiO_3 and Li_4SiO_4 samples were irradiated by 1.7 keV deuterium ions in a ECR facility in Hokkaido University, and then the deuterium retention and release behavior measured by TDS. For Li_2TiO_3, two desorption peaks, respectively at about 500 K and 650 K, might correspond to the de-trapping of Li-D and Ti-D bonds. For Li_4SiO_4, two desorption peaks are about 450K and 600K, respectively.

6. Dust

The understanding of the production of dust in fusion devices are needed because the dust may directly affect the safe operation of a next step device. The formation during plasma, distribution and basic characteristics of dust, such as morphology, size, composition and retention of hydrogen isotopes, were investigated on EAST and HT-7 [18]. The dust in the two devices had similar characteristics. It was also found that plasma parameters, displacement and configuration were main factors for the dust production. Hot spots produced during long pulse were also an important reason for the production of lots of dust particles. A dust capture experiment using SiO_2 aerogel probe showed hypervelocity dust particles would exist in HT-7, i.e. higher than 1km/s.

In summary, significant progress has been made in our collaboration researchs. The communications between each other are greatly strengthened. Not all results have been mentioned here. It is foreseen that more cooperations between China and Japan will proceed in the future.

[1] J.L. Chen et al., J. Nucl. Mater. 363–365 (2007) 1334.
[2] C.Y. Xie et al., J. Nucl. Mater. 363–365 (2007) 282.
[3] Q. Xu et al., J. Nucl. Mater. (2011) At press.
[4] G.-N. Luo et al., Phys. Scr. T128 (2007) 1.
[5] G.-N. Luo et al., J. Nucl. Mater. 363–365 (2007) 1241.
[6] F.L. Chong et al., J. Nucl. Mater. 363–365 (2007) 1201.
[7] Y. Yang et al., J. Nucl. Mater. 363–365 (2007) 839.
[8] Yaran Niu et al., J. Nucl. Mater. (2011) At press.
[9] Zhongshi Yang et al., J. Nucl. Mater. (2011) At press.
[10] Jing Wu et al., J. Nucl. Mater. (2011) At press.
[11] Y.W. Yu et al., J. Nucl. Mater. 390–391 (2009) 1051.
[12] J.S. Hu et al., J. Nucl. Mater. 366 (2007) 206.
[13] J.S. Hu et al., Fusion Eng. Des.. 83 (2008) 689.
[14] J.S. Hu et al., J. Nucl. Mater. 376 (2008) 207.
[15] J.S. Hu et al., J. Nucl. Mater. 363–365 (2007) 862.
[16] J.S. Hu et al., Plasma Phys. Control. Fusion 49 (2007) 421.
[17] J.S. Hu et al., J. Nucl. Mater. (2011) At press.
[18] M. Tang et al., J. Nucl. Mater. (2011) At press.

CUP collaborations on plasma wall interactions (12A)

N. Ashikawa[1]*, T. Hino[2], J.S. Hu[3], Wu[3], T. Ming[3] Z. Hunag[4], J.L. Chen[3], L.W. Yan[4], and N. Noda[1]

[1]*National Institute for Fusion Science, Oroshi-cho, Toki, Japan*

[2]*Laboratory of Plasma Physics and Engineering, Hokkaido University, Sapporo, Japan*

[3]*The Institute of Plasma Physics, Chinese Academy of Sciences, Hefei, China*

[4]*Southwestern Institute of Physics, Chengdu, China*

Japanese and Chinese researches on plasma wall interactions (12A) aggressively and continuously have been investigated in order to contribute to the present large fusion devices (LHD, EAST, HT-7 and HL-2A). In particular, characterizations of wall conditionings and analysis of collected dust particles using surface analyzer method, such as secondary electron microscope (SEM) and X-ray photoelectron spectroscopy (XPS), have been reported.

1) Boronization

Boronization has been performed in many fusion plasma devices as one of the most effective wall conditioning techniques. It is well known that the major advantages of boronization are (1) covering high Z first wall with low Z materials, (2) oxygen gettering, and (3) quick starting up of wall conditioning after opening the devices to air. The behavior of boronized walls is fairly complicated under physical and chemical processes such as mass transfer and composition changes due to sputtering and deposition of other materials. At present, two kinds of boronization supported by glow discharges and ICWC are operated in fusion devises. Three kinds of boron sources have been used by B_2H_6, $B_{10}H$(or D)$_{14}$ and $B(CH_3)_3$. Hence, characterizations of coated boron files depends on combinations of supporting discharges, boron sources, dilute gasses and materials of in-vessel components including plasma facing wall.

Material probes exposed to boronization supported by glow discharges or ICWC were analyzed using XPS with sputtering by argon (Ar) ions. From comparison of boron-oxide concentrations and other impurities, capacities of oxygen gettering and their processes have been estimated.

Figures 1 shows atomic concentrations of boron films at different depth positions in HT-7 analyzed by XPS. For example, a boron film by He-GDC boronization shows a boron concentration of 70% and carbon concentration of 20% as shown in Fig.1 (a). A boron film by D2-GDC boronization shows a boron concentration

of 50-55% and carbon concentration of 25-30% as shown in Fig.1 (b). Hence, carbon concentration into boron film by D2-GDC boronization is higher than by He-GDC.

Figure 2 shows narrow profiles for boron (B1s) peak at depth of 30 nm by XPS. This data indicates chemical bondings of boron and each chemical bondings locates as pure boron at about 188eV, boron-carbide at 189eV and boron-oxide at 189-192eV. A boron file by He-GDC boronization shows mainly boron-carbide bonding, but a boron file by D2-GDC boronization shows mainly boron-oxide. These boron –oxide are kept toward base materials as shown in Fig.3. For a reason of difference between He-GDC and D2-GDC, difference of wall conditions previous operation of boronization are considered.

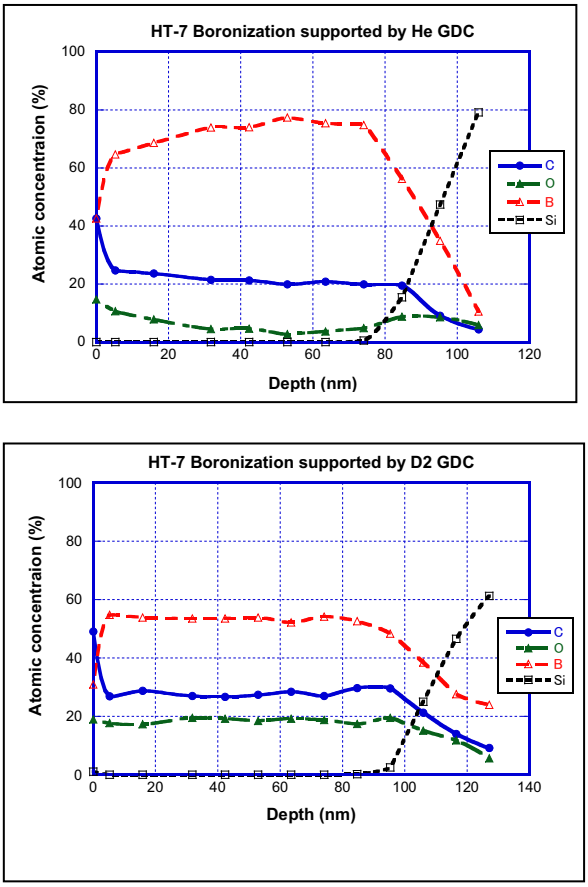

Fig.1 atomic concentrations of boron films by (a) He-GDC and (b) D2-GDC in HT-7

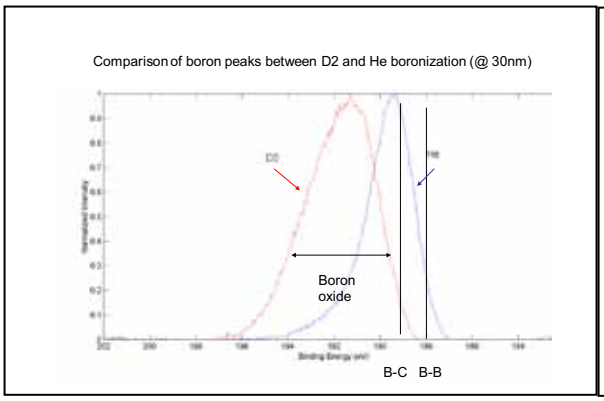

Fig.2 Narrow peak profiles of boron (B1s)

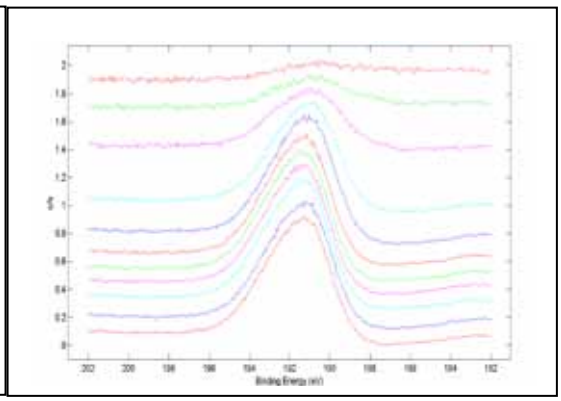

Fig.3 Depth profile of B1s narrow peak profiles of boron film by D2-GDC

2) Dust Analysis

Dust research is an important issue related to the accumulations of radioactive

impurities in core plasmas and the tritium retention in ITER, FFHR and other future devices. Thus, for understanding characteristics of dusts, their performance and compositions have been investigated in tokamaks and stellarator/heliotrons. Dust particles were collected in LHD, EAST, HT-7 and HL-2A, and then these morphologies, atomic concentrations, total amounts and size distributions of dust diameter are reported. These results relate plasma facing components, confined plasma geometries, plasma parameters and operational histories, and then many kinds of different type dust particles have been observed in each device. Investigations of collected dusts in ASIPP and SWIP were started under this CUP collaboration.

Figures 4 show surface morphologies of dust particle analyzed by SEM in (a) HL-2A, (b) HT-7 and (c)(d) LHD. At present, Chinese tokamaks such as EAST, HT-7 and HL-2A reported mixed materials dust particles and boron flakes. These shapes are flakes and size is over 10 microns. Source elements of dust particle depend on plasma facing wall and wall conditioning methods. For the case of carbon dust, this morphology, compositions indicates a growing process with chemical reactions of hydrocarbon. In LHD, a typical diameter of carbon dust is under 1 micron and these morphologies are sphere as shown in Fig. 4(c). Some of carbon dusts show an agglomeration shape with connecting small sphere carbon dust in LHD as shown in Fig.4 (d). From JT-60U results collected in 2010,

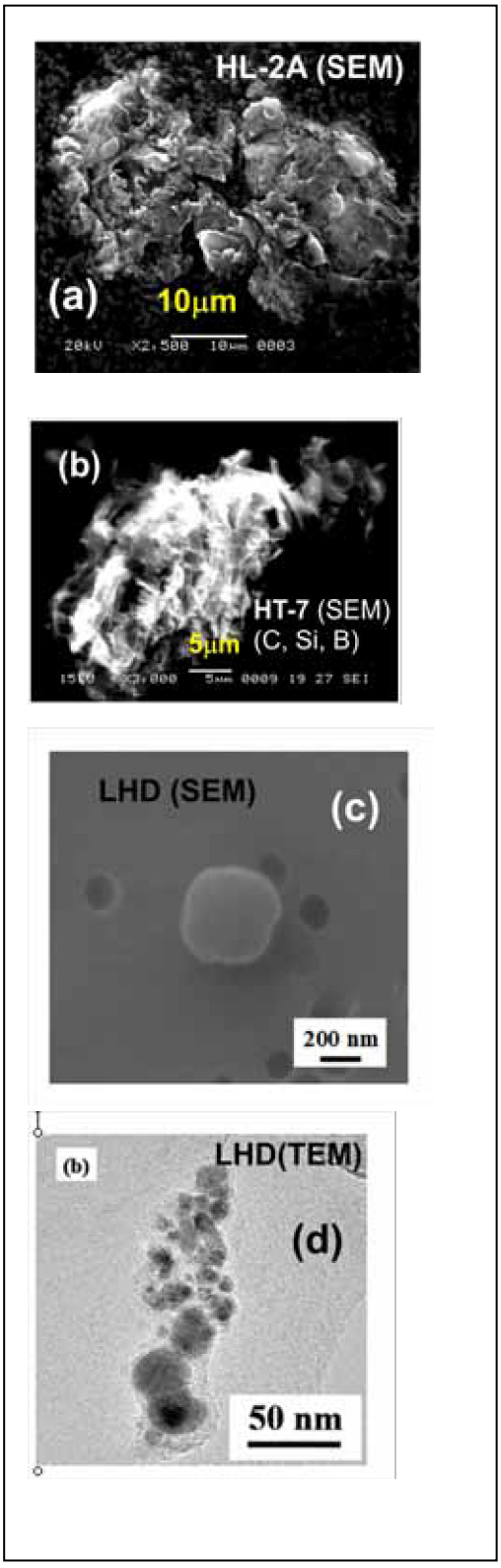

Fig.4 Morphologies of dust particles by SEM

many sphere carbon dusts are observed and large size of over 10 microns are also founded. To summarize these differences of compositions, shapes and size are important to understand a production and growing presses of dust particles.

Summary

Research accomplishments and seminars of "Atomic and Molecular Process in Plasmas (AMPP)" in 2006-2010

Daiji Kato, Nobuyuki Nakamura*, Takako Kato, and Shunsuke Ohtani*
e-mail: kato.daiji@nifs.ac.jp
National Institute for Fusion Science, Toki, Gifu 509-5292, JAPAN
*Institute for Laser Science, Univ. Electro-Commun., Chofu, Tokyo 185-8585, JAPAN

1 Introduction

Essential roles of atomic processes of heavy impurity ions and molecular processes in magnetic confinement fusion plasmas have long been recognized. It encouraged efforts of acquiring the spectroscopic and collision data, and had fostered basic studies on the atomic and molecular collisions in each country. Under the auspice of the JSPS-CAS Core-University Program (CUP), we conducted personal exchanges (China → Japan: 29 persons, and Japan → China: 18 persons, see Fig. 1) to share the atomic and molecular data and facilitate collaboration on database development. In this report, research accomplishments and seminars on the subject "Atomic and Molecular Process in Plasmas" in the last five years (2006-2010) are summarized.

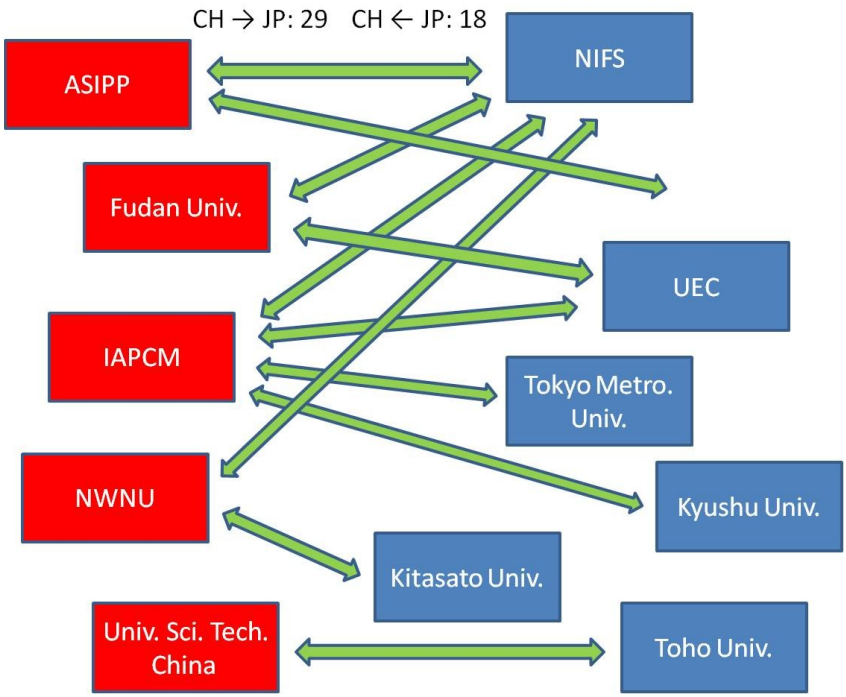

Fig.1 Personal exchanges in 2006-2010.

2 Research accomplishments

2.1 Atomic spectroscopy of heavy impurity ion spectra in Large Helical Device

Since the heavy impurity ions would not be fully ionized even in core plasmas, a significant amount of energies confined in the core plasmas is exhausted by high-energy photon emission of the impurity ions unless the impurity concentration is extremely low. Transport of the heavy impurity ions in the peripheral plasma is, therefore, a critical issue for development of steady-state plasmas.

Emission line spectra of the impurity ions can be used for diagnostics of local plasma parameters, e.g. electron density and temperature, and ion transport study. Fe pellet injection was used to measure Extreme-Ultra-Violet (EUV) spectra of highly charged Fe ions in Large-Helical-Device (LHD). The EUV measurement of the Fe spectra was also done by means of an Electron-Beam-Ion-Trap (EBIT). By analysis on differences in both spectra, it was fond that intensity ratios of some line pairs observed in LHD were changed significantly with electron density, while they were not changed with electron temperature. Referring independent measurements of radial electron density distributions, the Fe-ion transport in LHD after the Fe-pellet injection was investigated in terms of the intensity ratio.

In LHD (and any laboratory plasma, in principle), plasma temperature and density can be obtained by the independent measurements, *e.g.* laser Thomson scattering, FIR interferometry. Synthesized spectra with the collisional-radiative (CR) model are, therefore, used to study ionization and recombination dynamics and transport of impurity ions in LHD plasmas. Application of the CR models of impurity (Fe, C, Ne, O) ions developed in NIFS, which involved data collection of the impurity ions, to plasma diagnostics in EAST at ASIPP was discussed. The plasma diagnostics systems and data acquisition systems in LHD were also studied by Chinese visitors.

2.2 Theoretical evaluation of atomic collision data

Available data for electron-impact ionization cross section of M-shell Fe ions were surveyed for use in non-ionization-equilibrium plasma modeling. Benchmark test of a newly developed atomic code was done for the direct ionization cross sections of Na-like Fe ions. Good agreement with HULLAC code was obtained. Importance of indirect ionization processes (excitation-autoionization and resonant-excitation-double-autoionization) was clearly shown. Charge transfer cross sections in C^{3+} and He collisions over a wide range of collision energies were evaluated theoretically. Molecular-Orbital-Close-Coupling (MOCC) calculations have been performed precisely, but significant discrepancies from experimental measurements were found at low collision energies.

2.3 Divertor plasma diagnostics and modeling in a linear plasma device

Hydrogen molecules in highly vibrationally excited states can greatly enhance the production of negative ions, mainly through dissociative attachment of hydrogen molecules. Recent studies with divertor plasmas have suggested that the Molecular Assisted Recombination (MAR) has much larger reaction rates at an electron temperature of ~2-3 eV, at which the three-body and radiative plasma

recombination are not effective. MAR mainly results from the vibrational excitation, and would enhance the divertor plasma recombination at a relatively high electron temperature in a way greatly beneficial to the protection of divertor target plates by avoiding or reducing overheat and high flux ion bombardments on the plates. To study these hydrogen molecular behaviors, we need to understand the Vibrational Distribution Functions (VDF) of the molecules. Experimental determination of the VDF by Fulcher band spectroscopy, by $a^3\Sigma_g \rightarrow b^3\Sigma_u$ continuum emission has been studied.

Among these visible emissions of the hydrogen molecules in low temperature plasma, the Fulcher transition, $d^3\Pi_u \rightarrow a^3\Sigma_g$, was considered to be a good candidate because of its relatively strong emission intensity and few perturbations. By using the new fitting scheme to fit the rotational and vibrational temperatures using all the resolvable rovibrational lines and the new cross section data by using a semi-classical method to taking into account the rovibrational dependency, rovibrational distribution was measured in better accuracy in a linear plasma device to simulate edge plasmas, MAP-II in Univ. Tokyo.

2.4 Experimental studies on highly charged ions by means of Electron-Beam-Ion-Trap (EBIT)

EBIT is known as a versatile tool for study on electron-ion interaction. Atomic spectroscopy and measurements of electron collision cross sections for ions of virtually any charge state of any element are feasible with the EBIT, provided the electron beam is controlled properly. Dielectronic-Recombination (DR) in the EBIT was measured for several high-Z elements at Univ. Electro-Commun. (UEC), Japan. Theoretical calculations of the DR strengths were performed. In this collaboration, strong relativistic effects in the DR strengths were identified for the first time.

Profs. S. Ohtani and N. Nakamura in UEC helped design and construction of a new EBIT at Fudan Univ. Chinese young researchers visited UEC to learn operation of the EBIT at UEC. Dr. J. Sun (a student from Fudan Univ. under supervision of Ohtani) received the phD degree at UEC in Sept. 2008 for experimental studies on highly charged ion physics.

2.5 Charge eXchange Recombination Spectroscopy (CXRS) of ion-atom collisions

Personal exchanges to collaborate on CXRS by means of an Electron-Cyclotron-Resonance (ECR) ion source at Tokyo Metro. Univ. (TMU), Japan, have been conducted since 2007. State selective cross sections of electron transfer from H_2 and He gas targets to C, N, and O ions from the ECR ion source were calculated with two-center Atomic-Orbital-Close-Coupling (AOCC) code developed in IAPCM, China. The theoretical calculations were compared with measured polarization degrees of photon emission after electron captures. The results validated the code and explained collision energy dependence of the polarization degrees.

2.6 Electron energy loss spectroscopy

Electron scattering experiments have the capability for studies of atomic processes. In

particular, the electron energy-loss spectroscopy is one of the powerful tools for these studies. Electron energy-loss spectra of some simple molecules and rare gas atoms have been measured under this CUP since 2001. 1) Measurement of generalized oscillator strength (GOS) of the nitric oxide has been done. In this study, it was found that the GOS curves determined from the electron energy-loss spectra showed a strange behavior in small momentum transfer region. The theoretical calculations could not reproduce this strange behavior. 2) Sub-shell excitation of rare gas atoms was measured. When sub-shell excitation levels are coupled to the ionization continuum, the spectra have feature structures that are called Fano-profile. It was found that the line profile depended on the incident electron energy and the scattering angle.

2.7 Theoretical study on atomic processes in plasmas

After organizing the first "China-Japan Joint Seminar on Atomic and Molecular Processes in Plasma" in 2004, Profs. F. Koike of Kitasato University, Japan, and C.-Z. Dong of Northwest Normal University (NWNU), China, have started to visit each other and completed several papers on theoretical atomic physics in plasmas which had been accomplished by their collaboration. For the introduction of the frontier of the plasma diagnostics and related atomic physics to the young scientists in NWNU, Koike gave one or two lectures to them at every occasion of his visit. The titles of the lectures are as follows.

1) 2006: Several topics in multiple electron excitations of atoms
2) 2008: Time dependent aspects in atomic ionization realized by photo-excitation of atoms
3) 2010: Three-photon double ionization of Ar by extreme ultraviolet free electron laser: manifestation of intermediate resonances of Ar.
4) 2010: MCDF study of M1 visible transitions of W^{26+} arising from the ground state multiplets

The young scientists in NWNU, who use to be graduate students during the period of the present CUP activities, have now grown up to start their research work at various institutions in various counties as well as in China. Dr. X.-B. Ding has been granted COE fellowship of National Institute for Fusion Science (NIFS), Japan, from the fiscal year of 2010, who had been studying in

Fig. 2 Lecture by Koike at NWNU in Nov. 2006.

NWNU under the supervision of Prof. Dong.

2.8 Theoretical study on plasma screening effects in ion-atom collisions

Collision dynamics of ion-atom systems was studied by using the Two-Center Atomic Orbital Close-Coupling (TC-AOCC) and Molecular-Orbital-Close-Coupling (MOCC) methods in the Debye-Hückel model. The atomic orbitals and eigenenergies of $n \leq 6$ states for O^{7+} and $n \leq 2$ states for H were calculated as a function of the screening parameter and used in the AOCC dynamics scheme to calculate the electron capture cross sections in the energy range 1-100keV/u. With increasing the screening, the bound states centered on O^{7+} and H successively enter the continuum, thereby reducing the number of reaction channels in the discrete spectrum. Furthermore, the interaction screening introduces also significantly changes in the direct and exchange couplings, affecting thereby the magnitude and energy behavior of state-selective cross sections. These result in the change of charge exchange spectrum.

3 China-Japan joint seminars

[F. Koike (Kitasato Univ.) / C.-Z. Dong (NWNU)]

As one of the activities of the Core University Program (CUP) entitled "Atomic and Molecular Processes in Plasma", we have organized a series of three seminars entitled "China-Japan Joint Seminar on Atomic and Molecular Processes in Plasma". The first seminar was held on March 6 to 11'th March 2004 at Northwest Normal University, Lanzhou, China. The second seminar was held on 8 to 12'th October 2007 at Silk Road Dunhuang Hotel, Dunhuang, China. And the third seminar was recently held on 26 to 30'th October 2009 at Xian Jiaoda Nan Yang Hotel, Xi'an, China.

Since the first seminar in 2004 [1], the researchers from both Japan and China carried out a number of significant studies in atomic and molecular processes in relation to the fusion plasma. The succeeding two joint seminars have offered opportunities for them not only to present the collaborative studies but also to be acquainted with each other. The seminars also offered the place to exchange the information about the recent progress of their research activities and also to discuss about the plan of the future collaborations.

In the second seminar in 2007, the total number of 26 oral talks was presented by experts from Japan, China and EU, and the total number of 11 posters was presented by experts from China. The total number of the audience was about 38, in which 12 from Japan, 20 from China, and 4 from EU. The proceedings of the seminar have been issued collecting 23 oral talks and 11 posters that have been presented in the seminar, and they have been published in NIFS-PROC-73 [2]. In the third seminar in 2009, the total number of 38 oral talks was presented by experts from Japan, China and USA, and, furthermore, quite a few contributions were presented by posters. The total number of the officially registered participants was 54, in which 18 from Japan, 35 from China, and 1 from USA. The proceedings of the seminar have been issued collecting 34 papers from the delegates of the seminar, and they have been published in NIFS-PROC-81 [3]. In addition to the proceedings, the

total number of 16 papers from the delegates has been submitted to the journal “Plasma Science and Technology”.

This local organization of the seminars has been hosted by Northwest Normal University, and therefore the seminars have given an opportunity for young scientist from this university and the neighboring institutions in China to present their own studies and also to learn much about the frontier of the plasma science. The seminars have accepted a number of poster presentations from mainly the young scientists of Northwest Normal University. This fact suggests us that an active

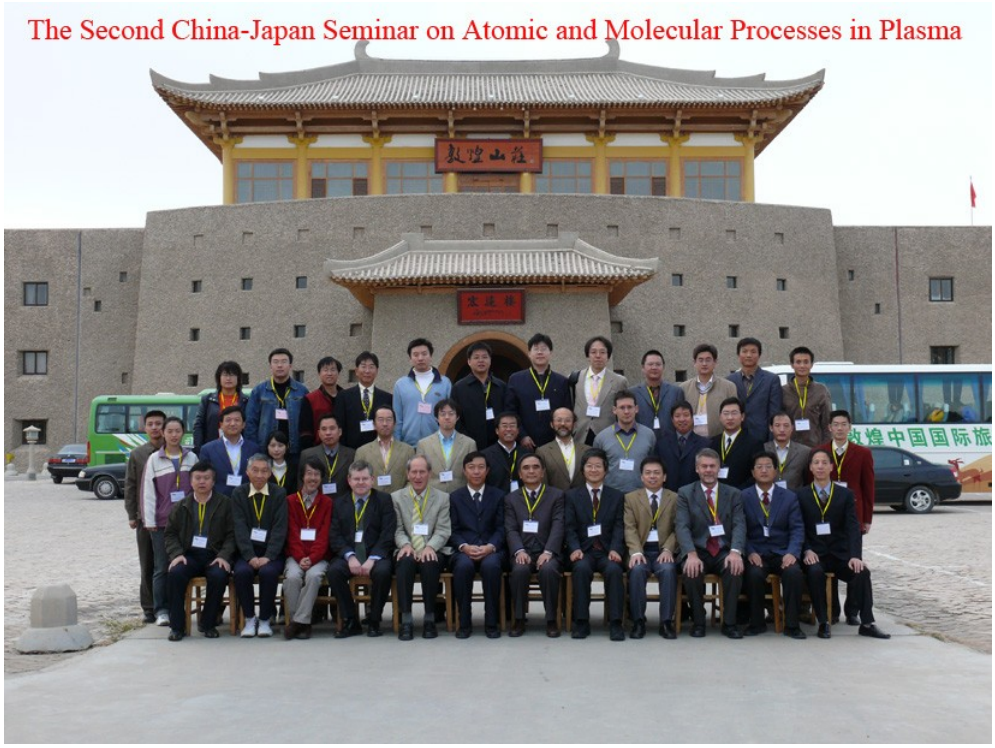

Fig. 3 group photo for the 2nd seminar at Silk Road Dunhuang Hotel.

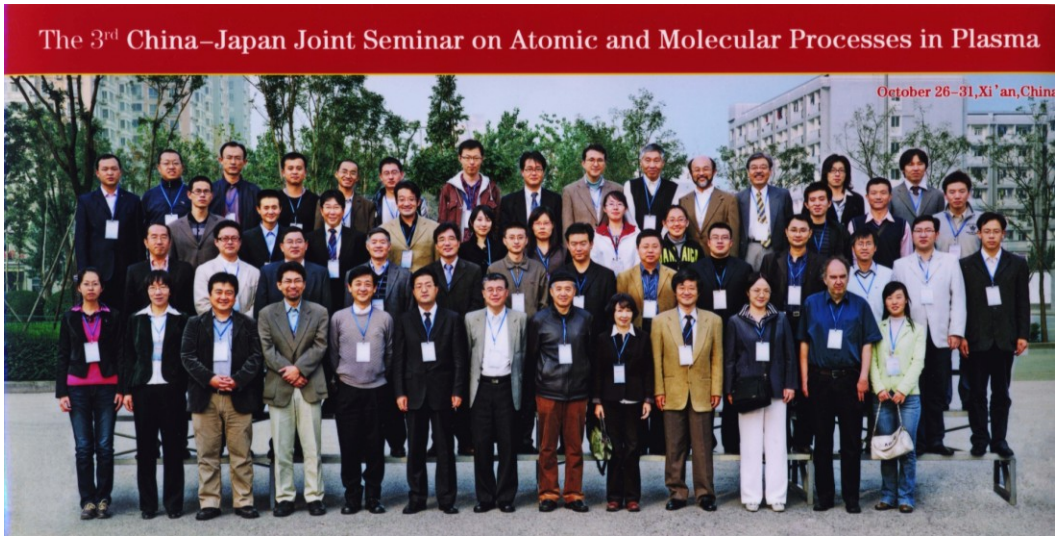

Fig. 4 group photo for the 3rd seminar at Xian Jiaoda Nan Yang Hotel.

group has grown up on the research of ion spectroscopy of high temperature plasmas that is needed for the diagnostics of the fusion plasma.

Fig. 5 Scientific sessions in the 3rd seminar at Xian Jiaoda Nan Yang Hotel, Xi'an.

4 Outlook

Feasibility study of tungsten divertor, which is an urgent task in ITER, requires atomic data of tungsten ions in peripheral plasmas. It includes evaluation of the radiation power and ion transport study with tungsten ions. Also, we need to dissipate high heat fluxes on the divertor plate, impurity gas puff into edge plasmas is a promising technique. Atomic data of the cooling gas, e.g. N, Ne, Ar, and Kr are required. Since electron-collision with those impurity ions plays principal roles in the radiation of edge plasmas, evaluation of electron collision cross sections and rate coefficients in low temperature plasmas are very important. Laboratory devices such as EBIT are used for measurements of the electron-collision and line emissions of the impurity ions. Recently, a new EBIT has been constructed in Fudan University (China), consulting the original design of Tokyo-EBIT in UEC (Japan). Continuous collaboration between them is necessary for further development of experimental studies with the EBITs. Collisional-radiative models with the atomic data are useful to develop diagnostics methods of plasma parameters with ion emission lines. Validation of the model is made through comparison with well defined plasma parameters in LHD and EAST. Collaboration with theoretical groups in China is also very important on this subject.

Accurate monitoring of tritium inventory and recycling are indispensable to demonstrate feasibility of the controlled nuclear fusion reactors. Comprehensive data set for atomic and molecular collisions involving hydrogen isotopes are required to increase practicality in the fuel recycling modeling and simulation. State-of-the-art quantum calculations of the collision data are, therefore, becoming more important. Through this CUP, we have learned good research groups also on this subject in China. Continuous collaboration is highly desirable.

We have successfully organized a series of joint seminars on "Atomic and Molecular Processes in Plasma" during the operation of the present Core University Program, and the contribution of these seminars to the progress and the initiation of collaborative research works between Japan and China has been found to be well substantial. It is strongly desirable to continue to organize the present

series of seminars.

Acknowledgments

Thanks to all of the contributors to this subject “Atomic and Molecular Process in Plasmas”.

Reference

[1] NIFS-PROC-59, F. Koike and C. Dong Eds., Feb. 2005.

[2] NIFS-PROC-73, F. Koike and C. Dong Eds., Mar. 2008.

[3] NIFS-PROC-81, F. Koike and C. Dong Eds, Jan. 2010.

Atomic and Molecular Processes in Plasmas

Jian-guo Wang

Through the CUP (13A) project, the scientists of China and Japan have done many excellent collaboration works in the field of atomic and molecular processes in plasmas. In this report, some important progress are introduced and the future prospect is expected.

The atomic and molecular (A+M) processes play an important role magnetic fusion plasmas. In the central (core) plasma, atomic processes determine the plasma radiation losses, impurity transport and alpha particle transport. In the edge and divertor plasma regions, the atomic and molecular processes determine the plasma cooling, volume plasma recombination, plasma momentum dissipation and particle and power exhaust. Those involves the photo processes (photo-excitation and photo-ionization, and their inverse processes: radiative decay and radiative recombination), electron impact processes (excitation, ionization and their inverse processes, dielectronic recombination) and heavy particle collisions (excitation, ionization and charge transfer). The related atoms and molecules include fusion materials and the impurities. The emitted photon spectra are often used to diagnose the plasma parameters.

In the CUP (13A) project, the scientists of China and Japan have done many collaborative works to investigate these A+M processes. We summarize some important progress here.

1. A+M processes in the edge and divertor of Tokamak plasmas

The edge and divertor plasmas of Tokamak have low temperatures and support existence of neutral and low charged atomic and molecular plasma impurities (generated due to plasma-wall interactions). The most abundant edge/divertor impurities are Be, B, C and their hydrides. The collision processes of these impurities with the main constituents of edge/divertor plasmas (e, H^+, H, H_2) have a strong effect on edge/divertor plasma properties (radiation losses, transport, etc) and also affect the dynamic plasma behavior (by, e.g., changing the plasma temperature and density gradients in these regions). Using a variety of methods, we studied the collision processes between basic edge/divertor plasma constituents (e, H^+, H, H_2) and the light element atomic and molecular plasma impurities such as: Li, Be, B, C, N, BeH, BeH_2 (and their single and multiply charged ions), and the accurate cross sections and rate coefficients have been presented.

We have calculated the elastic, momentum transfer and viscosity cross sections for the H^++Be, Be^++H, H^++C and C^++H collisions in the CM energy range 10^{-4}eV – 10keV by using the molecular-orbital close-coupling (MOCC) method with quantum-mechanical description of nuclear motion (QMOCC). The required molecular structure information for the BeH^+ and CH^+ ions was obtained by

employing the MRD-CI program package. As an example, figure 1 plots the results of $H^+ + Be(2s^2)$ [1].

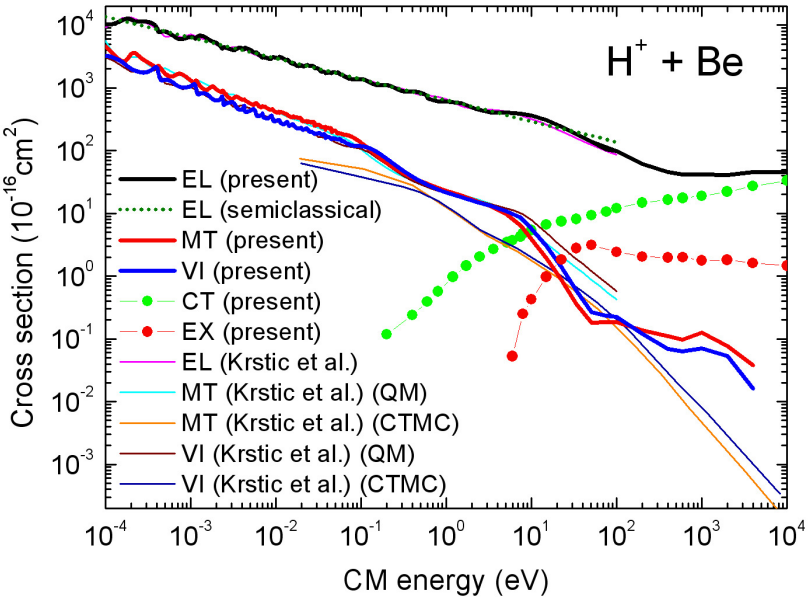

Figure 1. Elastic (EL), momentum transfer (MT) and viscosity (VI) cross sections of present calculations for $H^+ + Be(2s^2)$ collision, compared with those of Ref. [2]. The total charge transfer (CT) and target excitation (EX) cross sections from the present calculations are also shown.

2. A+M processes in the Debye plasmas

The atomic processes in Debye plasmas are investigated by a series of methods including the classical, semi-classical and quantum-mechanical ones. It's found that due to the plasma screening of the interactions both the binding energies and the number of bound states are reduced, while the radial extension of the wave functions become broader. Taking into account these plasma screening effects on the atomic structure and interactions, we have studied the photo processes [3], electron-impact processes [4] and heavy particle collisions [5] in a wide range of plasma screening conditions. Our work demonstrates that the screening effects are very important in Debye plasmas, which should be taken into account in the modeling and diagnostics of these plasmas. As examples, figure 2 and figure 3 plot the photo-ionization and electron impact excitation cross sections in a wide Debye length.

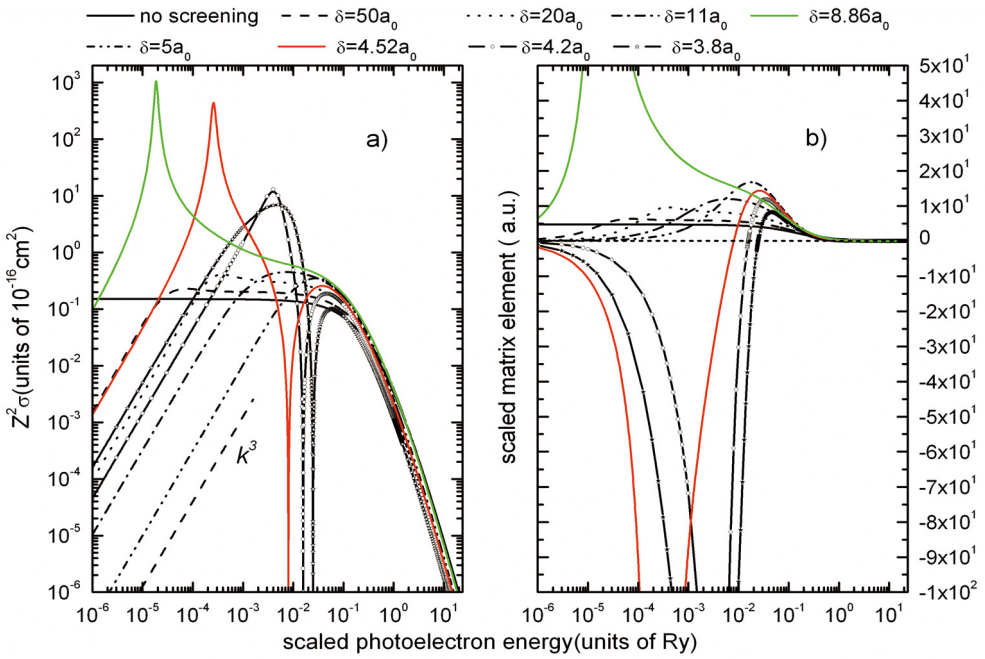

Figue 2. Scaled photoionization cross sections for the $2s$ state of hydrogen as function of the scaled photoelectron energy for the pure Coulomb case and for the screened case with scaled screening lengths $\delta = 50, 20, 11, 8.86, 5, 4.52, 4.2, 3.8 a_0$ (a). Panel (b): dipole matrix elements.

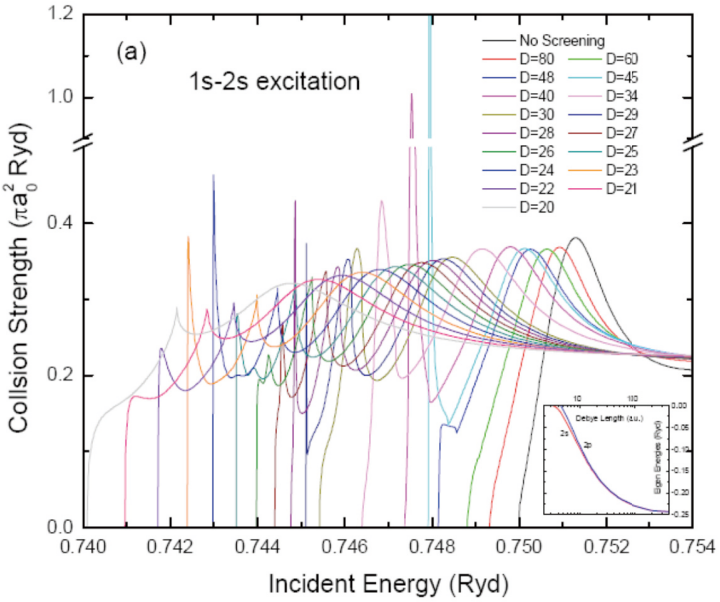

Figue 3. Dynamic evolution of 1s→2s collision strengths for hydrogen when the screening length varies.

3. Simulation of Charge Exchange Recombination Spectroscopy

The intensities of Charge Exchange Recombination Spectroscopy (CXRS) of α particle with atomic hydrogen Neutral Beam Injection (NBI) are calculated by solving the rate equations, including all kind of electron collision processes, in the quasi-static state approximation. The influence of electron collision processes on the CXRS signal

for He^+(n=4→3) at λ = 468.6 nm in various plasma conditions are discussed. In figure 4, the effects of electron collisions can be displayed clearly [6].

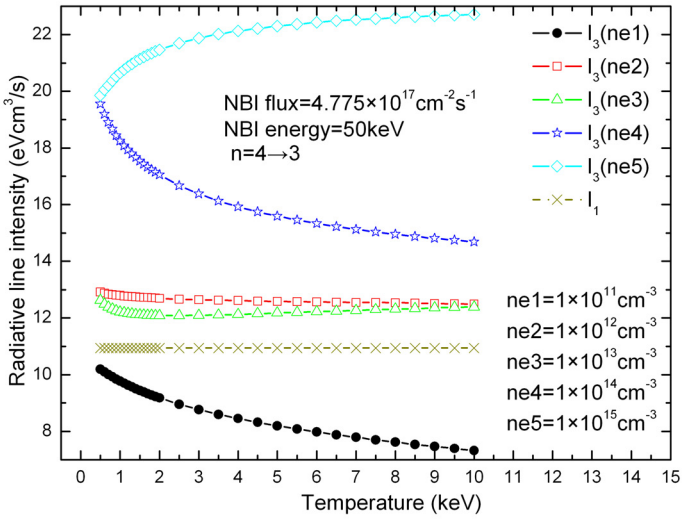

Figure 4. Intensity in the $He^+(n=4\rightarrow 3)$ line, as a function of plasma temperature, for varied electron densities using the model including the electron impact processes and the crosses is intensity I_1 with the model without the electron impact processes.

In summary, a good collaboration relation has been built between the scientists in China and Japan, and some important progress has been achieved through the collaborations. The CUP project is important for the research work in the field of atomic and molecular process in plasmas. It can be expected that a more great success will be achieved in future through the collaborations between China and Japan scientists.

References

[1] C. H. Liu, J. G. Wang and R. K. Janev, J. Phys. B At. Mol. Phys. **43**, 144006 (2010).

[2] P. S. Krstić and D. R. Shultz, J. Phys. B: At. Mol. Phys. **42,** 065207(2009).

[3] Y. Y. Qi, J. G. Wang, R. K. Janev, Phys. Rev. A **78**, 062511(2008); **80**, 032502(2009); **80**, 063404 (2009).

[4] S. B. Zhang, J. G. Wang, R. K. Janev, Phys. Rev. Lett. **104**, 023203 (2010); Phys. Rev. A **81**, 032707 (2010); Phys. Rev. A **81**, 065402 (2010).

[5] L. Liu, J. G. Wang, R. K. Janev, Phys. Rev. A **77**, 032709(2008); **77**, 042712 (2008); **79**, 052702(2009).

[6] X. J. Liu, J. G. Wang, Y. Z. Qu and B.J. Xiao, submitted to Phys. Plasmas (2011).

13A: Atomic and Molecular Processes in plasmas
Topical Talk

Atomic Processes of Highly Charged Heavy Ions Relevant to Hot Plasmas

NAKAMURA Nobuyuki
e-mail: n_nakamu@ils.uec.ac.jp
Institute for Laser Science, The University of Electro-Communications (ILS/UEC)
Chofu, Tokyo 182-8585, JAPAN

INTRODUCTION

Behavior of highly charged heavy impurities in hot plasmas is quite important, because they can not be fully ionized even in high temperature plasmas, and thus high energy radiations from them would result in serious radiation cooling of the plasmas. Studies of highly charged heavy ions are thus necessary to diagnose and control laboratory fusion plasmas. An electron beam ion trap (EBIT) [1] is a versatile device for studying such atomic data of highly charged ions (HCIs). It consists of a Penning-like ion trap and a high-energy, high-density electron beam going through the trap. HCIs are produced through the successive ionization events caused by the beam electrons, and trapped for hours while interacting with the high energy electrons. It is a powerful device to measure cross sections for various electron – HCI collision processes, such as ionization, recombination, excitation, and so on. Furthermore, trapped ions can be spectroscopically studied, which provides fundamental atomic data, such as transition wavelengths and probabilities. These atomic data are also important for fundamental atomic physics to study the relativistic effects on the atomic structure.

ELECTRON BEAM ION TRAP (EBIT)

Fig. 1 shows the principle of an EBIT. An EBIT consists of mainly four parts, an electron gun, a drift tube, an electron collector, and a magnet surrounding the drift tube. An electron beam emitted from the electron gun is compressed by the axial magnetic field produced by the magnet. The compressed high density electron beam ionizes trapped ions in the drift tube. HCIs are thus produced by successive electron impact ionization. Ions are confined by the axial well potential applied to the drift tube, and radially by the space charge of the high density electron beam. There are observation slits at the middle of the drift tube, which enable spectroscopic studies of the trapped HCIs. The trapped ions can also be extracted as a beam to the axial direction through the electron

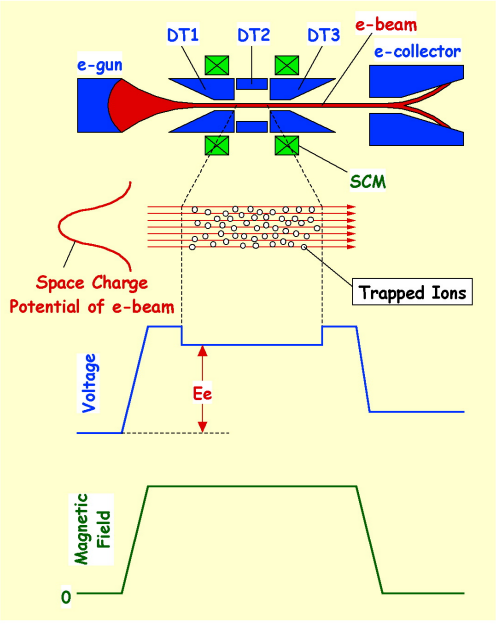

Fig. 1. Principle of an electron beam ion trap.

collector.

In 1996, Prof. Ohtani (UEC) constructed a high-energy EBIT in Tokyo [2]. We have been using the Tokyo-EBIT since then to study a wide range of electron-ion interactions and to measure the spectroscopic data of highly charged heavy ions. The left panel of Fig. 2 shows the picture of the Tokyo-EBIT. Almost 10 years later since the Tokyo-EBIT was built, i.e. around 2006, a new EBIT was built by Prof. Zou's group of Fudan University (Shanghai) [3]. The right panel of Fig. 2 shows the picture of the Shanghai-EBIT. From the early period of design and construction of the Shanghai EBIT, the Tokyo and the Shanghai groups have kept collaboration through frequent exchanges of researchers. The Shanghai-EBIT itself is one of the most important results of this CUP. The complementary use of the Tokyo- and the Shanghai-EBITs have enabled us to produce atomic data of HCIs efficiently.

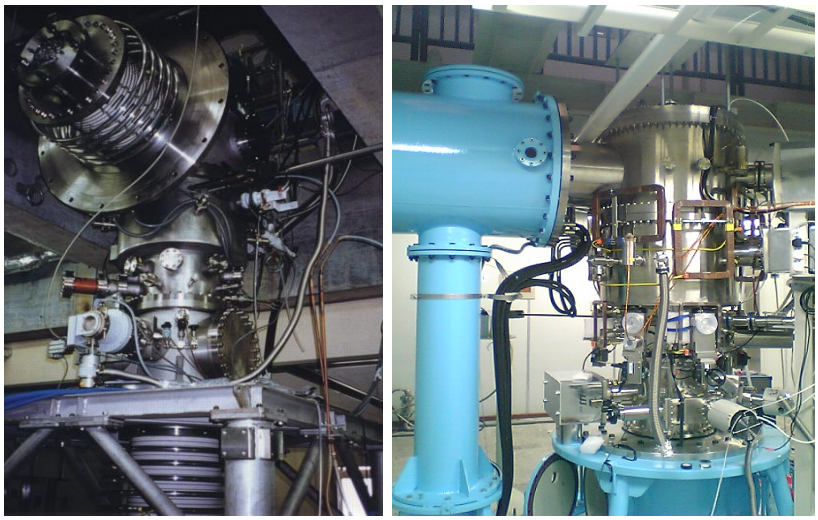

Fig.2. (left) Tokyo-EBIT at ILS/UEC Tokyo. (right) Shanghai-EBIT at Fudan University.

DIELECTRONIC RECOMBINATION (DR)

Dielectronic recombination (DR) of highly charged ions is one of the most important processes in plasmas. DR is a two-step electron-ion collision process, which is composed of dielectronic resonant electron capture and radiative stabilization of the doubly excited state produced in the dielectronic capture (Fig. 3). An EBIT is a useful device for studying DR processes of highly charged heavy ions since it has a quasi-monoenergetic electron beam whose energy can be easily and rapidly controlled. By using the Tokyo-EBIT, we have been studying DR processes through both X-ray observations [4] and ion abundance measurements [5]. The former has the advantage

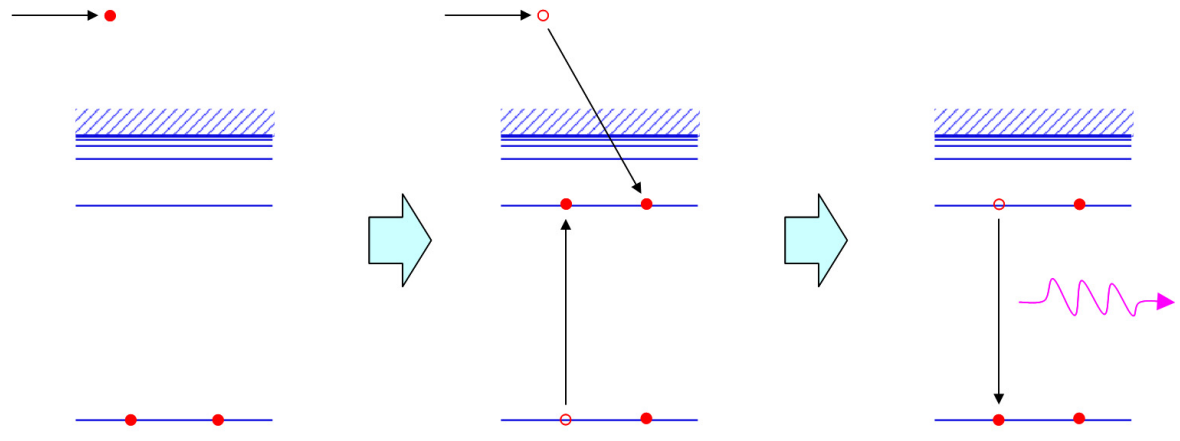

Fig. 3. Dielectronic recombination (DR) process.

that absolute cross sections can be obtained by normalizing the X-ray intensity of DR to that of radiative recombination (RR), for which reliable theoretical cross sections can be obtained. On the other hand, it has the disadvantage that it is difficult to resolve the charge states mixed in the EBIT due to the intrinsic energy resolution of a solid state Ge detector. In contrast, the latter has the advantage that charge-state resolved measurements are available although it is difficult to obtain absolute cross sections. The ion abundance measurement is thus suitable for open shell systems for which it is difficult to concentrate the abundance on a single charge state. Fig. 4 shows a typical result of the X-ray measurements performed for highly charged tungsten ions[6]. As seen in the figure, enhancement of X-ray intensity is found at the resonance energy. DR process is important not only for plasma physics but also for atomic physics. For example, Fig. 5 shows the experimental results of the resonant strength for KLL DR of Li-like ions as a function of the atomic number. As shown in the figure, the resonant strength has very strong dependence on atomic number. The theoretical calculation which includes only the Coulomb interaction completely fails to reproduce the experimental results. On the other hand, it is found that the theoretical results well reproduced the experiment when the generalized Breit interaction (GBI), one of the quantum electrodynamics (QED) effects is taken into account properly. This result showed that the QED effects affect the resonant strength significantly for highly charged heavy ions[5].

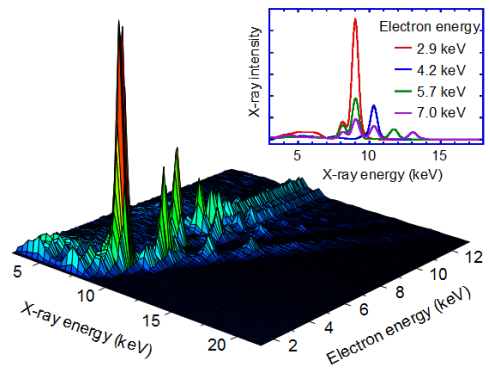

Fig. 4. X-ray observation of dielectronic recombination of highly charged tungsten ions.

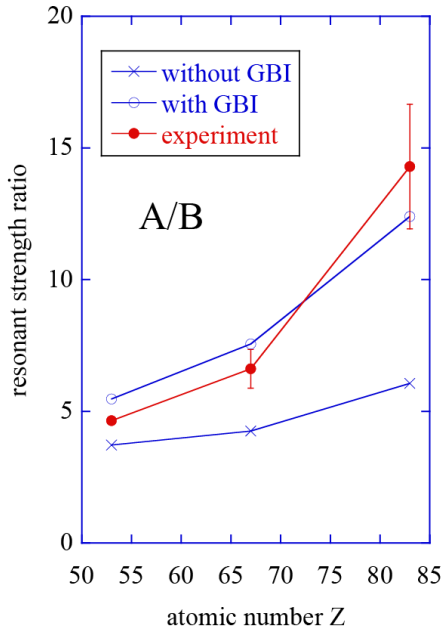

Fig. 5. Resonant strength ratios between the $[2s^2 2p_{1/2}]_1$ (A) and $[2s 2p_{1/2}^2]_1$ (B) resonant states. Red closed circles represent the present experiments while open circles and crosses theoretical values with and without the generalized Breit interaction, respectively.

SPECTROSCOPY

Tungsten is a major candidate for the divertor material of the next generation fusion reactor ITER. Spectroscopic studies of tungsten ions are thus necessary to diagnose and control the high temperature plasma in ITER. In particular, the visible lines of moderately charged ions (W^{q+} with q ~ 30 or less) are very important for the diagnostics of the edge plasmas because optical elements such as optical fibers, lenses and so on can be used. However, there is no identified line in the visible range except only one line. An EBIT is an useful device to observe and identify previously unreported lines because it reveals a simple spectrum with a narrow charge state distribution. By

observing the dependence of line intensity, one can identify the charge state of the ion emitting the line. For example, the spectra obtained at Ee = 330, 360, 400, and 450 eV are shown in Fig. 1. Each spectrum was obtained by a 1-hr exposure with an electron beam current of 10 mA. As seen in Figure 1, some lines show a sharp Ee dependence. For example, the lines marked by the arrows in Fig. 1(b) appeared when Ee was increased from 330 eV to 360 eV, and they almost disappeared when Ee was further increased to 400 eV. These lines are attributed to W^{16+}, because the lines appeared when Ee exceeded the ionization energy of W^{15+}. Similarly, the responsible ions for the lines marked by the arrows in Fig. 1(c) and (d) are W^{17+} and W^{18+}, respectively. These lines are the magnetic dipole transitions in the ground state fine structure levels. Detailed identification through the comparison with theoretical calculation is under progress[7,8].

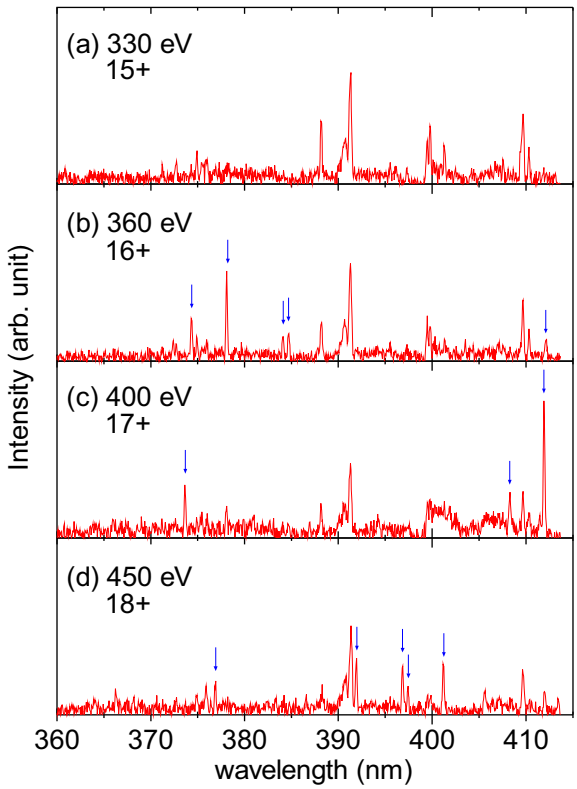

Fig. 6. Visible spectra of tungsten ions produced with an electron beam ion trap.

SUMMARY AND OUTLOOK

An electron beam ion trap is a versatile device for studying the atomic processes of highly charged ions. It is useful for the study of electron – ion collision processes and the spectroscopic investigation of highly charged ions. Though the CUP collaboration, atomic data relevant to hot plasmas have been accumulated. However, the atomic data required for the success of thermal fusion have been increasing, so that further collaboration is surely needed for future.

References

[1] R.E. Marrs et al., Phys. Rev. Lett. 60 (1988) 1715
[2] N. Nakamura et al., Phys. Scr. T73 (1997) 362
[3] Z. Xikai et al., J. Phys.: Conf. Ser. 2 (2004) 65
[4] H. Watanabe et al., J. Phys. B 34, 5095 (2001).
[5] N. Nakamura et al., Phys. Rev. Lett. 100, 073203 (2008).
[6] H. Watanabe et al., Plasma and Fusion Research 2 (2007) 027
[7] A. Komatsu et al., Phys. Scr., in press
[8] X.B.Ding et al. submitted to J. Phys. B

Progress and Outlook of Plasma Industrial Application (14C)

Rikizo Hatakeyama[1] and Motoyasu Sato[2]

[1]*Department of Electronic Engineering, Tohoku University, 6-6-05 Aza-Aoba, Aramaki, Aoba-ku, Sendai 980-8579, Japan E-mail: hatake@ecei.tohoku.ac.jp*
[2]*National Institute for Fusion Science, 322-6 Oroshi-cho, Toki 509-5292, Japan*
Email: satomoto@lhd.nifs.ac.jp

1. TRANSITION SUMMARY AND FUTURE DIRECTION

The two branches in the 14C framework were established in 2001. One is "Heating behavior of Blast Furnace Slag Bearing High Ti Under Microwave". Finally, the knowledge were extended to the researches. The mechanism of microwave processing has been extending to all the industries to be the most promising candidate for reducing the exhaust of carbon dioxide. The personal exchanges, such as done between Prof. N.Yoshikawa of Tohoku University and Professor Bai of Chongqing University, helped to progress the research and developments of microwave applications to the blast furnace.

Concerning the other branch, on the other hand, after a starting phase of 2001 the subject was settled to be "Development of High Pressure Plasmas for Environmental Application and Materials Processing" in 2002, which has been adopted thereafter till now. In this first term of 2001-2004, various kinds of equilibrium high-pressure arc discharge and nonequilibrium atmospheric-pressure corona and glow discharge plasmas in a wide range of frequencies were improved and developed to be applied to the purification of waste water and exhausted gases and processes for surface-engineering related materials, based on discussion and collaborations on the mutual interchange.

In addition to this development of high pressure plasmas for traditional environmental application and materials processing, special attention was directed to a nanotechnological application of gaseous plasmas in the second term of 2005-2007. Some examples of the researches concerned are nanoscopic-surface processes and syntheses of fullerenes, carbon natotubes, and carbon nanocoils using low pressure glow discharge plasmas and high pressure arc discharge plasmas.

Furthermore, in addition to environmental and nanotechnological investigations, aspects of biotechnological application have gradually been introduced to this program in the third term of 2008-2010 since the end of the second term. Some examples of the researches concerned are bacteria inactivation and medical instrument sterilization using low-temperature plasmas, and on-site inspection of food hygiene and measurement of atmospheric pollutants using atmospheric-pressure discharge plasmas.

11 (10 organizations) and 13 (4 organizations) scientists have been delegated from Japan to China and from China to Japan, respectively, for five years in 2006-2010 in the case of the branch "Development of High Pressure Plasmas for Environmental Application and Materials Processing", as listed in Table 1.

According to the stream of results achieved so far, one of the important future-subjects on plasma industrial application of JSPS-CAS Core University Program is predicted to be the fusion of science and technology among environmental, nanotechnological, biotechnological, and medical fields such as environmental nanomedicine using high-/low-pressures gaseous, liquid, and gas-liquid interfacial plasmas.

JSPS-CAS Core University Program (2006-2010)

"Development of High Pressure Plasmas for Enviromental Application and Materials Processing"

Country / Year	JAPAN → CHINA		CHINA → JAPAN	
2006	H. Takigawa (Toyohashi Univ. of Technol.)	S. Fan (Tsinghua Univ.)	J. Zhang (Donghua Univ.)	H. Sugai (Nagoya Univ.)
	H. Akiyama (Kumamoto Univ.)	Q. Zhang (Xi' an Jiaotong Univ.)	Z. Hu (Nanjing Univ.)	H. Takigawa (Toyohashi Univ. of Technol.)
2007	T. Fujiwara (Iwate Univ.)	Y. Leng (Southwest Jiaotong Univ.)	J. Nan (ASIP)	R. Hatakeyama (Tohoku Univ.)
	K. Yukimura (Doshisha Univ.)	N. Huang (Southwest Jiaotong Univ.)	Y. Lan (ASIPP)	M. Nagatsu (Shizuoka Univ.)
2008	M. Nagatsu (Shizuoka Univ.)	Y. Meng (ASIPP)	Y. Meng (ASIPP)	M. Nagatsu (Shizuoka Univ.)
	K. Terashima (Univ. of Tokyo)	H. Li (Tsinghua Univ.)	C. Cheng (ASIPP)	T. Fujiwara (Iwate Univ.)
2009	M. Kogoma (Sophia Univ.)	D. Wang (Dalian Univ. of Technol.)	X. Wang (ASIPP)	M. Nagatsu (Shizuoka Univ.)
	T. Hirata (Tokyo City Univ.)	C. Dong (Dalian Univ. of Technol.)	G. Ni (ASIPP)	H. Toyoda (Nagoya Univ.)
	H. Toyoda (Nagoya Univ.)	R. Liang (Fudan Univ.)	J. Shen (ASIPP)	T. Matsumura (Nagoya Univ.)
2010	T. Kaneko (Tohoku Univ.)	C. Liu (Tianjin Univ.)	S. Fang (ASIPP)	M. Nagatsu (Shizuoka Univ.)
	A. Mizuno (Toyohashi Univ. of Technol.)	K. Yan (Zhejiang Univ.)	L. Chen (ASIPP)	S. Hamaguchi (Osaka Univ.)
			J. Luo (Donghua Univ.)	K. Nakamura (Kyushu Univ.)
			Y. Meng (ASIPP)	H. Toyoda (Nagoya Univ.)

2. TYPICAL RESULTS

2.1 Discharge Methods for Atmospheric Pressure Plasma Production (T. Fujiwara: Iwate Univ.)

Discharge methods for production of atmospheric pressure plasma, metallic plasma sources for plasma-based ion implantation and deposition(PBII&D), and the mechanism and application of atmospheric pressure discharge were discussed in Tsinghua University, Southwest Jiaotong University, and Iwate University, respectively. In addition, the lecture of NO_x removal by non-thermal plasma was delivered in Yanshan University.

Consequently it is found that the multipoint barrier discharge is an effective method for the production of atmospheric pressure plasma, and the shunting arc discharge is a convenient plasma source of metals and semi-metals, such as titanium, carbon, silicon and tungsten, which promises to be a cost-effective technology for ion implantation and deposition.

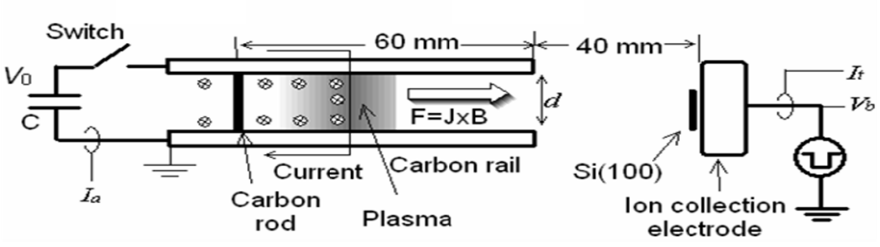

Fig. 1: Shunting arc discharge for hybrid plasma production and its magnetic drive for PBII&D.

[1] K. Takaki, Y. Hatanaka, K. Arima, S. Mukaigawa, and T. Fujiwara, *Vacuum* **83** (2008) 128.

[2] K.Takaki, S.Mukaigawa, T.Fujiwara, and K.Yukimura, *Surface & Coatings Technol.* **201** (2007) 6490.

2.2 Discharge Configuration with Single and Spiral-Type Electrodes (M. Kogoma: Sophia Univ.)

The waveform of the conduction current in the discharge of single-electrode configuration is much similar to that in the glow discharge in AP DBD rather than the filament discharge. We can see that the waveform of the conduction current in the discharge of single-electrode configuration is much similar to that in the glow discharge in AP DBD rather than the filament discharge [1] .

The gas temperatures of the Ar base capillary plasma discharge at various gas flow rates were determined by the spectroscopic analysis of OH *A-X* spectrum by Prof. Dezhen Wang et al [2]. The discussion about effect of gas flow on electrical discharge characteristics was presented and it is found that the heat removal by Ar gas flow plays the most important role in determining its electrical characteristics. The rotation temperature was estimated higher than 450K in Ar discharge .

Spiral type electrode configuration in tube discharge system has been developed by Okazaki and Kogoma using He base glow discharge under atmospheric pressure [3]. In the case of He discharge, the gas temperature is lower than 100 K that is much lower than in Ar base glow discharge. Because the thermal conductivity of He is ten times higher than in Ar . On the contrary, the specific heat Cp of He is ten times lower than in Ar. From the reason, in the He discharge , the escape energy by thermal conduction to the tube wall is much higher than that of the heat capacity conduction of flowing gas. The energy escaping system in He is very different from that of Ar. So, in the case of polymer deposition on the inner face of the tube, He base discharge is better choice than Ar base discharge on the view point of the gas temperature .

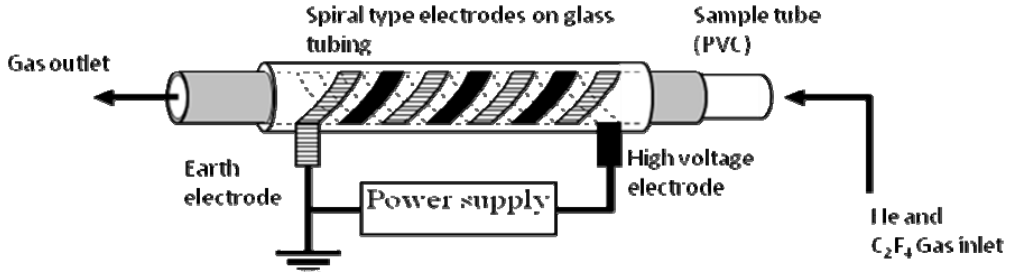

Fig. 2: Spiral type electrode system in tube discharge system.

[1] S. Z. Li, W. T. Huang, and D. Wang, *Phys. Plasmas* **16** (2009) 093501.
[2] S. Z. Li, W. T. Huang, and D. Wang, *IEEE Trans. Plasma Sci.* **37** (2009) 1825.
[3] S. Okazaki and M. Kogoma, *J. Photopolymer Sci. & Technol.* **6** (1993) 339.

2.3 Strip-Line Microwave Micro Atmospheric Plasma and Application to Neutralization (K. Terashima: Univ. of Tokyo)

We estimate the plasma parameters of strip-line microwave micro atmospheric plasma (SMMAP) such as rotational temperature (T_r) both from OH and N_2 rotational transitions (610–770 and 770–980 K in Ar, respectively), electron density (N_e) from Stark broadening (about 10^{13} /cm^3 in mixture of Ar and H_2), and the distribution of electric field before ignition of SMMAP (5×10^4 V/m at maximum, and applied voltage less than 5 V). Since the lower applied voltage of SMMAP might enable us to conduct efficient processing without electrostatic damage (ESD), we applied jet-type SMMAP to neutralization. The result of neutralization

showed that it can reduce surface charge from ±1000 to ±100 V for 0.2 s at 10 W with Ar gas flow within 4 V offset voltage, which provides efficient plasma processing without ESD.

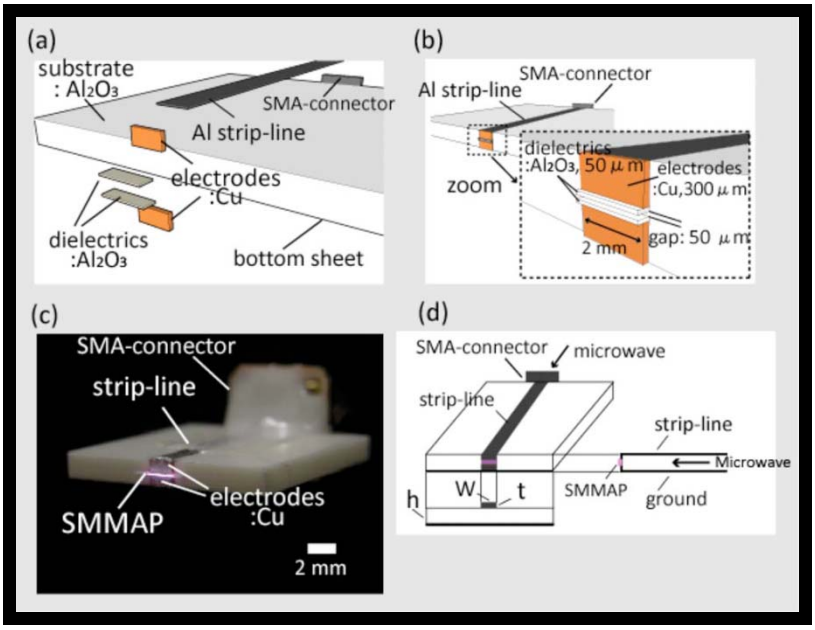

Fig. 3: (a) Components of SMMAP substrate, (b) SMMAP substrate and its close-up figure, (c) generation of SMMAP in air, and (d) cross section of SMMAP substrate.

[1] K. Ogata and K. Terashima, *J. Appl. Phys*. **106** (2009) 023301.

2.4 Discharge Plasmas in Water (H. Akiyama: Kumamoto Univ.)

Firstly the information exchange was carried out in the following way. Akiyama delivered a special lecture of "Pulsed Power Technologies and Application" for 90 minutes. Then graduate students of Xi'an Jiaotong University presented their research, and we discussed the problems on researches mentioned below.

- What is new researches of plasmas produced under an atmospheric pressure ?
- What is the know-how to make plasmas in water ?
- How to make a pulsed power generator using magnetic switches.
- What is the know-how to produce pulsed power with a shorter risetime.

Secondly the role share was taken up, i.e., a level-up of the production of discharge plasmas in water was necessary to develop applications of environment at Xi' an Jiaotong University. Akiyama did a guidance how to make discharge plasmas in water.

Thirdly an experiment on discharge plasmas in water was demonstrated because students at Xi'an Jiaotong University had not been able to produce discharge plasmas in water. Akiyama changed the experimental apparatus totally. Though the diameter of plasmas was small, the discharge plasmas were produced successfully during a Akiyama's short stay as shown in photograph. Another photograph was taken at that time for memory.

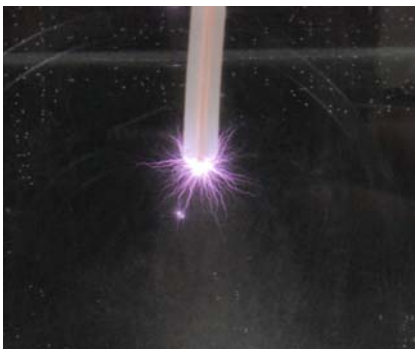

Fig. 4: Demonstration of plasma discharge in water.

2.5 Wet Electrostatic Precipitators for Higher Performance Accompanied by Simultaneous Removal of SO_2 and Discharge above w ater forRadical Injection to Water (A. Mizuno: Toyohashi Univ. of Technol.)

The wet electrostatic precipitation has attracted attention in Dalian Institute of Technology, and Zhejiang University since this system shows better performance of electrostatic precipitation of suspended dust particles. Especially when dust resistivity is very high, wet ESP does not cause reduction of efficiency due to breakdown of high resistivity dust on the collection electrode. This system can also absorb SO_2 simultaneously. Material against corrosion is of interest. These institutions have started research on this method.

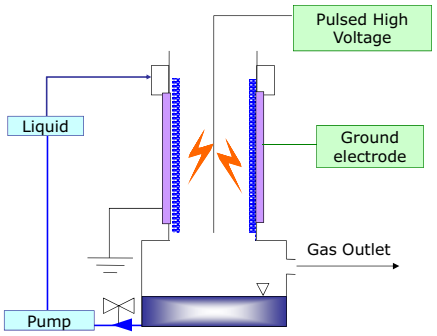

Fig. 5: Schematic of wet electrostatic precipitator.

Discharge above water, or in water is of interest in various researchers including Dalian Institute of Technology, Dalian Maritime University, Shanghai Jadong University and Zhejian University. Radicals produced by the ionization are effectively injected into water. This enables rapid oxidation of impurities in water and effective sterilization of bacteria and other microbes.

2.6 Environmental and Medical Applications of Plasma Technology (M. Nagatsu: Shizuoka Univ.)

Firstly we pursued an environmental application of plasma technology using 2.45 GHz miciro-wave surface plasma. It was experimentally verified that Ni ions are successfully removed for waste solution. Secondly this micro wave was also attempted to be utilized for a medical application. N_2 and N_2/O_2 plasmas were found to be effective for sterilization of G. Stearothermophillus spores. A possible mechanism of inactivation of spores is considered to be the VUV/UV effect in the N_2 plasma and the etching effect due to O radicals in the O_2 plasma. Furthermore, sterilization of G. Stearothermophillus spores was tried using atmospheric dielectric barrier discharge (DBD) plasmas. Inactivation of wrapped biological indicator was demonstrated using a flexible DBD plasma, and an effect of water vapor addition in addition to ozone and UV emission on sterilization property was apparently observed.

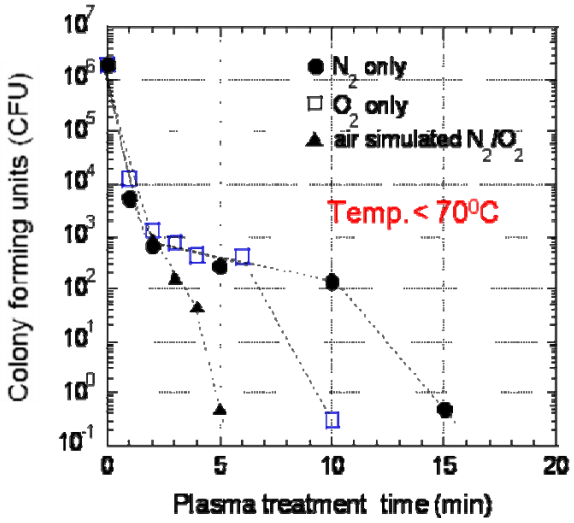

Fig. 6: Sterilization progress as a function of plasma treatment time.

[1] C. L. Chen, B. Liang, A. Ogino, X. Wang, and M. Nagatsu, *J. Phys. Chem. C* **113** (2009) 7659.
[2] H. Eto, Y. Ono, A.Ogino, and M.Nagatsu, *Appl. Phys. Lett.* **93** (2008) 221502.
[3] M. K. Singh, A. Ogino, and M. Nagatsu, *New J. Phys.* **11** (2009) 115027.
[4] Y. Zhao, M. K. Singh, A.Ogino, and M.Nagatsu, *Thin Solid Films* **518** (2010) 3590.

2.7 Micro-Spot Atmospheric Pressure Plasma Production for the Bio-Medical Application (T. Hirata: Tokyo City Univ.)

Plasma medicine covering medical treatments, burn wound, dermatitis, DNA introduction into cells and so on has recently attracted much attention. Especially in USA and EU, clinical test and treatment product development are on the move. However, mechanisms of medical treatment using plasmas are not clear because many factors such as electric field, electromagnetic field, proteins in the cells, and nitric oxide (NO) simultaneously operate more or less under the plasma irradiation to living bodies, tissues, and cells. Our goal is the clarification of the mechanisms and development of novel plasma applications. Here we report medical treatment and cell activation using micro-spot atmospheric pressure plasmas.

The device is a coaxial structure having a tungsten wire installed inside a glass capillary, and a grounded tubular electrode wrapped on the outside. The small animal used in the experiment involving plasma irradiation into living tissue was a Wistar male rat and is deeply anesthetized with the gas anesthesia. In an experiment testing the effects of plasma irradiation on rats that were artificially given burn wounds, no evidence of electric shock injuries was found in the irradiated areas. In fact, the observed evidence of healing and improvements of the burn wounds suggested the presence of healing effects due to ion/radical collisions on the right area.

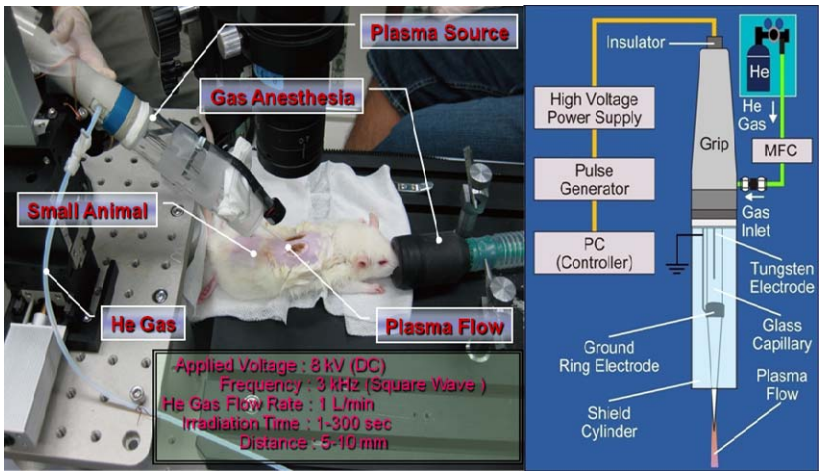

Fig. 7: Micro-spot atmospheric pressure plasma source and experimental configuration.

2.8 Nanotechnological and Biotechnological applications of liquid related plasmas (T. Kaneko: Tohoku Univ.)

The purpose of visit to Tianjin University and Dalian University of Technology was to discuss problems concerning creation of various kinds of nanoparticles and novel nano-bio composite materials, such as carbon nanotubes and DNA, using atmospheric pressure and novel gas-liquid interfacial plasmas, and concerning applications of the nano-bio composite materials to bio-sensor, drag delivery system, bio-medicine, environment, and so on.

In the former university the research subjects were generation of plasmas in contact with ionic liquid, synthesis of new kinds of catalysts for fuel cell using plasmas, and synthesis of nanopore and nanoparticles for biological/ environmental applications. Firstly the lecture titled "Generation of Gas-Liquid Interfacial Plasmas and Application to Novel Nano-Bio Material Synthesis" was given by Kaneko, and subsequently the effects of plasma ion irradiation to the ionic liquid and the synthesized nanoparticles was discussed effectively. Then the laboratory tour was held, where plasma sources such as gas-liquid interfacial plasma and atmospheric barrier discharge plasma, and measurement devices such as FTIR, UV-vis, SEM, STM, and so on were introduced.

In the latter university the subjects were the synthesis of carbon nanotubes using an arc discharge plasma, synthesis of graphene using an atmospheric pressure barrier discharge plasma, and nanoparticles synthesis for super-capacitor and fuel cell. The lecture titled "Fabrication of Infrared Solar Cells Using Plasma-Processed Carbon Nanotubes" was given by Kaneko, and subsequently the separation of metallic and semiconducting carbon nanotubes was discussed effectively. Then experimental equipments were introduced, which are related to an atmospheric pressure barrier discharge plasma for graphene synthesis, an arc discharge plasma for carbon nanotube synthesis, and measurement of surface areas of the nanopore and nanoparticles

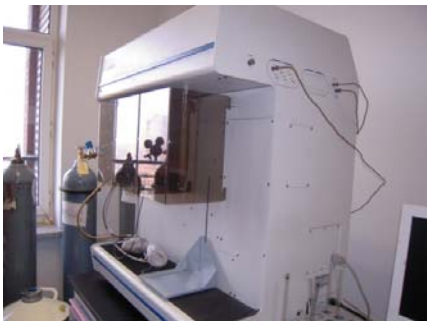

Fig. 8: Instrument for measurement of surface areas of the nanopore and nanoparticles.

3. A HIGHLIGHTENED TOPIC

— Generation of Gas-Liquid Interfacial Plasmas and Application to Novel Nano-Bio Material Synthesis (T. Kaneko and R. Hatakeyama: Tohoku Univ.) —

Recently, several works on gas-liquid interfacial discharge plasmas (GLIDPs) have been performed as fundamental and applied researches [1]. Among them, the synthesis of various kinds of nanoparticles using the plasma-liquid interfaces [2][3] is advantageous in that toxic stabilizers and reducing agents are unnecessary and the synthesis is continuous during the plasma irradiation. In addition, the nanoparticles conjugated with carbon nanotubes (CNTs), which are very fascinating materials in electronic, magnetic, and optical applications, could constitute promising nanoelectronics devices such as gas sensors [4], field-effect transistors, and so on. Up to now, electrochemical decoration [5] and supercritical fluid [6] methods have been utilized for the synthesis of the nanoparticles conjugated with the CNTs. However, the nanoparticles usually attach to the outside of the CNTs, and as a result, they easily agglutinate and change in quality by the heat or chemical reactions. Therefore, it has been claimed that the nanoparticles should be intercalated into the interlayer of the bundled CNTs. Based on these backgrounds, we attempt to develop a novel nanoparticles synthesis method using gas (plasma) / liquid (ionic liquids) interfacial fields under low gas pressures, where the various kinds of nanoparticles can be generated and intercalated into the

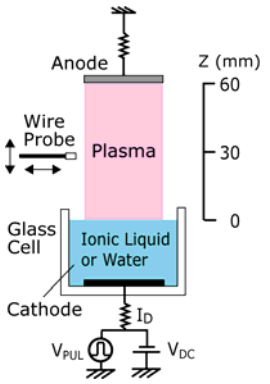

Fig. 9: Experimental apparatus. This discharge configuration is defined as "A-mode"

CNTs [7].

Figure 9 shows the schematic diagram of an experimental setup for the GLIDP [8], which has a glass cell with 15 mm inner diameter and 10 mm depth in a cylindrical glass chamber with 75 mm diameter and 200 mm length. A cathode electrode composed of liquid (an ionic liquid or water) is located inside the glass cell and DC or pulse power is supplied to the cathode electrode. On the other hand, a grounded anode electrode composed of a stainless steel (SUS) plate is set in the gas-phase region at a distance of 60 mm from the surface of the cathode electrode. This discharge configuration is defined as "A-mode". To examine the effects of the power supplied to the liquid electrode on discharge-related phenomena, the cathode electrode is switched to the SUS plate in the gas phase, and the liquid electrode is grounded instead, which is defined as "B-mode". Argon gas is adopted as a discharge gas, and the gas pressure P_{gas} is varied from 20 Pa to 40 kPa. A Langmuir probe is inserted at the position of z = 0–60 mm to measure the parameters of the plasma in contact with the ionic liquid (z = 0: surface of the cathode electrode).

We successfully generate ionic liquid incorporated plasmas at low gas pressures with high stability, similar to normal glow discharge plasmas. It is found that the secondary electrons are emitted from the ionic liquid more efficiently than the SUS electrode by the irradiation of the high energy ions to the cathode electrode in A-mode and electrons to the anode electrode in B-mode. Therefore, it is expected that the liquid electrode enhances the chemical reactions at the interface between the plasma and the ionic liquid, and is effective for the synthesis of nanomaterials.

This newly-developed novel gas-liquid interfacial plasmas can be utilized for the synthesis of the various kinds of nano-bio composite materials as shown in Fig. 10. Here, we introduce the synthesis of metal nanoparticles using the plasma irradiation to the liquid electrodes [9][10], and conjugate them with carbon nanotubes [11] for the purpose of controlling the particle size, inter-particle distance, optical and electrical properties, and so on. Furthermore, we attempt to synthesize the nanoparticles conjugated with DNA and insert them into the carbon nanotubes for applications to the bio sensor, drug delivery system, gene therapy, and so on. In addition, we demonstrate to create DNA encapsulated carbon nanotubes using a plasma ion irradiation method in an electrolyte plasma [12][13] and realize the control of electric properties of the carbon nanotubes by changing the base sequence of the encapsulated DNA [14].

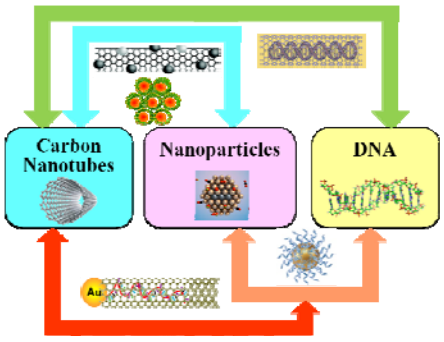

Fig. 10: Schematic model of the synthesis of conjugates between metal nanoparticles, carbon nanotubes, and DNA.

To synthesize the functionalized CNTs conjugated with nanoparticles, we attempt to make gold nanoparticles (AuNPs) using the CNTs as a template in the GLIDP. The bundled CNTs are impregnated with the Au chloride dissolved in the ionic liquid, and are exposed to the GLIDP in B-mode. As a result, the Au chloride is reduced inside the bundles of the CNTs by the electron irradiation and the AuNPs are synthesized. Since the CNTs inhibit the agglomeration of the AuNPs due to their small inside space, the uniform and small seized AuNPs are expected to be synthesized. Figure 11 presents the transmission electron microscope (TEM) image of AuNPs synthesized between the bundled CNTs in the ionic liquid for P_{gas} = 60 Pa, discharge current I_D = 1 mA, and plasma irradiation time t = 10 min. It is found that the high density, mono-dispersed, and small-seized (1~2 nm) AuNPs are synthesized by controlling the GLIDP. Furthermore, the density of the AuNPs can be controlled by changing the plasma irradiation time and the concentration of the Au chloride dissolved in the ionic liquid.

For the application to an effective DNA delivery system using CNTs as the vector, we

synthesize size-controlled AuNPs conjugated with DNA using pure water and a pulse power source in place of the ionic liquid and DC power source, respectively. Single-stranded DNA with 30 guanine bases (denoted as G_{30}) is used as the stabilizing agent. The Ar pressure is 40 kPa. Figure 12 gives the TEM images for products synthesized at different G_{30} concentrations. The AuNPs (~18 nm) synthesized without G_{30} precipitate quickly after the synthesis. In the presence of G_{30}, interestingly, the AuNPs drastically change to water-soluble products, which consist of the dispersedly small-sized AuNPs (~7 nm) (G_{30} concentrations less than ca. 1 μM). However, the AuNPs take on an agglomerated form (~31 nm) for G_{30} concentrations lager than ca. 1.5 μM. Therefore, the optimized DNA concentration is necessary to synthesize the small-sized DNA-AuNPs conjugate for the DNA delivery system.

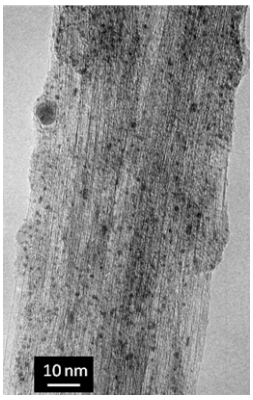

Fig. 11: TEM image of AuNPs synthesized using the CNTs as a template. P_{gas} = 60 Pa, I_D = 1 mA, t = 10 min.

Since it is demonstrated below that DNA can be encapsulated into the CNTs using a plasma ion irradiation method [12][13], we propose that the DNA–AuNPs could be encapsulated into or intercalated between the CNTs by adopting the same method. Alternatively, since the AuNPs can move in a light field [15], the DNA–AuNPs could be manipulated by the light, i.e., inserted into and extracted from the carbon nanotubes.

On the other hand, the CNTs encapsulating biomolecules such as DNA is the most promising material for the electronic modification, because DNA is well known to consist of four kinds of bases, each of which has a different electronic property. Since the base sequence has come to be easily controlled recently, the control of electrical characteristics of the CNTs can be performed by encapsulating DNA, the base sequence of which is properly selected.

The schematic of an experimental apparatus for DNA encapsulation inside CNTs is shown in Fig. 13(a). A direct-current (DC) electric field is applied to the DNA electrolyte plasma (DNA solution) by applying the DC bias voltage (V_{DC} = 10 V) between micro gap electrodes (d=1 mm) in order that the DNA negative ions are moved to the anode electrode coated with single-walled (SWNTs) and double-walled (DWNTs) carbon nanotubes in the same way as the plasma ion irradiation method in the gas phase plasmas [16], where the CNTs are treated by heat for opening their tips in advance and are aligned along the double-layer electric field in front of the anode electrode. In addition, a radio-frequency (RF) electric field in the electrolyte plasma, which is generated by the applied RF voltage (V_{RF} = 0-150 V, f_{RF} = 1 MHz), plays a role in stretching random-coil-shaped DNA molecules due to the interaction between induced dipoles in the DNA molecules and the external RF electric field (dielectrophoresis) [17]. The DNA irradiation time is fixed at t=10 min.

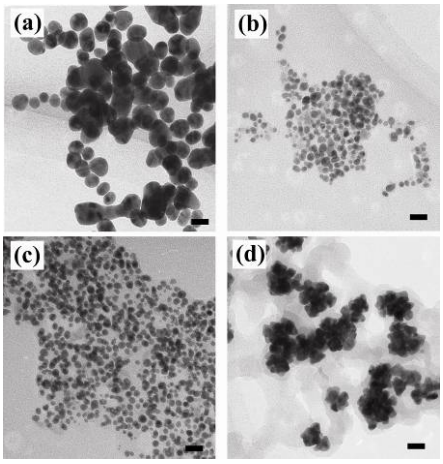

Fig. 12: TEM images of AuNPs synthesized with DNA concentrations of (a) 0, (b) 0.35, (c) 0.7, and (d) 1.75 μM. Scale bar is 20 nm. The TEM image of AuNPs synthesized without DNA is obtained by measuring the precipitate.

Several kinds of single-stranded DNA molecules which have different bases are used to be encapsulated into the SWNTs. By means of this plasma ion irradiation system, it has been realized that the DNA is encapsulated into the SWNTs [12].

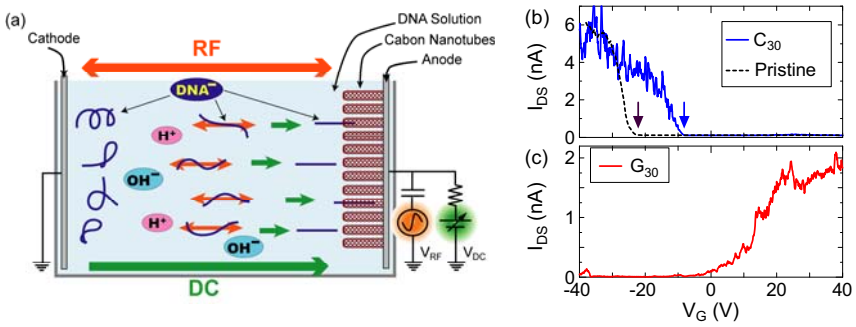

Fig. 13: (a) Schematic of experimental apparatus, and I_{DS} vs V_G characteristics for (b) pristine SWNT (dotted line) and C_{30} encapsulated SWNT (blue solid line), and (c) G_{30} encapsulated SWNT (red solid line).

Using the DNA encapsulated SWNTs (DNA@SWNTs), we fabricate the SWNT-based FET device. The electrical transport measurements, i.e., the source-drain current I_{DS} as a function of the gate voltage V_G for a fixed source-drain voltage V_{DS}, are performed at room temperature under vacuum conditions on a semiconductor parameter analyzer.

The transport property of the pristine semiconducting SWNTs is well known to exhibit the p-type characteristic as shown in Fig. 13(b) (dotted line). The transport property of the SWNTs encapsulating DNA with cytosine (C_{30}) is presented as a blue solid line in Fig. 13(b). The typical p-type characteristic is observed, however the threshold voltage for hole conductance is found to shift from –22 V to –8 V compared with that of the pristine SWNTs, indicating that the p-type characteristic of the SWNTs is enhanced by the encapsulation of C_{30}. In contrast, the SWNTs encapsulating DNA with guanine (G_{30}) drastically change to the n-type semiconductor, the transport property of which is presented in Fig. 13(c) [14].

Therefore, the base-sequence controlled DNA@SWNTs are expected to be applied to nano/bio photoelectronic devices and nanomedicine systems.

[1] P. Bruggeman and C. Leys, *J. Phys. D: Appl. Phys.* **42** (2009) 053001.
[2] S. A. Meiss, M. Rohnke, L. Kienle, et al., *ChemPhysChem* **8** (2007) 50.
[3] J. Hieda, N. Saito, and O. Takai, *J. Vac. Sci. Technol. A* **26** (2008) 854.
[4] J. Kong, N. R. Franklin, C. Zhou, M. G. Chapline, S. Peng, K. Cho, and H. Dai, *Science* **287** (2000) 622.
[5] G. G. Wildgoose, C. E. Banks, and R. G. Compton, *Small* **2** (2005) 182.
[6] X. Ye, Y. Lin, C. Wang, M. H. Engelhard, Y. Wang, and C. M. Wai, *J. Mater. Chem.* **14** (2004) 908.
[7] T. Kaneko, Q. Chen, T. Harada, and R. Hatakeyama, *Plasma Sources Sci. Technol.* in press.
[8] T. Kaneko, K. Baba, and R. Hatakeyama, *J. Appl. Phys*. **105** (2009) 103306.
[9] K. Baba, T. Kaneko, and R. Hatakeyama, *Appl. Phys. Express* **2** (2009) 035006.
[10] T. Kaneko, K. Baba, T. Harada, and R. Hatakeyama, *Plasma Process. Polym.* **6** (2009) 713.
[11] K. Baba, T. Kaneko, R. Hatakeyama, K. Motomiya, and K. Tohji, *Chem. Commun.* **46** (2010) 255.
[12] T. Okada, T. Kaneko, R. Hatakeyama, and K. Tohji, *Chem. Phys. Lett*. **417** (2006) 288.
[13] Y. F. Li, T. Kaneko, and R. Hatakeyama, *Small* **6** (2010) 729.
[14] T. Kaneko and R. Hatakeyama, *Appl. Phys. Express* **2** (2009) 127001.
[15] K. Wang, E. Schonbrun, and K.B. Crozier, *Nano. Lett.* **9** (2009) 2623.
[16] R. Hatakeyama, T. Kaneko, W. Oohara, Y. F. Li, T. Kato, K. Baba, and J. Shishido, *Plasma Source Sci. Technol.* **17** (2008) 024009.
[17] M. Washizu and O. Kurosawa, *IEEE Trans. Ind. Appl.* **26** (1990) 1165.

Synthesis Alkaline Anion-exchange Membrane by Plasma Polymerization

Y. D. Meng*, J. Hu* , C.X. Zhang* , Hirotaka Toyoda† and Masaaki Nagatsu ‡

* Institute of Plasma Physics, CAS, P.O. Box 1126, Hefei, Anhui, China 230031

† Department of Electrical Engineering and Computer Science Nagoya University

C3-1(631), Furo-cho, Chikusa-ku, Nagoya 464-8603 Japan

‡ Graduate School of Science and Technology, Shizuoka University

3-5-1 Johoku, Naka-ku, Hamamatsu, 432-8561 Japan

Abstract Plasma polymerization was developed for alkaline anion-exchange membranes synthesis using vinylbenzyl chloride as monomer. The membrane was deposited in the rear of plasma. X-ray photoelectron spectroscopy and attenuated total reflection Fourier transform infrared spectroscopy were used to characterize the chemical structure properties of plasma-polymerized membranes. Ion-exchange capacities of quaternized poly(vinylbenzyl chloride) (QPVBC) membranes were measured to evaluate their capability of hydroxyl ion transport. A mechanism of plasma polymerization using VBC as monomer that accounts for the competitive effects of free radicals polymerization and plasma ablation in the plasma polymerization process was proposed. Our results indicate that plasma discharge power influences the contents of functional groups and the structure of the plasma polymer membranes, which attribute to the coactions of polymerization and ablation. The properties of uniform morphology, good adhesion to the substrate, high thermal stability and satisfying anion conduction level suggest the potential application of QPVBC membrane deposited at discharge power of 20 W in alkaline direct methanol fuel cells.

1. Introduction

Direct methanol fuel cells (DMFCs) have been recognized as one of the most promising energy source for transportation, potable electronics and stationary applications in the future due to their high energy density and portability [1]. Most efforts have been directed toward proton exchange membrane direct methanol fuel cell (PEMDMFC) thanks to its numerous advantages. However, its slow kinetics at the anode, methanol crossover through the membrane and high cost due to the use of noble metals especially platinum (Pt) as catalyst constitute major obstacles for a widespread development in applications [2, 3]. To overcome these problems of PEMDMFC, there has been a growing interest in the development of alkaline direct methanol fuel cells (ADMFCs) using alkaline anion-exchange membranes (AAEMs) as polymer electrolyte, due to a summary of benefits: ⑴lower methanol permeability [1]; ⑵lower overpotentials associated with many electrochemical reactions at high pH [4, 5]; ⑶potential to forego noble metal catalysts [6].

Various methods have been exploited to prepare AAEMs which is recognized as one of the main technical challenges limiting ADMFC performance. Some important developments came from Varcoe and co-workers who prepared AAEMs by radiation grafting of vinylbenzyl chloride (VBC) onto completely or partially fluorinated polymers [7-10]. Several groups have reported the synthesis of AAEMs by performing a chloromethylation reaction on the polymer to form benzylic chloromethyl groups and then converting the benzylic chloromethyl groups into benzyltrimethylammonium cationic groups in subsequent steps [3, 11-16]. However, due to the weak adhesion to the electrode surface, AAEMs can be easily peeled off from the electrode resulting in high interfacial resistance and poor cell performance. Moreover, in order to enhance the chemical and thermal stability of AAEMs, crosslinkers such as glutaraldehyde are needed to get cross-linked structure, leading to low hydroxyl conductivity [17].

Plasma polymerization is under active study because of its effect on fabricating ion-exchange

membranes with good adhesion to electrode using electrode as substrate, a few microns thickness, uniform morphology, pinhole-free and flat surface structure, and highly cross-linked chemical structure [18-20]. In plasma polymerization process, exciting species such as electrons, ions and atoms generated in glow discharge bombard with monomer creating active species for polymerization and, as a result, depositing high cross-linked films on the substrate surface. However, the membrane structure can also be destroyed by plasma bombardment since the formation and degradation of polymers occur simultaneously in plasma polymerization process [21]. In after-glow discharge plasma polymerization (AGD-PP) system, plasma polymers can be generated and deposited away from the plasma discharge region, which allows lower destruction of membranes by plasma bombardment, and higher preservation of the membranes structure.

Vinylbenzyl chloride (VBC) is an excellent monomer for synthesis of AAEMs for having two functional groups: vinyl group for polymerization reaction and benzyl chloride group for quaternization. AAEMs prepared by radiation grafting of VBC onto fluorinated polymers obtained high hydroxyl conductivity and good cell performance [8-10, 22]. The VBC monomer has not been reported as having been used for preparing AAEMs by plasma polymerization so far. In this work, AAEMs were prepared from VBC monomer by forming poly(vinylbenzyl chloride) (PVBC) membranes in AGD-PP system, and then converting the benzylic chloromethyl groups into benzyltrimethylammonium cationic groups in subsequent quaternization and alkalization steps. Because of the low bond dissociation energy of the C-Cl bond in benzyl chloride groups, it is very important to investigate the effects of energy input level on the polymerization [23]. The objectives of this study are: ⑴ to prepare quaternized poly(vinylbenzyl chloride) (QPVBC) membranes with flat and uniform morphology, high thermal stability and high ion-exchange capacities for potential application in ADMFCs; ⑵ to establish the influence of plasma discharge power (energy input) on structure characteristics of the plasma-polymerized PVBC membranes to give information for further understanding the plasma polymerization process and improving the membranes performance.

2. Experimental details

2.1. Plasma polymerization

The plasma-polymerized membranes were synthesized in a capacitively coupled apparatus, depicted in **Fig. 1**. The after-glow discharge system consisted of a stainless steel reactor, vacuum pumps (a mechanical booster pump and a rotary pump), a gas flow control system that included mass flow controllers and reset valves, a radio frequency power supply with corresponding power coupling system, a substrate bias voltage supply and a monomer heater with a temperature control system. The plasma discharge was sustained by a 13.56 MHz power supply between two external electrodes in a Pyrex glass tube (upper part of the reactor), using argon as working gas. The upper part of the reactor was glow discharge region, and the lower part of it was the polymerization region. 4-vinylbenzyl chloride (95%, Alfa Aesar®), without any further

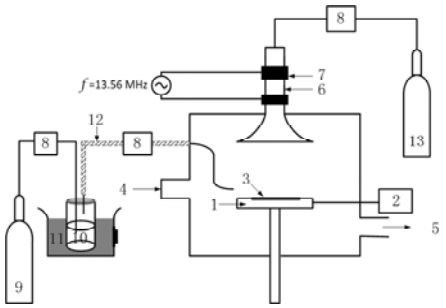

Fig. 1. Schematic diagram of the apparatus used for plasma polymerization. 1-Substrate holder, 2-bias voltage power source, 3-substrate, 4-watch window, 5-to pump, 6-Pyrex glass tube, 7-electrode, 8-gas mass flowmeter, 9-hydrogen liquid gas, 10-liquid monomer in glass test tube, 11-water bath, 12-heating wires, 13-argon liquid gas.

purification, was inlet into the deposition region from one side of the reactor as gaseous state carried by hydrogen. Heating wires were wrapped around the gas lines to avoid the condensation and polymerization of monomer. The flow rates of VBC monomer, hydrogen and argon were controlled by gas mass flow controllers, as shown in Fig. 1. A liquid nitrogen trap was placed in front of the pumps to avoid erosion of the vacuum pumping system by untreated monomer and by-products of the plasma polymerization. The constant parameters in these experiments were 60 Pa for the reactor total pressure (10 Pa for partial pressure of argon) and -10 V for the bias voltage. Silicon wafers [P-doped Si (100)], polytetrafluoroethylene (PTFE) porous membranes and stainless steel plates were used as the substrates.

2.2. Quaternization and alkalization of plasma polymerized membranes

The plasma-polymerized vinylbenzyl chloride (PVBC) membranes were soaked in 33 wt % trimethylamine (TMA, Shanghai Chemical Reagent Store, China) solution at room temperature for 48 h. After soaking, the membranes were washed with deionized water to remove excess TMA solution. The treated membranes were immersed in 1 M potassium hydroxide aqueous solution at room temperature for 48 h to convert the membranes from the Cl^- form into the OH^- form. Then, the membranes were washed by deionized water to remove any trapped potassium hydroxide and finally immersed in deionized water >48 h with frequent water changes.

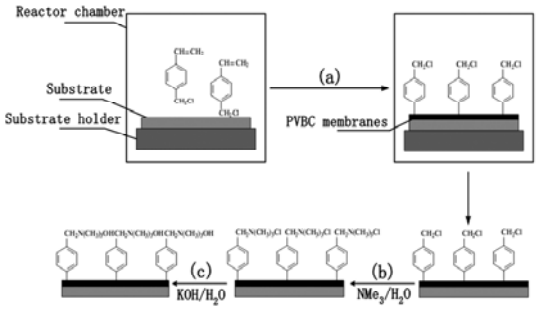

Fig. 2. Schematic diagram for synthesis: (a) plasma polymerization, (b) quaternization, and (c) alkalization.

The reaction sequence of the synthesis of the QPVBC membranes is shown in **Fig. 2**. From Fig. 2, it can be seen that the contents of quaternary ammonium groups in QPVBC membranes are greatly affected by the preservation of benzyl chloride groups in plasma polymerization process.

2.3. Characterization of membranes

The Sirion 200 (FEI, America) scanning electron microscope (SEM) at operation voltage of 5.0 kV was used to determine the cross-section morphology of the PVBC membranes. The chemical structure and composition of the PVBC membranes were analyzed by X-ray photoelectron spectroscopy (XPS) and attenuated total reflection Fourier transform infrared spectroscopy (ATR-FTIR). The XPS analysis was carried out using a Thermo ESCALAB 250 spectroscopy at a power of 150 W with a monochromatic Al Kα radiation at 1486.6 eV. The photoelectrons were detected with a hemispherical analyzer positioned at an angle of 90° with respect to the sample plane, which provided an integrated sampling depth of ~10 nm for XPS. XPS of PVBC membranes were recorded at pass energies of 70 eV for survey spectra and 20 eV for core level spectra. An additional electron gun was used to allow for surface neutralization during the measurements since the plasma polymerized membranes were nonconductive. The energy resolution was about 0.6 eV. The spectrometer energy scale calibration was checked by setting Ag $3d_{5/2}$ = 368.26 eV and the spectra were calibrated with respect to the C 1s peak at 284.6 eV. The curves were fitted with symmetrical Lorentz-Gauss functions. The ATR-FTIR analysis was performed in the range of 4000-670 cm^{-1} on Nicolet NEXUS 870 spectrometer. The spectra were obtained after 256 scans at 2 cm^{-1} resolution with subtracting the contributions from H_2O and CO_2 (gas). The differential thermal analysis (DTA) was used to observe the thermal stability of the

PVBC membranes using DTG-60H (SHIMADZU, Japan) thermal analyzer in flowing nitrogen from ambient temperature to 800 ℃ at a scanning rate of 10 ℃.

The ion-exchange capacities (IECs) of QPVBC membranes were measured by classical back titration method to evaluate the capability of hydroxyl ion transport. For IECs measurement, as reported previously [24], dry samples were accurately weighed and converted to the OH^- form in 1 M potassium hydroxide aqueous solution for 48 h. Three pieces of QPVBC membrane samples prepared in the same time were respectively equilibrated with 25 ml 0.005 M hydrochloric acid for 48 h and then back titrated by 0.005 M sodium hydroxide aqueous solution. IEC values of the samples were calculated as the following relation

$$\mathrm{IEC}\ (\mathrm{mmol}\times \mathrm{g}^{-1}) = \frac{n_{1,\mathrm{HCl}} - n_{2,\mathrm{HCl}}}{m_{\mathrm{dry}}} \qquad (1)$$

where $n_{1,\mathrm{HCl}}$ and $n_{2,\mathrm{HCl}}$ are the amount (mmol) of hydrochloric acid required before and after equilibrium, respectively, and m_{dry} is the mass (g) of the dried sample. The average value of the three samples calculated from Eq. 1 is the IEC value of the measured membrane.

3. Results and discussion

3.1 Morphology of PVBC membranes

The cross-section of plasma membranes deposited on silicon wafer at plasma discharge power of 10 W to 50 W, total pressure of 60 Pa and bias voltage of -10 V can be recorded by SEM image, shown in **Fig. 3.** The plasma-polymerized PVBC membranes are thin and flat with uniform structure at the level of the SEM observation. The thicknesses of the PVBC membranes deposited from 10 W to 50 W, based on SEM image, are 1740 nm, 2880 nm, 608 nm, 400 nm and 787 nm, respectively. From the cross-sectional view in **Fig. 3 (a)**, membrane deposited at 10 W peeled off from the substrate because of its poor practical adhesion to the substrate, suggesting hard preservation of membrane in the quaternization and alkalization steps and application in the ADMFC. However, as shown in **Fig. 3 (b), (c), (d) and (e)**, it is observed that the operation of higher discharge power (20 W to 50 W) improved the practical adhesion between membrane and substrate, and brought better morphology performance of plasma-polymerized membranes for potential application in ADMFC. Therefore, the discharge power of 20 W, 30 W, 40 W and 50 W was chosen for the further investigation.

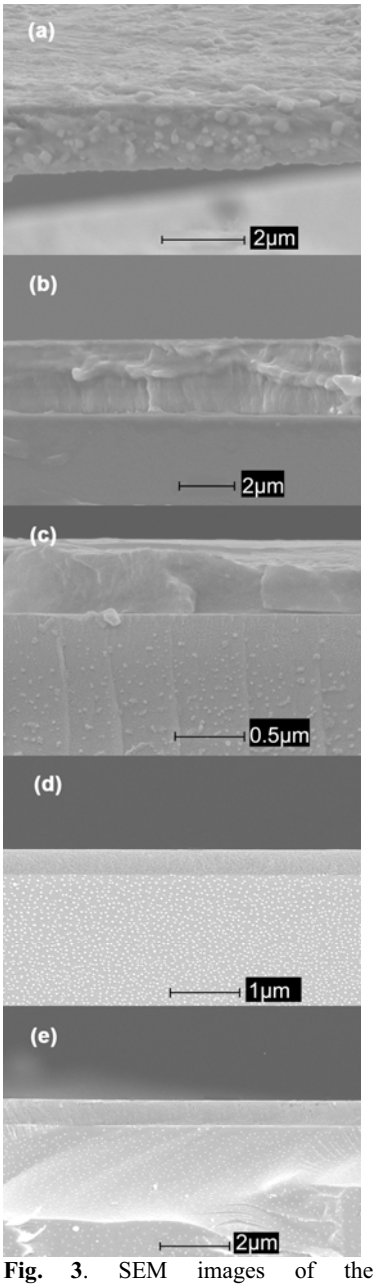

Fig. 3. SEM images of the cross-section morphology of PVBC membranes on silica wafer at total pressure of 60 Pa, bias voltage of -10 V and discharge power of: (a) 10 W, (b) 20 W, (c) 30 W, (d) 40 W and (e) 50 W.

3.2 IEC analysis

IEC is performed to determine the capability of hydroxyl ion transport, and of course, to evaluate the applicability in ADMFCs of obtained membranes. The IEC of QPVBC membrane deposited at discharge power of 20 W is 1.24 mmol/g, which is higher than those of VBC grafted FEP AAEM reported before [8]. **Fig. 4** shows the influence of plasma discharge power on the IECs of QPVBC membranes deposited at the total pressure of 60 Pa and bias voltage of -10 V. It can be observed that the IECs linearly decrease with increasing plasma discharge power from 20 W to 50 W. The operation of higher discharge power enhances the energy level of plasma, leading to more destruction in functional benzyl chloride groups, and thus decreases the IECs which associate with the contents of quaternary ammonium groups of QPVBC membranes. It can also be indicated that the contents of quaternary ammonium groups in QPVBC membranes are greatly influenced by plasma discharge power due to the damage of benzyl chloride groups in plasma polymerization. In this regard, the effects of plasma discharge power on the preservation of benzyl chloride groups of PVBC membranes should be elucidated.

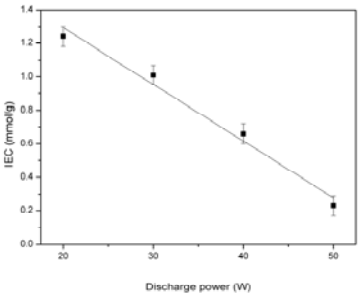

Fig. 4. Influence of plasma discharge power on the IECs of QPVBC membranes deposited on PTFE substrate at the total pressure of 60 Pa and bias voltage of -10 V.

3.3 ATR-FTIR analysis

The chemical structures of PVBC membranes deposited on stainless steel substrate at the total pressure of 60 Pa and bias voltage of -10 V, as a function of plasma discharge power, were analyzed by ATR-FTIR spectra, shown in **Fig. 5**. The absorption at 826 cm^{-1} and 3020 cm^{-1} related to the C-H deformation for para-substituted aromatics and aromatic C-H stretches, respectively, indicates the existence of the benzene ring structure in PVBC membranes at the discharge power of 20 W to 50 W [25, 26]. The peaks at 1265 cm^{-1} and 844 cm^{-1} are assigned to CH_2-Cl wag of benzyl chloride groups and C-Cl stretching vibrations, respectively, suggesting the preservation of the benzyl chloride groups in AGD-PP system[27, 28]. The decrease in the absorption at 1265 cm^{-1} at discharge power from 20 W to 50 W indicates greater polymer damage under the higher discharge power. The absorption at 961 cm^{-1} and 1654 cm^{-1} attributed to the *trans* CH wagging and C=C stretching, respectively, proves the existence of C=C bonds in C-C backbone [28].

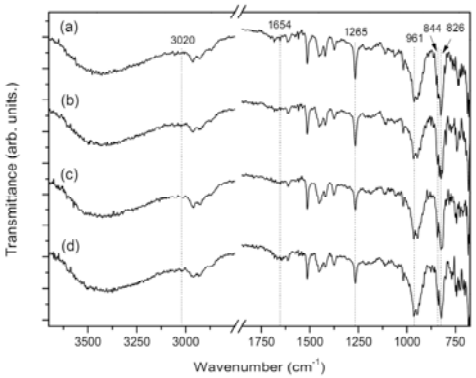

Fig. 5. Influence of plasma discharge power on ATR-FTIR spectra of the PVBC membranes deposited at total pressure of 60 Pa, bias voltage of -10 V: (a) 20 W, (b) 30 W, (c) 40 W and (d) 50 W.

3.3 XPS analysis

In order to characterize the changes in the contents of benzyl chloride groups, XPS data were conducted. **Table 1** shows the XPS results of PVBC membranes with the contents of O, N and Cl expressed as atom %, as a function of discharge power.

Table 1 XPS elemental analysis of plasma-polymerized PVBC membranes as a function of plasma discharge power deposited at total pressure of 60 Pa and bias voltage of -10 V.

PVBC membranes	C (atom %)	N (atom %)	O (atom %)	Cl (atom %)	Cl^{c*} (atom %)	Cl^- (atom %)
20 W, 60 Pa, -10 V	92.00	0.72	4.13	2.98	2.79	0.19
30 W, 60 Pa, -10 V	83.23	4.51	8.58	2.73	0.38	2.35
40 W, 60 Pa, -10 V	83.72	3.37	10.82	2.09	0.39	1.70
50 W, 60 Pa, -10 V	89.54	1.77	7.49	1.19	0.48	0.71

*Cl^c: covalently bonded chlorine species in benzyl chloride groups and polymer backbone

The Cl 2p core-level spectrum of the sample can be curve-fitted with two spin-orbit-split doublets, shown in Fig. 6, with the binding energy for Cl $2p_{3/2}$ peak components located at about 199.9 ± 0.2 eV attributable to the covalently bonded chlorine species in benzyl chloride groups and polymer backbone, and 197.4 ± 0.2 eV related to the ionic chloride (Cl^-) in HCl [29, 30]. The quantitative analysis confirms the high preservation of benzyl chloride groups in PVBC membranes at discharge power of 20 W. The huge decrement of covalently bonded chlorine species under the higher discharge power indicates an effect of plasma ablation [31]. From **Table 1** and **Fig. 6**, it can be seen that the plasma ablation of PVBC membranes at discharge power of 30 W compared with 20 W does not lead to large changes in the content of Cl, but changes in the content of Cl^c (covalently bonded chlorine species in benzyl chloride groups and polymer backbone) obviously. The decrease in the C-Cl fraction at discharge power from 20 W to 30 W indicates that most of the covalently bonded chlorine species might be destroyed by plasma ablation. Moreover, the increase in Cl^- fraction when the discharge power is up to 30 W from 20 W also proves the dissociation of C-Cl bonds and the formation of HCl on the surface of PVBC membranes. At the discharge power from 30 W to 50 W, there are slight changes in the content of Cl^c, whereas, the content of Cl^- decreases. Considering the air contamination during and after plasma polymerization process due to the trapped free radicals within the membrane network and on the membrane surface, the influence of oxygen and nitrogen on membrane chemical structure during plasma polymerization process is hard to estimate [32].

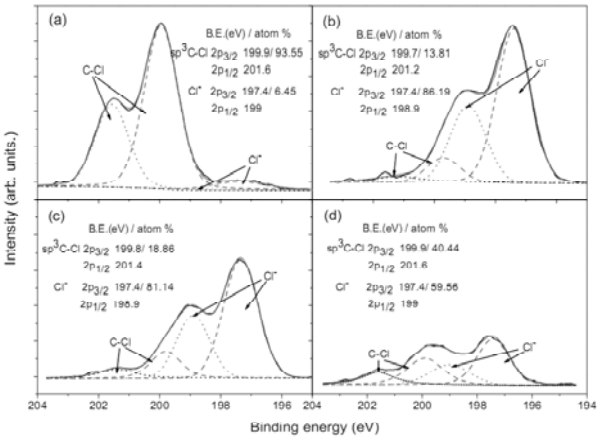

Fig. 6. Influence of plasma discharge power on XPS Cl 2p spectra of the PVBC membranes deposited at total pressure of 60 Pa, bias voltage of -10 V: (a) 20 W, (b) 30 W, (c) 40 W and (d) 50 W.

To acquire more information on the chemical structure characteristics of plasma-polymerized membranes influenced by the plasma discharge power, C 1s spectra were analyzed. As shown in **Fig. 7**, the C 1s peak is deconvolved into four peaks [30, 33-35]: peak (1) at 284.3 eV attributed to the sp^2 carbon atoms (C=C); peak (2) at 284.8 eV corresponded to the sp^3 carbon atoms (C-C and C-H); peak (3) at 286.1 eV related to sp^3 carbon

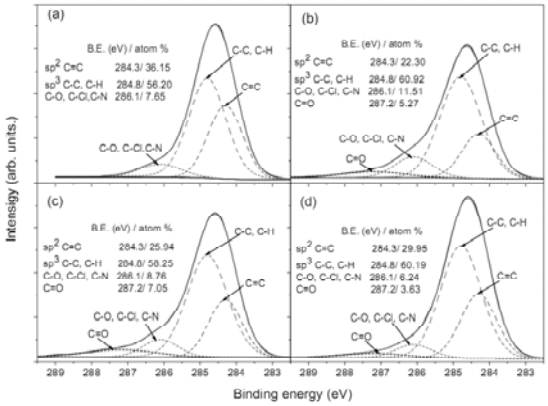

Fig. 7. Influence of plasma discharge power on XPS C 1s spectra of the PVBC membranes deposited at total pressure of 60 Pa, bias voltage of -10 V: (a) 20 W, (b) 30 W, (c) 40 W and (d) 50 W.

carrying one chlorine atom (chlorine fixed by a free radical process on two nonconjugated sp^2 carbon atoms) or to sp^3 carbon bonded to one oxygen atom (C-O); peak (4) at 287.2 eV assigned to the oxygenated groups (carbonyl). The initial decrease in the C=C fraction at discharge power from 20 W to 30 W is likely due to the occurrence of polymerization. Afterward, the C=C fraction increases at discharge power from 30 W to 50 W, whereas Cl^- content decreases and Cl^c content slightly increases. These changes suggest the occurrence of elimination reaction in C-C backbone with participation of chloridion through generating covalently bonded chlorine. A possible reaction mechanism based on XPS analysis might occur during the plasma polymerization process from VBC monomer, as shown in **Fig. 8**. Most studies of plasma polymerization mechanisms suggest that free radicals are the most likely reactive species involved in polymer formation under plasma conditions. It is believed that free radicals are generated firstly on the dissociated π bonds in C=C because of its low bond dissociation energy [23]. Dissociation can also be occurred in C-Cl bonds of benzyl chloride groups when the impinging particles energy is higher than its bond dissociation energy. Free radicals can further react with monomers and active species to form polymerized membranes. Chlorine radicals existing in plasma atmosphere can also react with active species. This process may produce C-Cl bonds in C-C backbone, as shown in **Fig. 8 (a)**. The benzyl chloride groups in polymer membranes might be further destroyed due to the high-energy particles bombardment (as an effect of plasma ablation on polymer), which indicates the decreasing of benzyl chloride groups contents by turning up the discharge power, as shown in **Fig. 8 (b)**. The mechanism of C=C fraction formation may be more complicated. A possibility is the occurrence of elimination reaction through eliminating covalent chlorine and beta hydrogen by the high-energy particles bombardment shown in **Fig. 8 (c)**. This gives reasons for the decrease of Cl^c content while Cl^- content increases. **Fig. 8 (d)** shows another possibility that the C=C bonds may be generated by a series of reactions including the formation of carbonium ion by high-energy particles bombardment, nucleophilic attack by chloridion and elimination reaction. This can be certified by the changes of C=C fraction and Cl^- content and the slight increase of Cl^c content at the discharge power from 30 W to 50 W.

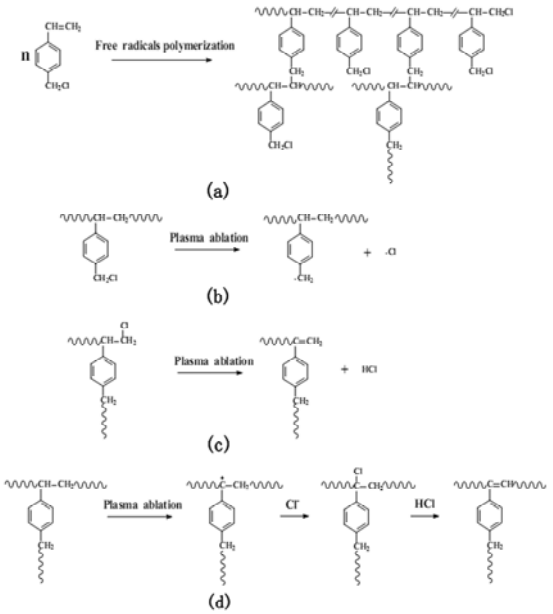

Fig. 8. Possible mechanism of plasma polymerization from VBC monomer. (a) formation of cross-linked PVBC membranes; (b) destruction of functional groups in PVBC membranes; (c) and (d) generation of C=C bonds in polymer backbone.

This mechanism indicates the competitive free radicals polymerization and plasma ablation in plasma polymerization process which affect the polymerization of monomers, and the structure of the functional membrane, respectively [31, 36]. It is believed that most of the chemical reactions occur between the plasma-generated radicals and the active species in the plasma atmosphere [37]. It may be, however, that many species in the plasma do not contribute to the plasma polymerization but rather contribute to the ablation [38]. The competitive nature of reactions is

highly dependent on the condition of plasma polymerization, in particular the energy input level. The density of free radicals and other reactive species increases in various degrees as the plasma discharge power increases. In the range of lower discharge power, the effect of plasma ablation is less obvious. In the range of higher discharge power, however, the effect of plasma ablation becomes a vital element to affect the membrane chemical structure when other plasma polymerization conditions keep constant. This result is crucial because the plasma discharge power as one of the most important parameters for the industrial application of plasma-polymerized electrolyte synthesis can directly influence the electron energy distributing function, the density of all the active species of the discharge, and then the membrane chemical structure [32]. Except for the reactions mechanism mentioned in Fig. 8, many other reactions may be involved in the plasma polymerization process due to the complexity of plasma polymerization mechanism [38]. Herein, we take the free radicals generated on the C=C bonds and benzyl chloride groups, C=C bonds generated by the reactions of covalent chlorine and chloridion as examples and illustrate the possible reactions on the plasma polymerization and plasma ablation.

3.5 Thermal stability

AAEMs with high thermal stability are desirable since operation of ADMFCs at elevated temperature would not only reduce thermodynamic voltage losses but also improve the electrokinetics [4]. The thermal stability of PVBC membranes deposited at discharge power of 20 W to 50 W was investigated by DTA in flowing nitrogen from ambient temperature to 800℃. The sample for DTA is PVBC membranes combined with PTFE substrate. In DTA trace, as shown in **Fig. 9**, the PVBC membranes are degraded mainly in two steps, with the first step ascribed to degradation of PVBC membranes in the range of 310-366 ℃, indicating the high thermal stability of PVBC membranes due to the highly cross-linked structure, and the second step related to the degradation of PTFE substrate in the range of 460-624 ℃ [39].

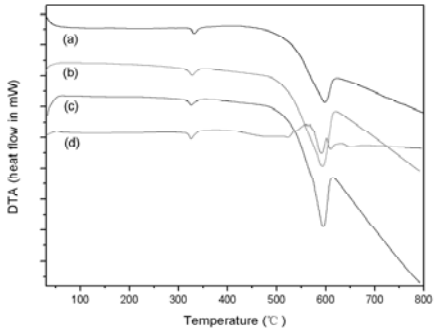

Fig. 9. Thermo gravimetric and differential thermal analysis of PVBC membranes with PTFE substrate deposited at total pressure of 60 Pa, bias voltage of -10 V and discharge power of: (a) 20 W, (b) 30 W, (c) 40 W and (d) 50 W.

4. Conclusion

In this work, we presented an approach to prepare quaternized poly(vinylbenzyl chloride) (QPVBC) membranes by after-glow discharge plasma polymerization, quaternization and alkalization process. SEM images showed that the plasma-polymerized membranes were flat and uniform. The operation of higher discharge power (20 W to 50 W) improved the practical adhesion between membrane and substrate, brought better morphology performance of plasma-polymerized membranes for potential application in ADMFC. DTA result indicated the high thermal stability of the PVBC membranes deposited at plasma discharge power from 20 W to 50 W. XPS and ATR-FTIR data showed the variation of the chemical structure properties of plasma-polymerized membranes as a function of plasma discharge power. A mechanism of plasma polymerization using VBC as monomer was proposed, indicating the competitive effects of free radicals polymerization and plasma ablation in the plasma polymerization process. Because of the enhancement of plasma ablation with increasing energy input,

plasma-polymerized membranes deposited at lower discharge power have higher contents of functional groups and less structure damage. As a result, it seems to be an effective way to fabricate QPVBC membranes by after-glow discharge plasma polymerization at total pressure of 60 Pa, bias voltage of -10 V and plasma discharge power of 20 W.

This article mainly discussed the influence of plasma discharge power on structure characteristics of the plasma-polymerized membranes. More characterization of the QPVBC membranes will be reported elsewhere. Since the variation of electron energy and free radical density can result in changes in the membrane structure characterization, further researches on the improvement of membranes performance by regulating the electron energy and free radical density and the application of QPVBC membranes in ADMFCs are in progress.

Acknowledgements

This research is financially supported by National Nature Science Foundation of China (No.10975162), the Institute of Plasma Physics, Chinese Academy of Sciences (No. 095GZ1156Y) and Core-University Program of Japan-China. We are also very grateful to Dr. Z.Q. Jiang from the Institute of Plasma Physics, Chinese Academy of Sciences for his kind assistance with our experiments.

References

[1] E.H. Yu, K. Scott, J. Power Sources 137 (2004) 248.
[2] Y. Wang, L. Li, L. Hu, L. Zhuang, J. Lu, B. Xu, Electrochem. Commun. 5 (2003) 662.
[3] S.F. Lu, J. Pan, A.B. Huang, L. Zhuang, J.T. Lu, P. Natl. Acad. Sci. USA 105 (2008) 20611.
[4] J.R. Varcoe, R.C.T. Slade, Fuel Cells 5 (2005) 187.
[5] K. Kordesch, J.C.T. Oliveira, Int. J. Hydrogen Energy 13 (1988) 411.
[6] J.R. Varcoe, R.C.T. Slade, G.L. Wright, Y.L. Chen, J. Phys. Chem. B 110 (2006) 21041.
[7] T.N. Danks, R.C.T. Slade, J.R. Varcoe, J. Mater. Chem. 13 (2003) 712.
[8] H. Herman, R.C.T. Slade, J.R. Varcoe, J. Membr. Sci. 218 (2003) 147.
[9] J.R. Varcoe, Phys. Chem. Chem. Phys. 9 (2007) 1479.
[10] J.R. Varcoe, R.C.T. Slade, E.L.H. Yee, S.D. Poynton, D.J. Driscoll, D.C. Apperley, Chem. Mater. 19 (2007) 2686.
[11] P. Zschocke, D. Quellmalz, J. Membr. Sci. 22 (1985) 325.
[12] G.-J. Hwang, H. Ohya, J. Membr. Sci. 149 (1998) 163.
[13] E.N. Komkova, D.F. Stamatialis, H. Strathmann, M. Wessling, J. Membr. Sci. 244 (2004) 25.
[14] M.R. Hibbs, M.A. Hickner, T.M. Alam, S.K. McIntyre, C.H. Fujimoto, C.J. Cornelius, Chem. Mater. 20 (2008) 2566.
[15] Y. Xiong, J. Fang, Q.H. Zeng, Q.L. Liu, J. Membr. Sci. 311 (2008) 319.
[16] G.G. Wang, Y.M. Weng, D. Chu, D. Xie, R.R. Chen, J. Membr. Sci. 326 (2009) 4.
[17] C.C. Yang, J. Membr. Sci. 288 (2007) 51.
[18] S. Roualdes, I. Topala, H. Mahdjoub, V. Rouessac, P. Sistat, J. Durand, J. Power Sources 158 (2006) 1270.
[19] K. Matsuoka, S. Chiba, Y. Iriyama, T. Abe, M. Matsuoka, K. Kikuchi, Z. Ogumi, Thin Solid Films 516 (2008) 3309.
[20] Z.Q. Jiang, Y.D. Meng, Z.J. Jiang, Y.C. Shi, Surf. Rev. Lett. 16 (2009) 297.
[21] H.U. Poll, M. Arzt, K.H. Wickleder, Eur. Polym. J. 12 (1976) 505.
[22] J.R. Varcoe, R.C.T. Slade, E.L.H. Yee, S.D. Poynton, D.J. Driscoll, J. Power Sources 173 (2007) 194.
[23] D.R. Lide, G. Baysinger, L.I. Berger, R.N. Goldberg, H.V. Kehiaian, K. Kuchitsu, G. Rosenblatt, D.L. Roth, D. Zwillinger, Handbook of Chemistry and Physics, CRC Press, Boca Raton, Florida, 2006.
[24] R.K. Nagarale, G.S. Gohil, V.K. Shahi, R. Rangarajan, Macromolecules 37 (2004) 10023.
[25] N. Sundaraganesan, H. Saleem, S. Mohan, M. Ramalingam, V. Sethuraman, Spectrochim. Acta A 62 (2005) 740.
[26] J. Reyes-Labarta, M. Herrero, P. Tiemblo, C. Mijangos, H. Reinecke, Polymer 44 (2003) 2263.
[27] D.O.H. Teare, D.C. Barwick, W.C.E. Schofield, R.P. Garrod, L.J. Ward, J.P.S. Badyal, Langmuir 21 (2005) 11425.
[28] S. Rajendran, T. Uma, J. Power Sources 88 (2000) 282.
[29] S.B. Roscoe, S. Yitzchaik, A.K. Kakkar, T.J. Marks, Z.Y. Xu, T.G. Zhang, W.P. Lin, G.K. Wong, Langmuir 12 (1996) 5338.
[30] E. Papirer, R. Lacroix, J.-B. Donnet, G. Nanse, P. Fioux, Carbon 33 (1995) 63.
[31] H. Yasuda, T. Yasuda, J. Polym. Sci. Pol. Chem. 38 (2000) 943.
[32] H. Biederman, Plasma Polymer Films, Imperial College Press, Covent Gardent, London, 2004.
[33] D. Briggs, G. Beamson, Anal. Chem. 64 (1992) 1729.
[34] T.I.T. Okpalugo, P. Papakonstantinou, H. Murphy, J. McLaughlin, N.M.D. Brown, Carbon 43 (2005) 153.

[35] F.J. Xu, E.T. Kang, K.G. Neoh, Macromolecules 38 (2005) 1573.
[36] A.R. Denaro, P.A. Owens, A. Crawshaw, Eur. Polym. J. 4 (1968) 93.
[37] C. Chen, B. Liang, D. Lu, A. Ogino, X. Wang, M. Nagatsu, Carbon 48 (2010) 939.
[38] H. Yasuda, Plasma Polymerization, Acadamic Press, INC, Orlando, Florida, 1985.
[39] T. Yu, H. Lin, K. Shen, L. Huang, Y. Chang, G. Jung, J. Huang, J. Polym. Res. 11 (2004) 217.

15A: Ultra high density plasma [fusion energy]

Key person 15-A
Graduate School Engineering Osaka University
Division of Electric, Electronic, and Information Engineering
Kazuo A. Tanaka

【Preface】
During the years of 2005 to 2010, we could perform a number of collaborative researches in this 15-A category.
From Japan, Osaka University, Kyoto University, University of Tokyo, Tokyo Institute of Technology, Utsunomiya University, Gifu University, Hiroshima University, JAERI, and Kansai Photon Institute participated into this program, From China, participated are SIOM, Beijing Institute of Physics, Shanghai Jiao Tong University, Science and Technology University of China, Dalian University, Southeast University, and Laser Fusion Institute.

【Acknowledgement】
We appreciate the support by director professor A. Komori and professor K. Toi in NIFS, and professors J.G. Li, and K.J. Wang from China. We appreciate the support from JSPS for this program.

【Summary of activities for each year】
Year 2006
As a second start of this 5- year project, we summarized our first 5 years of activity in October 2005 at Jiuzhaigou in China. We could collect more than 100 scientists from both Japan and China, and discussed how we proceed from 2006 for our collaboration research.
After this summary workshop, we did see a great progress both from fast ignition and high density science. In the area of fast ignition, target development has been conducted between Japan, Osaka University and Southeast University of China. In 2007, Professor K. Nagai and Professor Z. Gu agreed to have a target workshop. In terms of an experiment in fast ignition area, we published 2 Physical Review Letters papers, indicating that gold form target worked fairly well to increase fast electrons as additional heating source of fast ignition.

In January of 2007, we had a fast ignition workshop and professors Anle-Lei and Jian Zheng participated and presented their results in high energy density physics, and we could discuss the further collaboration.

Figure 1. Farewell party at Osaka University of professor Anle-Lei, SIOM, he played an important role in this Japan-China CUP program.

Year 2007
Professors T. Norimatsu, K. Nagai, Osaka University, and Zhong-Ze Gu, South East University (China) published 3 scientific papers on target fabrication for inertial fusion energy. They held a China-Japan bilateral seminar on target materials in Huangshan, China from July 2008 to August 1st. There they discussed the highly spherical capsule fabrication method, coating method and form material. And these information exchange and collaboration research plan will benefit research in both countries.
Professor Kodama, Osaka University, and professor Yugami, Utsunomiya University, have preceded their collaboration research with Shanghai Jiao Tong University on Terra-hertz generation. They visited Shanghai Jiao Tong University, and discussed the details of the collaboration with professors Zheng-Ming Sheng and Jie Zhang. Their plan is to conduct experiment in Japan and part of theoretical research being performed by Chinese side.
Professor KA. Tanaka, Osaka University, has preceded the collaboration research with a professor Anle-Lei of SIOM, and they published scientific paper in Physical Review E in 2007 about laser propagation in a relativistic regime in plasmas.

Year 2008,
Professor KA. Tanaka, H. Habara, Osaka University, and professor Anle-Lei of SIOM (China) summarized the research result on relativistic laser light self-focusing and this result was presented at American Institute of Physics invited talk by professor Anle-Lei and also the result has been published in the Physics of Plasma.
Professor K. Nagai and T. Norimatsu, Osaka University, and professor Z. Gu, Southeast University of China, held laser target workshop in Japan and summarized their collaboration research in several notable scientific journals such as Applied Physics Letters.
Professor N. Yugami and N. Higashiguchi of Utsunomiya University and professor Zheng-Ming Sheng of Beijing Institute of Physics have collaborated on the terra-hertz generation. Beijing Institute of Physics was responsible for simulation and experiment was being performed by the Japanese side. Professor K. Nagai of Tokyo Institute of Technology and Professor Z. Gu, Southeast University, have built up very strong tie on their collaboration research in the area of target development. They produced many good scientific papers. Professor K. Nagai visited Laser Fusion Institute at Mianyang and visited other facilities in China. This visit befitted in many ways to professor Nagai's research. From Chinese side, they requested to send post-doctor young scientists to Osaka University, especially to professor KA. Tanaka and professor N. Miyanaga. And this request is based on this long years' of active research exchange and reliable relations, and we would like to make these collaboration research more fruitful by using this long-term post-doctoral system by JSPS.

Fig. 2 Professors N. Yugami, Utsunomiya University and Z. Sheng, Shanghai Jiao Tong University discuss the Terahertz generation at SJTU.

Year 2009

In the area of laser plasma interaction, professors H. Habara and Y. Sakawa, Osaka University, professor N. Yugami, Utsunomiya University, and professor K. Nagai, Tokyo Institute of Technology, have visited China, and their specified areas are relativistic laser plasma interaction, non-collisional shock wave generation in laser plasma, terra-hertz generation and target fabrication respectively. Professor Z. Gu, Southeast University (China), visited for target fabrication to discuss with Professor K. Nagai (TIT). Dr. Z. Zhaozongqing and X. Zhang visited Japan for a relativistic laser plasma interaction as well as professor A. Lei of SIOM and professor J. Zheng, USTC, and professor J. Quang of Institute of Physics has visited Japan for the area of non-collisional shock wave generation.

As their collaboration research result, 13 scientific papers have been published, and a paper is planned to be published in Physical Review Letters soon.

Figure 2; the scene of discussion that Shanghai Jiao Tong University, where professor Yugami, Utsunomiya University, and professor Zheng-Ming Sheng discuss the terra-hertz generation.

Year 2010

Based on the collaboration research and unique ideas developed by professor KA. Tanaka and professor J. Zheng, Cherenkov radiation research has been published in Physical Review Letters by professor H. Habara and the further experiment has been planned. This research shows that relativistic electron energy spectra can be measured by making use of the characteristics of Cherenkov radiation. Professor J. Zheng of USTC (China) asked advice on the professor H. Habara's expertise on the laser systems. Professor J. Zheng planned to install 10 terra-watt laser system in the near future. They discussed possible collaboration research.

Professor H. Habara and KA. Tanaka, Osaka University, and professor Anle-Lei, SIOM, have continued their collaboration research on fast electron energy transport for fast ignition. Professor Anle-Lei participated in the experiment conducted at Osaka University and obtained understanding on the energy transport mechanism of fast electrons.

Professor K. Nagai, Tokyo Institute of Technology, and professor Zhongze Gu, Southeast University, continued their collaboration research on target fabrication. They discussed some research result on the nano-particles, nano-fibers and they discussed also those applications. These technical improvement performed by these scientists are beneficial to the laser plasma interaction research as well as the other application in the field such as medicine.

We have held a review seminar from Oct. 13th to 15th at Shanghai Jiao Tong University. Originally, Chinese key persons pointed out this seminar should be held in China, and this point was right because many Chinese young scientists and graduate students could participate and exchange a research information with Japanese scientists. All these collaboration research result would be published in the near future.

【PAPERS published under the collaboration of this CUP program】

1. Jian Zheng, K.A. Tanaka, T. Miyakoshi, Y. Kitagawa, R. Kodama, T. Kurahashi, and T. Yamanaka, "Spectrum of transition radiation from hot electrons generated in ultra-intense laser plasma interaction" Physics of Plasmas, Volume9, 3610, 2002.

2. Jian Zheng, K.A. Tanaka, Y. Sentoku, A.A. Offenberger, Y. Kitagawa, R. Kodama, T. Kurahashi, K. Mima, and T. Yamanaka, "Harmonic emission with cyclotron satellite structure due to strong magnetic fields produced by ultra-intense laser-plasma interaction" Physics of Plasmas, Volume9, 3193, 2002.

3. Z.M.Sheng, K.Mima, et al., "Stochastic Heating and Acceleration of electron in colliding laser fields in plasma" Physical Review Letters, Vol.88, 2002, 055004-1~4.

4. Y.Sentoku, K.Mima, Z.M. Sheng, et al., "High-energy ion generation in interaction of short laser pulse with high-density plasma", Appl.Phys., B74, 207-215, 2002.

5. Y.Sentoku, K.Mima, Z.M. Sheng, et al., "Three-dimensional particle-in-cell simulation of energetic electron generation and transport with relativistic laser pulses in overdense plasmas", Physical Review E,vol.65, 046408, 2002.

6. Jian Zheng, K.A. Tanaka, T. Miyakoshi, Y. Kitagawa, R. Kodama, T. Kurahashi, and T. Yamanaka, "Theoretical study of transition radiation from hot electrons generated in the laser-solid interaction" Physics of Plasmas, Volume10, 2994, 2003.

7. M.Suzuki, H.Daido, Il Woo Choi, Wei Yu, K.Mima, et al., "Time and space resolved Measurement of a gas puff laser- plsama X-ray source", Physics of Plasmas, 10,227, 2003.

8. Z.M. Sheng, et al., "Efficient Acceleration of Electron with counter propagating intense laser pulses in Vacuum and underdense plasma", Phys, Rev.E, 69,0164071, 2004.

9. Jian Zheng, K.A. Tanaka, T. Sato, T. Yabuuchi, T. Kurahashi, Y. Kitagawa, R. Kodama, T. Norimatsu, and T. Yamanaka, P "Study of Hot Electrons by Measurement of Optical Emission from the Rear Surface of a Metallic Foil Irradiated with Ultraintense Laser Pulse" Physical Review Letters, Volume92, 165001-1, 2004.

10. Y.T. Li, J. Zhang, Z.M. Sheng, J. Zheng, Z.L. Chen, R. Kodama, T. Matsuoka, M. Tampo, K.A. Tanaka, T. Tsutsumi, and T. Yabuuchi, "High-energy electrons produced in subpicosecond laser-plasma interactions from subrelativistic laser intensities to relativistic intensities" Physical Review E 69, 036405-1, 2004.

11. R. Kodama, Y. Sentoku, Z.L. Chen, G.R. Kumar, S.P. Hatchett, Y. Toyama, T.E. Cowan, R.R Freeman, J. Fuchs, Y. Izawa, M.H. Key, Y. Kitagawa, K. Kondo, T. Matsuoka, H. Nakamura, M. Nakatsutsumi, P.A. Norreys, T. Norimatsu, R.A. Snavely, R.B. Stephens, M. Tampo, K.A. Tanaka, and T. Yabuuchi, "Plasma devices to guide and collimate a high density of MeV electrons" Nature, Volume432, 1005, 2004.

12. Z.L. Chen, R. Kodama, M. Nakatsutsumi, H. Nakamura, M. Tampo, K.A. Tanaka, Y. Toyama, T. Tsutsumi, and T. Yabuuchi, "Enhancement of energetic electrons and protons by cone guiding of laser light" Physical Review E71, 036403-1, 2005

13. Jian Zheng, C.X. Yu, Z.J. Zheng, and K.A. Tanaka, "Cherenkov radiation generated by a beam of electrons revisited", Physics of Plasmas 12, 093105-1, 2005

14. Han Yang, Keiji Nagai, Xiangwei Zhao, Haihua Chen, Zhong-Ze Gu, "Fabrication of Photo-Encoded Beads for Bioanalysis", J Nanosci. Nanotechnol, 2005 in press

15. "Manipulation of radiation divergence of extreme ultraviolet emitted from laser plasma generated by nanostructure-controlled low-density SnO2 targets" Keiji Nagai, QinCui Gu, Zhong Ze Gu, et al., Applied Physics Letters, 2005 in press

16. K.A. TANAKA, R. Kodama, Y. Kitagawa, K. Kondo, et al., "Current Status of Fast Ignition Research Using a Long Pulse Laser for Implosion and a PW Laser for Heating", Physics Essays, Vol.18, 2006.

17. A.L.Lei, K.A. TANAKA, R. Kodama, G.R. Kumar, K.Nagai, T.Norimatsu, T. Yabuuchi and K.Mima, "Optimum Hot Electron Production with Low-Density Foams for Laser Fusion by Fast Ignition", Physical Review Letters, 255006 (2006)

18. H. Habara, K. Adumi, T. Yabuuchi, T. Nakamura, Z.L. Chen, M. Kashihara, R. Kodama, et al., "Surface Acceleration of Fast Electrons with Relativistic Self-Focusing in Preformed Plasma", Physical Review letters, **97,** 095004 (2006).

19. AL. Lei, A. Pukhov, R. Kodama, T. Yabuuchi, K. Adumi, K. Endo, R. R. Freeman, H. Habara, Y. Kitagawa, K. Kondo, G. R. Kumar, T. Matsuoka, K. Mima, H. Nagatomo, T. Norimatsu, O. Shorokhov, R. Snavely, X. Q. Yang, J. Zheng, and K. A. Tanaka, "Relativistic laser channeling in plasmas for fast ignition", Physical Review E.,76, 066403(2007).

20. R. Snavely, B. Zhang, K. Akli, Z. Chen, R. R. Freeman, P. Gu, S. P. Hatchett, D. Hey, J. Hill, M. H. Key, Y. Izawa, J. King, Y. Kitagawa, R. Kodama, A. B. Langdon, B. F. Lasinski, A. Lei, A. J. MacKinnon, P. Patel, R. Stephens, M. Tampo, K. A. Tanaka, R. Town, Y. Toyama, T. Tsutsumi,

S. C. Wilks, T. Yabuuchi, and J. Zheng, “Laser generated proton beam focusing and high temperature isochoric heating of solid matter”, PHYSICS OF PLASMAS 14, 092703 2007.

21. Toshinori YABUUCHI, Yasuhiko SENTOKU, Takeshi MATSUOKA, Hideaki HABARA, Ken ADUMI, Zenglin CHEN, Ryosuke KODAMA, Kiminori KONDO, Anle LEI, Kunioki MIMA, Motonobu TAMP, Tsuyoshi TANIMOTO and Kazuo A. TANAKA, “Influence of Electrostatic and Magnetic Fields on Hot Electron Emission in Ultra-Intense Laser Matter Interactions”, Plasma Fusion Research Vol.2, 15, (2007).

22. T. Yabuuchi, K. Adumi, H. Habara, R. Kodama, K. Kondo, T. Tanimoto, and K. A. Tanaka Y. Sentoku T. Matsuoka, Z. L. Chen, M. Tampo, A. L. Lei, and K. Mima, “On the behavior of ultraintense laser produced hot electrons in self-excited fields”, PHYSICS OF PLASMAS 14, 040706 2007.

23. Takeshi Higashiguchi, Nobuo Ohata, Kun Li, and Noboru Yugami, “Observation of temporal behavior of the emission frequency from an ultrashort, high-power, and compact millimeter-wave source”, Applied Physics Letters, vol. 90 111503 (2007).

24. T Matsuoka, A Lei1, T Yabuuchi, K Adumi, J Zheng, R Kodama, K Sawai, K Suzuki, Y Kitagawa, T Norimatsu, K Nagai, H Nagatomo, Y Izawa, K Mima, Y Sentoku and K A Tanaka “Focus optimization of relativistic self-focusing for anomalous laser penetration into overdense plasmas (super-penetration) ” PLASMA PHYSICS CONTROLLED FUSION 50 (2008) 105011

25. Tsuyoshi Tanimoto, Kazuhide Ohta, Hideaki Habara, Toshinori Yabuuchi, Ryousuke Kodama, Motonobu Tampo, Jian Zheng, and Kazuo A. Tanaka “Use of imaging plates at near saturation for high energy density particles” REVIEW OF SCIENTIFIC INSTRUMENTS 79, 10E910 2008

26. J Zheng, Z B Wang, C X Yu, X H Jiang, Z R Cao, Y K Ding and K A Tanaka “Influence of target geometry on the ion temperature of laser-produced plasmas” J. Phys.: Conf. Ser. 112 Volume 112 (2008) 022040 (4pp)

27. H Habara, G Xu, T Jitsuno, R Kodama, K Suzuki, K Sawai, C P J Barty, T Kawasaki, H Kitamura, K Kondo, K Mima, N Miyanaga, Y Nakata, H Shiraga, K A Tanaka, K Tsubakimoto and M C Rushford “Pulse compression using segmented grating in Gekko MII system, ILE” J. Phys.: Conf. Ser. 112 Volume 112 (2008) 032017 (4pp)

28. A Lei, W Yu, Y Tian, H Xu, X Wang, X Yang, V K Senecha, K A Tanaka and R Kodama “Effect of focus position on a high intensity laser propagation in a dense plasma” J. Phys.: Conf. Ser. 112 Volume 112 (2008) 022089 (4pp)

29. T Tanimoto, A L Lei, T Yabuuchi, H Habara, K Kondo, R Kodama, K Mima and K A Tanaka "Hot electron spatial distribution under presence of laser light self-focusing in over-dense plasmas" J. Phys.: Conf. Ser. 112 Volume 112 (2008) 022095 (4pp)

30. T Yabuuchi, Y Sentoku, H Habara, T Matsuoka, K Adumi, Z Chen, R Kodama, K Kondo, A L Lei, K Mima, M Tampo, T Tanimoto and K A Tanaka "Hot electron emission limited by self-excited fields from targets irradiated by ultra-intense laser pulses" J. Phys.: Conf. Ser. 112 Volume 112 (2008) 022093 (4pp)
31. W Yu, L Cao, H Xu, A Lei, X Yang, K A Tanaka and R Kodama "Plasma hole boring by multiple short-pulse lasers" J. Phys.: Conf. Ser. 112 Volume 112 (2008) 022100 (4pp)

32. A.L. Lei, K.A. Tanaka, R. Kodama, K. Adumi, H. Habara et al.," Study of ultraintense laser propagation in overdense plasmas for fast ignition", Physics of Plasmas 16 (2009) 056307.

33. H Habara, G Xu, T Jitsuno, R Kodama, K Suzuki, K Sawai, C P J Barty, T Kawasaki, H Kitamura, K Kondo, K Mima, N Miyanaga, Y Nakata, H Shiraga, K A Tanaka, K Tsubakimoto, and M C Rushford, "Pulse compression using segmented grating in Gekko MII system, ILE", Journal of Physics: Conference Series 112 (2008) 032017.

34. J Zheng, Z B Wang, C X Yu, X H Jiang, Z R Cao, Y K Ding and K A Tanaka, "Influence of target geometry on the ion temperature of laser-produced plasmas", Journal of Physics: Conference Series 112 (2008) 022040.

35. W. YU, L. CAO, M.Y. YU, H. CAI, H. XU1 X. YANG, A. LEI, K.A. TANAKA, AND R. KODAMA, "Plasma channeling by multiple short-pulse lasers", Laser and Particle Beams" (2009), 27, 109–114.

36. A.L. Lei, L. H. Cao, X. Q. Yang, K. A. Tanaka, R. Kodama, X. T. He, K. Mima, T. Nakamura T. Norimatsu, W. Yu, and W. Y. Zhang, "Guiding and confining fast electrons by transient electric and magnetic fields with a plasma inverse cone", PHYSICS OF PLASMAS 16, 020702 (2009).

37. Hideaki HABARA, Masashi YAMAMOTO, Takahiro KURAHASHI, Kenji KIDA and Kazuo A. TANAKA, "Development of High-Order Harmonic Light Spectrometer for Observation of Strong Magnetic Field Generated by Fast Electrons in Laser-Plasma Interactions", J. Plasma and Fusion Research ser. 8 (2009) 1214.

38. Soichiro SAKAE, Hiroyuki HAYASHI, Tomoaki KITABATAKE, Takuya MATSUMURA, Takuma ENDO and Takayoshi NORIMATSU, "Experiments on a Gas Gun for Target Injection in Inertial Fusion Energy", Plasma Fusion Res. 4, S1006 (2009).

39. Akifumi IWAMOTO, Takeshi FUJIMURA, Mitsuo NAKAI, Takayoshi NORIMATSU, Keiji NAGAI, Ryuji MAEKAWA and Hitoshi SAKAGAMI, “A Proposed Procedure for Temperature Control of the Cryogenic Target for the FIREX Project”, Plasma Fusion Res. 4, S1007 (2009).

40. Shengyin LI, Weidong WU, Xueming WANG, Feng WANG, Yongjian TANG and Weiguo SUN, “Properties of N-doped Diamond-like Carbon Films Prepared by the PLD Method”, Plasma Fusion Res. 4, S1008 (2009).

41. Cheng SUN, Xiang-Wei ZHAO, Yuan-Jin ZHAO, Rong ZHU and Zhong-Ze GU, “Fabrication of Colloidal Crystal Beads with Uniform Size by a Drop-Breaking Technique”, Plasma Fusion Res. 4, S1009 (2009).

42. Takeshi FUJIMURA, Mitsuo NAKAI, Akifumi IWAMOTO, Keiji NAGAI, Hirofumi HOMMA, Ken-ichi TANABE and Takayoshi NORIMATSU, “Manufacturing and Leak Check of Shell Targets for the FIREX-I Project”, Plasma Fusion Res. 4, S1010 (2009).

43. Fuyumi ITO, Naotake NAKAMURA, Takayoshi NORIMATSU and Keiji NAGAI, “Tin-Doped Resorcinol-Formaldehyde Aerogel with Decanano-Cell Structure”, Plasma Fusion Res. 4, S1011 (2009).

44. Hitoshi SAKAUCHI and Ryusuke TSUJI, “Compression of Arago Spot Images for Rapid Position Measurement of Inertial Fusion Energy Targets”, Plasma Fusion Res. 4, S1012 (2009).

45. T. Higashiguchi and N. Yugami, “Short pulse, high power microwave radiation source with a laser-induced sheet plasma mirror”, Journal of Applied Physics, Vol. 105, pp. 093301-1-093301-4 (2009)

46. M. Nakagawa, R. Kodama, T. Higashiguchi, and N. Yugami, “Generation of terahertz radiation via an electromagnetically induced transparency at ion acoustic frequency region in laser-produced dense plasmas”, Physical Review E, Vol. 80, p. 025402(R) (2009)

47. Linqin Ge, Jianyu Ji, Tian Tian, Zhongdang Xiao, Zhongze Gu, Takayoshi Norimatsu, Yoshinori Shimada, Hiroaki Nishimura, Shinsuke Fujioka, Keiji Nagai, ” Fabrication of the hollow SnO2 nanoparticles contained spheres as extreme ultraviolet (EUV) target”, Colloids and Surfaces A: Physicochem. Eng. Aspects, 358(1-3), 88-92 (2010).

48. Keiji Nagai, Kouhei Miyamoto, Tomokazu Iyoda.Cao Pan, Zhongze Gu, “Monolithic and Low-density (<50 mg/cm^3) Metaloxides Fabricated using Electrospinning:Vanadium Oxide and Copper”, Fusion Science and Technology, 59（1）, 216-220 (2011).

Japan-China CUP Summary: The last decade of 15B

(Laser Plasma: Theory and Simulation)

Key Persons: **TAKABE Hideaki (2009-2010)**
MIMA Kunioki (2001-2008)
Institute of Laser Engineering, Osaka University, Japan
ZHU Shaoping
Institute of Applied Physics and Computational Mathematics, Beijing, China
and **SHENG Zhengming**
Shanghai Jiao Tong University, Shanghai, China

We have carried out mainly focusing on the joint research focusing on the following topics in the last several years.

- **Fast Ignition Theory & Computation**
  - K. Mima, H. Sakagami, M. Murakami, H. Nagatomo (Japan)
  - Z-M Sheng, J Zheng, W-M Wang, J-F Wu (China)
- **Laser Particle Acceleration and Coulomb Explosion**
  - Kawata, M. Murakami (Japan)
  - Q. Kong, W. Yu
- **Modeling Astrophysical Collisionless Shocks**
  - Y. Sakawa, Y. Kuramitsu, T. Morita, H. Takabe
  - Y-T. Li, Q-L. Dong, J. Zhang
- **Photo-ionized Non-LTE Plasma**
  - S. Fujioka, H. Nishimura, H. Takabe
  - F-L .Wang, G. Zhao, J. Zhang

One of the great benefits though the program is the construction of human relation between the two countries. I hope Japan and China will show a leadership to construct a new era of East-Asia Union, and Asia-Union in the near future. Good example is EU. EU is going to try to construct the grate EU with a lot of investment to the east Europe. The enrichment of the science and technology by CUP program should be distributed to the other Asian counties in the coming years.

Official collaboration between Japan and China has lasted for more than 1,500 years.

Without a relatively short time, we have kept a good relation. One of the pioneers of Chinese large scale laser program, Prof. Deng Xing-ming, told in front of Japanese in our institute almost 30 years ago. “On the long way to go, we appreciate the power of a horse. Through a long time to go, we understand the mind of our fellows”. It is written as follows in Chinese and Japanese kanji-letters: I thank Prof. C. Liu who gave me the following hand writing.

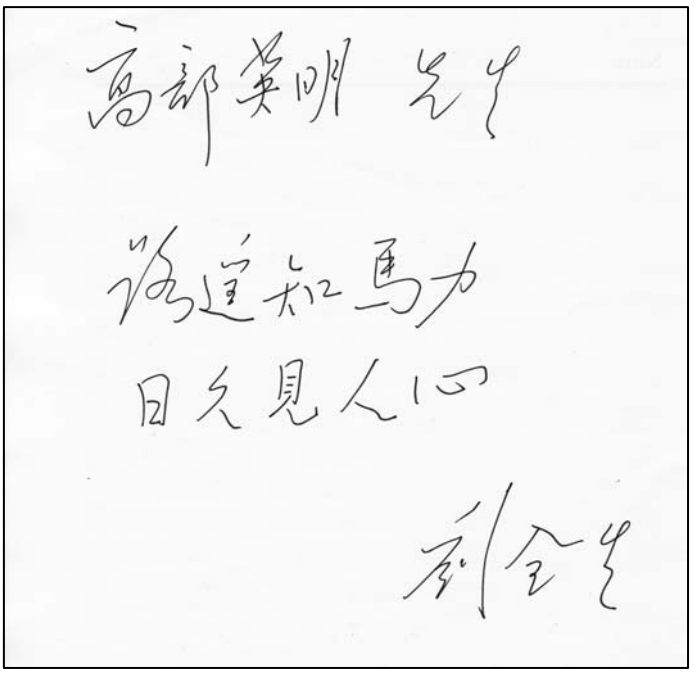

路遙知馬力

日久見人心

From left to right; S-P. Zhu, H. Takabe, X-T He, C. Liu, Z-M. Sheng(standing), and a Prof. SJTU. October 14, 2010 at faculty Club, Shanghai Jiao Tong University.

Some Progress on High Energy Density Physics under the China-Japan CUP Collaboration

Z. M. Sheng
Key Laboratory for Laser Plasmas (Ministry of Education) and Department of Physics, Shanghai Jiao Tong University and Beijing National Laboratory of Condensed Matter Physics, Institute of Physics, CAS, Beijing, China
zmsheng@sjtu.edu.cn

In the last 10 years we have witnessed rapidly increasing collaboration between China and Japan from economy to scientific research. From today's perspective, the China-Japan Core-University-Program (CUP) came timely when it was initiated 10 years ago. In the catalogues of I-5A (Study of Ultrahigh Density Plasma -- Inertial Confinement Fusion) and I-5B (Theory and simulation on Inertial Fusion Plasmas) of the program, there are totally 10 institutions from China, engaged in the research of high energy density physics and inertial fusion energy, have participated in the CUP collaboration. The program involves a large number of personal exchanges, quite a few joint experiments, more than 10 bi-lateral meetings and workshops. I find it is a very successful program from viewpoints of scientific achievements, cultural exchange, educating young generation of scientists. Based upon the CUP exchange program, we become real partners with our Japanese colleagues. Lots of young people (e.g. graduate students) have been involved in the program, which shall become the main force of future collaboration. Because of the CUP program, collaboration to work on the large facilities in both sides appears very fruitful. This may help to promote the share of using large facilities in the future. Thus CUP has paved a bright way for future long term collaboration. As a participant (and a key person in the last 5 years) of CUP, I have benefited greatly from this program both for my research and career development through close collaboration with Japanese colleagues. In this report, I will briefly introduce some Chinese programs and institutions working on high energy density physics (HEDP) and fundamental laser plasmas, including our Laboratory for Laser Plasmas newly established in Shanghai Jiao Tong University. Then I will highlight some recent research progress on fast ignition of fusion targets (theory and simulation) by some groups in China.

I. Chinese programs and institutions working on HEDP and fundamental laser plasmas

In the last 5 years, we have been witnessing the steady progress on laser-driven high energy density physics research. For example, the NIF laser aiming at the realization of central ignition was complete in LLNL in 2009 and the first integrated

ignition experiments were declared completed in October 2010. In Europe, a similar laser LMJ is expected to complete in 2012 in Bordeaux, France. Preliminary design for possible construction of HiPER (High Power laser Energy Research facility) laser for fast ignition of fusion targets starts in 2010. In the meanwhile, another European project called ELI (Extreme Light Infrastructure) started to construct in 2010, which is dedicated to the investigation and applications of laser-matter interaction at the highest intensity level (more than 2 orders of magnitude higher than today's laser power). In Japan, the LFEX laser, which can deliver energy up to 10 kJ in a 0.5-20 ps pulse, has been constructed at the Institute of Laser Engineering, Osaka University in 2009.

In China, the SG-II laser (8 beams with the output of 3kJ/1ns/3ω) was completed in 2000 in the Joint Laboratory for High Power Laser located inside the Shanghai Institute of Optics and Fine Mechanics, Chinese Academy of Sciences. The 9^{th} beam (3ns, 4.5kJ) for backlighting diagnostic was constructed in 2005. A petawatt laser beam for target heating in fast ignition research is under construction. The SG-III laser (48 beam with the output of 150-200kJ in 3ω) started to construct in Laser Fusion Research Center in Mianyang in 2008 [1]. In the meanwhile, systems delivering short intense laser pulses at the multi-hundred terawatt to near petawatt level have been constructed in the Institute of Physics, CAS, in Beijing, Shanghai Institute of Optics and Fine Mechanics, CAS, in Shanghai, and Laser Fusion Research Center in Mianyang.

Figure 1: The Extreme Light III(XL-III) in Institute of Physics (IoP), Chinese Academy of Sciences, Beijing, China. This Ti:sapphire laser facility was designed with top-able configuration and can output peak power to 350TW with pulse duration of 30fs per 20 minutes. With further upgrade works by using OPCPA as front stage amplifier and optimized multipass amplifiers in recent, now the facility is able to delivery laser pulse to 750TW, contrast ratio about 10^{-8}, central wavelength at 810nm, focused laser intensity up to 10^{21}W/cm^2. Upper: 527nm Nd:glass pump laser and 750TW Ti:sapphire facility. Bottom: Laser target chamber and diagnostic system (provided by Z.Y. Wei).

In China, institutions, laboratories, groups working on HEDP and fundamental laser plasmas include Shanghai Institute of Optics and Fine Mechanics/CAS, Institute of Physics/CAS, National Astronomical Observatory/CAS, Shanghai Institute of Laser Plasmas and Joint Laboratory for High Power Laser, Laser Fusion Research Center /CAEP, Beijing Institute of Applied Physics and Computational Mathematics, University of Science and Technology of China (USTC), Fudan University, Shanghai Jiao Tong University (SJTU), National University for Defense Technology, Zhejiang University, Beijing Normal University, etc. But at the moment, only a few of these institutions and laboratories have the capabilities to carry out experimental studies.

In SJTU, Laboratory for Laser Plasmas was newly established in 2010 as a key laboratory of the Ministry of Education of China. At present there are 16 research staffs in the laboratory. The main research topics are fundamental laser plasmas including relativistic laser plasmas, advanced particle acceleration and radiation from relativistic laser plasmas for applications, development of ultrafast diagnostics for material sciences, advanced high power laser technologies, etc. Planned new experimental facilities included: laser systems 200TW/5J/25fs/10Hz (commercial system), 20mJ/40fs/1kHz (commercial system), and 100J/100fs/10Hz (2-5 μm), which are funded; MeV ultrafast electron diffraction system, which is partially funded; 1PW/100J/100fs/0.1Hz with contrast ration over 10^{10}, which is not yet funded.

II. Some recent research progress on fast ig nition of fusion targets (theory and simulation)

For the fast ignition scheme of laser fusion, two key issues are how to convert the energy of high intensity lasers to hot electrons and how to deposit the hot electron energy to the pre-compressed fusion core. For these issues, the proper target design is very important to increase the energy coupling efficiency. Since the hot electrons produced usually have a large angular spread (typically larger than 50 degrees) and the distance from the critical surface to the fusion core is too long for hot electron transport, it is necessary to produce the hot electrons as close to the compressed core as possible. For this purpose, two methods have been proposed. One is so called the hole-boring by the laser ponderomotive force, which produces a plasma channel, and another is by use of cone-targets attached to fusion core.

When one adopts the hole-boring scheme, it has been found by simulation that the hole-boring process is not stable. When the intense laser makes hole-boring, the channel is not produced straight forward along the initial laser axis, instead, the channel bends during the course of hole-boring. This is due to fact that at the pulse front, the self-modulation and filamentation instabilities are produced, and they can

couple with the instability driven by (electron) beam-plasma interaction. The nonlinear development leads to unstable channeling propagation of the laser pulse. To solve this problem, Yu et al. found that more effective hole-boring can be produced by multiple short laser pulse trains than by a single long pulse [2]. In this case the plasma channel is formed more stably and with less laser energy. Figure 2 shows a comparison of the channel formation with a short laser pulse train and a relatively long pulse.

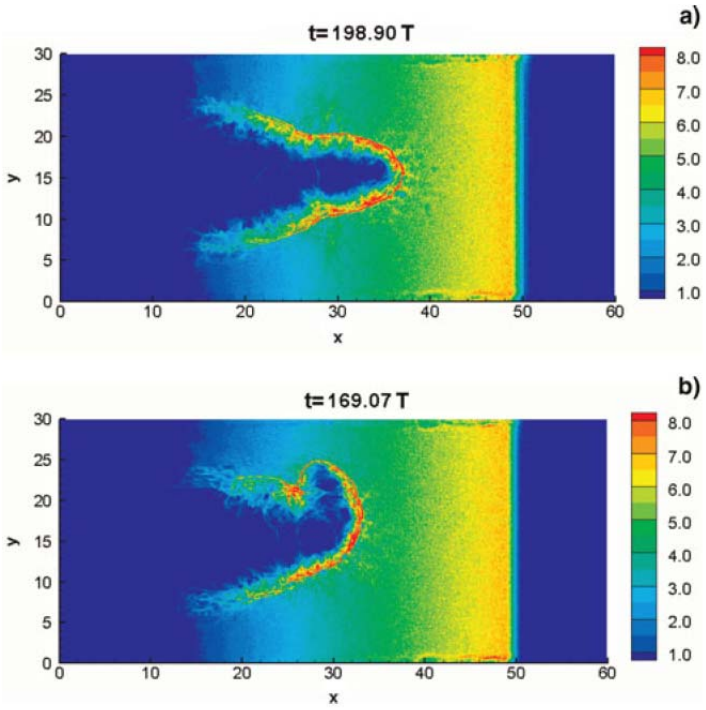

Figure 2: Comparison of the plasma channel formation with a short laser pulse train and a single long pulse (see Ref. 2).

When one adopts the cone target scheme as shown in Fig. 3(a), it is found that the hot electrons have large angle spreads. This reduces the energy coupling significantly. In order to improve this, Cai et al. came up with the double cone target design as shown in Fig. 3(b). The lower plots show comparison of the corresponding hot electron distributions. It is obvious that the hot electrons show much smaller angle spreads with the double cone target, which leads to enhanced energy coupling. Actually, it was found from simulation that coupling from laser to the high energy electrons which can deposit to DT core increases from 4.8% (for normal cone target) to 14.8% (for double cone target) [3]. The physical mechanism is that at the double cone layer boundaries, strong quasi-static electric and magnetic fields are induced as the first part of the hot electrons pass through the boundaries. The generated quasi-static fields tend to confine the hot electrons produced at a later stage.

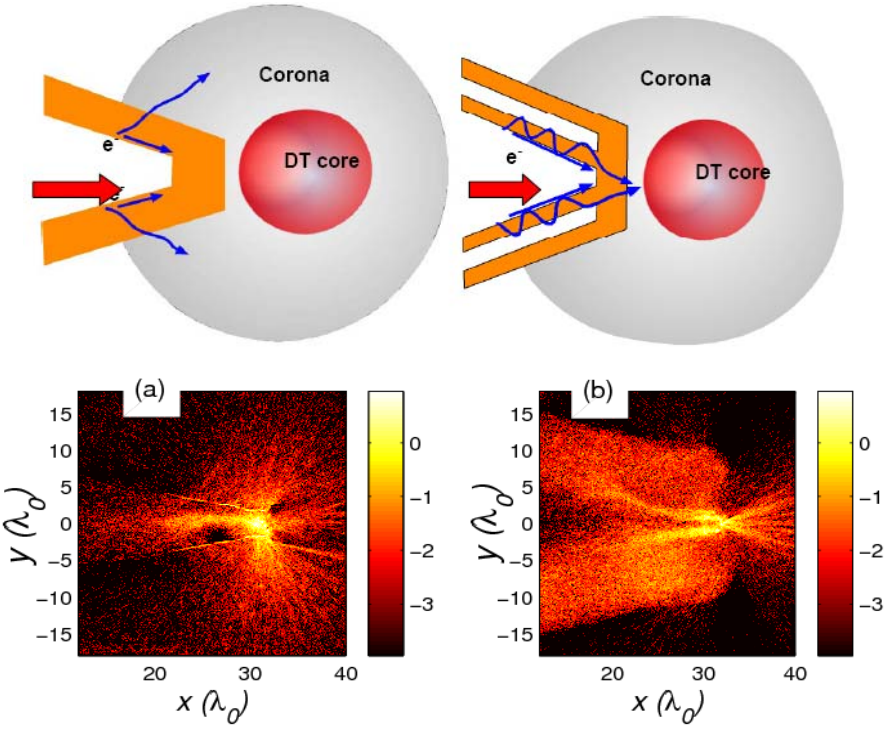

Figure 3: Comparison of the hot electron distributions in 2D space with a normal cone target (a) and a double-cone target (b) (see Ref. 3).

When a large flux of hot electrons (with currents larger than the Alvén current) propagates in dense plasma, large electrostatic fields can be induced. These fields drag background electrons to form a return current. For this system, there are a few new physics needed to be studied. The first one is how high the return current can be and the second one is how this system evolves under such conditions (large currents, high density, collisional effects, etc.). We have studied these problems analytically and numerically. For the first problem, based upon Fokker-Planck simulation, We have found that the electron distribution function (EDF) in a large dc electric field can be presented as a hybrid of a stationary and drifting Maxwellian. According to the form of EDF, we derive the hydrodynamic-like equation, which can be used as Spitzer's model but without the weak-field limit. For fast electron transport in the FI targets, it is found that the return current obtained with our new current model can compensate the beam current almost completely, whereas the one obtained with Spitzer's model cannot [4].

For the second problem, we find that collisional effects play significant role for the beam-plasma instabilities. In particular, we find the electrostatic instability (such as the two-stream instability) is attenuated and finally stabilized by collisional effects. However, the electromagnetic instability (such as the filamentation instability) is enhanced. The latter becomes dominant in the nonlinear evolution [5].

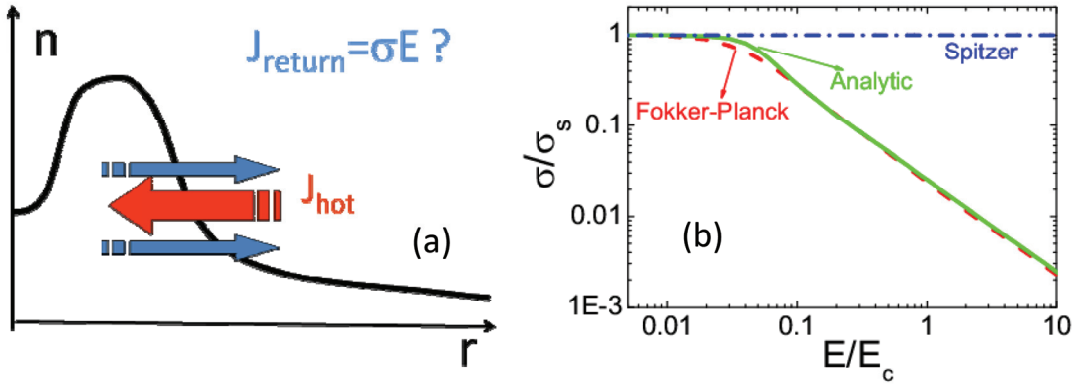

Figure 4: Schematic plot for the hot electron transport and return current formation in dense plasma (a); Comparison of the Plasma conductivities as functions of dc electric field, obtained by Spitzer's model and our new model (b).

Acknowledgements

The author wishes to express my gratitude to the JSPS, CAS, and other funding agencies such as National Science Foundation of China (NSFC) for the financial support. Thanks to the coordinators and key persons from both sides for their support. In the first five years, the key persons are Prof. Zunqi Lin and Prof. Kazuo A. Tanaka for I-5A, Prof. Shaoping Zhu and Prof. Kunioki Mima for I-5B. In the second five years, the key persons are Prof. Shaoping Zhu, Prof. Jianqiang Zhu, and myself from China, Prof. Kunioki Mima, Prof. Hideaki Takabe, and Prof. Kazuo A. Tanaka from Japan. Thanks to the participants of the CUP program for their contributions to make a successful program. Last but not the least thanks are due to the secretaries from both sides for their dedicated support. The author is also greatly indebted to Academician X.T. He for providing some information about SG II and SG III, as well as to Prof. Z.Y. Wei, Prof. W. Yu, and Dr. H.B. Cai for some figures shown in this report.

References

[1] W.G. Zheng et al., J. Phys.: Conf. Ser. 112, 032009 (2008).
[2] W. Yu et al., Laser and particle beams 109, 27(2009)
[3] H. B. Cai, K. Mima et al.., Phys. Rev. Lett. 102, 245001 (2009).
[4] S. M. Weng et al., Phys. Rev. Lett. 100, 185001 (2008).
[5] B. Hao et al., Phys. Rev. E 79, 046409 (2009).

Laboratory Astrophysics Joint Research with China Group Lead by Jie Zhang, President of Shanghai Jiao Tong University

H. Takabe
Institute of Laser Engineering and Graduate School of Science
Osaka University

Laboratory astrophysics is a new field to study a variety of plasma astrophysics phenomena in laboratory with use of intense and large-scale lasers originally developed for researching laser fusion. Laser fusion is to realize a miniature Sun in laboratory; that means it can be also used for study of stellar dynamics and many of plasma phenomena in the Universe. From the first proposal of the new research field, it has passed almost 15 years and it now attracts many laser plasma experimentalists to challenge a variety of topics. The author would like to report mainly the joint activities with China in the last decade supported by Japan-China CUP program.

1. Introduction

If you face to solve some physical phenomena in laboratory or in the Universe, you are required to select or decide which equations should be solved with what kind of boundary condition and with aid of physics data already known. It is more precise but not a cleaver way to couple many equations to solve complicated physical phenomena. Then, we are required to pick up the most important physics and describe the phenomena with the simplest equations. This "Modeling" is nothing but the most interesting element in researching science.

If the basic equations are relatively simple, we can solve them with analytical way. It is, however, not the case of modern physics, especially the case of astrophysics. Most of attractive phenomena observed with modern observational methods are expected to be ones as the result of coupling of a variety of physics. So-called integrated physics is required to be solved to understand the controlling physics and core of physics in the complicated phenomena.

This logic is the same even in the case of physics measured in laboratory, especially in the case of plasma physics. They can be, however, made simpler compared to the plasma physics in the Universe by controlling the initial and boundary conditions in the controlled experiments.

Anyway, it is usual that we have to solve the model equations with high-speed computer after reducing the model equations to digital relations. These numerical equations for the digital relation are also based on the new discipline developed in the last half century and are also interesting subjects. But, we yield the description to other textbooks or papers.

Numerical simulation has been said to be the third method to study science after experiment and theory. As the same as analytical case, if the basic equation is the same between the plasma in laboratory and that in the Universe we wish to understand, we can expect in a special case the same result after solving the equations. In order to understand this easily, let us think of the case of Navier-Stokes equation controlling the aerodynamic and hydrodynamic phenomena:

It is well known that this equation can be normalized with typical parameters of the targeted phenomena like

$$\mathrm{Re} = UL/\nu,$$

where Re is the very famous Reynold number of non-dimension. This means we can expect exactly the same physics regardless of the dimension of space and time scale under the condition that the Reynold number is kept the same.

This theoretical logic has been used in the design of aircrafts as wind tunnel experiment by

recent days. It might be interesting to point out that modern aircraft design has been replaced with computer simulation in the last few decades and Boeing 777 is designed about 70 % with computer. This is a good example of how the method of engineering changes after the maturity of new technology.

Such scaling law is called self-similarity of the physics and has been used mainly in solving nonlinear hydrodynamic equations. One of the most famous solutions is Taylor-Sedov self-similar solution for the case of a point explosion in a uniform gas. If the energy is 1 Mega-ton TNT (10^{17}Joule), the solution gives us the blast wave when hydrogen bomb explodes and if the energy is 10^{44} Joule, it gives the dynamics of supernova explosion. In the laboratory, we can make a small scale explosion with intense short pulse laser. If the energy of the laser is of the order of 100 Joule, we can obtain the blast wave in laboratory.

The idea of laboratory astrophysics is to demonstrate and clarify the physics controlling the phenomena in the Universe with model experiments with intense lasers in laboratory. The model experiments should be designed with corresponding scaling law and then the physics condition such as usually characterized with non-dimensional parameter should be kept the same.

The key words, compressible hydrodynamics, atomic physics, radiation hydrodynamics, shock wave and so on, are also the key words to study astrophysics. By designing the target and laser condition so that another typical physics can be modeled, we can carry out model experiments of magnetic reconnection, jets, radiation source for photo-ionization, equation of states of extremely high pressure, radiation opacity, compressible turbulent mixing, non-LTE atomic physics, nuclear astrophysics, and so on.

The achievable temperature by lasers covers a wide range of astrophysical plasma. There is only one way with intense lasers except for nuclear weapons to realize such high temperature comparable to many objects in the Universe. This is the reason why we propose Laboratory Astrophysics is an emerging new academic field in Astrophysics.

It is very important to summarize why we promote this field intensively. There are four purposes:

(1) Validation of computational codes used to study astrophysics by reproducing the result of the model experiment in laboratory.
(2) Expectation of new finding or new physics which we did not expect before the model experiment.
(3) Prediction of very new physics in the Universe which has not been found through many observations so far.
(4) Increase the attractiveness of Plasma Physics to apply it to astrophysics and deep insight in analyzing the model experiment data.

In the present paper, we cannot review all aspects of the proposal laboratory astrophysics subjects and results obtained so far. We recommend the reader to read the review article by the author [1] on a variety of proposals of model experiments and B. Remington et al. [2] on the comprehensive review mainly of the experimental data and its relation to astrophysics. The laboratory astrophysics has been promoted by bi-annual international conferences. In addition, Jie Zhang (President of AAPPS), Gang Zhao (NAOC), and H. Takabe has have organized Laboratory Astrophysics international conference four times in China..

In the present paper, we focus on the topics now carried out as project in our institute under collaboration with China and another countries. In Section 2, we focus on the subject of the photo-ionized non-LTE atomic physics issue. This is a model experiment of photo-ionization of a companion star by almost 1keV Planckian radiation source created by a compact objects, Black Hole and Neutron Star. In Section 3, we report our new theory for the formation of almost all collionless shocks in the Universe and the present status of the model experiment to demonstrate thatthis theory does work. In Section 4, we briefly summarize the future prospect of the laboratory astrophysics.

2. Atomic Physics of Hot Plasmas in the Universe

The spectral opacity and emissivity are fundamental ingredients to study a variety of subjects where

radiation transport becomes important in any dynamics of matter in the Universe. Recently, the first star in the Universe becomes a big topics and the physics becomes simpler for the star formation in the early Universe, because almost all matters are only Hydrogen and Helium whose atomic structure is very simple. The evolutional scenario of the stars strongly depends upon the metalicity of the Universe and it increases with time. The main reason is that the matter becomes optically thick after many of nucleo-synthesis in massive stars as time goes on. For example, the fraction of iron (Fe) in solar abundance is extremely small compared to the hydrogen, but it cannot be neglected in solving the radiation transport in general.

The metalicity dependence of the evolution of stars as function of the initial mass of stars is calculated, for example, by A. Heger et al[3]. Roughly speaking, in the early Universe massive stars are produced because heated energy by gravitational collapse can escape easily with the radiation transport and the radiation cannot drive stellar wind because of low opacity. As the age of Universe approaches to the present time, the increase of metalicity prevents the formation of very massive stars and it is said that the heaviest mass of the main sequence is about 40-60 solar mass.

It is obvious, therefore, that the detail information of the partially ionized metals in the Universe should be studied. With the aid of rapid progress of computational ability, very complicated atomic structure becomes able to be solved for *ab initio* model. For example, Grant code and Cowan code are two most famous codes for this purpose. It takes a long time even with the present super computer to obtain the atomic data for one configuration in the case of relatively many electrons system. More convenient and precise numerical modeling has been done, for example, by Klpapish et al. [4] and Igresias et al. [5]. That is para-potential method which is the equation of one-electron system with an effective potential so that the resultant atomic structure reproduce Hartree-Fock type consistent field model result. HULLAC code developed by Klapish et al. is now

available [4] and OPAL code is now widely used for opacity of astrophysics [5]. It should be noted that appearance of OPAL was critical to validate the theory of light curve of Nova [6].

It is not well known in Astrophysics area that OPAL code has been validated and improved with OPCITY experiment with intense lasers. This is very traditional laboratory astrophysics.

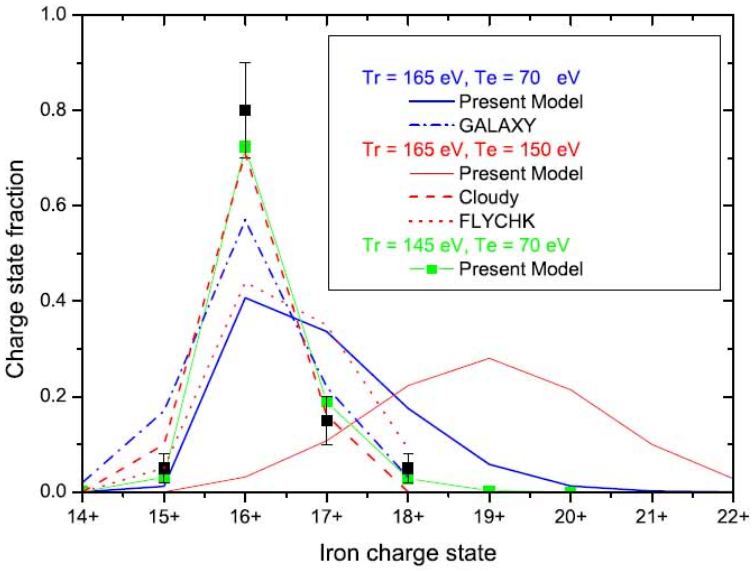

Figure-1

Recent topics already shifted to photo-ionized plasma[7]. Sandia National Lab in USA and our team are now leading the topics in the world. Sandia uses Z-Pinch machine to do experiment and mainly focus on the opacity of radiation heated matter. They compared their results with many codes used in astrophysics [8] and found difference among them. We have carried out the self emission [9] and absorption [10] experiment as Joint experiment with China. At the same time Feilu has developed a rate equation solver and compared it to the result by Sandia as shown in **Fig.1[11].**

In Fig. 1 the square data are Sandia experimental data. We have compared four different code results; our code, GALAXY, Cloudy, and FLYCHK. GALAXY and Cloudy have been developed in astrophysics and open code, while the FLYCHK is developed in laser plasma physics and widely used[12]. The main idea of our code is the same as FLYCHK, but the result is different from code to code. It is found that we can reproduce the experimental data when we assume the radiation temperature is 145 eV and the free electron temperature of the radiatively heated sample is 70 eV. The charge distribution is very sensitive to the temperature and over-ionization is clearly seen if we assume Tr=165 eV as shown in Fig. 1. It is surprising that Cloudy gives the best fit when we assume unphysical condition such as Tr=165 eV and Te=150eV. GALAXY gives the best fit at Tr=165 and Te= 70 eV. FLYCHK cannot give a good fit with any

combination of Tr and Te. You can see how difficult to model the photo-ionized plasma. We need more experimental data for verification and validation of the simulation codes. The code comparison would be needed with code developers from laser plasma and astrophysics.

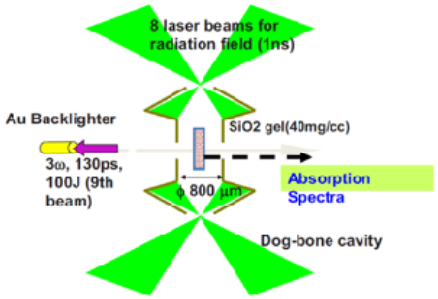

Figure-2

We describe laser-driven photoionized plasma experiments. First, we consider an experiment performed in the Shenguang II laser facility in Shanghai, China where a silicon gel sample placed in a "dog-bone" shaped *Hohlraum* cavity was driven by eight laser beams entering the *Hohlraum* in two groups of four beams through both ends of the cavity, as displayed in Fig. 2. The dog-bone shaped *Hohlraum*, which has cylindrical symmetry and is approximately 2.5 mm long by 0.8 mm in diameter, prevents the laser beams from directly interacting with the silicon-gel inside the main body of the *Hohlraum*.

It is the *Hohlraum* radiation field that actually heats and ionizes the silicon gel thus turning it into photo-ionized silicon plasma. The plasma was backlit with the x-ray flux from a gold laser-produced plasma, and the transmission spectrum through the silicon plasma recorded for detailed spectroscopic analysis. In a first approximation, the interpretation and modeling of the data assumed Saha equilibrium ionization and level population distribution with detail term accounting description of the energy level structure. Energy level and ionization potential values were computed with the flexible atomic structure code.

The transmission spectrum included absorption arising from $1s^2 2l^m n'l'$ to $1s^2 2l^{m+1}$ line transitions, where m is in the range from 1 to 8 in Be-through Na-like Si ions, and the spectral line shapes were Voigt profiles with a width dominated by instrumental broadening effects (FWHM~0.89eV). From the spectroscopic analysis of the transmission spectrum we extracted a density of 10 mgcm^{-3} and temperature equal to 56 eV, which is less than the radiation temperature (i.e., 80–100 eV)in the cavity. Also, it was possible to determine that 70% of absorption was due to ions in the ground state configuration (i.e., n'=2), 20% was due to excited ions with n'=3–6, and less than 5% from excited ions with n'>6.

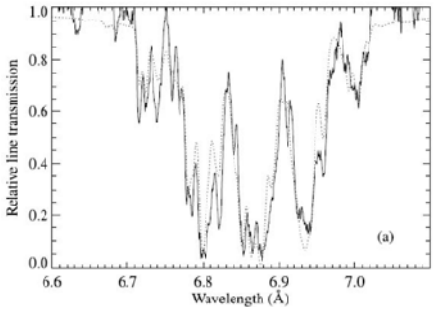

Figure-3

In Fig. 3, the comparison between experimental data and computational ones is shown [10]. In Fig. 3, the solid line is the experimental data and dotted line is the computational ones. It is clear the good agreement is obtained by using the temperature as adjustable parameter.

Another important aspect of photoionized plasma research is the observation and spectroscopic analysis of the radiation emitted by the plasma, i.e., the self-emission of the plasma. In this connection, we discuss an experiment fielded at the GEKKO XII laser facility of the Institute of Laser Engineering at Osaka University. In this experiment, the target was a gas-bag filled with nitrogen and placed inside a gold-coated dog-bone shape *Hohlraum* cavity, similar to the one used at the Shenguang II laser facility. The filling pressure of the gas bag is the nitrogen number density 1.4×10^{19} cm^{-3}. The almost Planckian radiation flux inside the cavity (radiation temperature of about 80 eV) drives the nitrogen gas turning it into a photo-ionized plasma [9].

The time evolution of the He- and H-like emission line spectra was recorded with a time-resolved spectrometer, and He- to H-like N ion line ratios were used to extract the plasma temperature. To this end, we have developed an atomic kinetics rate equation solver with detailed configuration accounting based on the screened hydrogenic atom approximation. The line transition energies and oscillator strengths were calculated with the HULLAC suite of atomic codes. From the analysis of the line ratio data we were able to determine electron and ion temperature of approximately 20 eV. The fractional populations of the plasma are displayed in [13] which also includes a comparison with results from the NIMP code. The calculations were done for a density of 0.325 mg cm^{-3}, electron and ion temperatures of 20 eV, and radiation temperature of 80 eV.

The next step in the development of this code will be to include inner-shell direct photoionization for treating plasmas made out of higher atomic number elements and relatively high radiation temperatures (~1 keV), as in the case of compact stars. Also, we are currently assuming that the bound electrons are in the ground state with only one electron in an excited state. In the cases of high radiation temperature,

K-shell electrons can also be ionized with X-rays of energies higher than the ionization threshold. Work is currently in progress to extend the atomic kinetics model to include this effect.

In the above experiments with gold cavities, we cannot model the situation of, for example, X-ray binary where high temperature thermal radiation with the radiation temperature of about 1 keV heats the surrounding cloud and the surface of a companion star as schematically shown in Fig. 9. It is reported for the cases of CYGNUS X-3[14] and VELA X-1[15], strong line emissions from the highly charge Si, S, Ar, Fe, etc. are observed in the strong continuum radiation as shown in Fig.10[14]. It is already identified that the continuum component stems from the radiation with thermal temperature of a few keV generated mainly in the inner region of the accretion disk of compact star, black hole candidate (Cyg X-3) and neutron star (Vela X-1). It is also identified that the line emissions stem from the surface plasma which is relatively very low temperature (Te=10eV) but strongly photo-ionized by the radiation.

In order to carry out a model experiment of such extreme phenomena, we need to produce the thermal X-ray source with its temperature of the order of keV. It is impossible to realize such temperature with cavity plasmas mentioned above. Recently, however, we could carry out the model experiment of X-ray binary situation by use of the thermal radiation from an imploded core spherically compressed with 12 beams[16]. It is early to report the details of the experimental data, but we could reproduced the line emission profiles stemming from He-like Si highly ionized by the thermal radiation of the compressed core with a Planckian radiation of 0.5 keV.

In our recent paper[16], it is concluded that the same spectral profiles can be demonstrated with this model experiment, but the theoretical analysis concluded that although the line hump beside the He-like resonance line observed in Chandra is speculated to be due to the forbidden line emission, our detail analysis of the experimental data suggests it is mainly due to three blended satellite emissions when K-shell electron is photo-ionized in Be-like Si ions. The readers who wish to know more details are recommended to contact the author by e-mail.

3. High Mach-Number Collisionless Shock Formation

Big laser facilities of intense lasers have been developed mainly for the purpose of laser driven inertial confinement fusion (ICF) and it is almost just before the demonstration of ignition and burn in a couple of years. Because of the maturity of the discipline of laser fusion research, the main topic in ICF has shifted mainly to the hydrodynamic phenomena of compressed high energy density (HED) plasma. There are a lot of researches of laboratory astrophysics with use of HED plasmas. In addition, opacity issue has been studied from the early stage of the research relating to astrophysics. We can find a lot of such topics in the review papers [1,2]

In the Universe, however, the density is very low and temperature is high in general. The collisionless nonlinear plasma physics becomes also very important. Although the use of intense laser can model such exciting and very essential physics to understand a lot of unknown physics in astrophysics, there are not so many activities to study the nonlinear physics of collisionless plasma, for example, with use of the characteristics of the high-velocity and high-temperature plasmas produced by intense lasers, whose density is in the range of 10^{20} cm^{-3}, flow velocity is almost 1,000 km/s, and Mach number is more than 20. Such plasmas can be easily produced as ablating plasmas irradiated by intense lasers on solid targets.

Laser plasmas with high flow velocity can be a good test-bed to clarify the extreme physics only seen in the Universe. The collisionless shock formation and resultant particle acceleration, for example, in supernova remnants (SNRs) are a typical example of such extreme phenomena. If we can clarify the formation of a collisionless shock in model experiment with intense lasers to confirm the simulation result of a newly proposed physical mechanics without external magnetic field as shown in our recent paper [17], it would be a striking message to Astrophysics. In our recent paper based on two-dimensional PIC (particle in cell) simulation, we proposed the collisionless shock formation mediated by Weibel instability. The physics mechanism of its nonlinear evolution and structure formation are clarified for the non-relativistic shocks such as SNRs. It is noted that the collisionless shock formation mediated by Weibel instability was demonstrated numerically in highly relativistic electron-positron plasmas by one of the authors [18] before the present work.

They are now very hot topics in high-energy astrophysics that how relativistic collisonless shock waves are produced in the electron-positron fireball in gamma-ray bursts [18,19], how relativistic collisonless bow shocks are produced by cosmological jets (AGN jets) [20], and so on. It has been believed quite a long time that the background magnetic field needs to help the formation of the collisonless shock in the Universe. Actually our galaxy is full of magnetic field of average 3 μG. This is mainly because the collsionless shock really observed by satellites in the space is the bow shock of the earth magnetosphere

and in this case it is clearly concluded that the magnetic field is essential to the formation of the collisionless shock. It is, therefore, reasonable to think that some external magnetic field should be essential to form and maintain the observed collisonless shocks in the Universe.

It is natural to guess that there should be a uniform external magnetic field, when we see the very smooth and cylindrically symmetric X-ray image of SN1006 SNR as shown in Fig. 4-(a) [21]. It is, however, an exceptional case and most of the SNRs do not show clear structure globally and have sharp edges locally [22]. It is more natural to think of the physics scenario for the formation of the collisionless shock without any help of external magnetic field in the Universe.

Figure 4-(a)

It is important to compare the shock thickness to average Coulomb mean free path in the case of typical SNR. In Fig. 4-(b), the left edge of the x-ray image of SN1006 taken by Chandra X-ray satellite is shown with the stretched special distribution of the X-ray intensity [23]. It should be noted that the typical temperature and density at the rear of the shock front is $T_i \sim 15$keV ($T_e \sim 0.5 \sim 1$ keV) and $n_i \sim 1$ cm^{-3} and the corresponding proton Coulomb mean-free-path is estimated to be $4\text{x}10^{19}$ cm (=13 pc). The diameter of SN1006 is about 10 pc (= $3\text{x}10^{19}$ cm). The shock front width which is here defined to be that of the sharp intensity front in Fig. 4-(b) is about 0.04pc (=$1.2\text{x}10^{17}$cm) [23] (it should be noted that it is much thinner than this width). As a result, it is concluded that the thickness of the shock front of SN1006 SNR is less than 1 % of the radius and the Coulomb mean free path is 400 times longer than the shock front thickness; namely, the shock should be the collisionless shock.

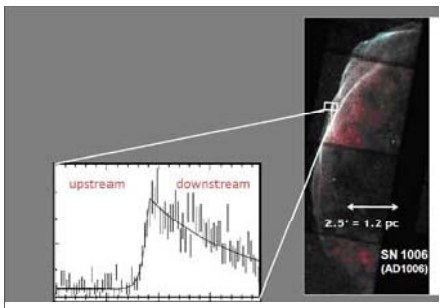

Figure 4-(b)

The explosion energy of a typical supernova (SN) is 10^{44} J and the proto-SN material is ejected with the velocity of the order of 10,000km/s by a shock wave generated by the gravitational collapse of the core of a massive star (Type II SN) or by a shock wave driven by the detonation wave in thermonuclear burning of C/O white dwarfs (Type Ia). The ejected material does snow-plow the interstellar gas for one hundred years and when the snow-plowed mass becomes roughly equal to the ejected mass, so-called Taylor-Sedov blast wave is generated and the shock front velocity decrease as $(\text{time})^{-3/5}$. The reverse shock is also produced to heat up the ejecting plasma [24]. The hydrodynamic instability of such SN explosion was the first target for modeling dynamics of astrophysical phenomena [25] and the intensive experimental studies have been carried out as reviewed in [2].

It should be noted that the velocity of the collisionless shock of SN1006 in Fig. 11 is U_s = 3,000 km/s evaluated through the observation over 11 years [26]. Typical values for the supernova remnants are given in Ref. [24] and (t, R_{sh}, U_{sh}) = (100, 2, 8000), (1000, 5, 2000), (10000, 12.5, 500), where t is the time after explosion in the unit of years, R_{sh} is the shock front radius in the unit of pc (=$3.1\text{x}10^{18}$cm), and U_{sh} is the velocity of the shock front in km/s unit, respectively.

Such blast wave phenomena were observed in laboratory in the early stage of laser plasma research as shown, for example, in Ref. [27]. The laser energy of 100 J heats the surface of solid aluminum to produce the ejecting material (ablating plasma) with the velocity of several 100 km/s and it expands in Nitrogen gas in target chamber to clearly produce Taylor-Sedov blast wave [27]. Its time evolution and energy dependence, density dependence etc. have been studied intensively and the Taylor-Sedov self-similarity has been confirmed experimentally.

It should be noted that the big and essential difference of SNR shock compared to the laser shock is not the difference of the energy: it is the difference of 42 orders of magnitude, but the difference of physics. The shock wave of the SNRs is the collisionless plasma shock as described previously, but the laser shock wave is in general the collisional hydrodynamic shock wave. In the laser shock, the mean free path is almost the same as the thickness of the shock front. In addition, the collisionless shock accompanies the electric and magnetic fields which play essential role in accelerating charged particle, namely the origin of cosmic rays.

In the case of the formation of the collisionless shock, the external magnetic field or a generation of the magnetic field is essential and the Larmor radius which is extremely shorter than the Coulomb mean free path determines the thickness of the collisionless shock surface (transition region). For example, proton Larmor radius with velocity 10^3 km/s in 3 μG magnetic field is $3x10^9$ cm extremely shorter than the radius of SNRs. In Fig. 11, X-ray emission from the shock surface stems from up-shifted cyclotron emission ($\omega=\gamma^2\omega_{ce}$; γ: Lorentz factor) from ultra-relativistic electron with the energy of about 10 TeV[21]. The up-shifted photon energy of the cyclotron emission is given in the form:

$$h\nu_{rce} = 2\ \text{keV}\left(\frac{B}{10\mu G}\right)\left(\frac{E_e}{10^{14}eV}\right)^2,$$

where E_e is the energy of accelerated electron.

Such direct observation of continuum X-ray emission approved that electrons are accelerated near the collisonless shock surface and ions are also expected to be accelerated at the same time [28]. Such acceleration physics is a long-standing question of the origin of Cosmic-ray[29]. In Ref. 29, there is an explanation of well accepted acceleration mechanism, Diffusive Shock Acceleration (DSA), based on a statistical model proposed by E. Fermi[30]. Chandra X-ray satellite provided us with highly spatial resolved image of SN1006[23] and it was suggested that there should be some amplification mechanism of magnetic field near the shock front. It is recently inferred from observation that the magnitude of magnetic field is about 1 mG and seems to be the result of an amplification more than 100 time stronger at the shock front of another young SNR[31]. This observation also supports the self-generated magnetic field scenario explained below.

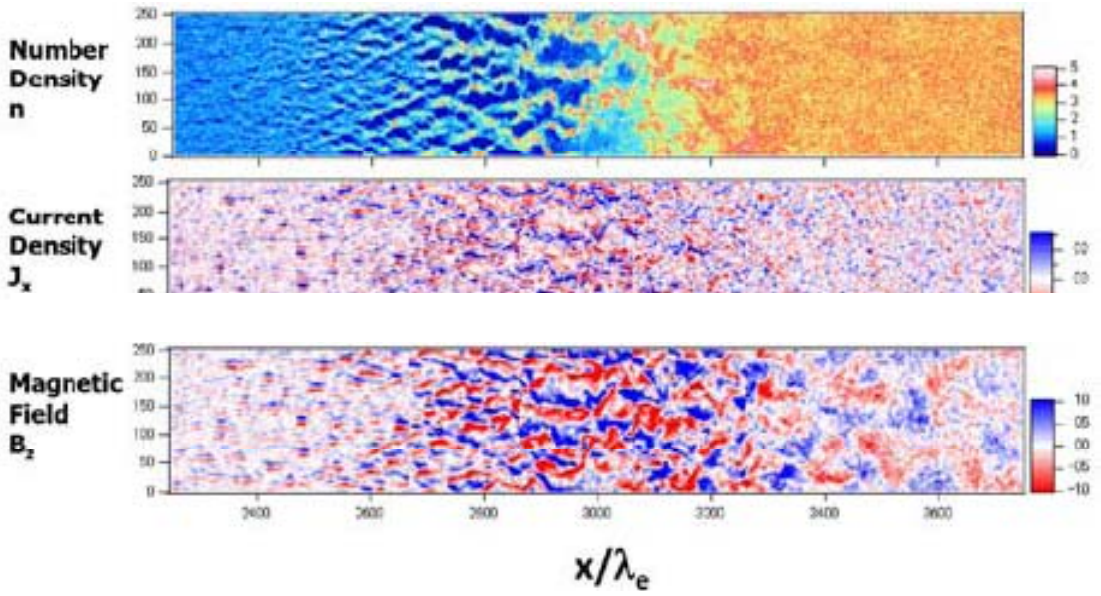

Figure 5

We have carried out two-dimensional Particle-in-Cell (PIC) simulations in x-y plane with different mass ratio of ion to electron and different plasma velocity in non-relativistic region[17]. In Fig. 5, the typical snapshots of the ion density, total electric current in x-direction, and magnetic filed in z-direction are shown when almost steady-state collisionless shock wave is produced in the counter streaming system. It should be noted that the two counter streams of plasmas start to penetrate to each other at time = 0 at the right boundary. It takes about $\omega_{pi}t = 500$ to see the formation of the steadily propagating shock front, where ω_{pi} is the ion plasma frequency. It is clearly seen in Fig. 5 that the filamentary structure of the density appears near the left edge and the thickness of the filament grows with the decrease of the number of the filaments. This is well known filament coalescence phenomena predicted in 1970s [32].

Relating to the fast ignition laser fusion [33], there are many papers published on the highly nonlinear stage of Weibel instability[34]. The Weibel instability is induced when the velocity distribution is anisotropic in velocity space [34]. In the present case, electron and ions have the same velocity and plasma flow to the right and left co-exist at the same place. This is a very asymmetric velocity distribution and is unstable to Weibel instability. In the simulations, we also observed electrostatic two stream instability. It grows near the front of the counter stream and gets into nonlinear stage, but the electric field does not increase compared to the case of one-dimensional simulation, where

particle trapping is seen in highly nonlinear stage [35]. Instead, the Weibel instability becomes dominant. Initially, the electron moves to make current channels, then the ions start to move so that the filamental currents increase. However, ambipolar filed prevents both electron and ions make different current channels. In the late nonlinear phase, the ion heavier than electron sustains the current and current filaments coalescence to become larger size filaments as known well [32].

When the magnitude of the magnetic field increased as seen from the left to right in Fig. 5, the size of the filaments also increases and the mean velocity of the ions almost vanished to stagnate in the central region. Because of the deceleration of ion flow by the induced magnetic field, the ion density increases as see on the right in Fig. 5. This is the formation scenario of the collisionless shock mediated by Weibel instability. It is also found that about 2 % of the ion kinetic energy density is converted to the energy density of the magnetic field in the region where the density increases. It must be noted that only 2% (the effective β=50) is enough to modify the straight orbit of the ion flow.

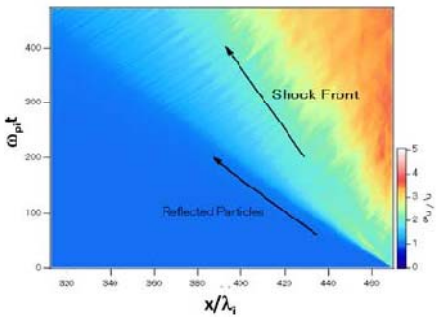

Figure 6

In Fig. 6, space-time evolution of the ion density averaged in the y-direction is shown in order to see the shock wave formation, where $\lambda_i = c\omega_{pi}^{-1}$ is the ion inertial length. The injected particles from the left travel as indicated "Reflected Particles" and they travel to the left-above corner in Fig. 6. It is clearly seen that at the time longer than $\omega_{pi}t$=200, the shock wave is already produced and it propagate to the left as steady state. It should be noted that such time scale becomes shorter by a factor in general in three-dimensional case as well studied, for example, nonlinear stage of the Rayleigh-Taylor and/or Richtmyer-Meshkov instabilities. It is natural that the increase of the number of freedom leads the time for nonlinear evolution faster.

The thickness of the shock front is about 100 ion inertial length ($c\omega_{pi}^{-1}$), and it is found in Ref. 17 that the thickness is independent on the flow velocity and mass ratio. It is also found that the counter stream is also unstable to the electro-static instability and the electric field is predominant near the front of the shock wave due to the two stream instability, but the energy of the electric field is kept much less than that of the magnetic field in the region where Weibel instability grows and proceeds to the nonlinear stage[17].

The basic equations governing the physics described above are Vlasov equations to the electron and ion, and Maxwell equations. If we can produce the counter streaming plasmas in the collisionless condition, we can do a model experiment to clarify if the present new scenario does work in the Universe. It is widely accepted that any simulation code should be verified and validated with model experiments [36]. In Ref. 36, it is mentioned that $3.5 Billion NIF (National Ignition Facility) [37] was funded in order to verify and validate the reliability of 3-D integrated codes for nuclear weapons. It is regarded as a reasonable facility and cost in USA for improving the reliability of the integrated codes for nuclear weapons under SBSS (Science Based Stockpile Stewardship) program [38].

There was a model experiment long time ago in UK to demonstrate the formation of collisionless shock with laser produced plasmas. Pioneering work was done by A. Bell et al [39] who observed the bow shock image around the spherical obstacle modeling the earth in laser ablating plasma modeling solar wind. In this case, external magnetic field has been imposed to help the formation of the collisionless shock. Subsequent and intensive works have been done by N. Woolsey's group to demonstrate the difference of stagnating shock formation with and without magnetic fields [40]. Their works should be appreciated, while the present proposal is very different from their work as the readers have already seen in this article.

IWe carried out a joint experiment in China with Shenguang-II facility in Shanghai [41,42] for the better scheme. The experimental data are in the process for publication from both of Japan and China.

We do not describe the details of the scaling law, while the readers who are interested in it are recommended to see the paper [43]. By use of the resultant scaling law, we can estimate how large plasma is necessary to follow from the growth of the linear instability, nonlinear phase, and substantial growth of magnetic field to the structure formation of the collisionless shock. If we can produce the counter-streaming plasma with velocity of 1000 km/s and the density is 10^{20} cm^{-3}, the scaling law says the thickness of the collisionless shock is 3 mm. It is note that this parameter allows sufficient collionless phenomena.

In order to measure the whole scenario from the beginning to the shock formation, we might need plasma whose size is 5 mm cube. Then, we can calculate how much flow velocity energy this cube has

very simply. It is 10 kJ. We can conclude that we need a big laser like OMEGA-EP and NIF for the critical demonstration of the formation of the collisionless shock formation and resultant particle acceleration.

4. Conclusion

In the present paper, we have introduced the concept of Laboratory astrophysics and explained the present status of two topics; one is the topic regarding photo-ionized plasma, and the other is the collisionless shock formation in the Universe.

The laser can produce the pressure of 40 Mbar, the highest pressure of Jupiter, with ablation pressure and such equation of state studies are also carried out in our institute. The most important issue in this study is how to keep the compressed matter cool as inside of Jupiter. This requires the same kind of technique as laser fusion requires, namely laser pulse tailoring. We hope the progress of techniques also brings new subjects as targets for Laboratory Astrophysics.

References

[1] H. Takabe, Prog. Theo. Phys. Suppl. **143**, 202 (2001).
[2] B. Remington et al. Review of Modern Physics, **78**, 755-807 (2006).
[3] A. Heger et al., The Astrophysical Journal, **591**:288-300 (2003).
[4] E. Klapish, Comput. Phys. Commun. 2, 239 (1971).
[5] F.J. Rogers and C.A. Iglesias, Science 263, 50 (1994) ; http.//www phys.11nl.gov/V-Div/O PAL/.
[6] M . Kato and L Hachisu , Astrophys . J . 437 , 802(1994)
[7] M. E. Foord et al.: Phys. Rev. Lett. 93 (2004) 055002.
[8] M. E. Foord et al.: J. Quant. Spectrosc. Radiat. Transfer. 99 (2006) 712.
[9] F. L. Wang et al., Physics of Plasmas 15, 073108 (2008).
[10] H. G. Wei et al., The Astrophysical Journal, 683:577–583, 2008
[11] F-L. Wang et al., J. Phys. Soc . Jpn. **78**, 064301 (2009)
[12] H. K. Chung, W. L. Morgan and R. W. Lee: J. Quant. Spectrosc. Radiat. Transfer. 81 (2003) 10
[13] R. C. Mancini et al., Physics of Plasmas 16, 041001 (2009).
[14] F. Paerels, et al., Astrophys. J. Lett. **533**, L135 (2000); S. Kitamoto et al., Publ. Astron. Soc. Jpn **46**, L105-108 (1994); K. Kawashima and S. Kitamoto, Publ. Astron. Soc. Jpn **48**, L113 (1996).
[15] S. Watanabe, et al., Astrophys. J. **651**, 421 (2006).
[16] S. Fujioka, H. Takabe et al., Nature-Physics **5**, 821-825 (2009).
[17] T. N. Kato and H. Takabe, Astrophys. J. Lett., **681**, L93-L96 (2008).
[18] T. N. Kato, Astrophys. J., **668**, 974 (2007)
[19] A. Spitkovsky, Astrophys.J **673**, L39 (2008).
[20] P. L. Biermann, edited by J. M. Matthews, *High Energy Astrophysics: Models and Observations from MeV to EeV*, p. 217 (World Scientific Publ., 1994)
[21] G. Cassam-Chenai et al. to be published in ApJ (2008).
[22] A. Bamba et al., Astrophys. J. **621**, 793-802 (2005).
[23] A. Bamba et al., Astrophys. J. **589**, 827 (2003).
[24] F. Shu, *Gas Dynamics, The Physics of Astrophysics II,* (University Science Books, 1992), Chapter 17, p. 230.
[25] H. Takabe, *ICF and supernova explosion,* Jpn Plasma Fusion Res. **69**, 1285-1300 (1993) *in Japanese*.
[26] P. Ghavamian et al., ApJ, **572** 888 (2002).
[27] J. Grun et al, Phy. Rev. Lett. **66**, 2738 (1991); Laser Part. Beams **21**, 529 (2003).
[28] K. Koyama et al., Nature **378**, 255 (1995).
[29] A. M. Hillas, J. Phys. G; Nucl. Part. Phys. **51** R95-R131 (2005).
[30] E. Fermi, Phys. Rev. **75**, 1169-74 (1949); Astrophys. J **119**, 1-6 (1954).
[31] Y. Uchiyama et al., Nature **449** 576-578 (2007).
[32] R. Lee and M. Lampe, Phys. Rev. Lett. **31**, 1390 (1973)
[33] M. Tabak et al., Phys. Plasmas **1,** 1626 (1994); K. Mima, J. Phys.: Conference Series **12,** 012005 (2008).
[34] R. L. Morse and C. W. Nielson, Phys. Fluids **14**, 830 (1971).
[35] F. F. Chen, *Introduction to Plasma Physics* (Plenum Press, 1974), Chap. 7.
[36] D. E. Post and L. G. Volta, Physics Today, Vol. 58, No. 1 (2005).
[37] E. I. Moses, J. Phys.: Conference Series **12,** 012003 (2008).
[38] http://nnsa.energy.gov/
[39] A. Bell et al., Phys. Rev. A 38, 1363(1988).
[40] N C Woolsey et al J. Phys.: Conf. Ser. **112** , 042009 (2008).
[41] W. Y. Zhang and X. T. He, J. Physics: Conference Series **12**, 032001 (2008).
[42] T. Morita, et al., Physics of Plasmas 17, 122702 (2010).
[43] H. Takabe, et al., Plasma Physics and Controlled Fusion **50**, 124057 (2008)

Summary of CUP Collaborations for Fusion Reactor Technologies

Takeo MUROGA
National Institute for Fusion Science, Toki, Gifu 509-5292, Japan

1. Program overview

The collaborative researches in Fusion Reactor Technologies have been carried out by four tasks on Low Activation Materials, Tritium/Blanket, Superconducting Magnet and Advanced Reactor Design/Technology Integrations. The key person and task leaders in the CUP collaboration period are summarized in Table 1. Every fiscal year, about 20 persons and 200 person x days of assignments from China to Japan and about15 persons and 80 person x days of assignments from Japan to China were performed. Also carried out were four CUP seminars during the period. The program contributed to education of young scientists by exchanging them as visitors for collaborative researches or by accepting them as graduate students in Japanese Universities.

2. Research highlights

The research highlights for the four tasks are summarized as follows.

Low activation materials:
Comparison of Japanese and Chinese candidate materials (RAFM, V-alloys)
Fabrication technology and characterization (RAFM, SiC)
Characterization of low activation materials using Chinese and Japanese infrastructures (TEM, Accelerator, Corrosion test system)

Tritium/Blanket:

Table 1. Key persons and task leaders for the category of fusion reactor technologies

	FY 2001-2005		FY 2006~FY2010	
	China	Japan	China	Japan
Key Person	Peide Weng Songtao Wu	T. Muroga H. Takahashi S. Tanaka	Damao Yao ↓ Yu Wu Yuntao Song	T. Muroga S. Ohnuki
Low activation materials	Jinnan Yu	A. Kohyama	Farong Wan	S. Ohnuki
Tritium/Blanket	Zengyu Xu	S. Tanaka	Kaiming Feng	S. Tanaka ↓ Y. Oya
Reactor Design	Yican Wu	T. Muroga	Yican Wu	T. Muroga
Superconducting technology	Peide Weng Songtao Wu	S. Yamada	Damao Yao Yu Wu Yuntao Song	S. Yamada

Characterization of solid breeders using Japanese infrastructures
Modeling and simulation of H and D behavior
Discussion on tritium managements in fusion blanket
Discussion on possible collaboration on ITER-TBM

Reactor Design and Key Technology:
Neutronics evaluation of Japanese and Chinese blanket materials
Contribution to FFHR and FDS designs
Thermofluid investigation
Design comparison of convection flowing test facilities

Superconducting magnet technology:
Information exchange and discussion on Chinese and Japanese device technologies
Superconducting magnet system for fusion device
Cryogenic system for fusion device
HTc superconducor and its application for SC device
Test system for superconducting conductor and magnets

3. CUP Seminars and education

Four CUP seminars were carried out during the period for overall fusion technologies

First seminar : July 29-Aug. 2, 2002, Lanzhou
Task detailed planning
Initial tuning of the collaboration.

Second seminar : Oct. 4-6, 2004, Sendai
Interim review

Third seminar : Oct. 23-25, 2007, Guilin
Planning toward the completion of CUP

Fourth seminar : Oct. 19-22, 2010, Uji
Grand summary

It should be noted that the CUP collaboration also enhanced education by receiving young Chinese scientists as assignees for collaborative work in Japan or as students in Japanese Universities. As for SOKENDAI, seven students majoring fusion technologies from the CUP relevant institutes entered the University, out of which five obtained the Doctoral Degree and two are staying in the Ph.D course.

4. Examples of the collaboration

4-1 Neutronics and rector design

Chinese reactor design people participated in the NIFS design studies (Force Free Helical Reactor- FFHR). Among the example of the effort is adoption of carbon reflector with enrichment of Li-6 enhanced Tritium Breeding Ratio to ~1.4 for the FFHR molten-salt Flibe blanket. Also carried out was CAD and Monte Carlo Computing for FFHR which included conversion between CAD model and Monte Carlo computing model.

Tritium transport analysis for FFHR Flibe system was carried out for analyzing overall tritium balance of

FFHR-2 system. Tritium recovery from Flibe and tritium permeation from the blanket to the vacuum vessel were estimated considering the effects of Tritium Permeation Reduction Factor (TPRF).

Analysis of activation properties of vanadium Alloys (NIFS-HEAT, SWIP-HEAT and US-HEAT) were carried out in which radioactivity of candidate V-alloys were compared considering the difference in the impurity levels. For the Japanese and Chinese alloys, ^{60}Co dominates the dose rate to 50 years. After the cooling time of ~100 years, the dose rate of Japanese candidate (NIFS-HEAT-2) is dominated by ^{94}Nb and that of Chinese candidate (SWIP-Heat) by ^{26}Al with minor contribution by ^{94}Nb.

4-2 Thermofluid Design and R&D

Both Japan and China operates or constructs liquid breeder loops for thermofluid and/or mass-transfer studies, e.g. Forced convection Li-Pb loop at Kyoto U, Thermal convection Li loop of U-Tokyo/NIFS, Thermal convection Li-Pb loop at ASIPP and Liquid metal MHD test loop at SWIP. Comparison of the design including thermofluid analyses was made by the collaboration. Also carried out was the MHD analysis for liquid metal blanket. The results were applied to characterizing test conditions for compatibility tests of structural materials with liquid breeders.

4-3 Characterization and Improvement of Candidate Alloys (Vanadium Alloys)

Low activation vanadium alloys are the common candidates of low activation structural materials for Japan and China. Comparison of Japanese (NIFS-HEAT) and Chinese (SWIP-HEAT) V-4Cr-4Ti candidates were carried out. First efforts were made for hydrogen embrittlement of Chinese and Japanese candidates[5]. Effects of hydrogen charging on tensile properties were compared. SWIP-HEAT was more sensitive to hydrogen. The difference in the oxygen level (NIFS-HEAT-2 : 140wppm, SWIP-Heat : 900 wppm) seems to be the source of the difference. After the collaboration, SWIP-Heat has made a progress and the oxygen level was reduced to ~200wppm.

Improvement of vanadium alloys were also explored, for example, V-W-Ti for improving hydrogen embrittlement resistance[6] and fine precipitation and cold working for improving resistance to thermal creep deformation of V-4Cr-4Ti was examined. High density of Ti-CNO precipitates were formed by double heat treatment to V-4Cr-4Ti. The fine precipitates were stabilized by cold working. The precipitates suppressed thermal creep deformation
Suppression of Thermal Creep Deformation by Cold Work followed by Annealing for NIFS and SWIP-HEAT were shown to be obvious in high stress range.

4-4 Characterization of Candidate Alloys (RAFM)

Japan was developing two reference 8~9Cr-2W reduced activation ferritic/martensitic (RAFM) steels, F82H and JLF-1. During the CUP collaboration, China fabricated its first candidate RAFM named CLAM. Comparison of JLF-1 and CLAM was carried out in the CUP framework.

The mechanical properties of CLAM steel were compared with those of JLF-1 steel by tensile and impact tests. The tensile results of CLAM showed the ultimate strength and yield strength were 670 MPa and 512 MPa at room temperature, and 373 MPa and 327 MPa at 873 K, respectively, which were higher than those of JLF-1. The Ductile-Brittle Transition Temperature (DBTT) of CLAM was 171 K by tests with one-third size Charpy V-notch specimens, and was 16 K lower than that of JLF-1. The microstructural analysis by SEM and TEM indicated that the prior austenite grain size and lath width for CLAM were smaller than those for JLF-1. The finer grain and lath structure was considered as one of main reasons for the better strength and DBTT for CLAM.

In the later tests, however, CLAM was shown to be more sensitive to thermal aging than JLF-1. Thus the initial mechanical properties and their stability were shown to be the trade-off.

SWIP is making another reference RAFM steel named CLF-1. Characterization of this alloy was also carried out in the later stage of CUP collaboration.

4-5. Component Fabrication Technology

Fabrication technology is the key to the success of Test Blanket Module project using ITER. Fabrication of blanket cooling channel by HIP (Hot Isostatic Press) process was carried out at ASIPP and tested at NIFS, including tensile, fracture, creep and hardness test. The key process for the properties of the joint was shown to be the degassing before the hipping.

Characterization of r ectangular CLAM Pipe was carried out using the samples extracted from the tube. Hardness of as rolled pipe showed that the harness peak is located at interfaces between a corner and a straight section. Tensile properties after standard heat treatment showed comparable properties to those of standard CLAM properties.

Fabrication of EB welding was carried out in NIFS followed by characterization of the resulting products.

4-6. Compatibility Tests

Compatibility of RAFM and Li-Pb is the common interest to China and Japan. Both countries installed unique test apparatus for the corrosion test. Comparative studies using a static immersion facility in ASIPP and a flowing test facility in NIFS showed the effect of the flow on the corrosion process. Exposure to Li-Pb resulted in dissolution of carbide precipitates at the grain boundaries.

5. Future directions for the collaboration

The Core University Program will end in March 2011. Various means to continue and extend the collaboration activities are under exploration. Smaller scale interaction by the both side including periodical mutual visit for short collaboration will be continues by the NIFS budget, in addition to the expected subsequent collaboration programs.

6. Summary

The achievements in fusion engineering are highlighted by comparison of Japanese and Chinese candidate materials, characterization of materials using infrastructures of the both countries, contribution to the reactor/blanket design activities and discussion on device technologies. The program has also contributed to education. The Japan-China Symposia are good opportunities for planning, tuning, discussing and summarizing the program. The collaboration will be continued using available programs and opportunities.

Summary on the researcher exchanges from FY2006-2011 from Chinese side (Basic Research of Nuclear Fusion Reactor Engineering)20-A,D,E,F

Y.WU & Y.SONG
Institute of plasma physics, Chinese Academy of Sciences

From 2006-2010, there are many research activities carried out in the field of “basic research of nuclear fusion reactor engineering” between Japan and China. This field includes: “study on reduced activation material for fusion”, “development of superconducting key technology for advanced fusion reactor”, “study of tritium behavior in solid and liquid breed material”, “advanced reactor design and technological integration”. More than 10 researchers from China visited National Institute for Fusion Science and other Japanese institute & university every year. Several JSPS-CAS CUP Program Seminars were held in China.
Based on EAST, LHD operation, JT-60 upgrade construction, ITER project, demonstration fusion reactor design, we can foresee that many co-operations can be carried out widely in this field.

1、Persons in charge and actual results

Table1 shows the persons in charge the different field from 2006 to 2011. Many researchers take part in the JSPS-CAS CUP Program Seminar and obtained a lot of achievement. Table 2 lists the persons visited in Japan from China in respective field from 2006 to 2011.

Table1 Persons in charge in different years

	FY2001-2005		FY2006~2011	
	CHINA	JAPAN	CHINA	JAPAN
Key person	Peide Weng Songtao wu	T.Muroga H.Takahashi S.Tanaka	Yu Wu Yuntao Song	T.Muroga S.Ohnuki
Low activation materials	Jinnan Yu	A.Kohyama	Farong Wan	S.Ohnuki
Tritium/Blanket	Zengyu Xu	S.Tanaka	Kaiming Feng	S.Tanaka
Reactor Design	Yican Wu	T.Muroga	Yican Wu	T.Muroga
Superconducting technology	Peide Weng Songtao Wu	S.Yamada	Yu Wu	S.Yamada

Table2 Persons visited in Japan from China in respective fields (2006-2011)

	Persons
Study on reduced activation material for fusion	Peng Lei, Wan Farong, He Ping, Huang Yina, Qiao Jiasheng, Wu Qingsheng.

Development of superconducting key technology for advanced fusion reactor	Yao Dayao, Huang Yiyun, Qian Jing, Liu Huajun, Chen Yonghua, Y.Song,Wang Yingqiao, Zhang Qiyong, Yuan Chuan yan, Cao Lei, Ji Xiang, Fu Bao
Study of tritium behavior in solid and liquid breed material	Feng Kaiming, Luo Tianyong, Li Zaixin, Zhao Zhou, Liu Haibo
Advanced reactor design and technological integration	Huang Qunying, Gao Sheng, Song Yong, Huang Bo, Wang Guozhong, Zeng Qin,

2、2007 and 2010 JSPS-CAS CUP Program Seminar

There are two JSPS-CAS CUP Program Seminar held in China from 2007 to 2011. One is CJS-9--9th China-Japan Symposium, 23rd-26th, Oct. 2007, Guilin, China and the other is JSPS-CAS CUP Seminar, 18th-21th, Oct. 2010,Xi'an，China.

(1) CJS-9--9th China-Japan Symposium, 23rd-26th, Oct. 2007, Guilin, China

This symposium main discussed on Materials for Advanced Energy Systems and Fission & Fusion Engineering Jointed with CAS-JSPS Core-University Program Seminar on Fusion Materials, System and Design Integration.

The organizers are Prof. K.M.FENG from SWIPP, China and Prof. A.KIMURA from Kyoto University, Japan. About 100 researchers, professors and engineers from China, Japan and USA participated in this symposium, including 8 invitation talks, 11 plenary talks and 70 parallel talks were organized. These presentations covered system &design integration, blanket & first wall technology, fission &fusion materials, radiation damage, calculation codes and data base, super-conducting magnet and related ITER technologies. In ASIPP, Prof. W.Y.WU, Dr. C.L. LIU, Ms L.M.Bao and et al participated in this symposium. The symposium offered a good chance for communication and our participants experienced a little, especially for the young guys.

The group photo after the symposium

(2) JSPS-CAS CUP Seminar, 18th-21th, Oct. 2010,Xi'an，China

This seminar with the title of superconducting key technology for advanced fusion device has had rich academic achievements on the ITER, LHD, JT-60SA, W-7X, EAST, AMS magnet, HV insulation, power supply system and cryogenic system.

On this seminar, there are 33 attendees giving their reports and exchange their achievements. They come from 13 organization including Japan and China, universities, institutes and companies.

The group photo after the symposium

3. Study on reduced activation material for fusion

Main subjects of "study on reduced activation material for fusion" are discussed. There are irradiation experiment by ions and electrons for advanced ferritic steels; fabrication and evaluation of advanced SiC/C; assignment of young scientists including Dr. Course students for progressing studies.

Effect o f Electr on Irradiation o n Ch ina Low Activation Martensitic steels (CLAM)

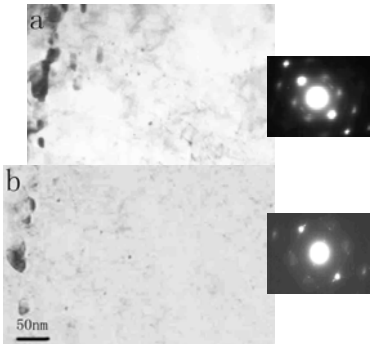

CLAM steels with Si before (a) and after (b) irradiation to 14 dpa at 723K on (111) crystal plane

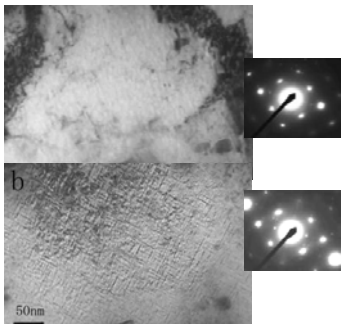

CLAM steels without Si before (a) and after (b) irradiation to 14 dpa at 723K on (111) crystal plane

The research on effect of Electron Irradiation on China Low Activation Martensitic steels shows that the Si has stabilizing effect on damage structural evolution.

Microstructure change in deuteriu m ions implanted CLAM steel under electron irradiation

As RAFM steel is considered to be the primary candidate for use as a structural material in fusion power reactors, research on CLAM (China Low Activation Martensitic) steel is also ongoing. Microstructural changes in CLAM steel that was implanted with deuterium ions under 1250keV of electron irradiation was investigated at temperatures from R.T. to 873K. Under the electron irradiation, both the growth and shrinkage of the defect clusters produced by deuterium ion implantation was observed.

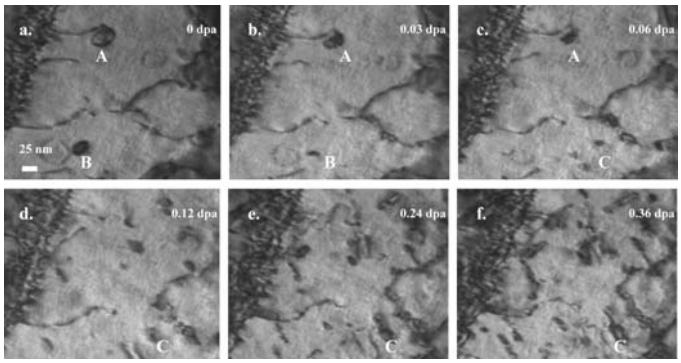

Irradiation Experiments on CLAM—Hokkaido University

Irradiation/helium induced effects is one of key issues in the current fusion materials programs. In-situ observation of microstructure change on China Low Activation Martensitic (CLAM) steel was carried out during electron-helium dual beam irradiation to 28dpa using High Voltage Electron Microscope and accelerator.
Evolutions of dislocation loops and helium bubbles were investigated.

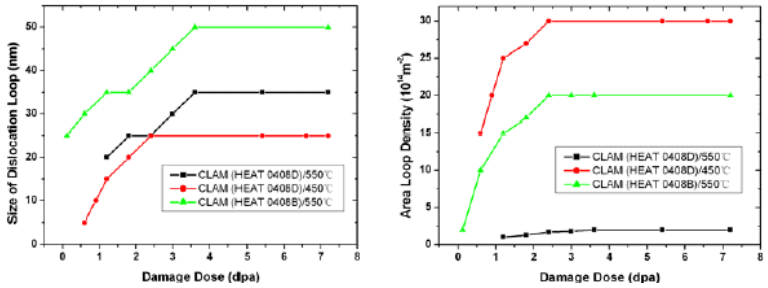

Changes of sizes and area densities of dislocation loops with damage at 550℃ and 450℃

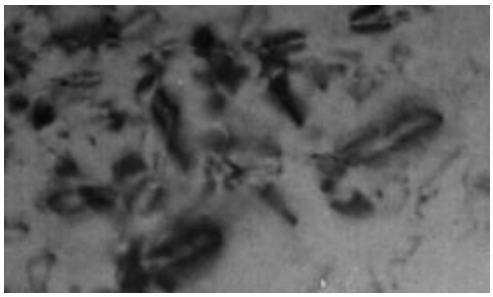

Dislocation loops

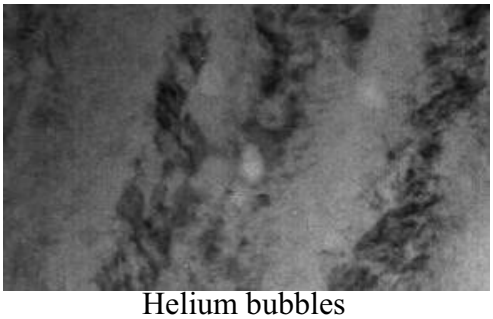

Helium bubbles

4. Development of superconducting key technology for advanced fusion for fusion reactor

Main subjects of "development of superconducting key technology for advanced fusion for fusion reactor" are discussed. The key discussion are key technologies of the power supplies of the EAST, LHD and ITER; ITER related technology, high voltage power supplies for plasma heating devices: NBI, ECH, FW-MG; cryogenic technology for superconducting tokamak; superconducting tokamak in-vessel components; peration scheme of fusion power plan: Bi-production of electricity and hydrogen fuel, hybrid energy transfer line, etc.

ITER superconducting conductor

The latest progress about ITER conductor sample including PF, TF, CC and Feeder conductor are reported. 4 conductor samples which are TFCN1, TFCN2, TFCN3, PFCN1(PF2) finished the qualification test at CRPP. All of testing results showed good performance met the PA requirements well. PFCN2(PF5) is testing in Sultan test facility, it seems OK.

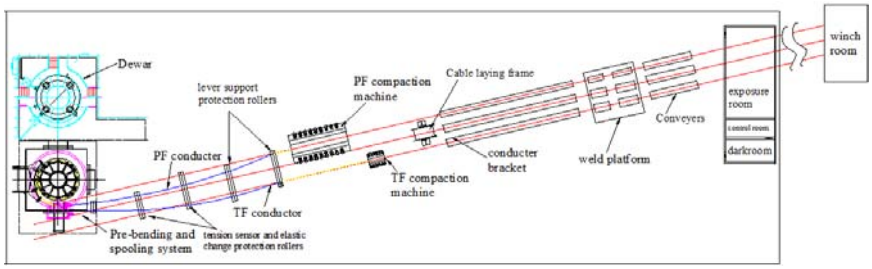

ITER Feeder and Helical coils

In discussion on ITER Feeder and Helical coils, Y. Song et al., discussed "Analysis of the magnetic shielding of the ITER magnet feeder cubicles", in NIFS.

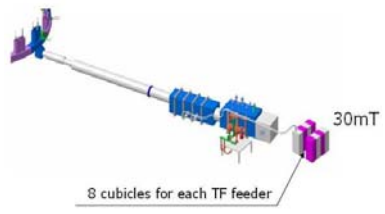

Figure : The cubicles for the TF feeder System in ITER.

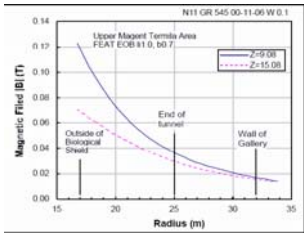

Figure : Stray field from the ITER magnet

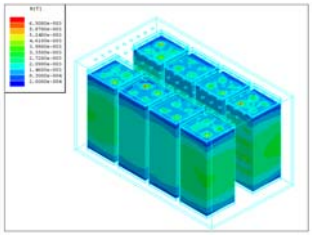

Figure : The magnet field inside the shielded cubicles.

N. Yanagi et al., discussed "Proposal of Split and Segmented-type Helical Coils for the Heliotron Fusion Energy Reactor", at CUP seminar held in Huangshan mountain.

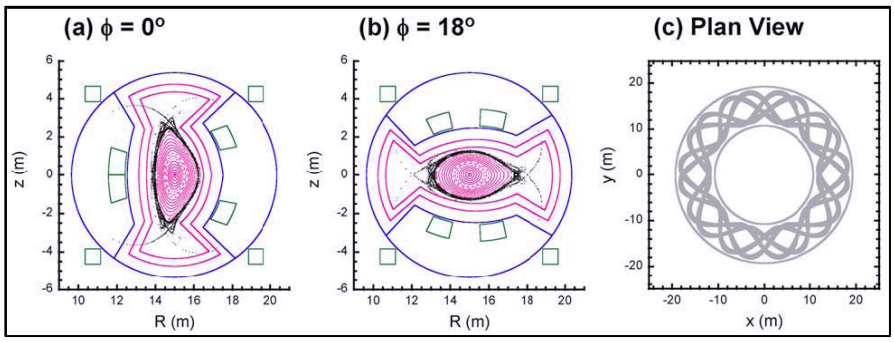

Vacuum magnetic surfaces of FFHR-2S at (a) toroidal angle φ = 0° and (b) φ = 18°.A planview of the coil system is shown in (c).

ITER power supply procurement package of China

ITER power supply procurement package of China is also reported at CUP seminar.

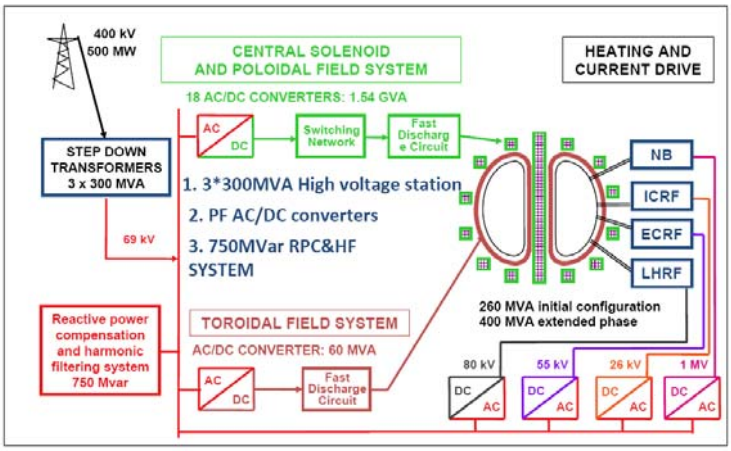

LHD, JT60SA and EAST Superconducting Tech

In LHD, JT60SA and EAST Superconducting Tech discussion, Sub-cooling cryostat installed to the valve box, mechanical behavior of the superconducting magnet system for LHD-type fusion reactor, JT-60SA EF conductors tested in the NIFS superconductor test facility, EAST Passive Stabilizers updated, design of graphite tiles for plasma facing surface are discussed.

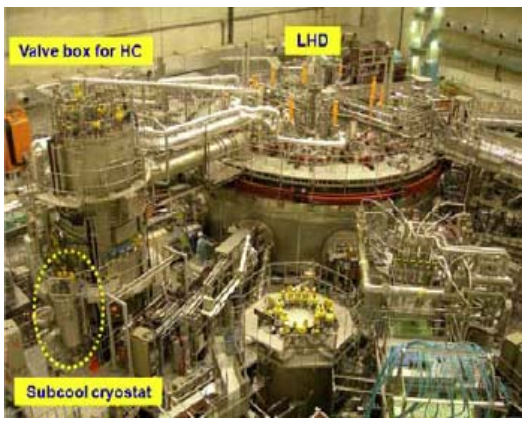

Large Helical Device (LHD)

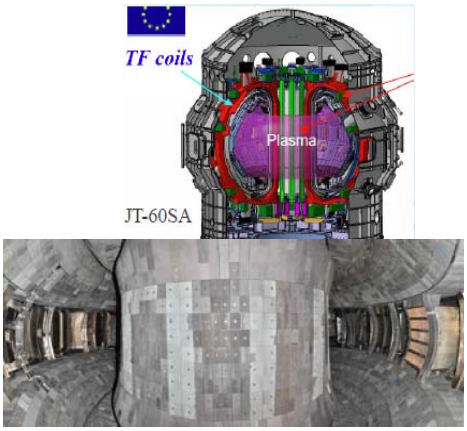

5. Study of tritium behavior in solid and liquid breed material

Main subjects are discussed in discussion on the study of tritium behavior in solid and liquid breed material: Tritium release behavior, irradiation defects analyses by TDS, XPS and FTIR, and simulation for tritium behavior in ternary lithium oxide for safety analysis of TBM. There are the discussion of cooperation and personal exchange on solid breeder field with two host universities are performed, Related cooperation research subjects on solid breeder field are also discussed, the tritium related studies for fusion engineering have been carried out and a series of D2+ implantation experiments on Li3TaO4 have been performed.

Effects of deuterium irradiation on the surface of Li4SiO4

In discussion on effects of deuterium irradiation on the surface of Li4SiO4, It was observed by Li-1s XPS spectra that almost all of the lithium on the surface for 3keV D2+-irradiated Li4SiO4 was removed in the range from 380K to 450K.

The D2 TDS desorption spectra consisted of two stages, showing the good correspondence between the release behavior of deuterium in the present study and that of tritium for neutron-irradiated Li4SiO4.

TDS results obviously showed that the deuterium retention for Li4SiO4 depended on the irradiation temperature.

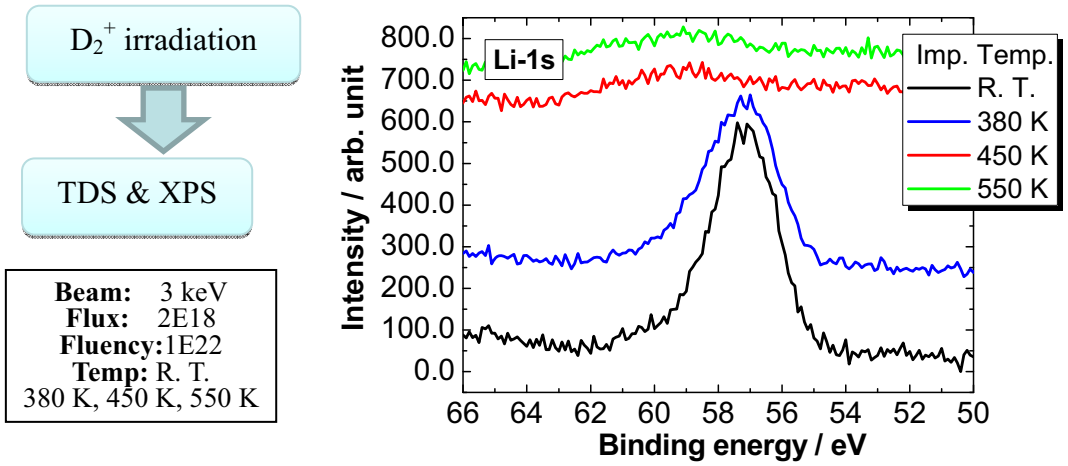

Study of tritium behavior in solid and liquid breeder materials

On study of tritium behavior in solid and liquid breeder materials, develop and test different ideas of ITER-TBM are discussed. It should be one of the aims of the ITER Project. China plans to develop own TBM concept for testing during ITER operation period based on China's DEMO definition and development strategy. The preliminary design and performance analysis of Helium-cooled Solid Breeder (HC-SB)Test Blanket Module (TBM) have been carried out.

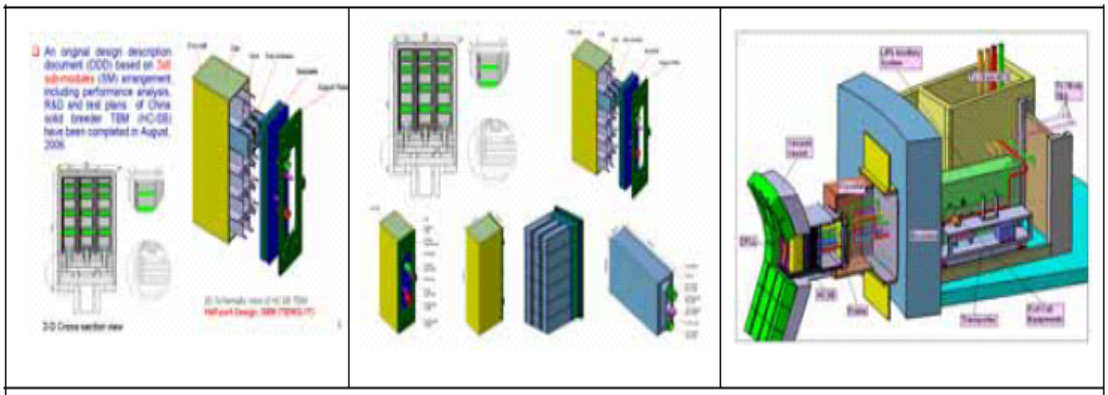

Fig.1 Progress and status on China HCSB TBM

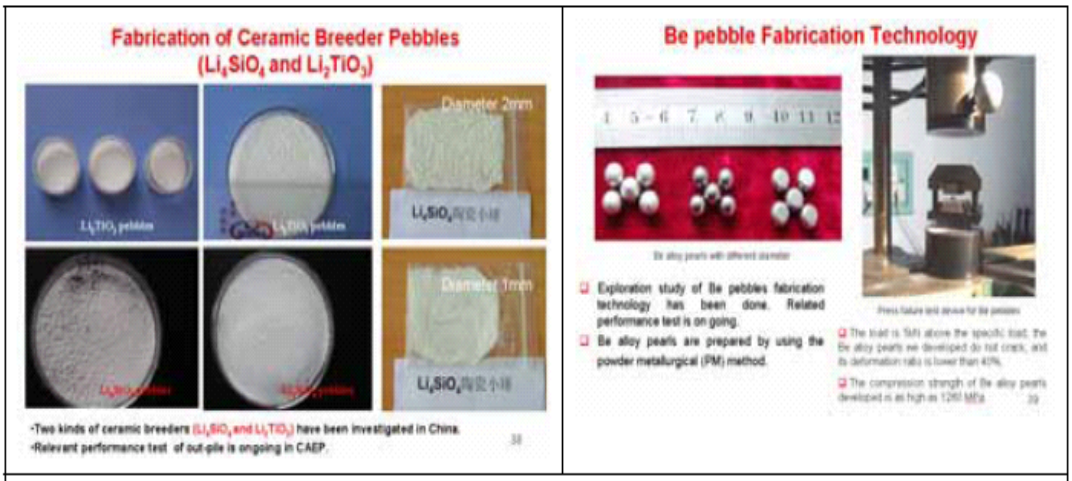

Fig.2 Relevant R&D activities of ChineseHCSB TBM

6. Advanced reactor design and technological integration

Main subjects of "advanced reactor design and technological integration" such as reactor design and design data-base; neutronics design and database; key materials technology and data base, thermofluid and thermal/structural analysis are discussed.

Emphasis of the collaboration are Reactor design and design data-base, Neutronics design and database; Key materials technology and data base; thermal creep, corrosion, joining technology; Thermofluid and thermal/structural analysis including design of flowing teat facility and so on.

Corrosion Tests of CLAM in Li-Pb

On study of Corrosion Tests of CLAM in Li-Pb, Exposure to Li-Pb resulted in dissolution of carbide precipitates at the grain boundaries is discussed.

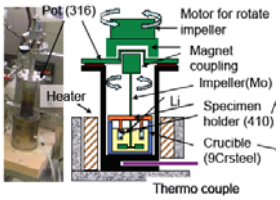

Test apparatus for corrosion tests in flowing Li-Pb

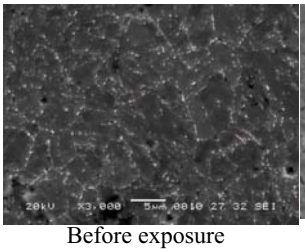

Before exposure

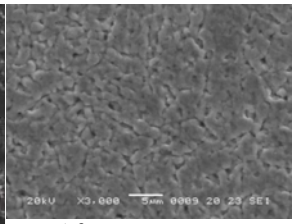

After exposure at 600C for 250 hr

Exposure to Li-Pb resulted in dissolution of carbide precipitates at the grain boundaries

Tritium Management in FLiBe Blanket for FFHR2—NIFS

On study of Tritium Management in FLiBe Blanket for FFHR2—NIFS, a tritium analysis model of the FLiBe blanket system was developed and the preliminary analysis on tritium permeation and extraction for FLiBe blanket system were done; the factors which affected tritium extraction and permeation were calculated and evaluated; the results of the presented analysis shows that further R&D efforts are required for FFHR2 tritium system to guarantee the tritium self-sufficient and safety.

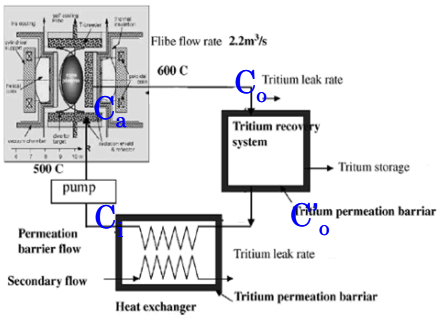

Tritium balance of FFHR-2 system

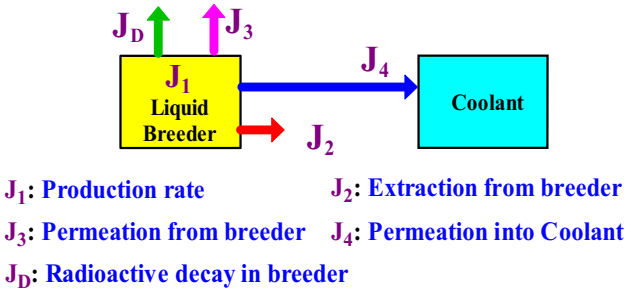

Tritium analysis model for FLiBe blanket

Tests of CLAM HIP Joints at NIFS

On study of tests of CLAM HIP Joints at NIFS, Charpy impact Test is reported. The test results show that outgassing before Hipping is critically important to maintain toughness of the joint.

With outgassing at 1273K before HIP (Ductile Fracture)

Without outgassing (Brittle Fracture)

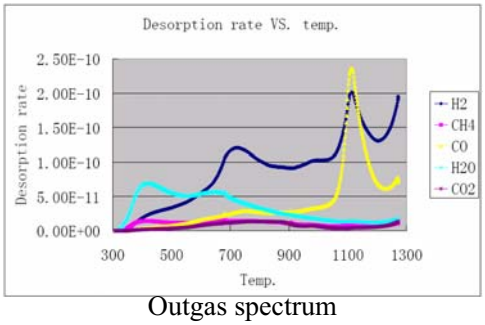

Outgas spectrum

CAD model of FFHR and Neutronics

There are many CAD model reported on FFHR and Neutronics. The main concern is conversion between CAD model and Monte Carlo computing model.

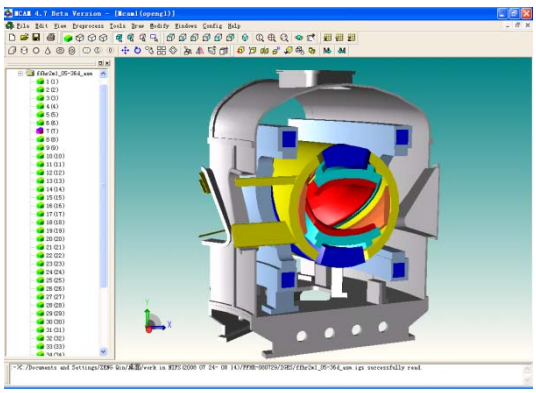

FFHR CAD model

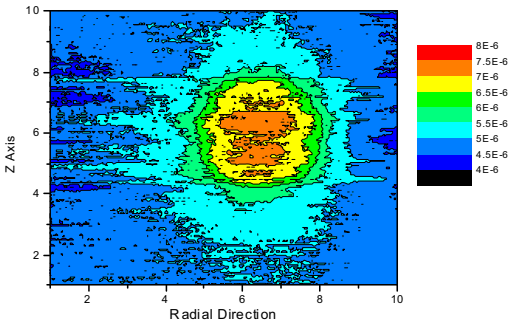

Neutron flux distribution

Thermal Creep of Vanadium Alloys

On the discussion of thermal Creep of Vanadium Alloys, Suppression of Thermal Creep Deformation by Cold Work and Annealing (SAACW) for NIFS and SWIP Vanadium Alloys is reported.

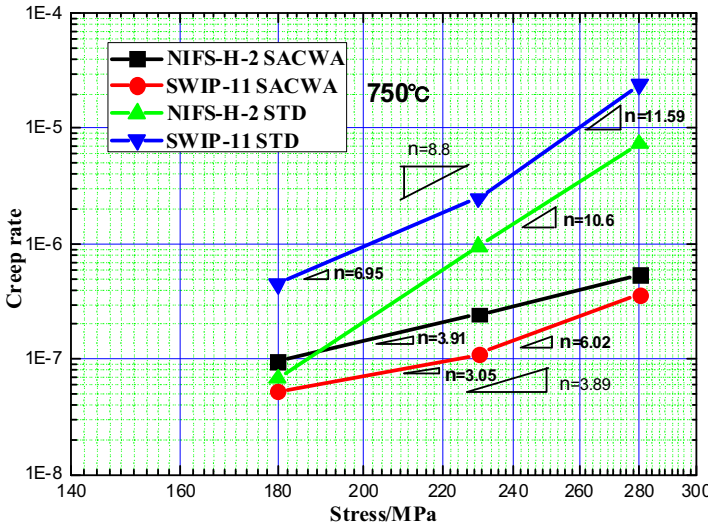

7. Summary and Prospect on future cooperation

Based on the ITER procurement package, some key engineering technique will be researched and developed in the future work, including,

(1) Conductor design;
(2) Design and manufacturing of HTS-CL;
(3) Design of components of Feeders;
(4) Research of insulation material;
(5) Design of superconducting joint;
(6) Establishing the testing platform;
(7) Research of magnetic shielding technique;
(8) Design of date acquisition system, research of the circuit of quench protecting and others;

Based on the engineer experience of LHD and EAST Superconducting Tokamak, some main engineering researches we can cooperate:

(1) Collaboration with some key components design, analysis and optimization for high power, long pulse heating system of ICRF antenna and NBI.
(2) Cooperation with design and optimization for inner components of vacuum vessel.
(3) Cooperation with design and optimization for diagnosis system.

Front research of future advanced fusion reactor:

(1) Research of tritium behavior in solid and liquid breeder materials.
(2) Breeding blanket design
(3) Fusion related neutronics experiment and analysis
(4) Study on reduced activation materials for fusion

Based on EAST, LHD operation, JT-60 upgrade construction, ITER project,

demonstration fusion reactor design, we can foresee that many co-operations can be carried out widely in this field. Small symposium tight with special engineering topic is welcome.

Hydrogen Fuel Society and Hybrid Energy Transfer Line of Hydrogen and Electricity

S. Yamada,

National Institute for Fusion Science, Toki, Gifu, 509-5292, Japan
yamadas@LHD.nifs.ac.jp

Abstract

Applicability of 1 GW class hybrid energy transfer line (HETL) of hydrogen and electricity is investigated in this report. The rated current is 10 kA, and operation voltage is 100 kV (+ 50 kV and -50 kV for ground). Delivery capacity of the liquid hydrogen is 100 tons per day. Re-cooling station of the liquid hydrogen is placed on every 10 km of the unit section. High J_c performance under high temperature region around 20 K requires for the SC wire. The special multi-filamentary magnesium diboride (MgB_2) wire was developed to suppress the I_c degradation against bending strain. Structure of a coaxial stranded cable is proposed for the design of 10 kA MgB_2 cable. Pressure of liquid hydrogen from 0.4 to 0.6 MPa was chosen, in order to keep the liquid phase up to 25 K. It was confirmed that this HETL is one of the attractive energy transportation system which combines hydrogen fuel and SC power transmission.

1. Introduction

Thermo-nuclear fusion is recognized to be a clean and unexhausted energy resource because the fuel can be extracted from sea water unlimitedly. It also has a big advantage of less CO_2 emission, of which character would contribute to avoiding green house effect on the earth. Integrated energy transportation system will be necessary for the hydrogen society in near future.

The conceptual design studies on force-free helical-type fusion reactor, FFHR, have been carried out with collaborations between the universities and National Institute for Fusion Science in Japan [1]. The SC helical coil system reduces the centering force by compensating with the hoop force. The FFHR can also produce the current-less steady-state plasma with no dangerous disruptions. These are great advantages for the force-free helical-type D-T reactors. To allow the flexibility in operation, co-generation system of electricity and hydrogen is one of potential candidates. In this system, hydrogen is made from the steam electrolysis, in which thermal energy of the steam can be obtained from the waste heat of the divertor and/or the radiation shield components outside of the breeder blanket [2]. Hydrogen has to be packaged by compression or liquefaction, transported by trailer or pipeline, stored, and transferred to the end users. The Energy Super-Grid that delivers electricity and hydrogen in the integrated energy pipelines in the USA was proposed [3]. World Energy Transmission System is also discussed to assess the global network of the SC power cables and fuel pipelines [4]. These reports deal the qualitative analysis and/or principle proposals.

In this report, 1 GW class hybrid energy transfer line of hydrogen and electricity is proposed on the basis of experience of the SC bus-lines with total length of 500 meters [5, 6]. Total efficiency of the hybrid energy transfer line system under 1000 km delivery is also investigated in this report.

2. Fusion Power Plant with Electrolyzer

To assess the technical potential of the FFHR operation style, dedicated hydrogen production from

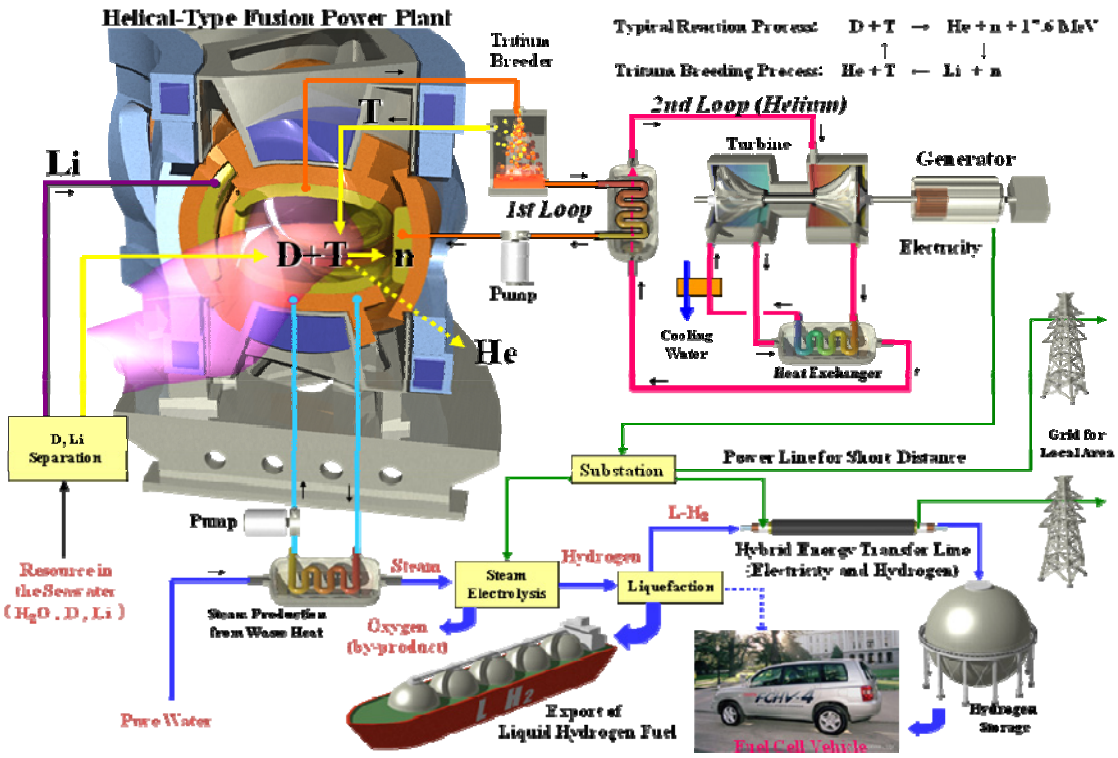

Fig. 1 Schematic drawing of the fusion power plant with hydrogen fuel production.

electrolysis by the electric power of 1 GW have been investigated. Schematic illustration of cogeneration of electricity and hydrogen is shown in Figure 1. Gaseous hydrogen of 700 tons per day can be produced. The steam of 6,354 tons per day at 150 °C is necessary in this case. In FFHR, about 450 MW of thermal power is delivered via the scrape-off layer plasma to the divertors. The energy is necessary to compress and/or liquefy the hydrogen for packing and delivering it to the end users. The compression works depends on the thermodynamics of the compression process. The energy consumption of a multi-stage hydrogen compressor is about half-way between the two theoretical limits of an isothermal and adiabatic compression process. About 17.4 MW of electrical power is

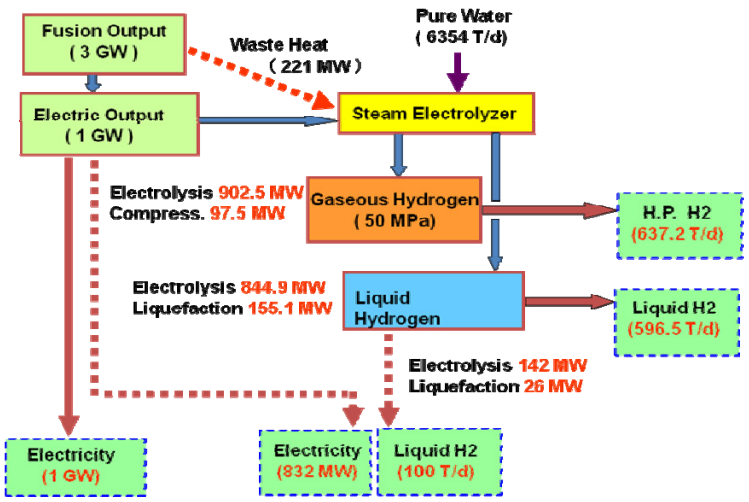

Fig. 2 Power flow from fusion output to power generation and electrolysis..

needed for the compression of 100 tons per day of hydrogen from 0.1 MPa to 50 MPa. Even more energy is needed to compact hydrogen by liquefaction. Required power of the helium compressors is about 2.7 times larger than that of the hydrogen compressors. The total power consumption of the hydrogen liquefaction system of 100 tons per day is 26 MW [2].

Figure 2 gives power flow diagram from fusion output to power generation and electrolysis. The four different styles of plant outputs are investigated: (A) pressurized hydrogen of 625 tons per day, (B) liquid hydrogen of 574 tons per day, (C) 1 GW of power generation, and (D) 0.824 GW of electricity production plus 100 tons per day of liquid hydrogen. Case (A) and case (B) are dedicated hydrogen production and these cases are desirable as the infrastructure for the future fuel cell society. Case (C) is suitable for a largely constant level of power demand as well as a nuclear fission power plant. Case (D) has the flexibility in plant operation. Electrical power to the grid can be modulated if the excess electricity were used for the hydrogen production, at the constant power generation. This fraction rate of case (D) is also appropriate for the levelization between on-peak and off-peak demand. In the following sections, transportation method of case (D) is investigated [2].

3. Hybrid Energy Transfer Line of Hydrogen and Electricity

The characteristics of the HETL are, 1) low energy consumption system for long transportation, 2) low-voltage high-current power line system, and 3) integrated energy transportation system. It is desired for the new needs which combine hydrogen fuel and SC power transmission. The total length of 100 km is selected to assess the engineering potential of the HETL [6].

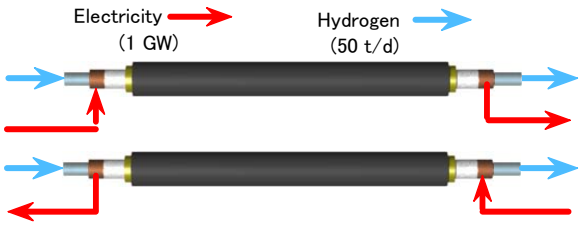

Fig.3 Schematic drawing of the HETL.

The HETL system requires high reliability and safety as well as the conventional power grid and natural-gas pipe line. The major concepts for the HETL are as follows. (1) Unit length of a HETL is 500 m. (2) The hydrogen re-cooling station is placed on every 10 km. (3) Delivery capacity of the liquid hydrogen is 100 tons per day. (4) Transmission capacity of the superconducting (SC) cable is 1 GW, and available current is 10 kA. Operation voltage between the lines is 100 kV, and operation voltage between the line and ground is +50 kV and -50 kV. Schematic illustration of HETL is shown in Figure 3. Design parameter of the HETL is summarized in Table 1.

Table 1 Design parameters of hybrid energy transfer line.

Items	Target values
Target distance	
total length to end user	100 km
length between the cooling stations	10 km
unit length of a HETL	500 m
Power Transmission	
operation voltage between the lines	100 kV (+50 kV and -50 kV)
maximum operation current	dc 10 kA
Hydrogen Transportation	
Transportation capacity	100 tons/day (1.16 kg/s)
Operation temperature	17 – 24 K
Pressure of liquid hydrogen	0.4 – 0.6 MPa

3.1 Structure of the HETL

The HETL system should be flexible and robust, because of the transportation by cable drums and installation on site. The SC cable should have the large margins for the operation current in the limited area. Magnesium diboride (MgB_2) wire is one of the potential candidates for 10 kA class cable, since the core Jc of more than 1000 A/mm^2 under the liquid helium was observed in various MgB_2 wires. The 10 kA class SC cable for the HETL was designed on the basis data of the MgB_2 wires with a diameter of 1.3 mm. Operation current of an MgB_2 strand at liquid hydrogen temperature was determined to 20 A (core Jc=100 A/mm2). Cross-sectional view of the MgB_2 is shown in Fig. 4 (a), and schematic drawing of the HETL is shown in Fig. 4 (b).

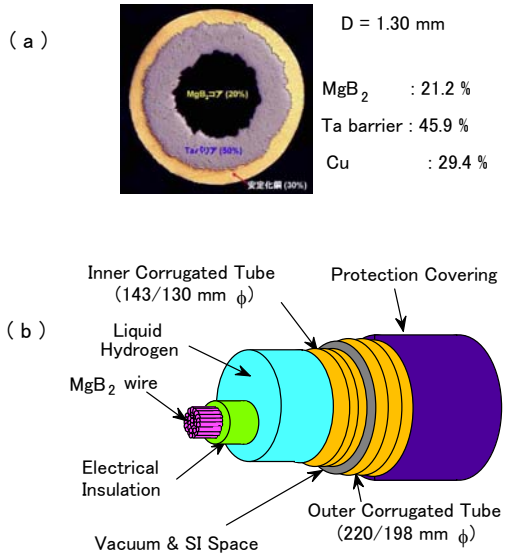

Fig. 4 Cross-sectional view of MgB_2 (a) and structure of the HETL (b)

3.2 Pressure loss of 10 km HETL

Transfer line consists of the SC cable, space for liquid hydrogen, electrical insulation layer, inner corrugated tube, vacuum space for thermal insulation, outer corrugated tube and so forth. Area of liquid hydrogen is 103 cm^2 (equivalent diameter of 114 mm). We assume the inlet temperature for 17 K, and flow rate of each channel for 50 tons/day. Friction factor in large flow rate regime, λ, was estimated by Nikuradse's equation. Pressure loss ΔP is expressed by following Fanning's equation.

$$\Delta P = 4\lambda\rho\frac{v^2}{2}\frac{L}{D} \qquad (1)$$

Where, ρ is density of the fluid, and v is velocity. The calculation result of the pressure loss as a function of pressurized hydrogen temperature is shown in Fig. 5. When the pressure of liquid hydrogen increases, boiling temperature becomes high. Density of liquid hydrogen is 0.071 g/cm^3 which is more than one order smaller than that of liquid nitrogen. Pressurization of liquid hydrogen enables to expand operation temperature region of the MgB_2 cable, and to absorb the head loss of the installation route. In order to obtain the operation temperature of MgB_2 cable from 17 K to 25 K, the pressure of liquid hydrogen from 0.4 to 0.6 MPa was chosen [6].

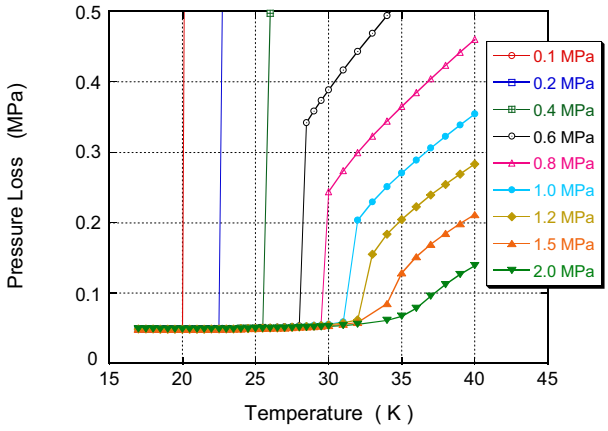

Fig. 5 Pressure loss of 10 km long HETL as a function of hydrogen temperature.

3.3 Heat load and required refrigerator

Reduction of the heat load into the transfer line is one of the important subjects

to realize the low-loss HETL system. Following are effective methods to reduce the heat leak; 1) high vacuum degree (for convection), 2) increase in number of super-insulation sheet (for radiation), and 3) slender and long spacer (for conduction) [10]. Purging with clean and dry gas before evacuation is also important to obtain a high vacuum degree for the long cryogenic tube. Taking into consideration of the above mentioned methods, the heat load of 1.0 W/m is realizable. Temperature rise of liquid hydrogen after 10 km transportation is calculated as a function of heat load. When a heat load is 1 W/m, the temperature rise is 2 K. Even if the heat load is 2 W/m, the temperature rise is 4 K. Cryostable condition can be sustained, when the inlet temperature is less than 20 K.

When the heat load is 1 W/m per one-way, refrigeration capacity of 20 kW @17 K is necessary. Cryogenic refrigeration is a complex process involving Carnot cycles and physical effects that do not obey the theoretical law. Nevertheless, the Carnot function is used as a reference for the process analysis. Power consumption of the refrigerator, *P,* can be estimated as shown in the following equation.

$$P = W_L \frac{T_H - T_L}{T_L} \frac{1}{\eta} \tag{2}$$

The refrigerator operates between T_H (=300 K) and T_L (=17 K). W_L is the refrigeration capacity, and η is efficiency of the Carnot cycle. Here, 0.25 was assumed as a value of η. Required power of the 20 kW refrigerators is estimated to 1.32 MW. The total power consumption for the energy transfer system of 100 km long becomes 13.2 MW. This value is equivalent to 1.32 % to the transportation capacity of 1GW.

4. Conclusions

Design studies of 1 GW class hybrid energy transfer line of hydrogen and electricity is performed. The results are concluded as follows; (1) Power transmission capacity of the dc power line is 1 GW, and capacity of the liquid hydrogen transportation is 100 tons per day. (2) To keep the liquid state of hydrogen anywhere in the unit section, the temperature and pressure of the inlet point were selected to 17 K and 0.4 MPa. (3) When the heat leak into the liquid hydrogen is 1.0 W/m (expected value), the temperature at the outlet becomes 18.1 K. It was confirmed that this HETL is one of the attractive energy transportation system which combines hydrogen fuel and SC power transmission

Acknowledgements

This work is supported by a grant from NIFS with ULAA005 and by the collaboration of JSPS-CAS Core University Program on Plasma and Nuclear Fusion. The authors would express their appreciation to Prof. A. Sagara and Prof. S. Imagawa in NIFS, and Prof. Y. Song in ASIPP for their kind advices.

Reference

[1] Sagara A et al, Nuclear Fusion **45** (2005) pp. 258-263.
[2] Yamada S. et al, Fusion Engineering and Design **82** (2007) pp. 2817-2823.
[3] Overbye T. J. et al, National Energy Supergrid Workshop Rept., Palo Alto, Nov. 6-8, 2002
[4] Grant P M et al., WETS`03 Workshop Report, Meudon, France June, 2003.
[5] Yamada S. et al., IEEE Transactions on Applied Superconductivity (2002) pp. 1328-1331.
[6] Yamada S. et al., to be published in Journal of Physics: Conference Series (Proc. of 9th EUCAS) .
[7] Hishinuma Y. et al, Fusion Engineering and Design **81** (2006) pp.2467-2471.

In-situ Observation of Radiation Damage in Reduced Activation Ferritic Steels by means of HVEM-ion Accelerator Facility

Somei OHNUKI[1] and Farong WAN[2]
[1]Hokkaido University, Sapporo, Hokkaido 060-8074, Japan
[2]University of Science and Technology Beijing, Beijing, China
Corresponding: ohnuki@eng.hokudai.ac.jp

Typical fusion reaction is $^{2}H + {}^{3}H \rightarrow {}^{4}He$ (3.52 MeV) + n (14 MeV), where high energy neutron irradiation is the most serious term for materials degradation. Figure 1 shows Materials Issues for Fusion Reactors. Radiation damage by 14MeV neutron irradiation, that the structural materials produce the dimensional change (swelling), hardening, embrittlement and high radioactivity. Fig. 1 shows main materials issues for blanket materials in fusion system. Therefore the low activation materials with anti-radiation damage have been studied. The final goal of fusion engineering is evaluation of material degradation and life time, especially on mechanical properties.

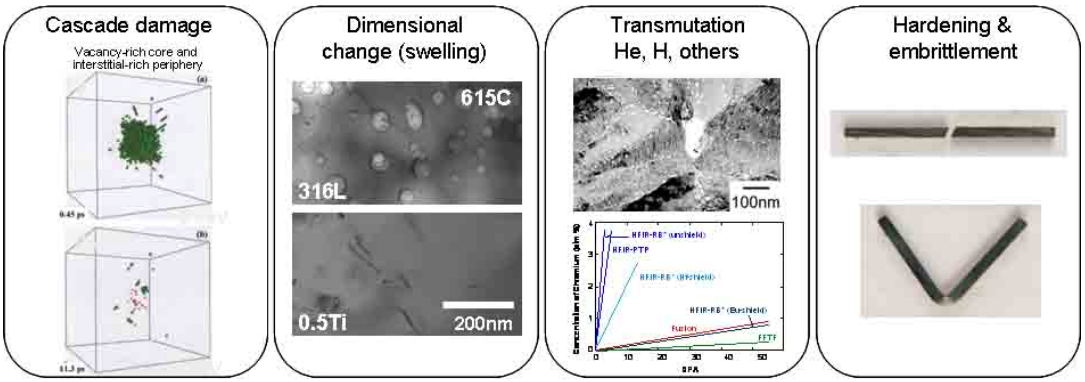

Fig. 1. Materials Issues for blanket.

Fig. 2 shows a multi-scale modeling for developing radiation damage studies for fusion reactor materials. There are many methods for evaluation of degradation, but the correlation between microstructures and mechanical properties is the most important for fusion engineering field.

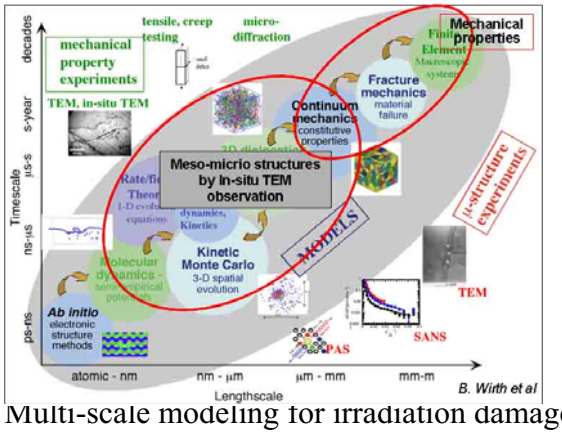

Fig. 2 Multi-scale modeling for irradiation damage

Hokkaido University has installed multi-beam irradiation facility combining with atomic resolution high voltage electron microscope and ion-accelerators, as shown in fig.3. By using the facility several groups have used for in-situ observation of damage structure in nuclear reactor materials [1] and systhesization of non-stoichiometric phases [2]. At this time an example of in-situ observation for damage development in fusion and fission reactor materials will be introduced during an electron-helium ion irradiation.

Fig.3 Multi-beam irradiation facility in Hokkaido University

Ferritic/martensitic steels are candidates for fusion reactors, however, there are main materials issues such as irradiation embrittlement and elevation in ductile-brittle transition temperature. Now days, migration energy of point defects influence evolution of irradiation-induced dislocation loops, and hydrogen and/or helium created by nuclear transmutation reaction are becoming important terms in “Multi-scale modeling” applying for solving such macroscopic materials behavior.

For measuring practical or average of migration energies for vacancies and interstitials, Kiritani et. al. proposed following equations.
For vacancies,

$$\ln\left(\frac{dL}{dt}\right) = C_2 - \frac{E_V^M}{2kT}$$

and for self-interstitial atoms,

$$C_{LS} = C_3 \exp\left(\frac{E_I^M}{2kT}\right)$$

where, C_I,C_V: concentration of I and V, M: mobility, P: damage rate [dpa/s], Z: reaction site number, C_S: sink density, L: diameter of loop, a: radial difference due to the absorption of a point defect, k: Boltzman constant, T: temperature [K], C_1, C_2 , C_3 : constant.
Finally we get simple relations, vacancy migration energy is two times of the slope, and then interstitial migration energy is two times of the slope.

In order to investigate the effect of helium on migration energy of vacancies or interstitials in Fe-Cr model alloys, two types of irradiations, electron single irradiation and electron-helium dual irradiation and their in situ observations were performed at 300 - 500 ℃. The acceleration voltage of electron in JEOL ARHVEM was 1250 kV, and the voltage of He ion was 100 kV. The damage rate was 10x10-4 dpa/s, and the injection rate was 10 He ppm/dpa.

At the beginning of the electron-irradiation interstitial-type dislocation loops were nucleated and then grew on <001> and <111>, as shown in Fig. 4. In the case of dual-beam irradiation, the loops were nucleated with much higher number density, and the grown with continuing irradiation, as shown in Fig. 5. By using simple method based on Kiritani and Yoshida [3], the migration energy of interstitials was evaluated as 0.2 eV in both types of irradiations, and that of vacancies was evaluated as 0.95 eV in electron-irradiation and 1.5 eV in dual beam irradiation, as shown in fig. 7. The difference of two energies, 0.5 eV, could be assumed to be net binding energy of vacancy and helium atom. These results are reasonable comparing to the results from other materials, as shown in Table 1.

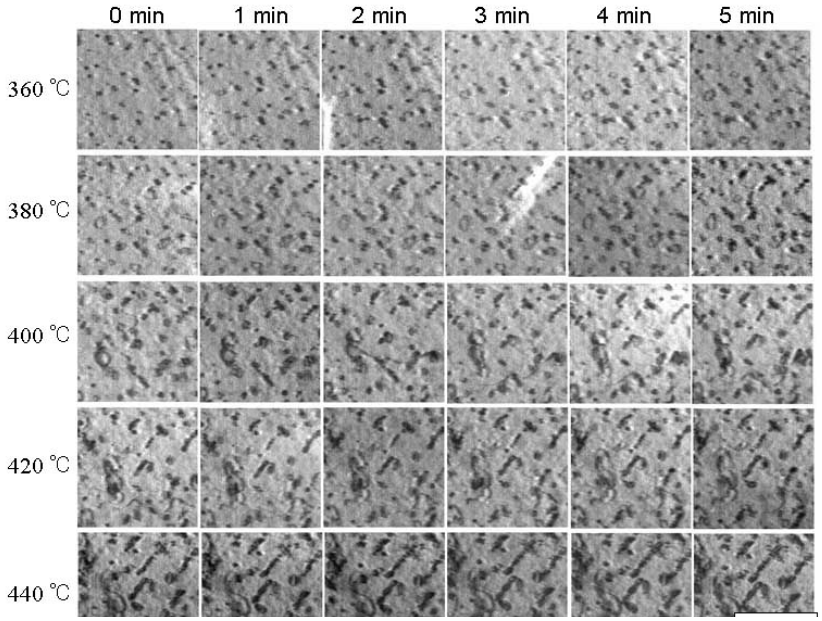

FIG. 4. Continuous growth of dislocation loops during electron-irradiation at different temperature

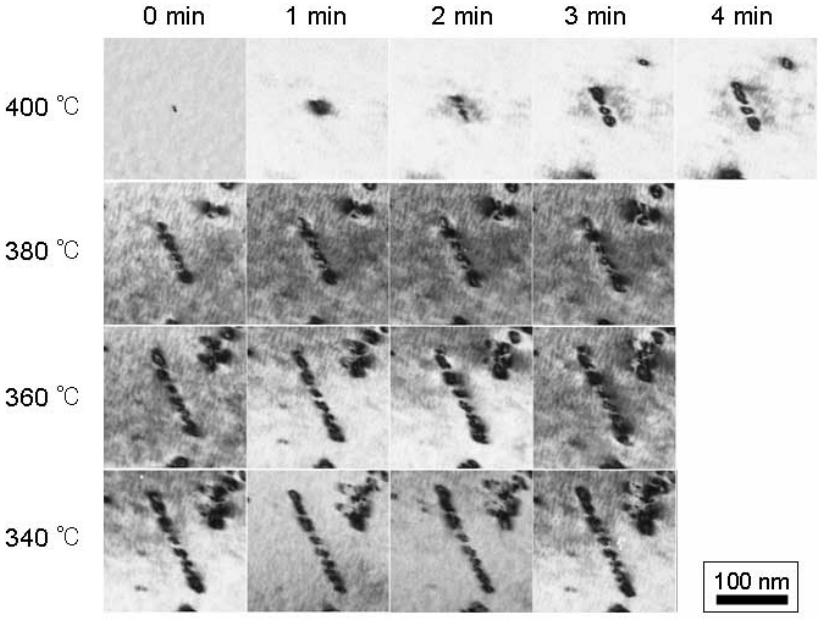

FIG. 5. Continuous growth of dislocation loops during electron-He ion irradiation at different temperature

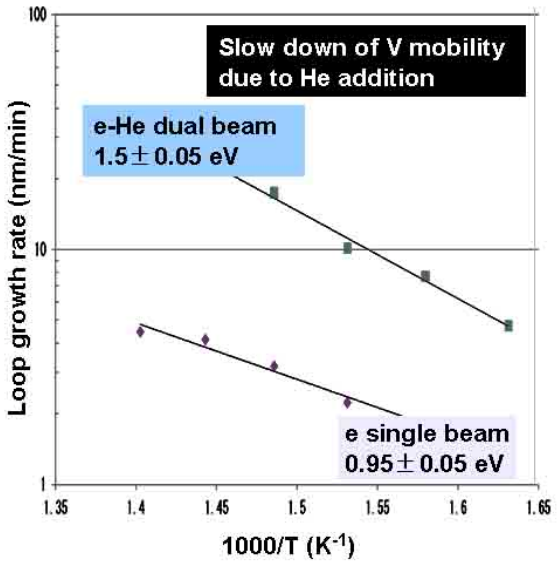

FIG. 6. Arrhenius plot for vacancy migration energy.

TABLE 1. Net migration energies from electron-irradiation experiments

Materials	Vacancy migration energy (eV)	Interstitial migration energy (eV)	
Fe-Ni-Cr without He	1.04	0.9	Hidaka et al.
20 appmHe/dpa	1.19	0.9	Hidaka et al.
70 appmHe/dpa	1.53	-	Hidaka et al.
Fe	0.7 – 1.0	0.2 – 0.3	Kiritani, Yoshida,

Summary

We studied about the role of in-situ TEM on radiation damage evaluation for fusion reactor materials. Several terms are very important, 1) atomic simulations of cascade damage for damage efficiency and cluster nucleation, 2) microstructural development for loop & void formation and dissolution & coarsening of precipitates, and 3) mechanical properties for radiation-hardening and radiation- embrittlement. Our conclusion is the in-situ TEM observation is key method for estimate the materials degradation after practical parameter fitting, Orowan equation for hardening estimation and DBTT Shift estimation

References

[1] K. Oka, S. Ohnuki, S. Yamashita, N. Akasaka, H. Tanigawa, *Mater. Trans*., 48 (2007)2563-2566

[2] S. Watanabe, *Mater. Sci. Forum*, 561-565 (2007) 2021

[3] M. Kiritani et al., *J. Phys. Japan,* 38 (1975)

Study of tritium behavior in solid breeder materials

Yasuhisa Oya[1]*, Takuji Oda[2], Tianyong Luo[3], Xiaojun Chen[4], Kaiming Feng[3], Satoru Tanaka[2], Kenji Okuno[1]

[1]Radioscience Research Laboratory, Faculty of Science, Shizuoka University, 836, Ohya, Suruga-ku, Shizuoka 422-8529, Japan.
[2]The University of Tokyo, 7-3-1, Hongo, Bunkyo-ku, Tokyo 113-8656, Japan.
[3]Southwestern Institute of Physics, Chengdu 610041, P. R.China.
[4]China Academy of Engineering Physics, Maiyang, P. R. China.
syoya@ipc.shizuoka.ac.jp

Abstract

The elucidation of tritium behavior in solid breeder materials for future fusion reactor is one of the key issues for fusion safety and fuel recycling. In especially, the dynamics and detailed chemical behavior of tritium in the materials are important for TBM design and future DEMO design.Under the CUP (Core University Program) program, ternary lithium oxide was focused on and various experiments using XPS, TDS and FTIR were performed. The comparison of D desorption behavior for D_2^+ implanted ternary lithium oxide was compared to that of T desorption one for neutron irradiated ternary lithium oxide. Molecular simulation research was also done to understand the stability of tritium in TBM. This paper summarized achievements for these issues performed under CUP tasks of 20B and 20E between Japan and China.

I. INTRODUCTION

In the future fusion reactor, the recovery of tritium will be one of important issues for the development of reactor design. For ITER, TBM design is undergoing in all over the world. To understand actual tritium recovery, it is important to elucidate the mechanism of tritium behavior in tritium breeder materials. In CUP program, fundamental study of tritium behavior in solid breeder materials which were the candidate TBM materials for both of Japan and China, was performed [1]. To achieve these issues, the combination usage of experimental research and simulation work were useful. In the present study, ternary lithium oxide was focused on and various experiments using XPS, TDS and FTIR were performed. Molecular simulation research was also done to understand the stability of tritium in TBM. This paper summarized achievements for these issues performed under CUP tasks of 20B and 20E between Japan and China.

II. EXPERIMENTAL

To elucidate tritium behavior, various ternary lithium oxides, namely Li_2TiO_3, $LiTaO_3$, Li_3TaO_4 and Li_4SiO_4 were used. The D_2^+ implantation experiment was performed up to the fluence of 1×10^{22} D m^{-2}. Thereafter, the sample was transferred to TDS chanber and TDS experiment was performed with a heating rate of 0.5 K s^{-1}. The desorbed species were measured by a quadruple mass spectrometer. The chemical states of consistuate atoms were observed by XPS. To compare the D desorption for D_2^+ implanted ternary lithium oxide, neutron irradiation was performed and the desorption behavior of tritium produced by ^{6}Li (n, α) T was observed by proportional counters. The behavior of O-D bonds were also analyzed by FT-IR. Following research topics were done under CUP program.

- ✓ Comparison of Tritium desorption behavior for D_2^+ implanted Li_2TiO_3 and thermal neutron irradiated Li_2TiO_3
- ✓ Effects of deuterium irradiation on the surface of Li_4SiO_4
- ✓ The deuterium trapping state for $LiTaO_3$ was compared to that for Li_3TaO_4
- ✓ Evaluation of O-D behavior in Li_3TaO_4 for understanding the stability of O-D bond

Some simulation researches were also done for understanding the experimental results and predicting the tritium behavior in various conditions.

Following research topics were studied

- ✓ Defect (O vacancy) migration energy in SiO_2, as a preliminary calculation of lithium silicate
- ✓ Modeling of ceramics pebble packing behavior

III. RESULTS

3-1. Comparison of TDS spectra for D_2^+ implanted Li_2TiO_3 and thermal neutron irradiated Li_2TiO_3[2-4]

Fig. 1 shows D_2 and D_2O TDS spectra for D_2^+ implanted Li_2TiO_3. In addition, tritium release and annihilation behavior of radiation defects for neutron-irradiated Li_2TiO_3 as a function of heating temperature were shown in Fig. 2. It was found that there were four deuterium trapping states in D_2^+-implanted Li_2TiO_3, which were assigned as follows;

(1)D trapped near the surface without interacting with oxygen
(2) D trapped near the surface with interacting with oxygen
(3) D trapped at E'-center in the bulk
(4) D trapped by oxygen with forming O-D bonds.

Comparison of these results with those for neutron-irradiated Li_2TiO_3 shows that the desorption of hydrogen isotope absorbed on the surface was observed only for ion implantation case. On the contrary, the desorption of hydrogen isotope trapped in the bulk, which could be found for both of ion implantation and neutron irradiation,

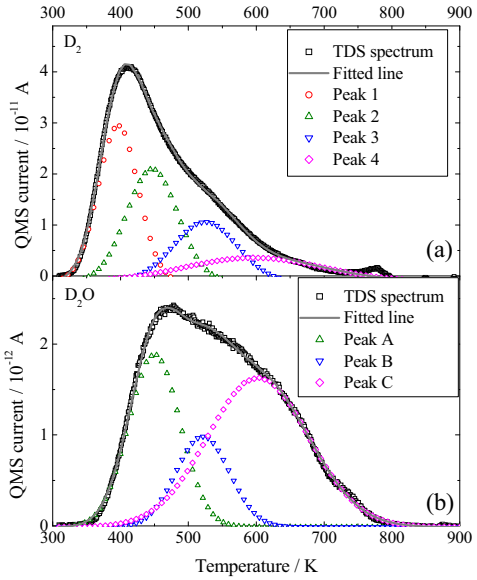

were found to be more complicated than the surface raction: they were independent of implantation temperature, indicating that the implanted deuterium could be trapped at E'-center in lower temperature and trapped by oxygen with the formation of O-D bonds in higher temperature region where E'-center could be annihilated due to the recovery of oxygen via diffusion, and therefore the deuterium retention in the bulk could become constant until the decomposition of O-D bond could be proceeded.

Recently, Raman analysis on nonstoichiometry of Li_2TiO_3 are undergoing to elucidate the influence of lithium concentration on tritium behavior. Fig. 3 shows the preliminary results for the Raman spectra for $Li_{2.0}TiO_3$, $Li_{2.2}TiO_3$, $Li_{2.4}TiO_3$. It was found that Raman spectrum of Li_2TiO_3 was broadened by addition of Li. Especially, additional peak emerges at around 800 cm^{-1}. It can be said that Raman spec. is useful to analyze the degree of nonstoichiometry of Li_2TiO_3. Further study will reveal more detail information.

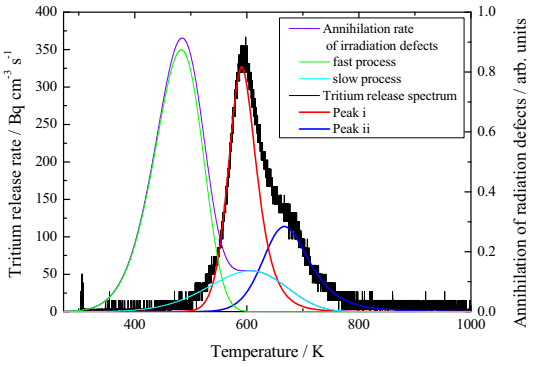

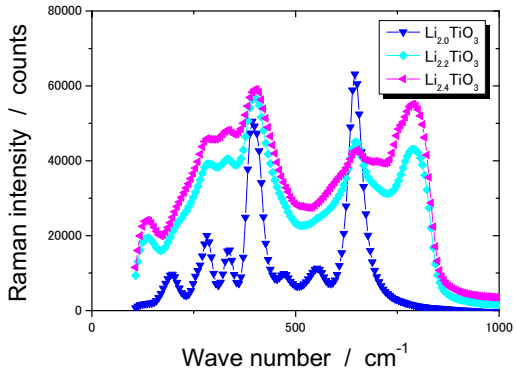

3-2. Deuterium trapping state for $LiTaO_3$ was compared to that for Li_3TaO_4[5]

Lithium tantalate is also considered as one of typical ternary lithium oxides. Li_3TaO_4 as one of lithium tantalite with higher lithium density has been developed at CAEP. In this study, lithium tantalite with different lithium density were picked up and deuterium retention behavior and O-D bond formation behavior were stided. Fig. 4 shows the D_2 TDS spectra for $LiTaO_3$ and Li_3TaO_4. It was found that the D_2 TDS spectrum for $LiTaO_3$ was consisted of 3 peaks as shown in Fig. 4(a). The first stage corresponds to the desorption of D adsorbed on the surface, the second could be that trapped by the defects caused by D_2^+ implantation, and the third would be that trapped as O-D bond. The ratio of O-D bond to total oxygen was gradually decreased with increasing of implantation temperature. For Li_3TaO_4, The TDS spectra extened toward higher temperature side and some of D was desorbed in higher temperature region. The D retention in $LiTaO_3$ was 3 times more than that in Li_3TaO_4. It can be said that the D retention behavior was quite different between lithium tantalates with different chemical composition. FTIR study was performed to clarify the behavior of O-D bond formation,. Fig.5 shows FTIR spectra for $LiTaO_3$ and Li_3TaO_4. In $LiTaO_3$, three peaks were observed at 2580 cm^{-1}, 2560 cm^{-1}, and 2480 cm^{-1}. In Li_3TaO_4, a broad peak was observed at 2540 cm^{-1}. The shapes of these peaks were not changed as the ion fluence increased. The peak intensities almost proportionally increased as the ion fluence increased. This significant difference in existence states of irradiated deuterium would come not only from crystalline structure, but also from composition, because a lithium vacancy is considered to act as an trapping site of hydrogen isotopes in $LiTaO_3$.

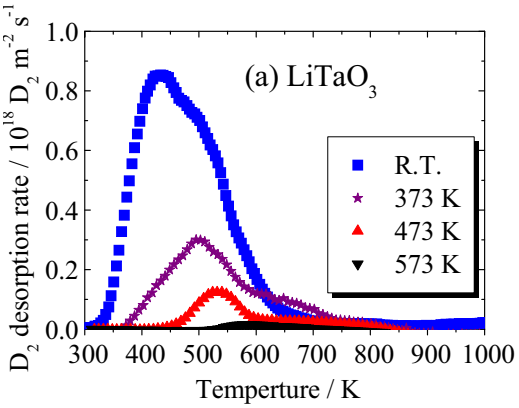

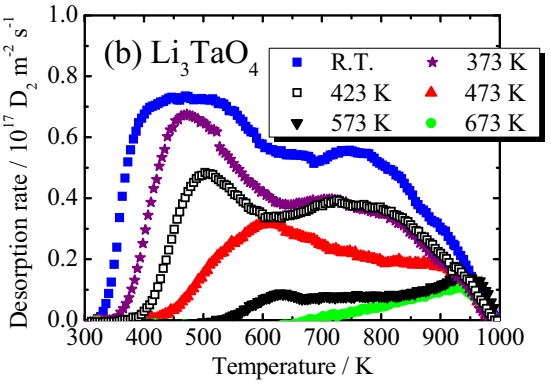

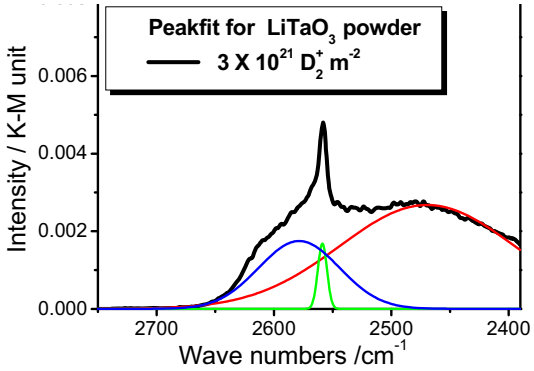

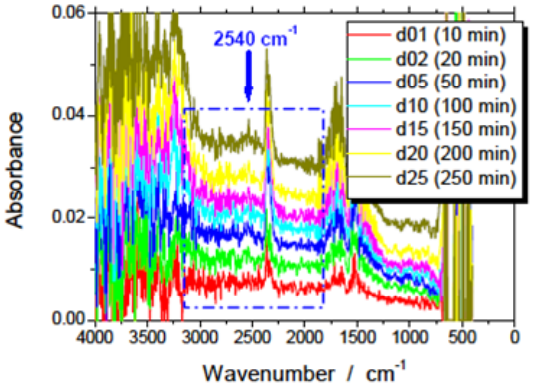

3-3. Effects of deuterium irradiation on the surface of Li_4SiO_4

Tritium recovery for Li_4SiO_4 is one of key research theme for China TBM design activities. To provide the scientific knowledge, D_2^+ implantation experiments were performed as a function of temperature. In addition, some of defect will be introduced by neutron irradiation in actual TBM. So, the defect migration energy was simulated as a preliminary study by using SiO_2 crystal.

Figs. 6 show Li 1s XPS spectra and the comparison of hydrogen isotope desorption for neutron irradiated

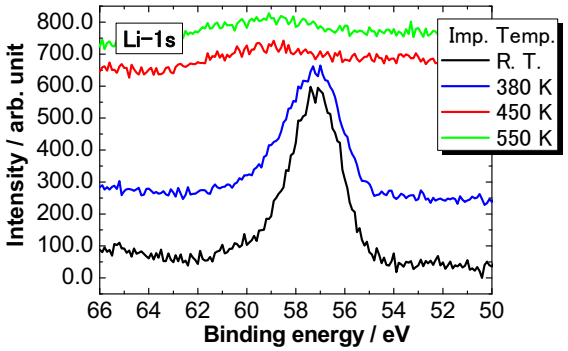

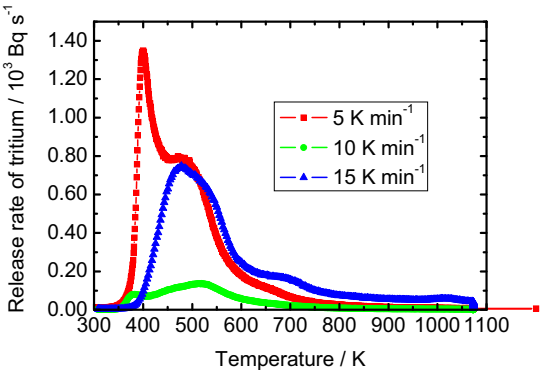

(b)

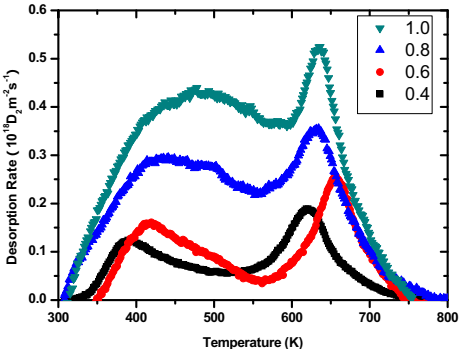

(a)

Li_4SiO_4 and D_2^+ implanted Li_4SiO_4 was summarized in Fig.7. It was observed by Li 1s XPS spectra that almost all of the lithium on the surface for 3keV D_2^+-irradiated Li_4SiO_4 was removed in the range from 380K to 450K. The D_2 TDS desorption spectra consisted of two stages, showing the good correspondence between the desorption behavior of deuterium in the present study and that of tritium for neutron-irradiated Li_4SiO_4. However the hydrogen isotope retention in each desorption stage was clearly different. In addition, the chemical form of hydrogen isotope for neutron irradiated Li_4SiO_4 was DTO, although that for D_2^+ implanted Li_4SiO_4 was D_2. This different would be caused by the difference of experimental condition, He purge gas condisiton or vaccum condition.

Preliminary simulation work was done using GLUP3.1 [6] to evaluate the defect migration behavior by using SiO_2 as a simple model. Fig. 8 shows the configurations along a migration path for SiO_2. Oxygen atom was stimulated to migrate inside SiO_2 crystal and energy difference was calculated. Fig. 9 shows the typical results for simulation. It was found that the migration energy can be calculated to be 2.5 eV. In the future work, Li_4SiO_4 cryslta will be adopted and migration energy will be also estimated. These results will be used for the simulation of actual tritium behavior in fusion reactor.

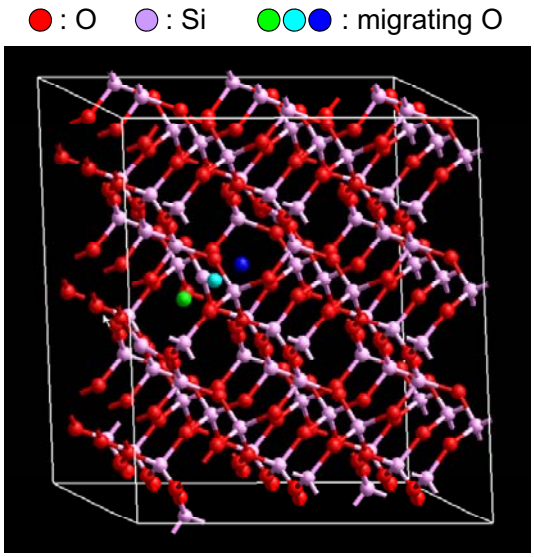

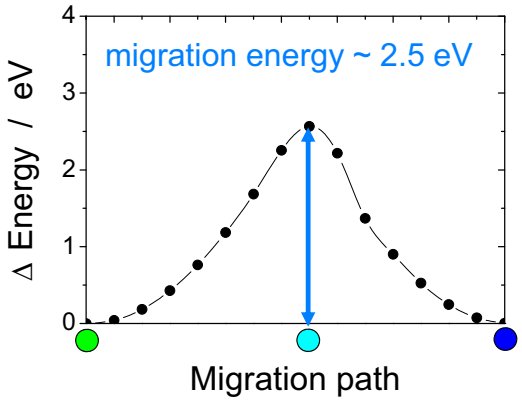

IV. CONCLUSIONS

To elucidate tritium behavior in ternary lithium oxides, various fundamental researches were performed under Japan-China CUP program. These activements will suppy the scientific knowledge about tritium recovery development and contribute the TBM design. The summary of key topics derived in this work is as follows;

Four deuterium trapping states were found for Li_2TiO_3. Most of deuterium trapping states in bulk are D trapped at E'-center and D trapped by oxygen with forming O-D bonds. It was considered that the O-D bond and the reduced tantalum atom on the surface of $LiTaO_3$ would be formed due to the formation of irradiation defects induced by D_2^+-irradiation. The D retention in $LiTaO_3$ is largely dependent on the implantation temperature. Using in-situ FT-IR analysis during 3 keV D_2^+ irradiation, the influence of material composition on the behavior of hydrogen isotopes were analyzed. The different existence states between Li_3TaO_4 and $LiTaO_3$ were clearly observed. The chemical states of lithium, oxygen and silicon on the surface of Li_4SiO_4 were changed by D_2^+ irradiation indicating the formation of irradiation defects. The TDS desorption stages consisted of two stages, showing the good correspondence between the release behavior of deuterium in the present study and that of tritium for neutron-irradiated Li_4SiO_4. Using molecular dynamics simulation, defects migration energy were evaluated. O vacancy migration energy was obtained as ~ 2.5 eV.

At present, we are still planning neutron irradiation for ternary lithium oxide to confirm tritium desorption behavior and compare with the ion irradiation results, which will lead not only for the fabrication of pebble but also the development of tritium recovery technique for both of China and Japan TBM and future fusion reactor.

ACKNOWLEDGMENTS

This study was performed under Japan-China CUP program. This work was also supported by the center for instrumental analysis at Shizuoka University.

REFERENCES

[1] K.M. Feng et al., "Overview of design and R&D of solid breeder TBM in China, Fusion Eng. Des. 83, 1149-1156 (2008).

[2] M. Oyaidzu, Y. Nishikawa, T. Suda, A. Yoshikawa, Y. Oya and K. Okuno, "Study on chemical behavior of energetic deuterium implanted into Li_2TiO_3," Fusion Technol., 52, 1002–1006 (2007).

[3] Yuji Inagaki, Haibo Liu, Hirotada Ishikawa, Sachiko Suzuki, Akira Yoshikawa, Kaiming Feng, Yasuhisa Oya and Kenji Okuno, "Role of lithium on chemical states and retention behavior of tritium in Li_2TiO_3" Fusion Sci. Technol., 56, 821-825 (2009).

[4] Sachiko Suzuki, Makoto Kobayashi, Rie Kurata, Wanjing Wang, Toshiyuki Fujii, Hajimu Yamana, Kaiming Feng, Yasuhisa Oya and Kenji Okuno, "Elucidation of Annihilation Processes of Defects Induced by γ-

irradiation in Li_2TiO_3", Fusion Eng. Des., in press.

[5] Tianyong Luo, Takuji Oda, Yasuhisa Oya, Satoru Tanaka, "IR observation on O–D vibration in $LiNbO_3$ and $LiTaO_3$ single crystal irradiated by 3 keV D_2^+", J. Nucl. Mater., 382 (2008) 46-50.

[6] P. Vashishta, Rajiv K. Kalia, José P. Rino, and Ingvar Ebbsjö, "Interaction potential for SiO_2: A molecular-dynamics study of structural correlations" Phys. Rev. B, 41, 12197-12209 (1990)

Analysis on Tritium Management in FLiBe Blanket for Force-Free Helical Reactor FFHR2

Yong Song [a], Akio Sagara [b], Takeo Muroga [b], Qunying Huang [a,c], Muyi Ni [c], Yican Wu [a,c], FDS Team

[a] *Institute of Plasma Physics, Chinese Academy of Sciences, Hefei, Anhui, 230031, China*

[b] *Reactor Engineering Research Center, National Institute of Fusion Sciences, Oroshi-cho, Toki 509-5292, Japan*

[c] *School of Nuclear Science and Technology, University of Science and Technology of China, Hefei, Anhui, 230027, China*

Abstract: In FFHR2 design, FLiBe has been selected as a self-cooling tritium breeder for low reactivity with oxygen and water and lower conductivity. Considering the fugacity of the tritium, particular care and adequate mitigation measures should be applied for the effectively extract tritium from breeder and control the tritium release to the environment. In this paper, a tritium analysis model of the FLiBe blanket system was developed and the preliminary analysis on tritium permeation and extraction for FLiBe blanket system were done. The factors which affected tritium extraction and permeation were calculated and evaluated, such as the heat exchanger material, tritium permeation reduction factor (TPRF) in blanket, proportion of FLiBe flow in tritium recover system (TRS) and efficiency of TRS etc. The results of the analysis showed that further R&D efforts were required for FFHR2 tritium system to guarantee the tritium self-sufficient and safety, for example reasonable quality of tritium permeation barriers on blanket, requirement for the TRS and fabrication technology of the heat exchanger etc..

Key words: Tritium; Permeation; Extraction; FLiBe

1. Introduction

Force-free helical reactor (FFHR) is a demo-relevant helical-type D-T fusion reactor based on the great amount of R&D results obtained in the LHD project. FLiBe has attractive merits on safety aspects: low tritium solubility, low reactivity with air and water, low pressure operation, and low MHD resistance which is compatible with high magnetic field designs. Thus FLiBe has been selected as a self-cooling tritium breeder in FFHR2 designs [1].

Tritium is one of the nuclear fuels and the significant radioactive sources for fusion reactors. Thus the tritium control in a breeding blanket is a key issue in terms of both tritium self-sufficiency and safety of the fusion plant. Considering the fugacity of the tritium and its low solubility in FLiBe, particular care and adequate mitigation measures are to be applied in the FLiBe blanket system in order to keep the tritium release rate to the environment below the allowable level i.e.10Ci/day [2].

In this paper, preliminary analysis on tritium management in FLiBe blanket for FFHR2 was done. The factors which affected tritium extraction and permeation were calculated and evaluated, such as the different heat exchanger, proportion of FLiBe flow in tritium recover system (TRS), efficiency of TRS, and tritium permeation reduction factor (TPRF) in blanket etc.

2. Analysis Method and Model

The tritium flow model of the entire FFHR2 blanket system was developed, which included the FLiBe blanket and major components of the auxiliary system. A schematic chart of this model was shown in Fig.1.

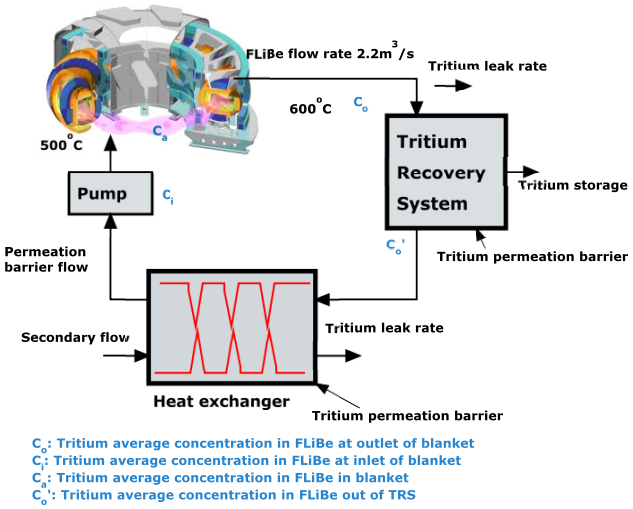

Fig.1 Tritium flow model of FFHR-2 system

Based on the tritium flow mode, a simplify tritium analysis model for FLiBe blanket system was developed, and shown in Fig.2. Utilizing the mass balance theory, an equation can be written as:

$$\frac{\partial M_{T/FLiBe}}{\partial t} = J_1 - J_2 - J_3 - J_4 - J_D \quad (1)$$

where $M_{T/FLiBe}$ is the tritium inventory in FLiBe, J_1 is tritium production rate, J_2 is tritium extraction from breeder, J_3 is tritium permeation from breeder, J_4 is tritium permeation into coolant, J_D is tritium radioactive decay in breeder.

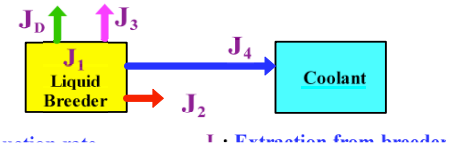

Fig.2 Tritium analysis model for FLiBe blanket

In the liquid FLiBe, the tritium chemical form will be T_2 [1]. The fast liquid FLiBe flow rate, the rising of helium in liquid breeder ($Li + n \rightarrow T + He$), the temperature gradients produce convection which develop an approximate uniform tritium concentration in the blanket. In analysis, we use average tritium concentration in breeder (C_a), neglect the tritium transport in the liquid breeder and consider only the diffusion in the steel walls to get conservative permeation result[3]. The average concentration (C_a) and tritium average pressure (P) were calculated by the following formula:

$$C_a = \frac{C_i + C_o}{2} = \left(1 - \frac{1}{2}\alpha\eta_{Li}\right)C_o \quad (2)$$

$$P = \frac{C}{K_H} \quad (3)$$

where K_H is tritium gas solubility constant for the molten salt (FLiBe), η_{Li} is efficiency of TRS, α is proportion of FLiBe flow into TRS.

In blanket, the tritium in FLiBe will diffuse into the structural material, and then permeate through blanket to other devices. To simulate this process, the diffusion limited permeation model is used. In the model, the tritium permeation flow rate (J) through a wall is proportional to the difference of the square roots of tritium partial pressures[4]:

$$J = \frac{1}{TPRF}\frac{A}{d}D_s K_s \sqrt{P_a} \quad (4)$$

Where K_s is tritium solubility in structure material, D is tritium diffusivity in structure material, and A is permeation area, d is the permeation distance. By means of the formula above, permeation from FLiBe system (J_3), and the permeation into secondary coolant in HX (J_4) were all considered in detail.

In the TRS, the tritium will be extracted from FLiBe and transport to the reactor core as a fuel supply. The extraction flux (J_2) is calculated:

$$J_2 = \alpha\eta_{Li}G_{Li}C_o = \alpha\eta G_{Li}K_{Ho}P_o \quad (5)$$

where G_{Li} is liquid breeder flow rate of FLiBe.

For short half-life of tritium, the radioactive decay can't be neglected. In this case, the tritium radioactive decay flux (J_D) of FFHR2 can be calculated by following formula.

$$J_D = \lambda V_{FLiBe}C_a = \lambda V_{FLiBe}\left(1 - \frac{1}{2}\alpha\eta_{Li}\right)K_{Ho}P_o \quad (6)$$

Where λ is 5.64%/yr, V_{FLiBe} is volume of breeder.

3. Conditions for Analysis

In FFHR2 operation, the fusion power is designed to be 1GW and the flow rate of FLiBe to be 4.4×10^6g/s (the density FLiBe is 2×10^6g/m^3). In steady state operation, 190g T will be bred per day in blanket of FFHR2, then transported to TRS and extracted from FLiBe. The tritium solubility in FLiBe as T_2 is 5.3×10^{-13}wtfr·Pa [5].

Refer to the designs of blanket and the auxiliary system for FFHR2, structure and material parameters of these components are showed in table.1. And the tritium related parameters are presented in table.2:

Table 1 Structure and Material for FFHR2 Blanket

Component	A (m^2)	d (m)	Material
Blanket [6]	489	0.010	JLF-1
Heat Exchanger (HX) [7]	700	0.001	Ta/Nb/W/Sic
Pipe from blanket to TRS	10	0.005	sus316
Pipe from TRS to HX	15	0.005	sus316
Pipe from HX to blanket	15	0.005	sus316

- For the FLiBe corrosion and neutron irradiation, it is considered to fabricate tritium permeation barrier on the exterior of FLiBe blanket, and the TPRF is 50 referenced other liquid blanket design [8].
- All the auxiliary piping have an aluminize coating on the exterior, and the TPRF would reach 1000 for a 50μm layer [9].
- The SiC composite and W have low tritium permeability, thus it don't need fabricate tritium permeation barrier on the substrate material surface.

Table 2 Tritium Parameters for Materials

T permeability through F82H (550°C) [10]	5.06×10^{-11} g/m.s.$Pa^{0.5}$
T permeability through W (600 °C) [10]	1.09×10^{-13} g/m.s.$Pa^{0.5}$
T permeability through SiC (600 °C) [11]	5.24×10^{-19} g/m.s.$Pa^{0.5}$
T permeability through Nb (600 °C) [7]	1.18×10^{-9} g/m.s.$Pa^{0.5}$
T permeability through Ta (600 °C) [12]	3.23×10^{-7} g/m.s.$Pa^{0.5}$
T permeability through sus316 (600°C) [3]	9.7×10^{-11} g/m.s.$Pa^{0.5}$

4. Analysis and results

4.1 Sensitive Analysis

A. Effect of material selection for heat exchanger

Based on the assumed conditions, the tritium extraction and permeation were calculated by changing the heat exchanger material without coating in this case, and the results were showed in Fig.3-4. Selected Nb alloy and Ta alloy as HX material, most of tritium would permeate into secondary loop for their high tritium permeability. While SiC composite and W alloy have low tritium permeability, thus less tritium would permeate into secondary loop but more would be extracted. In addition, considering the difficulty of SiC fabrication based on current technology, W alloy was more reasonable selection for HX structure material [13].

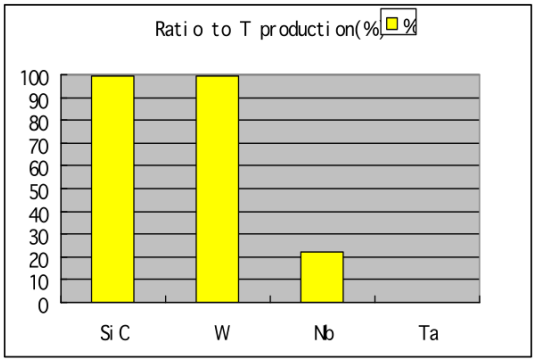

Fig. 3 T recovery vs. HX

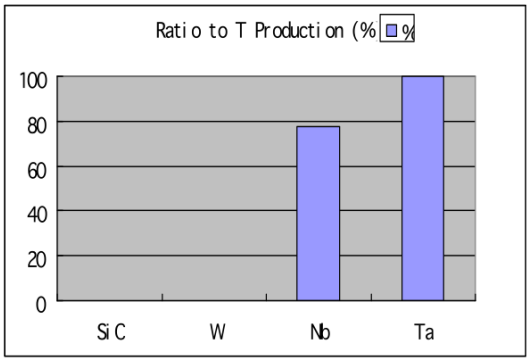

Fig. 4 T leak into secondary flow vs. HX

B. Effect of proportion of FLiBe flow in TRS (α)

In this analysis, using W alloy as HX material, the tritium extraction and permeation were calculated by changing α. The results were showed in Fig.5-6. When α reach to 0.2, tritium extraction and permeation would be changed slowly with increasing α, and the change limit in 1% when α increase from 0.2 to 1. More FLiBe flow into the TRS, the requirement of TRS would be increased and more heat in FLiBe would be lost in TRS. The analysis showed that it was reasonable to choose proportion of FLiBe into TRS as 0.2 for FLiBe blanket design.

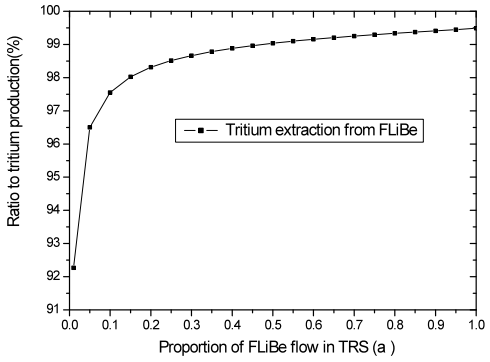

Fig. 5 T recovery vs. α

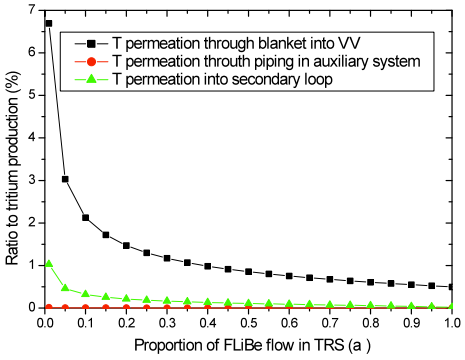

Fig. 6 T permeation vs. α

C. Effect of efficiency of TRS (η)

In the analysis, the HX material was W alloy and α was 0.2, the tritium extraction and tritium average pressure in FLiBe were calculated by changing η. As showed in Fig.7-8, when η increased from 0.01 to 0.98, tritium extraction from FLiBe would be increased little (from 94.5% to 98.3%). But the tritium average pressure in FLiBe would be reduced largely (from ~44000 Pa to ~4300 Pa). High tritium pressure in FLiBe means high tritium inventory in blanket, which would increase the potential dangers for fusion reactor operation. For safety reason, it needed get high η to reduce the tritium inventory in FLiBe, which would increase the requirement of technology and

cost for TRS. So it was needed to design reasonable efficiency for the TRS. The tritium average pressure in FLiBe would below 5000 Pa when η reaching 0.85. Maybe η as 0.85 was an acceptable design.

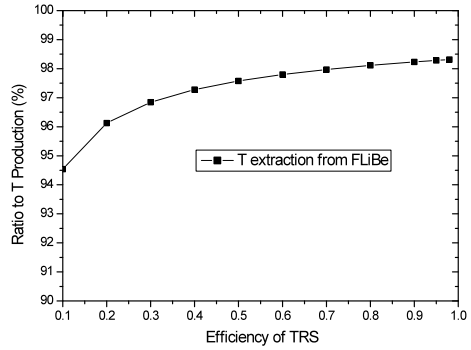

Fig. 7 T recovery vs. η

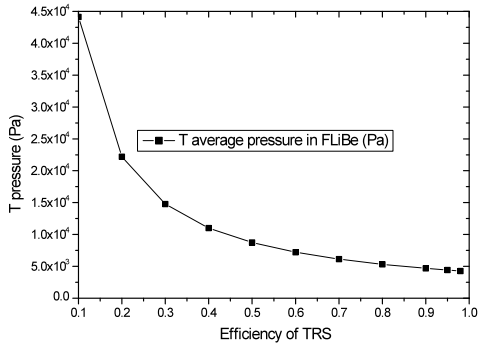

Fig. 8 T pressure vs. η

D. Effect of TPRF in FLiBe blanket

In the analysis, the heat exchanger material was W alloy, α was 0.2 and η was 0.85, the tritium extraction and permeation were calculated by changing the TPRF on FLiBe blanket. The results were shown in the Fig.9-10,

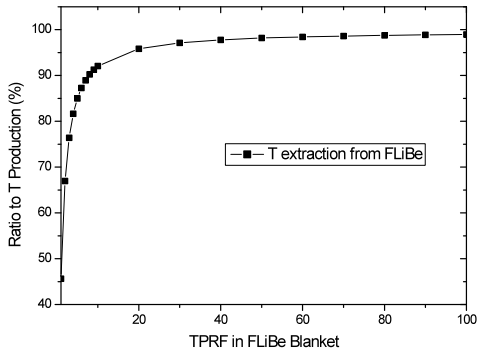

Fig. 9 T recovery vs. TPRF

When the TPRF reached ~20 or became larger on blanket, more than ~95% of bred tritium would be recovered from FLiBe, and the tritium average pressure in FLiBe and permeation through blanket would change slowly. Thus it was reasonable to choose TPRF for 20 on FLiBe blanket in FFHR2 tritium system design. It was needn't to get very high quality tritium permeation barrier for FLiBe blanket. However, the permeation barrier compatible with good thermal conductivity was essential.

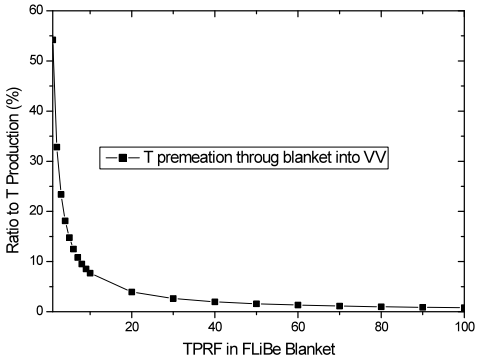

Fig. 10 T permeation through blanket vs. TPRF

4.2 Analysis Results

Basing on the sensitive analysis, the tritium extraction, permeation and tritium pressure in FLiBe were calculated, where HX material was W alloy, α was 0.2, η was 0.85 and TPRF was 20 in blanket respectively. The results were showed in the table3:

Table 3 Tritium analysis results of FLiBe blanket for FFHR2

T recover in TRS	1.7251E+06 Ci/day
T permeation into VV	7.0683E+04 Ci/day
T leak from blanket to TRS	1.1578E+01 Ci/day
T leak from TRS to HX	1.5822E+01 Ci/day
T leak from HX to blanket	1.5822E+01 Ci/day
T leak through secondary flow	4.1386E+03 Ci/day

- The fusion power of FFHR2 is 1GW, which means 1.4495E+06 Ci-T/day will be burned up in plasma. Tritium recovered from FLiBe in TRS is 1.7251E+06 Ci/day (9.5841E+01%), which is enough for FFHR2 burn up.
- The tritium permeation through blanket into VV is 7.0683E+04Ci/day, which must be transported to isotope separation system (ISS) by vacuum pump and stored for fueling. According to ITER [14], the impurity stream from VV is disposed to reduce the tritium content by a factor of ~10^7 before releasing into the atmosphere, thus most of tritium permeation into VV will be reused and the tritium release into environment from VV can be neglected.
- The total tritium inventory of permeation into the auxiliary system building is 4.3223E+01Ci/day. To

keep the tritium release into environment below the allowable level i.e.10Ci/day, an effective Vent Detritiation System (VDS) is needed for FFHR2 to process all effluent gas from reactor confinement building for final detritiation before release into the environment.

- Tritium permeation into secondary loop can't be neglected (4.1386E+03Ci/day), thus an effective coolant purification system (CPS) should be designed for FFHR2.

5. Conclusions

In this paper, a tritium analysis model of the FLiBe blanket system was developed and the preliminary analysis on tritium permeation and extraction for FLiBe blanket system were done. The factors which affected tritium extraction and permeation were calculated and evaluated, such as the heat exchanger material, proportion of FLiBe flow in tritium recover system (TRS), efficiency of TRS and tritium permeation reduction factor (TPRF) in blanket etc.

Based on the assumed operation condition, tritium recovery from FLiBe in TRS was enough for FFHR2 burn up. To control the tritium leak rate into auxiliary system building less than 10Ci/day, an effective VDS was needed for FFHR2 to process all effluent gas from reactor confinement building. In addition, an effective CPS should be designed for for secondary loop.

In addition, further R&D efforts were required for FFHR2 to guarantee the tritium self-sufficiency and safety, for example fabrication technology of the heat exchanger, requirement for the TRS and reasonable quality of tritium permeation barriers on blanket, etc..

Acknowledgements

This work was partly supported by the JSPS-CAS Core -University Program in the field of "Plasma and Nuclear Fusion". We would further like to thank the great help from the members of FDS Team in ASIPP and USTC in this research.

References:

[1] A. Sagara, S. Imagawa, O. Mitarai, et al., Improved structure and long-life blanket concepts for heliotron reactors, Nucl. Fusion 45 (2005) 258–263.

[2] S. Fukada, A. Morisaki, A. Sagara, T. Terai, Control of tritium in FFHR-2 self-cooled Flibe blanket, Fusion Engineering and Design 81 (2006) 477–483.

[3] G. Gervasini, F. Reiter. Tritium Inventory and Permeation in Separately cooled Liquid Breeder Blankets. J. Nucl. Mater., 1989, 168(3): 304-311.

[4] W. Farabolini, A. Ciampichetti, F. Dabbene, M.A. Fütterer, L. Giancarli, et al., Tritium control modeling for a helium cooled lithium–lead blanket of a fusion power reactor, Fusion Eng. Des. 81 (2006) 753–762.

[5] S. Fukada, A design for recovery of tritium from Flibe loop in FFHR-2. Fusion Power Plants and Related Advanced Technologies, Feb. 5, 2007.

[6] A. Sagara, O. Mitarai, T. Tanaka, S. Imagawa, Y. Kozaki, M. Kobayashi, et al., Optimization activities on design studies of LHD-type reactor FFHR, Fusion Engineering and Design 83 (2008) 1690–1695.

[7] B. Merrill, S. Malang, Tritium Permeation and Extraction Issues for the ARIES-CS, ARIES Meeting, University of Wisconsin, June 15th, 2005.

[8] Y. Song, Q. Huang, Y. Wang, M. Ni, Analysis on tritium controlling of the dual-cooled lithium lead blanket for fusion power reactor FDS-II. Fusion Engineering and Design 84 (2009) 1779–1783.

[9] C.P.C. Wong, M. Abdou, J. Blanchard, P. Calderoni, D.P. Carosella, M. Dagher, et al., Design Description Document for the U.S. Dual Coolant Pb-17Li (DCLL) Test Blanket Module, TBWG Meeting, Nov 15, 2005.

[10] E. Serra, G. Benamati, O. V. Ogorodnikova, Hydrogen isotopes transport parameters in fusion reactor materials, Journal of Nuclear Materials 255 (1998) 105-115.

[11] R. A. Causey, W. R. Eampler, The use of Silicon Carbide as a tritium permeation barrier, Journal of Nuclear Materials 220-222 (1995) 823-826.

[12] P.X. Wang, J.S. Song, Helium in Material and the Permeation of Tritium, National defence industrial publication company of China (2002).

[13] N. Baluc, K. Abe, J.L. Boutard, et al., Status of R&D activities on materials for fusion power reactors, Nucl. Fusion 47 (2007) S696–S717.

[14] H. Yoshida, O. Kveton, J. Koonce, D. Holland, R. Haange, Status of the ITER Tritium Plant design, Fusion Eng. Des. 39-40 (1998)875-882.

Study on theory and simulation of plasma MHD and micro-turbulence and transport in toroidal plasmas

Y. Kishimoto, Z. Gao*), J.Q. Li, and Ding Li**)
Graduate School of Energy Science, Kyoto Universuty
* Department of Engineering Physics, Tsinghua University, China
** University of Science and Technology of China

Abstract:
The subject under these categories 30A and 30B aims at studying the characteristics of MHD stability and micro-turbulence in toroidal magnetic fusion plasmas through establishing theoretical models and developing massively parallelized simulation codes to understand the plasma transport property and improve the confinement performance. This focus is on the multi-scale nature of MHD fluctuations and micro-turbulence with various kinds of flows including the low-frequency zonal flows and finite frequency geodesic acoustic modes(GAMs), low-frequency longer wavelength Kelvin-Helmholtz(KH) structures, radially elongated streamers. Furthermore, the local and nonlocal transport properties are explored by comparing the statistic analyses of experimental observations in stellarators and tokamaks with the simulations of intermittent transport dynamics. In past 10 years, lots of important results have been achieved through close collaboration between Japanese and Chinese colleagues. Collaborating partner framework has been established among institutions. Here the main achievements and activities on the study of MHD, micro-turbulence and transport as well as the computational analyses are briefly summarized.

Objectives:

It is aimed at basic understandings of micro-turbulence and MHD dynamics, which regulate stability and confinement of core plasmas, and their theoretical and computational modeling in toroidal plasmas. Specifically the multi-scale nature of turbulence and MHD in toroidal plasmas is investigated and the control methodology for the achievement of high performance plasmas is explored (see Fig.1).

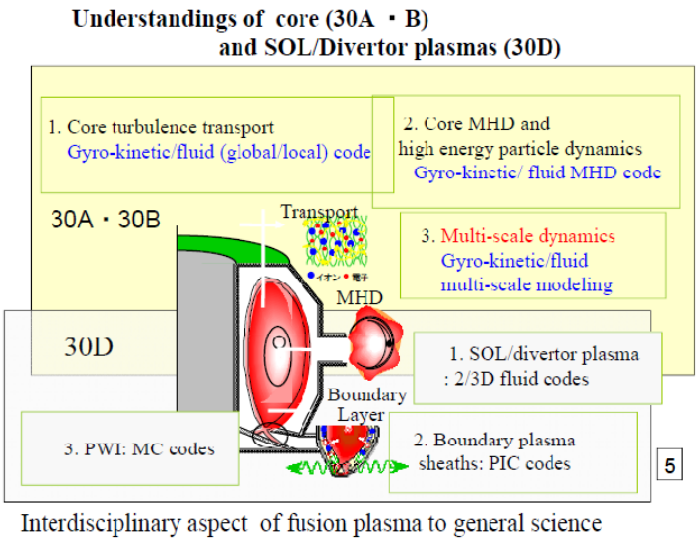

Fig.1 Schematic view of the subjects 30A and 30B and the relation with other one, 30D in the theory and simulation in magnetically confined fusion plasmas.

Overview of the activities and achievements

In past 10 years, 30 visits (261 days) from Japan to China and 33 visits (687 days) from China to Japan have been performed to exchange newly achieved results and discuss the collaboration subjects (see table1). The institutions that joined the 30A and 30B in the CUP program is also shown in Fig. 2. Several seminars and jointed workshops have been organized to present research progress and to propose and summarize the cooperation activities (see Fi.3 and Fig.4). More than 18 collaborative papers have been published in refereed journals such as Physical Review Letters, Physics of Plasmas, Nuclear Fusion, and others. Lots of presentations have been talked in various international academic conferences and workshops such as IAEA Fusion Energy Conference. In addition, this program has activated young scientists from both sides to start first international academic exchange and make international collaboration through their research visits to partner institutions. Many excellent young scientists working on the theory, simulation and experimental data analyses have grown into main cooperative researchers in the fields through the experiences under this program.

Exchanges of scientists: 30A

	2001	2002	2003	2004	2005	2006	2007	2008	2009	2010	
J → C	2(24)	1(12)	1(13)	2(15)	2(14)	3(23)	2(28)	2(12)	2(13)	2(14)	18(168)
C → J	1(42)	1(42)	2(31)	1(22)	2(42)	2(43)	3(47)	2(35)	2(30)	2(20)	18(362)

Exchanges of scientists: 30B

	2001	2002	2003	2004	2005	2006	2007	2008	2009	2010	
J → C	1(12)	1(8)	1(9)	1(8)	1(7)	1(7)	1(10)	1(4)	2(14)	2(14)	12(93)
C → J	1(43)	1(42)	1(40)	1(32)	1(21)	2(28)	2(35)	2(28)	2(28)	2(28)	15(325)

Table 1 Number of scientist and the days who visit Japan and China in the program 30A and 30B. 30 visits (261 days) from Japan to China and 33 visits (687 days) from China to Japan had been achieved.

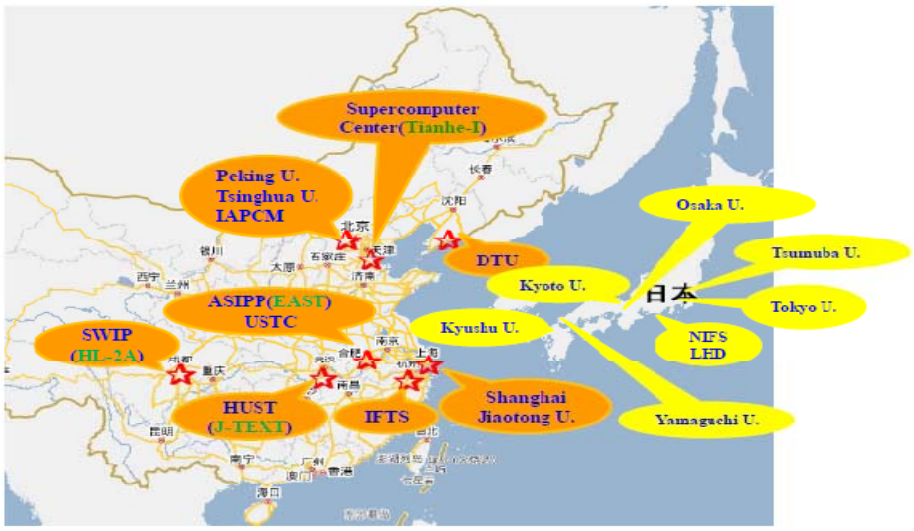

Fig.2 Institutions that joined the 30A and 30B in the CUP program

Fig.3　Mini-Workshop on “Physics and Modeling of Multi-scale Interaction in Plasmas”, Dec. 2-3, 2010, Kyoto University. We had for Chinese guests, Z. Gao (Tsinghau Univ.), H. Cai (USTC), C. Xiao (Peking Univ.), Z. Wang (Dalian Univ.)

Fig.4　China-Japan CUP Seminar on “Modeling of Theory and Simulation of Fusion Plasmas”,　August 30-Sepetember 2, 2010 Beijing, CHINA

Typical achievements

(1) Study on MHD fluctuations in toroidal plasmas

In magnetic fusion plasmas, the MHD activity such as the major disruption is a serious thread on the plasma confinement performance. The classical and/or neoclassical tearing mode and/or the double tearing mode (DTM) are of typical MHD fluctuations, which are the main drive force of the magnetic reconnection. These fluctuations also commonly appear in astrophysical plasmas. To understand the fast magnetic reconnection and the explosive process, the theoretical and numerical analyses of the tearing modes are performed intensively with the aid of large-scale simulations. In this issue, the following main results have been achieved.

The sawtooth driven neoclassical tearing modes in HL-2A tokamak plasmas have been investigated. It is found that as the islands grow, the overlap of neighboring islands can lead to field line missing and fast mode growth, and cause tokamak disruptions. With the toroidal geometry, the neoclassical effect caused by Trapped Particles with "Banana Orbits" can lead to Bootstrap Current and neoclassical resistivity. Correspondingly Neoclassical Tearing Mode (NTM) are excited with island equation

$$I\frac{dw}{dt} \approx \Delta' + 9.26\varepsilon_s^{1/2}\frac{\beta_s'}{s(r_s)}\frac{w}{w^2 + w_d^2}$$

with $I \approx 2S$, $\varepsilon_s \equiv r_s / R_0$, $s(r_s)$, and β_s being inversed aspect ratio, magnetic shear, and plasma beta on $r = r_s$ respectively. Differential rotations of tokamak plasmas can however suppress the island growth, though the mechanism for the rotations is yet unclear. Suppressed by the shear flow, Rutherford islands can be saturated in a low level. Nevertheless, the resonant Fourier component of intrinsic Error Field is able to interact with corresponding island to cause mode locking. The saturated rotation island can grow again if locked to the error field, and lead to island overlap and disruption. It is a typical boundary driven reconnection process. The other driven source can be the "seed" island induced by sawteeth. Then the sawtooth driven neoclassical tearing modes in HL-2A tokamak plasmas are discussed. Furthermore, the bursty phenomena are investigated in various plasmas, which are often found in many fast growth processes, such as solar flares, substorm onsets, sawtooth crashes, and tokamak major disruptions and are also observed in geo environment such as lightning and sprite discharges, as well as laser generated air plasmas. The methods developed in related studies can have wide applications to other fields. It has been discussed the possible applications in laser guide plasma jets and linear machine simulated divertor plasmas.

Anomalous resistivity generation for fast magnetic reconnection is a long-standing problem. A fast magnetic reconnection event observed by Cluster spacecraft near the reconnection X-point has been investigated. The power spectrum of the electric field around the lower-hybrid (LH) frequency is measured to compute the anomalous resistivity in comparison with the effective resistivity calculated from electrical field and current data. Also the fast reconnection rate is estimated from magnetic field and flow data to compare with the reconnection electrical field computed from the current density data and anomalous resistivity calculation. It is found that, the anomalous resistivity induced by LH frequency turbulence near the X-point is sufficient to trigger fast reconnection.

Scaling laws of fast growth of collisionless double tearing modes in the linear phase are studied numerically by a reduced magnetohydrodynamics model in a cylindrical plasma. It is found that, the scaling

of the linear growth rate changes gradually from $\gamma \sim d_e^1/\gamma \sim \rho_s^{2/3}$ to $\gamma \sim d_e^3/\gamma \sim \rho_s^1$ as the rational surface separation Δr_s increases in the case $\rho_s << d_e$, with d_e the electron inertial skin depth and ρ_s the ion sound gyroradius. These numerical scaling laws are testified to be reasonable in comparison with previous analytical theories, based on the similarity of physical characteristics of the same categories in tearing modes, where is the linear instability parameter for tearing modes. Finally, the characteristics of the spectrum of unstable DTMs under the influence of d_e and ρ_s for small Δr_s are discussed, and the second unstable eigenmode with different mode numbers are obtained and analyzed.

(2) Study on micro-scale drift wave turbulence in toroidal plasmas

Micro-turbulence is believed as a plausible fluctuation to respond to the anomalous trasnport in magnetic fusion plamsas. The short wavelength drift wave instabilities driven by the ion and/or electron temperature gradient (ITG/ETG) are intensively investigated based on gyrokinetic dispersion relation in a slab geometry through solving an integal code. An analytical analysis is performed first to clarify the physics mechanisms for the modes in a shearless slab. The correlation between the growth rate and the real frequency of the modes is discussed in detail. The electron temperature gradient is found to have strong influences on the modes in short wavelength regions. Several series of the short wavelength modes are then identified with a kinetic integral equation code in a sheared slab. The radial widths of the modes are found to be comparable with the conventional ITG modes and not short, although the poloidal wavelengths are short. The lowest odd mode usually dominates in the weak magnetic shear and low beta regime. However, the fundamental mode seems to be important in tokamak plasmas because the higher order modes are easily stabilized by finite beta and/or by magnetic shear. The fundamental short wavelength mode cannot be stabilized by beta when the magnetic gradient drift effect is taken into account. The modes are excited by both finite ITG and ETG, and may be stabilized by magnetic shear.

Series of ion temperature gradient (ITG) driven modes in the short wavelength region are investigated with a gyrokinetic integral equation code in toroidal plasmas. These instabilities exist even if electrons are assumed adiabatic. However, nonadiabatic electron response can influence these short wavelength ITG (SWITG) modes, especially the fundamental l=0 mode. At typical parameters, excitation of the l=0 mode requires that both ITG and ETG exceed thresholds, while the l=1 and l=2 modes with higher harmonic eigenfunctions persist unstable even at flat temperature gradient. Dependence of the SWITG modes on other parameters is also investigated. The l=1 mode with an odd potential eigenfunction grows faster than the l=0 mode and may be dominant in low ETG, high beta, weak positive magnetic shear, and/or weak toroidicity regions.

(3) Study on secondary large-scale structures in micro-turbulence in toroidal plasmas

Turbulent transport depends on both turbulence structure (spatial spectra) and fluctuation amplitude, which are represented by effective nonlinear decorrelation length and decorrelation time. Studying the saturation mechanism and estimating the saturation amplitude of drift wave turbulence are of importance in understanding the turbulent transport and improving the confinement performance. Several works have been done on this issue.

Typical secondary large-scale structure in magnetic fusion plasmas is the zonal flows including the geodesic acoustic mode (GAM) mode. A series of GAM eigenmodes is derived, which includes the standard GAM, a branch of lowfrequency mode, and a series of ISW-like modes. Eigenfrequencies of these modes are obtained analytically from a linear gyrokinetic model in collisionless toroidal plasmas with a constant electrostatic potential around a magnetic surface. The ISW-like modes have a discrete frequency spectrum roughly with a progression of $\sqrt{n\pi}$ times the transit frequency and strongly damped. The low-frequency eigenmode has a rigid zero frequency for low q but oscillates with a finite frequency for q and relaxes on the scaling with the order of transit frequency . Considering different damping rates of these modes, only a few (the least damped and/or the most excited) modes may play a role in the turbulence dynamics.

Plasma elongation effects on temperature gradient driven instabilities and geodesic acoustic modes have been investigated with gyrokinetic theory and a local MHD equilibrium model. In particular, the focus is on the effect of the elongation κ, including its radial derivative $s_\kappa = (r/\kappa)(\partial \kappa / \partial r)$, in the large aspect ratio limit. An analytical formula of the dependence of the GAM frequency on the elongation is given. It is found that the GAM frequency sharply decreases with increasing elongation, which comes from the modification of ion classical polarization balanced by that of curvature drift polarization. The dependence of the critical threshold of the ETG/ITG instability on the elongation is numerically studied and a semi-analytical formula is given. Plasma shaping effects on the GAM are further revisited analytically in the large orbit drift width limit. Comparing with results from the small orbit drift width expansion method, the behavior of the real frequency is almost the same but the effect on the damping rate is different due to the change of dominant resonant mechanism, from low order harmonic transit resonance to high order harmonic resonance, or equivalently, to the magnetic drift resonance. As a result, although the GAM frequency decreases with an increasing elongation, the damping is weakened mildly in the large orbit drift width limit, which is quite different from the result in the low small orbit drift limit, where the damping is enhanced exponentially with the decrease in frequency. Also, in the large orbit drift width limit, the dependence of the GAM damping rate on inverse aspect ratio is analytically obtained. As the inverse aspect ratio increases, the frequency behaves as a weakly decreasing parabola function, and the damping rate increases parabolically, but more rapidly than the frequency decreases. The GAM with longer radial wavelength is more easily damped by the finite aspect ratio effect. It is also found that the Shafranov shift gradient has the similar effect as the inverse aspect ratio.

The effects of GAMs on the toroidal ion temperature gradient turbulence and associated transport near the critical gradient regime in tokamak plasma are investigated based on global Landau-fluid simulations and extended predator-prey modeling analyses. A new type of intermittent dynamics of transport accompanied with the emission and propagation of the GAMs, i.e., GAM intermittency, has been found. The intermittent bursts are triggered by the onset of spatially propagating GAMs when the turbulent energy exceeds a critical value. The GAMs suffer collisionless damping during the propagation and nonlocally transfer local turbulence energy to wide radial region. The stationary zonal flows gradually increase due to the accumulation of non-damped residual part over many periods of quasi-periodic intermittent bursts and eventually quench the turbulence, leading to a nonlinear upshift of the linear critical gradient; namely, the Dimits shift. This process is categorized as a new class of transient dynamics, referred to as growing

intermittency. The Dimits shift is found to be established through this dynamical process. An extended minimal predator-prey model with collisionless damping of the GAMs is proposed, which qualitatively reproduce the main features of the growing intermittency and approximately predict its various time scales observed in the simulations.

(4) Study on multi-scale MHD and micro-scale drift wave turbulence in toroidal plasmas

Micro-turbulence is believed to be responsible for the anomalous transport in MCF plasmas. To explore the underlying mechanisms governing the transport and understanding the experimental observations in tokamak and stellarator discharges, gyrokinetic and gyrofluid simulation codes have been developed collaboratively and then applied for several specific physics problems. The interaction between two-dimensional vortex flows and microturbulence is studied numerically using gyrofluid simulations. It is shown that, qualitatively different from usual mean flows, vortex flows can dramatically suppress microturbulence even with weak flow shear. A generic suppression mechanism is identified as the multiplied effect of both radial and poloidal mode couplings, which induce the formation of a new global mode. Furthermore, an oscillatory zonal flow is found to form through interaction between the vortex flows and microturbulence. Furthermore, the focus is put on the effect of magnetic shear. It is shown that the vortex flow can effectively stabilize the ITG mode by inducing both radial and poloidal mode couplings. Furthermore, decreasing magnetic shear is identified to weaken the stabilizing role of the vortex flow. The effects of the magnetic shear on the ITG mode structure and on the growth rate in the presence of various shear flows are obtained and the relevant mechanisms are discussed in detail.

Characteristics of ion temperature gradient ITG instability in the presence of a magnetic island are investigated numerically using a gyrofluid model. It is shown that when the magnetic island is wide enough to produce a broad distribution of rational surfaces near the O-point region, the ITG perturbations at these rational surfaces form a radially global-type eigenmode with a fast growth rate, which is referred to as the magnetic-island-induced ITG mode. Moreover, the magnetic island also causes both radial and poloidal mode couplings, which play a stabilizing role.

The direct nonlinear interaction of mixed-scale resistive MHD and ITG turbulence has been investigated by performing 5-field gyrofluid simulation in slab geometry to focus on the understanding of the underlying interaction mechanism. Simulations show that the evolution of the mixed scale electromagnetic turbulence experiences four phases under complex nonlinear interaction and finally arrives at a dynamic quasi-steady state. The spatial structure of the multi-scale electromagnetic turbulence is characterized by the MHD fluctuation, namely the mixed-scale turbulence has a power-law scaling spectrum typical of MHD fluctuation. Nevertheless, the spectral amplitude is enhanced to a higher level at all scales by the ITG instability. An oscillatory ZF with finite frequency is found for the first time in slab plasma due to the cross-scale nonlinear interaction of turbulence. It is identified that the finite frequency of the oscillatory ZF originates from an oscillating electromagnetic torque exerting on the plasma, in which the micro-instability provides the free energy. As a result, the turbulent ion heat transport is not efficiently suppressed by a robust oscillatory ZF. These results imply that the cross-scale interaction in multi-scale turbulence may nonlinearly provide new energy flow channels as a source or sink.

(5) Publication list in refereed journals

1. Zhe Gao, H. Sanuki and K. Itoh, J. Q. Dong, Temperature gradient driven short wavelength modes in sheared slab plasmas, Phys. Plasmas 10, 2832 (2003)
2. Zhe Gao, J. Q. Dong, H. Sanuki , Effects of flow shear on temperature gradient driven short wavelength modes, Phys. Plasmas 11, 3054 (2004)
3. Zhe Gao, H. Sanuki and K. Itoh, J. Q. Dong, Short wavelength electron temperature gradient instability in toroidal plasmas, Phys. Plasmas 12, 022502 (2005)
4. Zhe Gao, H. Sanuki and K. Itoh, J. Q. Dong, Short wavelength electron temperature gradient instability in toroidal plasmas, Phys. Plasmas 12,022503 (2005)
5. Zhe Gao, H. Sanuki and K. Itoh, J. Q. Dong, Multiple eigenmodes of geodesic acoustic mode in collisionless plasmas, Phys. Plasmas 13, 100702 (2006)
6. Deng Zhou, Electromagnetic geodesic modes in tokamak plasmas, Phys. Plasmas 14(2007)104502.
7. Hao Wang, Aike Wang, Qing-Wei Yang, Xuan-Tong Ding, Jiaqi Dong,H.Sanuki and K.Itoh, HL-2A tokamak disruption forecasting based on an artificial network, Chinese Physics 12 (2007)123738.
8. Yemin Hu, Tokamak plasma equilibria with a zero total toroidal current, Phys. Plasmas
9. Zhe Gao, K. Itoh, H. Sanuki, and J. Q. Dong, Eigenmode analysis of geodesic acoustic modes, Physics of Plasmas 15, 072511 (2008)
10. Zhe Gao, Ping Wang, and H. Sanuki, Plasma shaping effects on the geodesic acoustic mode in toroidally axisymmetric plasmas, Physics of Plasmas 15, 072511 (2008)
11. Zheng-Xiong Wang, Xiaogang Wang, J. Q. Dong, Y. Kishimoto, and J. Q. Li, Shear flows induced by nonlinear evolution of double tearing modes, Physics of Plasmas 15, 082109 (2008)
12. Jiquan Li and Y. Kishimoto, Role of secondary long wavelength structures in the saturation of electron temperature gradient driven turbulence, Physics of Plasmas 15, 112504 (2008)
13. J Q Li, Y Kishimoto, N Miyato, K Miki, J Anderson and B R Shi, Gyrofluid simulation on the nonlinear excitation and radial structure of geodesic acoustic modes in ITG turbulence, Journal of Physics: Conference Series 123, 012027 (2008)
14. Jiquan Li, Y. Kishimoto, Y. Kouduki, Z.X. Wang and M. Janvier, Finite frequency zonal flows in multi-scale plasma turbulence including resistive MHD and drift wave instabilities, Nucl. Fusion 49 (2009) 095007 (8pp)
15. Z. X. Wang, J. Q. Li, J. Q. Dong, and Y. Kishimoto, Generic Mechanism of Microturbulence Suppression by Vortex Flows, PHYSICAL REVIEW LETTERS 103, 015004 (2009)
16. Z. X. Wang, J. Q. Li, Y. Kishimoto, and J. Q. Dong, Magnetic-island-induced ion temperature gradient mode, PHYSICS OF PLASMAS 16, 060703 (2009)
17. Z. Gao, L.L. Peng, P. Wang, J. Q. Dong, H. Sanuki, Plasma Elongation Effects on Temperature Gradient-Driven Instabilities and Geodesic Acoustic Modes, Nuclear Fusion 49, 045014 (2009)
18. Z. X. Wang, J. Q. Li, J. Q. Dong, and Y. Kishimoto, Stabilization of ion temperature gradient driven instability by a vortex flow, Physics of plasmas 18, 012110(2011)

Acknowledgements

In summarizing the 10 years history of Japan-China Core University Program, I would like to greatly appreciate Prof.Ding Li, Prof. H. Sanuki, Prof. J.Q. Dong who have led the theory and computation projects (30A and 30B) over the last decade. Without their aggressive and intensive encouragements and supports, the program had not reached the great success.

Prof. H. Sanuki gave the following message when we had a seminar (China-Japan CUP Seminar on "Modeling of Theory and Simulation of Fusion Plasmas", August 30-Sepetember 2, 2010 Beijing, CHINA, see Fig.4),

When we would discuss the future collaboration program, as my friend, Prof. Dong Jiaqi(SWIP) pointed out in his visit report(2000), we should remember that that there are no country boards for science(科学没有国界：kexue meiyu guojie) and science belong to the whole human being ; sciences all over the world should work together for a bright future all over the world. To realize so, one of the important issues is the mutual understandings. Associated with this point, recently I study a Chinese proverb by 荀子. （宥座之器）；

I also thank to my colleagues Prof. Zhe Gao, Prof. S. Wang, J.Q. Li who had provided significant contribution for arranging the program. Finally, I would like to deeply acknowledge to Prof. Toi and Prof. Komori for supporting our theoretical and computational activity in this program.

China-Japan Core University Program : [30C]

"Physics of self-organization in complex plasmas"

Project leaders: Ritoku Horiuchi (NIFS, Japan), Zhu Shaoping (IAPCM, China)
Email: horiuchi.ritoku@nifs.ac.jp

1. Purpose:

Self-organization phenomena are commonly observed in various complex plasmas such as solar flare, experimental plasmas, fusion plasmas and so on. The purpose of this collaboration research is to extract common properties based on theory and numerical simulation and clarify physics of self-organization in complex plasmas.

2. Overview of research activities

Each year a few scientists from both countries visited the member institutions in the partner country for the collaborations and two or three seminars on self-organization in complex plasmas were held during their stay in China and Japan, respectively. During the five years of successful operation for 2006-2010, 16 exchange visits and 11 seminars were carried out (Table 1). The seminars and the subsequent discussions covered the following topics; macroscopic self-organization and related physical mechanism on MHD dynamo, energy relaxation process, magnetic reconnection, intermittent phenomena in macro and micro plasma physics, cross-hierarchy phenomena in fusion plasmas, complexity in laser-plasma interaction, radiative diffusion and transfer process, development of multi-scale/multi-physics simulation model, and so on.

	2006	2007	2008	2009	2010	total
J to C	1	1	1	2	1	6
C to J	1	2	2	3	2	10
seminar	2	2	2	3	2	11

Table 1. Exchange visits and seminars

3. Main results in the collaboration research

Main results obtained from these collaboration works are summarized as follows:

A) Many interesting self-organization phenomena with common features appear in complex plasmas, regardless of whether it is controlled by microscopic physics or macroscopic physics.

B) Their dynamical behaviors are strongly dependent on openness of a system and multi-hierarchy nature in phenomena.

- Self-organization takes place intermittently in an open system with energy inflow, while it is realized through step-wise relation in a close system. The typical example of intermittent self-organization in a macroscopic system is spontaneous generation and sudden reversal of dipole magnetic field by MHD dynamo, as shown in Fig. 1 [Jinhong Li and A. Kageyama, 2002]. Inner core which consists of hot metallic component supplies the energy into the outer core region. It is found that the constant energy supply play a key role in triggering sudden change of the dipole polarity.

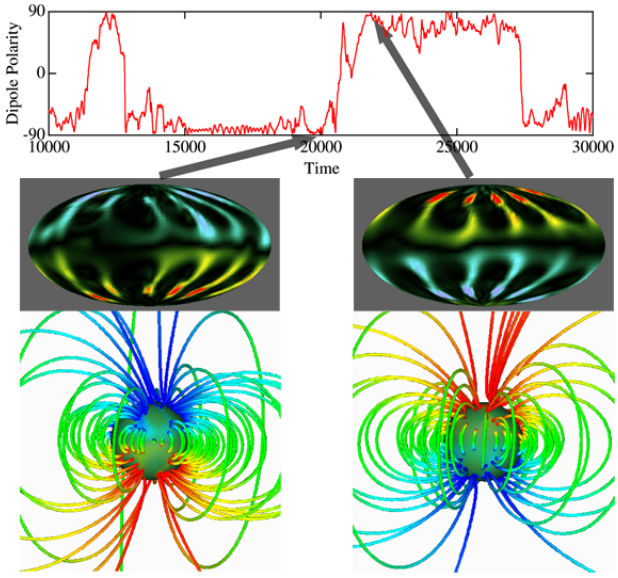

Fig.1 Spontaneous generation and sudden reversal of dipole magnetic field by MHD dynamo where time history of dipole polarity (top), spatial profiles of radial magnetic field at outer boundary (middle), and magnetic field lines (bottom) before and after the reversal are plotted.

- Dynamical behavior of microscopic collisionless reconnection is strongly coupled with macroscopic physics such as the way of energy supply into a microscopic system. For this study we have developed particle simulation code with an open boundaries (PASMO) in which the information of

macroscopic physics is introduced into the system as boundary conditions. A series of the PIC simulations have disclosed that collisionless driven reconnection takes place intermittently when plasma inflow at upstream boundaries satisfies some condition [Wenbing Pei and R. Horiuchi, 2001]. Figure 2 demonstrates an intermittent reconnection in microscopic open system. Magnetic islands are often generated in the central current sheet and the system never reaches a steady state.

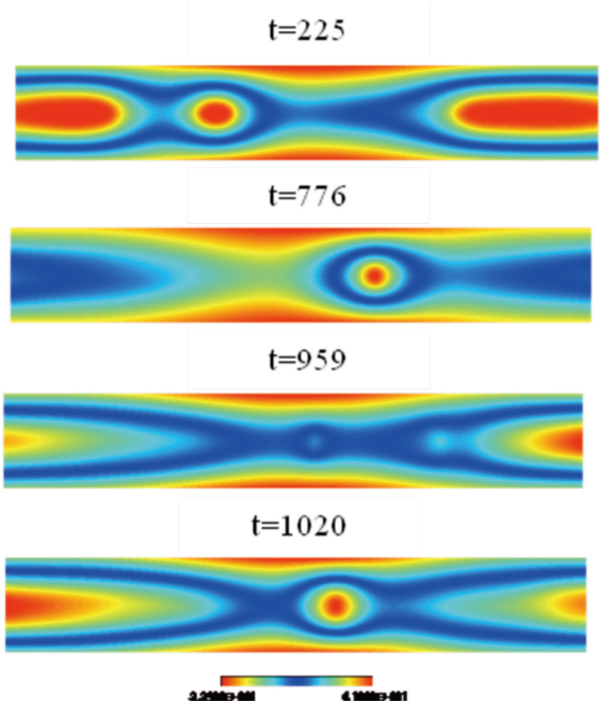

Fig. 2 Two-dimensional particle simulation of intermittent collisionless reconnection in an open system where magnetic flux profiles at four different times are plotted.

C) Many new aspects of magnetic reconnection have been disclosed as one of dominant processes controlling self-organization in both macro and micro hierarchies. Figure 3 shows a typical result of particle simulation studies of collisionless driven reconnection [Bin Li, S. R. Horiuchi, 2008]. Energy transfer mechanism of collisionless reconnection in the electron dissipation region is studied. The mechanisms in the upstream and downstream direction are found to be quite different, which are deeply related to the two-scale structure of the electron dissipation region.

D) Various large-scale simulation models and a series of simulation codes related to this research project have been developed.

E) The information exchanges on the software and hardware infrastructures such as multi-scale/multi-physics simulation algorism and scientific visualization of complex plasmas have been done through the mutual visits and seminars. Multi-hierarchy simulation model (**MARIS**) to interlock three different simulation models based on domain decomposition method has been developed on Japanese side, while **JASMIN** (J Adaptive Structured Mesh applications INfrastructure), which supports the large scale parallel simulations on adaptive structured mesh (SAMR) using massively parallel processing machines (MPP), is developed on Chinese side.

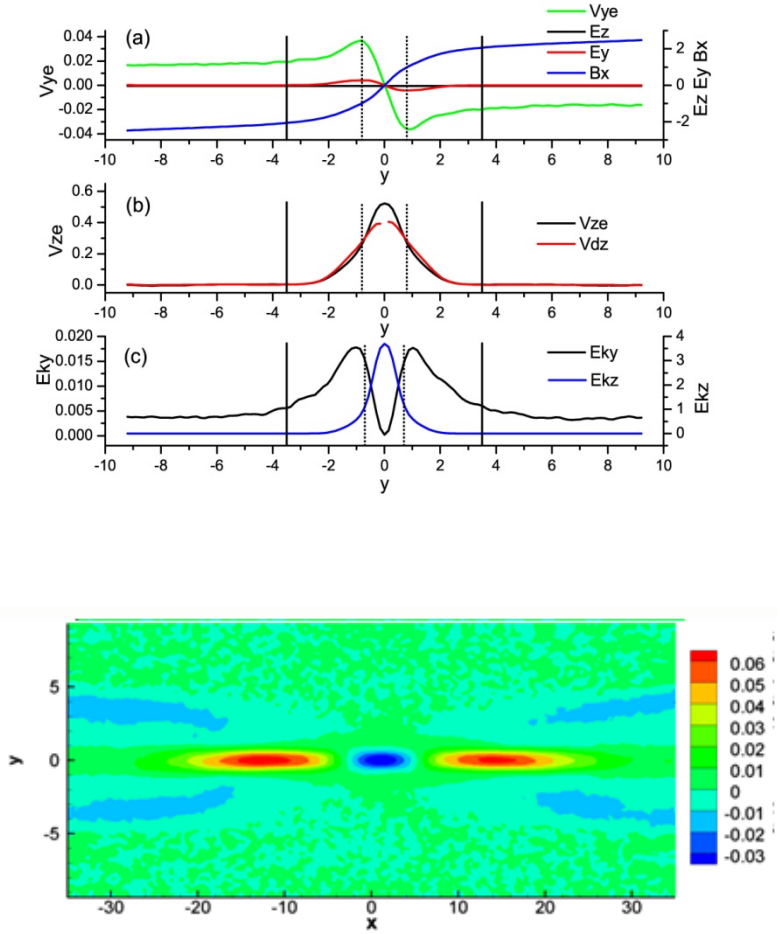

Fig. 3 Structure of electron dissipation region (bottom), and spatial profiles of several physical quantities in the downstream direction (top).

We hope to continue the collaboration studies in numerical simulation techniques and physics of self-organization in complex plasmas.

Summary of 30D
- Modeling of edge and divertor plasma and control of impurities and recycling particles –

Tomita Yukihiro (冨田幸博)[1] and Zhu Sizheng (朱思铮)[2]

[1]*National Institute for Fusion Science, 322-6 Oroshi-cho, Toki 509-5292 Japan*

[2]*Institute of Plasma Physics, the Chinese Academy of Sciences, Hefei 230031 China*

1. Introduction

During ten years we collaborated on the following subjects under the CUP program

1) Analysis on operation spaces by using CSD (Core-SOLDivertor) model in EAST (ASIPP) and HL-2A (SWIP) tokamaks;

In this collaboration research the objective is qualitative understanding of overall features of plasma operation space.

2) Researches of dust characteristics in fusion plasmas;

The purpose of this collaboration research is to analyze the charging and the dynamics of dust particles and investigate the control method to suppress the generation of dust particles from the plasma-facing wall.

3) Impurity transport study in EAST and HL-2A;

Nowadays we started the collaboration research to study the generation and redeposition of impurities from the plasma-facing wall.

2. Overview of collaboration research activities

The exchanges of scientist are tabulated in Table 1, where the first and second columns are exchanges from Japan to China and vice versa, respectively.

Table 1. Exchange program of category 30D.

	2001	2002	2003	2004	2005	2006	2007	2008	2009	2010	2011
J → C	1	1	1	0	1	1	1	2	2	2	2
C → J	0	0	0	1	1	1	1	2	2	2	1
papers	0	0	0	1	3	3	2	1	2	2	1

The initial period only one scientist visits each country. After the collaboration research becomes active, a number of exchanges increased. The lower column in the Table 1 indicates the number of papers published in the refereed journals under the CUP collaboration researches.

3. Main results from collaboration researches

The main results of the collaboration researches are briefly summarized in the following section.

3.1. Analysis on EAST LHCD Operation Space by using Simple Core-SOL-Divertor Model [1]

Consistency between the edge plasma operation and the core plasma operation is an important issue for the design of ITER and the future fusion power plant. In the case of the ITER divertor predictive modeling, the fitting scaling laws for divertor plasma property are built with a two dimensional (2D) divertor transport code, and these are used as boundary conditions for the core plasma analysis. Prior to such detailed and massive calculations by multi-dimensional transport codes, it is useful to understand qualitatively the overall features of plasma operational space including the requirements for the SOL and divertor plasmas. For this purpose, we are developing a simple Core-SOL-Divertor model (CSD model). In this study, we extend the core plasma model in which the hybrid operation can be taken into account, and apply this CSD model to investigate the relationship between the plasma discharge duration and the plasma operational space of low hybrid current drive (LHCD) experiments for the EAST tokamak.

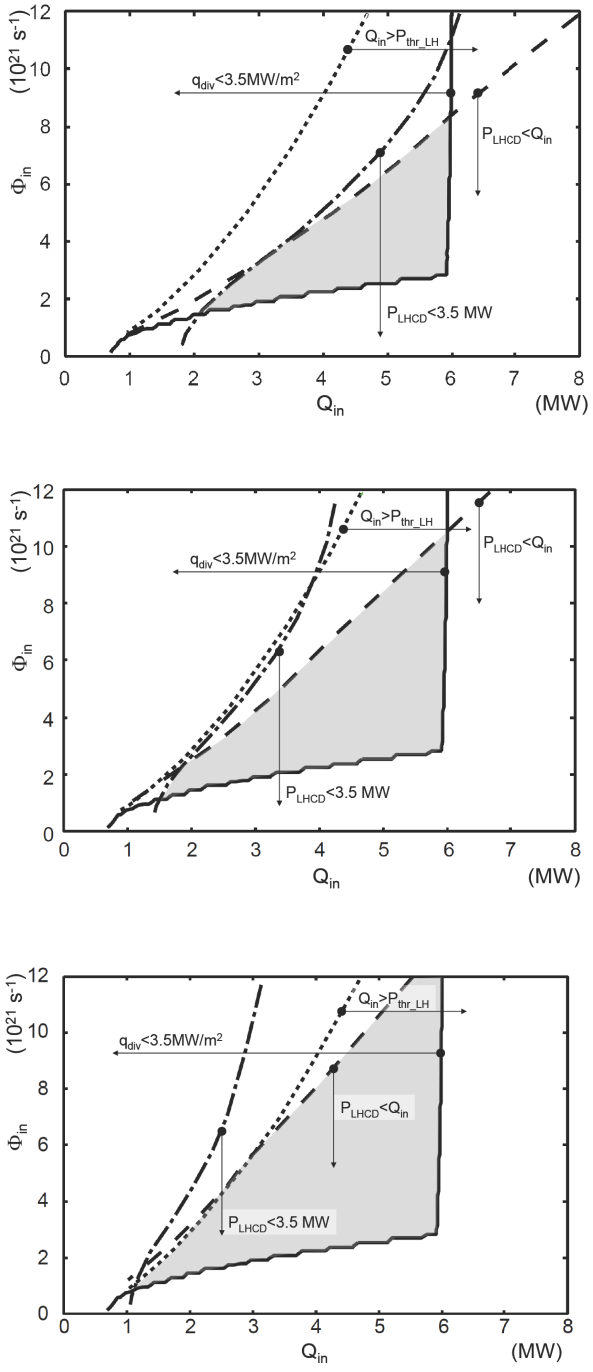

Fig.1 Operational space of LHCD operation and dependence on the fraction of ohmic current fraction f_{ohm}, (*a*) f_{ohm}=0%, (*b*) f_{ohm}=30%, and (*c*) f_{ohm}=50%,

The dependence of the operational space on the fraction of the ohmic current to the total plasma current f_{ohm} is investigated. In this series of investigation, the remaining parameters except the key parameter in the following methods are kept at the same values as those in Fig.1 (*a*). Fig.1 (*b*) shows the operational space for the hybrid operation case of f_{ohm} = 0.3 (which roughly corresponds to the plasma operation duration of 33 sec). The upper boundaries of the LHCD current drive and the power balance requirement move to higher particle flux region, which corresponds to

the high density region. When the fraction of the ohmic current to the total plasma current increases up to f_{ohm} = 0.5. (which roughly corresponds to the plasma operation duration of 20 sec), the boundaries of the LHCD current drive and the power balance requirement move to higher particle flux region and the boundary of the LH transition condition limits the upper operational space in the low heating region of Q_{in} < 3.0 MW. In the future, comparison with these results and the two dimensional divertor transport code B2-EIRINE will be carried out, and the high recycling or detachment operation point for the LHCD H-mode operation will be assessed.

3.2. Release Conditions of Dust Particle from Plasma-Facing Wall [2]

The presence of dust particles in fusion devices is one of the interesting topics as well as in the astrophysical, space, laboratory, and processing plasmas. In present fusion devices (TEXTOR-94, ASDEX-U, LHD, etc.), the dust particles were collected and analyzed their characteristics, where the dust radii are widely ranged between 10 nm and 100 mm. The components of them were mainly of carbon and constituents of stainless steel, which are used for most plasma-facing walls and vacuum vessels. One of the particular notices in fusion devices is associated with absorption of radioactive tritium. After operation of plasma discharges, the disposal of the radioactive dusts is one of key issues from the viewpoint of the safety. In this study we theoretically investigate the effect of the gravitational force on release conditions of the spherical dust particles attached on the plasma-facing wall, which is important to understand the behavior of the dust in the divertor plasma. We have estimated the release conditions of the spherical dust particles from the plasma-facing wall without the gravitational effect, where the threshold wall potential and the critical dust radius were discussed. In this analysis, the effects of the gravitational force directed toward or from the wall are discussed.

In Fig. 2, the critical dust radii normalized by the Debye radius are shown as a function of the wall potential ϕ_w for the case of hydrogen plasma, where the threshold wall potential $-e\,\phi_w^{th} / T_e$ is 1.40. The parameter δ_{gg} in Fig.2 indicates the effect of the gravitational force

$$\delta_{gg} \equiv \frac{\rho_d (g/cc)}{n_{se,19}\sqrt{n_{se,19}\,T_e(eV)}},$$

where $n_{se,19}$ is the plasma density at the sheath edge in the unit of 10^{19} m^{-3}. Here δ_{gg} = 0 corresponds to the dust particle on the vertical wall. The smaller dusts than the critical radius can be released. The larger the gravitational effect becomes, the smaller the released region becomes. In the case of the carbon dust in a plasma with high

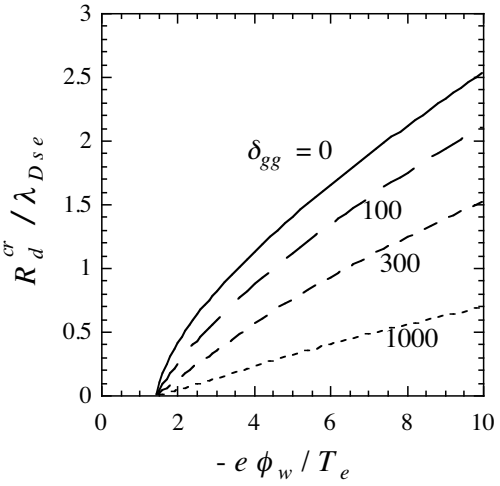

Fig.2 Critical dust radius as a function of the normalized wall potential for the gravitational parameter δ_{gg} = 0, 100, 300, and 1000, where the threshold wall potential $-e\,\phi_w^{th} / T_e$ is 1.40. The smaller dust than the critical one can release from the wall.

density 10^{18} m^{-3} and T_e = 10 eV, which corresponds to a divertor plasma in fusion devices, the gravitational parameter as low as 20. On the other hand, the low density plasma 10^{16} m^{-3} with T_e = 3 eV increases the gravitational parameter up to 10^4, where the released particle is quite rare.

The gravitational directed force from the wall easily releases the dust particle from the wall. The particle is released even if the wall potential is shallower than the threshold (Fig.3. (*a*) with δ_{gg} = 100 and the same parameters as in Fig.2). In Fig.3 the dust particle in the shaded regions can be released. The released region in the deeper potential and the smaller radius corresponds to that of the gravitational force directed toward the wall. At the released dust region in the shallower wall potential, where the repulsive electrostatic force is very weak, the gravitational force make the dust particle release. The larger gravitational effect expands the released dust region in the shallower potential and merges it into the released dust region in the deeper potential (Fig.3(*b*) with δ_{gg} = 159.6). The still more large gravitational effect with δ_{gg} = 300 makes the two released regions overlap. A dominant force divides the domain in Fig.3 into four parts. In the shallower potential and the larger dust region, the gravitational force, which is proportional to R_d^3, is dominant. The strong electrostatic force releases the dust from the wall in the deeper potential and the smaller dust particle, because the electrostatic force is proportional to R_d^2. In the pinned dust region with the deeper wall potential and the larger dust particle, the Coulomb scattering force pushes the dust toward the wall, which is proportional to R_d^4. On the other hand in the shallower potential with the smaller dust, the ion drag force due to absorption of ions by the dust is larger than the other forces. These results show adjusting the plasma parameters such as plasma density and temperature as well as biasing the wall potential controls the size of the released dust particle.

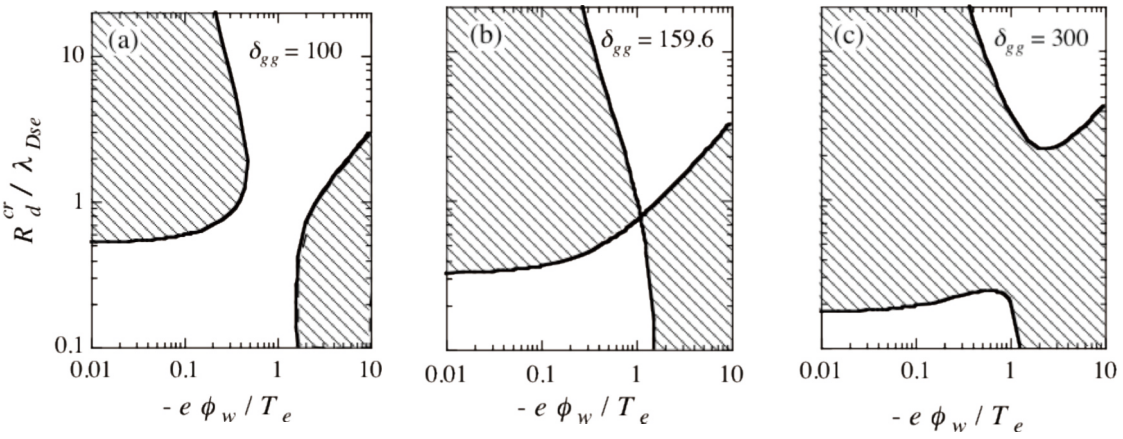

Fig.3 The critical radius as a function of the wall potential for the cases δ_{gg} = 100 (a), 159.6 (b), and 300 (c) with the same parameters as in Fig.2. A dust particle in the shaded regions can be released.

We investigated the effect of the gravitational force on release conditions of the spherical dust particle on the plasma-facing wall. For release of the dust, when the gravitational force is directed toward the wall, the strong enough electric field is required and there exists the threshold wall potential, which does not depend on the macroscopic plasma quantities, but the shape of the dust.

At the wall potential deeper than the threshold, we found the existence of the critical dust radius for release, where the smaller dust than the critical one is released by the repulsive electrostatic force and the ion drag force due to the Coulomb scattering pushes the larger dust particle toward the wall. In the case of the gravitational force directed from the wall, the gravitational force releases the dust particle even if the wall potential is shallower than the threshold wall potential. From these results it was clarified that we can control the size of the released dust particle by adjusting the plasma quantities such as plasma density and temperature as well as the wall potential. If the released dust is as large as the order of the Debye length, the multi dimensional study by using the computer simulation is necessary to investigate the release conditions of the dust particle. These results are useful to investigate the dynamic phenomena of the dust particle in the divertor and SOL plasmas as well as the core plasma in fusion devices.

References

[1] R. Hiwatari, A. Hatayama, S. Zhu and Y. Tomita, Plasma Science and Technology, Vol. 11, No.4, Aug (2009) 389 - 393.

[2] Y. Tomita, R. Smirnov, S. Zhu, Plasma Science and Technology, Vol.8, No.1, (2006) 122-124.

Understanding for multi-scale interaction of fusion plasmas and future collaboration

Y. Kishimoto
Graduate School of Energy Science, Kyoto Universuty

Abstract

One of the most important outcomes in the last decade in theory and simulation of Japan-China Core University Program (CUP) is an exploration of the understandings of multi-scale interaction among different scale fluctuations and the impact on the dynamics and structure in turbulent transport in magnetically confined fusion plasmas. We have systematically studied various kinds of interaction dynamics, e.g. the effect of large scale vortex flows due to the MHD event, the effect of magnetic island on the micro-turbulence, etc., and identified energy transfer channel. These studies have led to an important physical background for providing new control methodologies using internal and/or intrinsic mechanism in realizing high performance plasmas.

1. Introduction

Over 10 years (2001-2010), we have had very excellent and productive collaborations between China and Japan based of theory and simulation of turbulent transport and MHD via items 30A and 30B. It has been well known that fusion plasmas is generally subject to various kind of instabilities and fluctuations at differing spatio-temporal scales due to varied magnetic configuration as shown in Fig.1[1]. Micro-scale fluctuations ranging from ion to electron gyro-radius cause turbulent transport and deteriorate the plasma confinement performance and those of macro-scale in device size, i.e. magneto-hydrodynamics modes, sometimes lead to unexpected sudden termination of plasma discharge referred to as disruption. Besides fluctuations originated from linear free energy sources such as pressure and current gradients, the importance of nonlinear driven secondary modes such as zonal

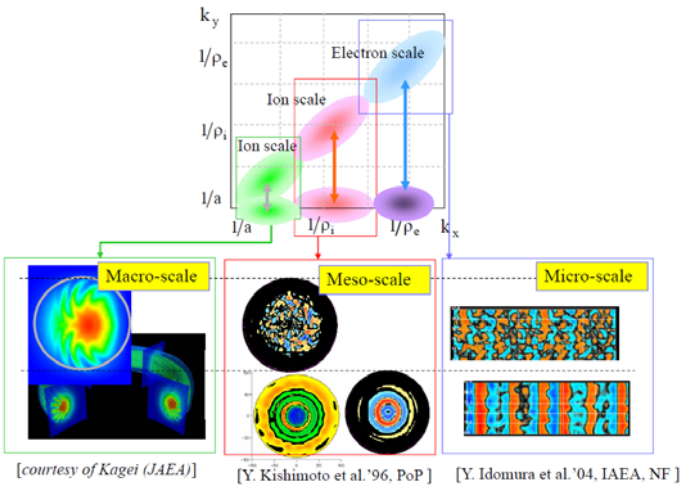

Fig.1 Distribution of fluctuation in radial and poloidal wave number space. Typical structures of fluctuation, MHD internal kink-ballooning mode, ITG mode, and ETG mode.

modes (zonal flows, fields and pressures), which free energy is originated from those already developed fluctuations, has been recognized. Specifically, zonal flows have been extensively investigated since they regulate the turbulence suppressing the maternal turbulence and then improving confinement [2]. It is noticed that not only ITG and ETG types of micro-turbulence but also large scale MHD modes can lead to the generation of global scale zonal flows once non-ideal MHD effect, e.g. two fluid effect, is taken into account. [3] Motivated by these nonlinear paradigm related to secondary instability, we have extended the idea to more general cases including cross scale interaction and/or coupling among different fluctuations as also shown in Fig.1 [4].

2. Effect of large scale vortex flows (VFs) on micro-turbulence [5,6]

As an example of the multi-scale interaction, we here investigate the roles of the vortex flows (VFs) in the evolution of microturbulence by imposing an external VF into the ion temperature gradient (ITG) driven turbulence system for transparence and simplicity. It is found that via 2D flow-shearing effect the VFs can dramatically suppress microturbulence even with weak flow-shearing, which is qualitatively different from the usual mean flows that destabilize microturbulence with weak flow-shearing. The mechanism is identified as the multiplied effect of both radial and poloidal mode couplings. Moreover, an oscillatory zonal flow (ZF) is shown to form through interaction between VFs and microturbulence. The result can be applied to various turbulence studies of plasma and fluid physics.

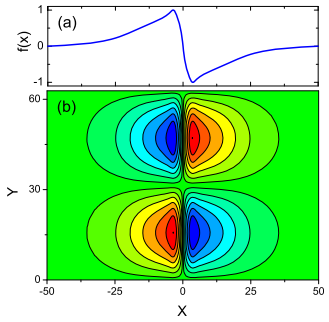

Fig.2 The radial profile (a) and structure contour (b) of VF.

A stationary large scale VF may be represented with the stream function,

$$\phi_T = \phi_{TX}(x)\sin(k_T y) = \phi_m f(x)\sin(k_T y),$$

where $f(x)$ and k_T are the normalized radial profile and poloidal wave number. The representative structure of a VF with two vortices on each side of the rational surface is shown in Fig. 2. Two extreme cases include the MFs with $\phi_T = \phi_m f(x)$ and the streamer-like flows (SFs) with $\phi_T = \phi_m \sin(k_T y)$. The VFs may then be understood as a multiplied combination of these two anisotropic structures. The

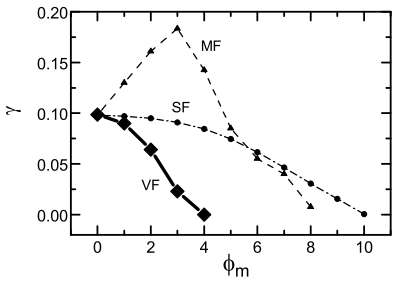

Fig.3 Growth rate γ of linear ITG mode in 2D simulations versus magnitude ϕ_m of VF (with diamonds), MF (with triangles), and SF (with dots).

nonlinear electrostatic gyrofluid model in a slab geometry is adopted The nonlinear equations extended from usual turbulence model are employed to simulate the time evolution of ITG perturbations in presence of the VFs.

To examine the stabilizing role of VFs, Fig. 3 plots the linear ITG growth rate γ in presence of VFs, MFs, and SFs for comparison. It is observed that γ dramatically decreases with increasing the VF amplitude, showing a strong stabilizing effect. This prominent effect is distinct from that of usual MFs, especially with weak flow-shearing. Guided by the linear stabilization by the VFs, three-dimensional (3D) nonlinear simulations are performed to study their role in suppressing turbulence. ZFs are known to interact with microturbulence.

ZFs are generated nonlinearly through the Reynolds stress and play an important role in reducing transport. In the present equation framework, the ZF is not only driven by ITG turbulence, but also produced through the coupling between ITG and VFs. Fig. 4(a) plots the radial profiles of $\chi_i(x)$ in the 3D ZF-included simulations. Besides the transport reduction by robust ZFs, the suppression role of VFs is still clearly exhibited locally in the region with strong radial flow-shearing. Most interestingly, different transport events associated with the ZF dynamics take place. It is noticed that the transport profile may be divided into three regions according to the level as marked in Fig.4(a). The central region (I) with strong radial flow-shearing displays a transport reduction by the VFs. The ZF is weak locally due to the suppressed turbulence by the VFs. However, the transport level in the regions (II) with weak radial flow-shearing is higher than that in the regions (III) with almost no radial flow-shearing ($\phi_T \approx 0$). It is found that the ZFs become oscillatory mainly in the regions (II), as shown in Fig. 4(b) by the time history of the ZFs in the quasisteady state.

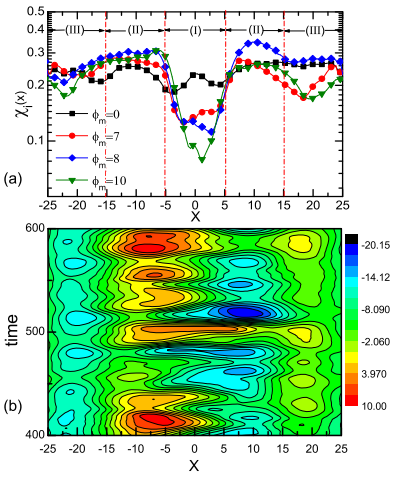

Fig.4 (a) Radial profile of conductivity $\chi_i(x)$ in 3D ZF-included simulations in presence of VFs. (b) Time evolution of ZF profile, $\phi_m = 10$.

The ZF frequency is estimated to be approximately the same as that of $k_y = 0.1$ ITG component as plotted in Fig.5. The oscillatory ZF component is identified to originate from the interaction between VFs and ITG fluctuations as expressed in the ZF equation

$$\partial_t \nabla_\perp^2 \tilde{\phi}_{0,0} = [\tilde{\phi}, \nabla_\perp^2 \tilde{\phi}]_{0,0} + [\phi_{TX}, \nabla_\perp^2 \tilde{\phi}_{k_y=0.1}]_{0,0} + \mu_\perp \nabla_\perp^4 \tilde{\phi}_{0,0}$$

Besides a low frequency ω_{q1} part driven by the Reynolds stress $[\tilde{\phi},\nabla_{\perp}^{2}\tilde{\phi}]_{0,0}$ as usual, another frequency of ZFs ω_{q2} is created via the term $[\phi_{TX},\nabla_{\perp}^{2}\tilde{\phi}_{k_y=0.1}]_{0,0}$ that satisfies the frequency matching relation $\omega_{q2}=\omega_{TX}+\omega_{k_y=0.1}$. Here $\omega_{TX}=0$ has been assumed for stationary VFs so that the ZF frequency is consistently the same as the frequency $\omega_{k_y=0.1}$. Hence the finite frequency of the ZFs reduces their effective suppression role in the regions (II). On the basis of sheared flow suppression, the resultant transport structure in the present simulations is consistent with the characteristics of the internal transport barriers in current tokamak discharges. On the other hand, the results may shed light on the understanding of the multiscale interactions among micro-turbulence, ZFs, and large-scale VFs. In the present simulations, the effect of the VFs on the equilibrium is estimated to be weak since the amplitude of the VFs is in the order of micro-fluctuations. It need be checked self-consistently in a toroidal simulation in the further, though equilibria with large-scale VFs were observed in experiments.

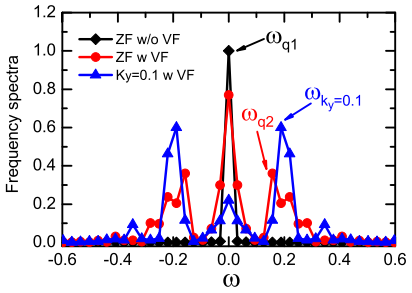

Fig.5. Characteristic frequency spectra of ZF and $k_y=0.1$ ITG component in 3D ZF-included simulations, $\phi_m=10$

We have also investigated the characteristics of ion temperature gradient (ITG) instability in the presence of a magnetic island are investigated numerically using a gyrofluid model [7]. It is shown that when the magnetic island is wide enough to produce a broad distribution of rational surfaces near the O-point region, the ITG perturbations at these rational surfaces will form a radially global-type eigenmode with a fast growth rate, which is referred to as the magnetic-island-induced ion temperature gradient (MITG) mode. Moreover, the magnetic island also causes both radial and poloidal mode couplings, which play a stabilizing role.

3. Effect of magnetic island on micro-turbulence and MITG mode [7]

We have investigated the characteristics of ion temperature gradient (ITG) instability in the presence of a magnetic island are investigated numerically using a gyrofluid model. It is shown that when the magnetic island is wide enough to produce a broad distribution of rational surfaces near the O-point region, the ITG perturbations at these rational surfaces will form a radially global-type eigenmode with a fast growth rate, which is referred to as the magnetic-island-induced ion temperature gradient (MITG) mode. The mode structure is shown in Fig. 6. Moreover, the magnetic island also causes both radial and poloidal mode couplings, which play a stabilizing role. The result in this work can still provide the most fundamental insight into the physical

mechanisms presented, though the initial pressure profile with respect to the magnetic flux surfaces is not treated self-consistently. It has been tested using a self-consistent 5-field gyrofluid model that when the island width exceeds a critical value in the quasisteady state, all harmonics begin to grow exponentially again with a faster growth rate than the linear one. It confirms the unique features of the MITG mode for a wide magnetic island convincingly. Detailed results of such a self-consistent nonlinear simulation will be presented in the near future. On the other hand, the quasilinear modification of plasma profiles for a larger magnetic island ought to be considered, which is beyond the scope of the present model. In addition, it has already been checked in the gyrofluid simulation that the enhanced Landau damping due to the magnetic island leads to a minor (up to ~10%) reduction of the growth rate of the MITG mode for a wide island. Nevertheless, it does not change the characteristics of the MITG mode and the understanding of the physical mechanisms reported.

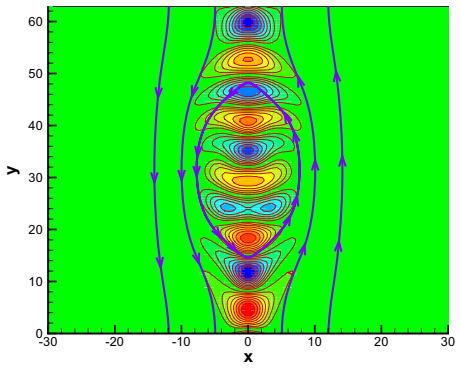

Fig.6. Typical contours of linear potential perturbations in the presence of the magnetic island with $w = 19\rho_i$ when $\eta_i = 4.2$. The thick stream-lines with arrows represent the magnetic field lines.

4. Multi-scale multi-mode MHD and micro-turbulence in magnetic fusion plasmas [8,9,10]

We have performed direct numerical simulations of multi-scale multi-mode MHD and micro-turbulence at ion gyro-radius scale are performed based on gyrofluid model. We focus on the nonlinear evolution of both MHD magnetic island and micro-turbulence in a dynamically interacting system involving all zonal mode components. Here we report the progress on the understanding of nonlinear interaction mechanism with two remarkable findings: (1) A novel short wavelength ITG instability induced by a MHD magnetic island as a consequence of the breakdown of the frozen-in law. The new instability is identified to be characterized by a substantially lower stability threshold and a global structure propagating in the ion diamagnetic drift direction. (2) A magnetic island seesaw oscillation due to the interaction with micro-turbulence. A minimal model is proposed to numerically illustrate the seesaw mechanism. It is identified that fluctuating electromagnetic (EM) torque due to the polarization current produced by the coupling with micro-turbulence may drive the island seesaw in the case with full reconnection. Such mechanisms offer new insights in understanding complex nonlinear interaction among multi-scale multi-mode fluctuations in fusion plasmas.

Conclusions

As can be imagined from Fig.1, a large amount of rich phenomena ascribed to such cross scale couplings can be expected, which may significantly increase a freedom for the control of the fusion plasma in achieving better confinement. For instance, the active excitation of fluctuations of a scale might lead to the suppression of those another scales. In order to explore the paradigm of such cross scale coupling, we have investigated the interaction dynamics based on two approaches. One is the element based approach to identify the mechanism, specifically energy transfer channel, of cross scale coupling. Here we have investigated the effect of large scale vortex flows and also magnetic island[7], which are assumed to be generated from large scale MHD events and/or long wavelength secondary instabilities, on meso-scale ITG turbulence. The other is a full interaction simulation covering two scale fluctuations, i.e. macro-scale MHD/tearing mode and meso-scale ITG mode self-consistently, based on gyro-fluid modeling. Here, we have found that various types of mode coupling among different scale fluctuations and associated constraints play an important role in regulating the interaction dynamics.

Acknowledgements

In summarizing the 10 years history of Japan-China Core University Program, I would like to greatly appreciate Prof.Ding Li, Prof. H. Sanuki, Prof. J.Q. Dong who have led the theory and computation projects (30A and 30B) over the last decade. Without their aggressive and intensive encouragements and supports, the program had not reached the great success. I also thank to my colleagues Prof. Zhe Gao, Prof. S. Wang, J.Q. Li who had provided significant contribution for arranging the program. Finally, I would like to deeply acknowledge to Prof. Toi and Prof. Komori for supporting our theoretical and computational activity in this program.

References

[1] E.J. Doyle, et al., Y. Kishimoto, et al., Nucl. Fusion 47(6), S18 (2007)

[2] L. Chen, Z. Lin and R. White, Phys. Plasmas 7, 3129(2000)

[3] T. Matsumoto, H. Naitou, S. Tokuda and Y. Kishimoto, Phys. Plasmas **12**, 092505 (2005)

[4] J.Q. Li and Y. Kishimoto, Phys. Plasmas 15, 112504 (2008)

[5] Z. X. Wang, J. Q. Li, J. Q. Dong, and Y. Kishimoto, Phys. Rev. Lett. 103, 015004 (2009)

[6] Z. X. Wang, J. Q. Li, J. Q. Dong, and Y. Kishimoto, Phys. Plasmas 18, 012110(2011)

[7] Z. X. Wang, J. Q. Li, Y. Kishimoto, and J. Q. Dong, Phys. Plasmas 16, 060703 (2009)

[8] J Q Li, Y Kishimoto, N Miyato, K Miki, J Anderson and B R Shi, Journal of Physics: Conference Series 123, 012027 (2008)

[9] J.Q. Li, Y. Kishimoto, Y. Kouduki, Z.X. Wang and M. Janvier, Nucl. Fusion 49, 095007 (2009),
[10] J.Q. Li, Y. Kishimoto, and Z. X. Wang, THC/P4-16, 23rd IAEA Fusion Energy Conference (Daejon, Korea)

Some points on rf physics in magnetic fusion plasmas

Zhe Gao (高喆)
Tsinghua University, Beijing 100084, CHINA
gaozhe@tsinghua.edu.cn

Abstract: Some points on rf physics in fusion plasmas are presented in this report, which may provide collaboration opportunities between the fusion communities in Japan and China in the post-CUP period.

1. Introduction

Rf waves are employed in magnetic fusion devices to heat the plasma, drive the plasma current to non-inductively sustain the confinement, control the profile, and influence MHD activities by localized heating or current drive. Therefore, the rf physics plays a very important role in high performance steady discharge of fusion plasma. Over more than half a century, we knew much about the rf physics and achieved great progress in rf application in fusion plasma. However, frankly speaking, still much about the rf physics is unknown, which prevents the application of rf in ITER and future fusion reactors. The rf physics we mentioned generally concerns the coupling of rf wave to plasma, wave propagation, absorption, and the response of plasma to rf power. However, these processes are closely integrated with the plasma dynamics both in core and in the periphery. [1] Varying with different frequency domains, different problems exists. In this report, we show some examples in ECRF, LHW, ICRF and Alfven wave domain, respectively, and hope to provide future collaboration opportunities between the fusion communities in Japan and China in the post-CUP period.

2. Some examples in different frequency domains

2.1 ECRF

The electron cyclotron wave has On the ECRF, the theory/simulation agrees well with the experiment. However, different collision models employed in the ECH/ECCD code should be considered carefully. For example, ECH/ECCD code was

benchmark under ITER conditions by Prater et al.[2] It was found that, when it is used to off –axis current drive, the difference between codes is little, within 10%. However, when it is used to central current drive, the strong difference appears. This behaviors was thought to be related with momentum conservation or non-conservation. The physics is further related with the steady or unsteady consideration, i.e. the Ohkawa effect is considered or not. In mathematics, the conservation may be lost when the approximation is employed in the collision operators, especially the treatment of relativistic effect. Recently, a group in ASIPP study this problem.[3] It is found that, at the ITER parameter, the weak-relativistic treatment is enough accurate for modeling the ECCD.

2.2 LHW

On the LHW, two processes are mentioned here. One is whether the LHW can contribute to the ITER-like plasma. It is known that the application of LHW is limited the density threshold, which is given the physics of slow wave-fast wave conversion. However, it is unfortunately that the actual operation limit is far lower than this theoretical limit. In recent FTU experiment,[4] the density operation limit increased dramatically through increasing the outer electron temperature, which was believed to attribute to the decrease of spectral broadening through control of parametric instabilities. Another problem arises that the spectral broadening effect was considered to be valuable to increase the amount absorbing power of LHW due to the rare of resonant electron at very high speed. The physics need to be investigated further.

The other case about LHW is what is the physical mechanism of LHW flow drive and whether this flow drive effect is repeatable and controllable. In C-mod experiment, [5] a strong flow was observed accompanying with LHCD. The mechanism of resonant pinch effect is developed [6] to explain this phenomena, where a sensitive dependence on the fine structure of the absorbing spectrum and a close relation to particle transport are given. However, a more quantities theory is still required.

2.3 ICRF

Among many problems about ICRF, the development of the full wave solver is emphasized since the ray tracing assumption is not valid any longer. The TORIC code [7] is widely used to predict the propagation and absorption of ICRF. The AORSA code[8] is developed to remove the limit of finite Larmor radius, but need to solve more huge number of Fourier space modes. Comparison of these two code is performed and a similarity is shown in many case. Fukuyama and his group developed a series of nice full wave solver: TASK/WM, TASK/WF [9], which may help to advance the understanding of ICRF physics.

The success of all these ICRF-based heating and plasma control techniques depends on the efficiency with which the high power electromagnetic waves can be coupled into the plasma from an external launching structure that is inserted into the plasma vessel. Uncertain issues to affect the coupling exist. The most possible candidate is the rf sheath effect.[10] Due to the change of boundary condition from metal to rf sheath, a series of bounded eigenmode is generated with typical global dispersion relation and structure. Then, the coupling of wave is strongly influenced. On this issue, there are still too many problems to be solved.

2.4 Alfven wave

Alfven wave was considered as an attractive mechanism of driving plasma current because of its potential high efficiency, no density limit and the convenience of high power RF generating and launching. However, electron trapping may dramatically reduce the current drive efficiency in the subthermal resonant regime. Although the scheme of increasing the drive efficiency by helicity injection has been considered for decades, this nonresonant current drive may be overestimated. We [11] examine the collisionless nonresonant force by low frequency wave and found that the collisionless nonresonant force from quasi-linear electromagnetic terms is cancelled by the nonlinear kinetic pressure force, and then, in collisionless plasmas, all the ponderomotive forces by low frequency waves are depending on the Landau resonant absorbing. Therefore, the current drive efficiency is strongly influenced by the

behaviors of trapped electrons in the low frequency wave field, i.e., the pinch effect and the enhancement of the bootstrap current.

For the sake of clarifying the physics involved, a research program on Alfven wave current drive is ongoing at the SUNIST spherical tokamak (R/a=0.30m/0.23m). The Alfven wave antenna system is designed [12] and installed, which consists of four models in toroidal direction and two antenna straps in poloidal direction for each module. Preliminary experiment was performed. It is shown the impedance of antenna agrees with the MHD calculation.

3. Summary

Rf physics plays a very important role in high performance steady discharge of fusion plasma. Through more than half a century, we knew much about it, but, frankly speaking, still much unknown. Japan has a solid study on this topic both in experiments and in theory/simulation. China also has a big project on the rf power system equipment and the rf physics as well. There should be many collaboration opportunities in the rf physics between the fusion communities in Japan and China.

Acknowledgement

This work is supported by the NSFC, under Grant No. 10990214, the Major State Basic Research Development Program of China, under Grant Nos. 2009GB105002 and 2008GB717804, and the JSPS-CAS Core University Program in 'Plasma and Nuclear Fusion'. The author would like to thank Prof. Sanuki and many staffs at NIFS for the kindly help and discussion during his stay in NIFS. Also thanks to Prof. Kishimoto, Prof. Tomita, Prof. LI Jiquan and other colleagues for the kindly hospitality and extensive discussion not only on physics but also on the collaboration arrangement

Reference:

[1] D A Batchelor, et al., Plasma Sc. Tech. 9, 312 (2007)

[2]R. Prater, et al., Nucl. Fusion 48, 035006 (2008)

[3] Y. J. Hu, Y. M. Hu, and Y. R. Lin-Liu, Phys. Plasma 18, 022504 (2011)

[4] R. Cesario, et al., Nature Commun. 1, 55 (2010)

[5] A. Ince-Cushman et al., Phys. Rev. Lett. 102, 035002 (2009). J. E. Rice et al Nucl. Fusion 49 025004 (2009)

[6] Z. Gao, S.J.Wang, H. Qin and N.J. Fisch, IAEA FEC2010 TH-W/P4-2

[7] M Brambilla, Plasma Phys. Control. Fusion 41, 1 (1999)

[8] E, F.Jaeger, et al, Physics of plasmas 9, 1973 (2002)

[9] A. Fukuyama, China- Japan CUP seminar on Modeling of Theory and Simulation of Fusion Plasmas, August 30-Sepetember 2, 2010 Beijing, CHINA

[10] J. R. Myra et al., Phys. Plasmas 11, 1786 (2004).

[11] Z. Gao, N. J. Fisch, and H Qin, Phys. Plasmas **13**, 112307 (2006), Z. Gao, N. J. Fisch, H. Qin and J. R. Myra, Physics of Plasmas 14, 084502 (2007).

[12] Y. Tan, Z. Gao and Y. X. He, Fusion Eng. Design 84, 2064 (2009)

Future Collaboration Researches on Peripheral Plasmas

Tomita Yukihiro (冨田幸博)
National Institute for Fusion Science, 322-6 Oroshi-cho, Toki 509-5292 Japan
tomita@nifs.ac.jp

1. Introduction

The following subjects are proposed for our future collaboration researches

1. Analysis on operation space by using CSD (Core-SOL Divertor) model in HL-2A (SWIP) tokamak
2. Researches of dust dynamics in plasma
   2.1 Interaction between dust and PFW (ASIPP)
   2.2 Dust characteristics in HL-2A plasma (SWIP)
3. Impurity transport study near PFW (Plasma-Facing Wall)
   3.1 PWI (Plasma Wall Interaction) study by using tungsten marker-tile (ASIPP)
   3.2 Impurity transport and redeposition on first mirror (SWIP)

2. Future collaboration researches

2.1 Analysis on operation space by using CSD (Core-SOL Divertor) model in HL-2A (SWIP) tokamak: R. Hiwatari (CRIEPI), A. Hatayama (Keio Univ.), Y. Tomita (NIFS),
T. Takizuka (JAEA), Zhu Ting-Ru, Tang Chang-Jian (Sichuan Univ.)
and Peng Xiao-Dong (SWIP)

The objectives of this collaboration research is to investigate the influences of impurity seeding, gas puffing and bootstrap current on the overall operation features in HL-2A tokamak.

In the Fig.1 the shaded region indicates the possible operation region for the LHCD operation in HL-2A. The boundaries come from the several constraints. The maximum of the heat flux is limited by the heat flux in the divertor range. Available current drive power is a key factor for the maximum of the particle flux and the minimum of is closely linked to the divertor heat load. Based on these ideas, we discuss the influence of several important factors for the operation of tokamak plasma. We investigate the effect of impurity seeding in the SOL-divertor region for the overall operation of tokamak plasma in the qualitative sense. The figure 2 shows the change of heat flux in the divertor range when we increase the impurity radiation loss fraction and the value of is taken as 0.3, 0.5, 0.6. We obtained the result of the increase of operation space when the impurity seeding.

In this collaboration research, we apply the ITER scaling. In future we have to confirm the several scaling from the experiments in the HL-2A.

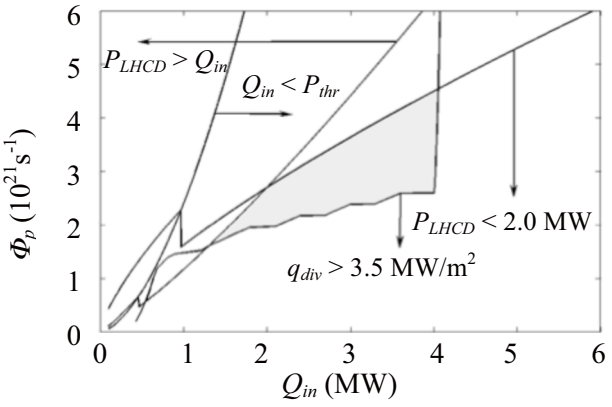

Fig.1 Operational space (shaded region) of LHCD operation under the constraints.

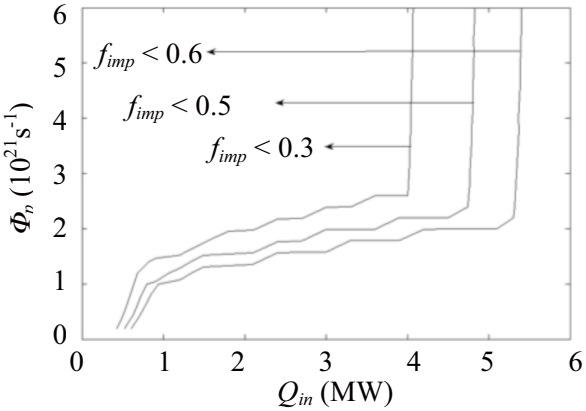

Fig.2 Operational space of LHCD operation and dependence on the fraction of impurity fraction f_{imp} = 0.3, 0.5 and 0.6 in HL-2A tokamak.

2.2 Researches of dust dynamics in plasma

2.2.1 Interaction between dust and PFW (ASIPP): Y. Tomita, N. Ashikawa (NIFS), M. Nagata (Univ. Hyogo), LUO Guangnan, HONG Rongjie (ASIPP)

In ASIPP there is an experimental plan to investigate the interaction between a dust particle with high speed and the plasma-facing wall. In order to carry out the experiment, we have to consider the acceleration of the dust particle to several hundreds m/sec. One of the ways to do this is the Magneto-Plasma-Dynamic Arcjet (MPDA). At first we investigated the acceleration of a dust in simplified plasma. In Fig.3 the orbits of the tungsten dust particle are sown, where cylindrical plasma exists to the *z* direction with the Gaussian distribution of the FWHM of 20 cm. The plasma density, electron temperature and ion temperature at the center are 10^{18} m^{-3}, 10 eV and 3 eV, respectively. The plasma ion flow directs to axial direction with the local ion sound speed. The dust particles are dropped down from the height of 50 cm without the initial speed.

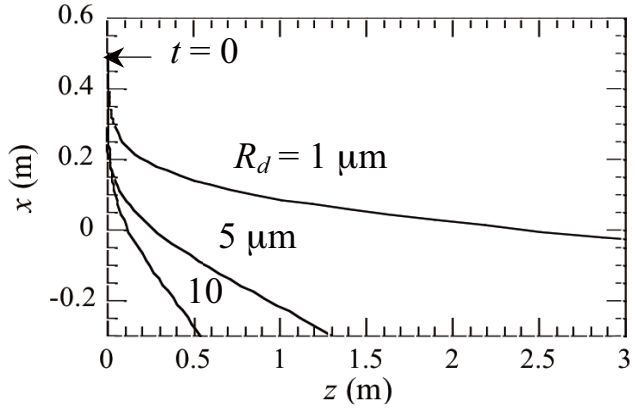

Fig.3 Orbits of dust particles in cylindrical plasma. Tungsten dust particles with the size of 1 μm, 5μm and 10 μm are dropped from the upper position of 50 cm.

The dust particle is accelerated to the axial direction due to the friction forces of plasma ions, which consists of the friction force due to the absorption of plasma ions and that due to the Coulomb scattering of ions. The smaller dust particle is accelerated along the plasma. On the other hand the larger dust particle falls down due to the gravity. The smaller dust with 1 μm radius is accelerated up to 100 m/sec during around 40 msec. The larger dust of 10 μm is accelerated to 5 m/sec.
We will continue the collaboration research to confirm the acceleration method of the few hundreds m/sec.

2.2.2 Dust characteristics in HL-2A plasma (SWIP) : Y. Tomita, N. Ashikawa (NIFS), PAN Yudong, HUANG Zhihui and YAN Longwen (SWIP)

We have been studied the dust dynamics in the SOL divertor plasma in HL-2A. Near future there is an experimental plan of the dust injection in SWIP in order to investigate the dust characteristics: dust charging and dynamics in fusion plasma. During the collaboration researches the fundamental characteristics of charging of a dust particle and its dynamics in SOL/divertor plasma in tokamaks are studied. We found that according to the OML (Orbit Motion Limited) theory, the charging time is so fast (~ nanoseconds) compared to the dynamics process of the dust particle in SOL/divertor plasma (~milliseconds), which means the equilibrium charge state is enough as the local charge state. It was clarified that the equilibrium charge $Z_{d,eq}$ is determined by the form as $Z_{d,eq} / R_d T_e$, which is a function of the normalized relative speed of plasma ion flow to the velocity of the dust particle and the plasma temperature ratio. After the investigation of the dominant forces on the dust particle, the friction forces due to the plasma ion absorption and ion Coulomb scattering are the same order for the low relative speed. The critical radius of a dust particle, where the gravity is

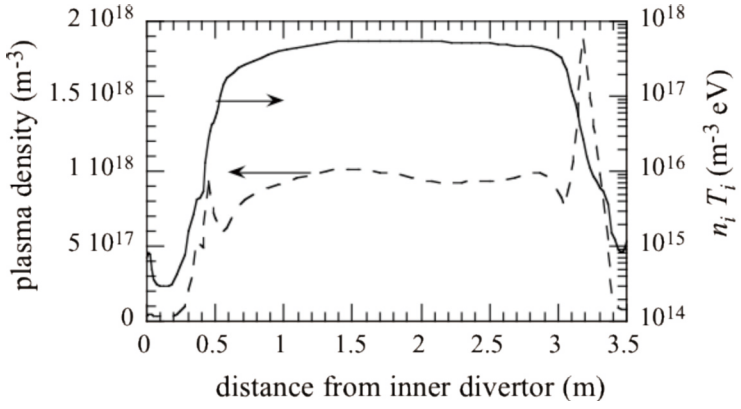

Fig. 4 The spatial distribution of plasma density and ion pressure along the poloidal direction as a function the distance from the inner divertor to the outer one.

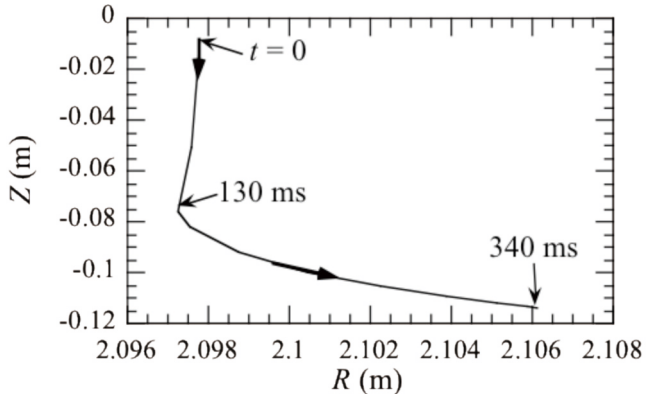

Fig. 5 The orbit of carbon dust particle with 10 μm, where the injection position is on the mid plane of the low field side.

larger than the friction forces due to plasma ions, is obtained. The model of the dust charging and the dynamics in fusion plasmas is applied to the HL-2A plasma. The background plasma parameters in the SOL/divertor region of the HL-2A tokamak, necessary for the dynamics study of the dust particle, is given by the B2-EIRENE code with the single null configuration. In Fig. 4 the typical plasma density and the ion pressure are shown along the poloidal direction in the SOL region, where the heat flow from the core region to the SOL region is 500 kW and the density at the core region is 10^{18} m^{-3}. The orbit of the carbon dust with 10 μm without the initial speed is shown in Fig. 5. At the initial phase the dust particle fallen down due to the gravity and during the falling down it is accelerated to the toroidal direction due to the friction force of absorption of plasma ions and the Coulomb force. The speed of the toroidal direction produces the centrifugal force outward. Then it moves out the plasma region. In order to investigate the characteristics in SOL divertor plasma the dust particle has to be accelerated initially. During the collaboration research the optimization of the experiment, i.e. dust size, injection position, initial dust speed and the diagnostics of dust dynamics, is studied.

2.3 Impurity transport study near PFW (Plasma-Facing Wall)

2.3.1 PWI (Plasma Wall Interaction) study by using tungsten marker-tile (ASIPP) :

G. Kawamura, Y. Tomita (NIFS), LUO Guangnan, XU Qian, DING Lui, WU Jing (ASIPP)

The objective of this collaboration research is to investigate damage of the tungsten PFW and impurity transport/redeposition near PFW in the EAST tokamak. The SiC and tungsten marker tiles have already installed in EAST in order study the impurity transport. So far in NIFS simulation model for impurity transport in LHD divertor region by ERO (erosion and redeposition) code is developed. On the other hand in ASIPP the ERO and EDDY codes are used to analyze the impurity transport. The target of this collaboration research is to develop simulation model and perform benchmark test between the ERO and EDDY codes for erosion and W transport.

2.3.2 Impurity transport and redeposition on first mirror (SWIP):

G. Kawamura, Y. Tomita (NIFS), ZHOU Yan, YAN Longwen (SWIP)

The objective of this collaboration research is to investigate the reason of the reduction of reflectivity of the first mirror on center conductor due to the impurity redeposition. Here the ERO code is applied to study the impurity transport during the glow discharge cleaning and the main discharge. In future the method to prevent the impurity redeposition might be developed.

Invitation to collaboration on the development of HTS magnet technology for fusion reactors

Nagato Yanagi
National Institute for Fusion Science, Toki, Gifu, 509-5292 Japan
E-mail: yanagi@LHD.nifs.ac.jp

Abstract

Feasibility studies on applying high-temperature superconductors (HTS) to fusion reactor magnets are being carried out. In the conceptual design of the heliotron-type fusion reactor FFHR, the HTS is a counter option to the presently well developed low-temperature superconducting (LTS) magnet technology. The HTS shows potentials of providing a number of benefits, such as the elevated temperature operations for securing high stability and low refrigeration power as well as the possibility that large coils could be constructed by jointing the segments. However, there are many engineering issues to be solved for developing large-current capacity conductors and the winding technology. In this respect, we consider that the development of HTS magnet technology could be a good international collaboration in the near future, especially among Asian countries.

Keywords : heliotron, FFHR, high-temperature superconductor, segmented fabrication

1. Introduction

The technology for fabricating large-scale superconducting magnets of fusion experimental devices using Low-Temperature Superconductors (LTS), represented by Nb_3Sn and NbTi, has been well established through the extensive R&D programs for the ITER project. It should be also reminded that the constructions of many existing and under-construction devices, such as LHD, EAST, KSTAR, SST-1, W7-X, JT-60SA and former devices, have contributed profoundly on the development of related technologies, especially with force-cooled cable-in-conduit conductors (CICC). However, if we consider the future extension of the superconducting magnet technology to construct DEMO reactors and to realize the proliferation of commercial fusion power plants, High-Temperature Superconductors (HTS), represented by Ytrium-based coated-conductors, should be regarded as a good counter option to LTS due to the following reasons:

(1) Higher cryogenic stability at elevated temperature operation (> 20 K)
(2) Higher current density in the winding package
(3) Higher mechanical strength of the winding package (due to the substrates of YBCO tapes and thicker conductor jackets)
(4) Lower refrigeration power at elevated temperature operation
(5) No need of liquid helium (useful in the preservation of helium resources)
(6) Simpler cooling system with refrigerators and coils
(7) Possibility for fabricating big and continuous coils with segments and joints
(8) Possibility for carrying out cold tests of conductors and/or coils at 77 K
(9) Future decrease of cost by mass production of HTS wires for electrical applications

According to these advantages, the HTS option has already been investigated in the conceptual design studies for some fusion demos, despite the well-recognized disadvantages, such as the immature technology for producing long-length wires, higher cost at present, and difficulty for making transposition of wires. A recent example of the HTS option for the conceptual design studies of fusion magnets is seen in the LHD-type fusion reactor FFHR. In this paper, the present status about the HTS design option for FFHR is described. A proposal is also given for future international collaborations about the development of HTS magnet technology.

2. HTS option for the FFHR magnet system

Based on the steadfast progress of high-density and high-temperature plasma experiments in the Large Helical Device (LHD) [1, 2], the conceptual design studies on the heliotron-type fusion energy reactor FFHR are being conducted on both physics and engineering issues [3]. For FFHR, a heliotron magnetic configuration similar to that of LHD is employed so that the confined plasma is current-free, suitable for steady-state operations and free from disruptions. Though configuration optimization is still being pursued, the present design for a commercial reactor, FFHR-2m2, gives a major radius of 17 m with a toroidal magnetic field of 5.1 T in order to generate ~3 GW of fusion power. The stored magnetic energy of the superconducting magnet system is ~160 GJ.

One of the most important engineering issues is the selection of superconducting material and cabling method. The primary option for FFHR is to use A15-type low-temperature superconductors (LTS), and Nb_3Al should be a good candidate due to its better resistance to strain compared to Nb_3Sn. For Nb_3Al, cable-in-conduit (CIC) conductors with force-cooling with supercritical helium will be employed, which is regarded as an extension of the ITER technology [4]. Another option with LTS is to incorporate solid-type conductors with aluminum-alloy jacket and the windings are indirectly cooled by cooling panels [5]. For these LTS options, long-length LTS conductors will have to be fabricated, transferred to the site, heat treated and wound using a big winding machine.

On the other hand, high-temperature superconductors (HTS) are considered to be a competitive candidate to be applied for fusion reactors [6-10] based on the recent development of the wire production technology owing to the advantages listed in the Introduction. The present proposal is to employ RE123-based coated-conductors, represented by YBCO [11] and/or GdBCO [12], which are also called the second generation HTS.

Fig. 1(a) shows the present design of the HTS conductor, which is supposed to have a nominal current of 100 kA at the maximum magnetic field of 13 T. The operating temperature is 20 K. The HTS wires are supplied in tape forms and are simply stacked together in a rather thin layer of ~6 mm thickness at the center of the conductor. In this case, the bending strain is limited to be 0.05%, which is one order of magnitude smaller than the allowable maximum strain for HTS tapes [13]. Good mechanical properties are secured also by using a stainless-steel jacket. The present idea is to simply stack a number of tapes, but we may also consider transpositions, such as by employing the Roebel-type conductors [14] to obtain uniform current distribution among tapes and reduce AC losses. We use copper stabilizers to assure the stability and safety in case of a normal-transition.

We here note that a proof-of-principle experiment of HTS conductors have been successfully

carried out using Ag-sheathed Bi-2223 tapes, which showed 10 kA critical current at 8 T and 20 K with a conductor size 12 mm by 7.5 mm [15]. It was also confirmed that the stability margin was about two orders of magnitude higher than that of LTS. We have also achieved even higher critical current with a similar conductor employing YBCO and GdBCO tapes; the details of this experiment will be reported elsewhere.

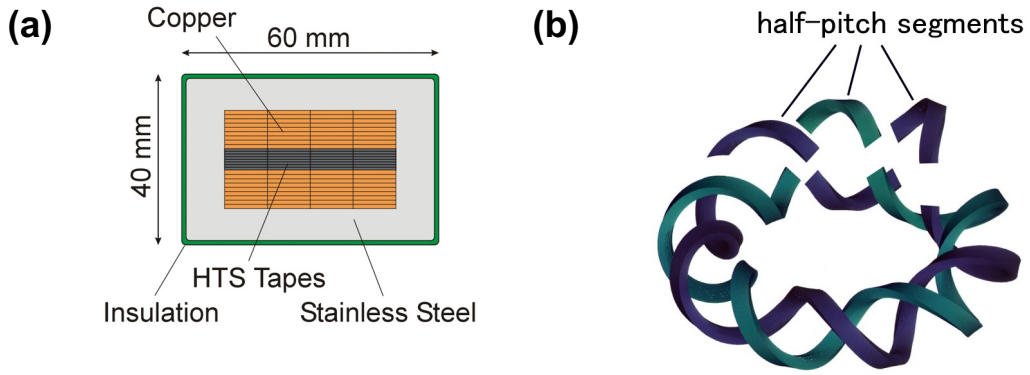

Fig. 1. (a) Design of high-temperature superconductor with 100 kA current capacity and (b) illustrative image of segmented fabrication of the helical coils.

3. Segmented fabrication of helical coils

The present design of the FFHR-2m2 requires a pair of continuous helical coils with a ~40 m diameter. Each helical coil has about 400 turns of windings. The three-dimensional winding process of helical coils with a huge size as FFHR is a difficult task.

In this respect, as an alternative idea to the conventional winding method of continuous conductors, we have proposed a "segmented-type" fabrication [16] based on the idea of "demountable" helical coils [17-19]. The basic concept is illustrated in Fig. 1(b). We first fabricate the half-pitch segments of the helical coils in factories, and they are transferred to the site, assembled and jointed. If this is possible, there would be no need to construct a huge winding machine with a ~40 m diameter. This concept was originally proposed in the 1980's by K. Uo (the founder of the heliotron project) with mechanical joints with NbTi superconductors [17]. Though intense efforts were made by conducting R&D's at that time, it was concluded that the joint resistance was too high to be admitted for the required refrigeration power at 4 K. Then, in 2002, there was a ground breaking proposal by H. Hashizume that the same concept could be realized using HTS at elevated temperature operations. This is because the joule heating generated at joints could be more easily removed using the surplus refrigeration power if the refrigerator was designed to meet the demand of a 4 K magnet system (without joints) [18-19].

4. Segmented fabrication of helical coils with segmented conductors

As discussed in Refs. 17 and 18, helical coils assembled with mechanical joints may have a further possibility that they can be demountable (or "remountable") for maintenance or in case of any failure of the helical coils. However, the difficult issue is how we can make a realistic proposal for making mechanical joints. It seems that some advanced technology is required [19]. In this

connection, we considered that employing the conventional soldering lap joints could be a good alternative to mechanical joints. In this case, we do not include demountability and we may focus only on the construction. However, it seems also very difficult when we try to make a concrete design with lap joints. Note that we have more than 400 turns of conductors in each coil pack and each conductor should be jointed securely and simultaneously. Moreover, another big problem is found in the estimated weight of each half-segment; a crude estimation shows several hundred tons for the FFHR-2m2 design, which is too difficult to be prefabricated in factories and transported to the site. And thus, it seems very difficult to consider this option.

In this respect, we here make a new proposal that instead of jointing half-pitch coil segments, the half-pitch conductor segments could be jointed. Figure 2(a) shows an illustrative image of this method. In this method, the helical coil casing (that installs the windings) should be first assembled by jointing half-pitch segments along the entire torus. And then the pieces of conductors, preformed into helical shapes in factories or on site, would be installed into the casings. We should note that the conductor pieces could also be cold tested in liquid nitrogen prior to the installation, if required. Moreover, there is another advantage that we do not have to produce high-performance HTS wires over a long length. Instead, we need high-performance wires with rather short length, which is easier to be supplied with lower cost.

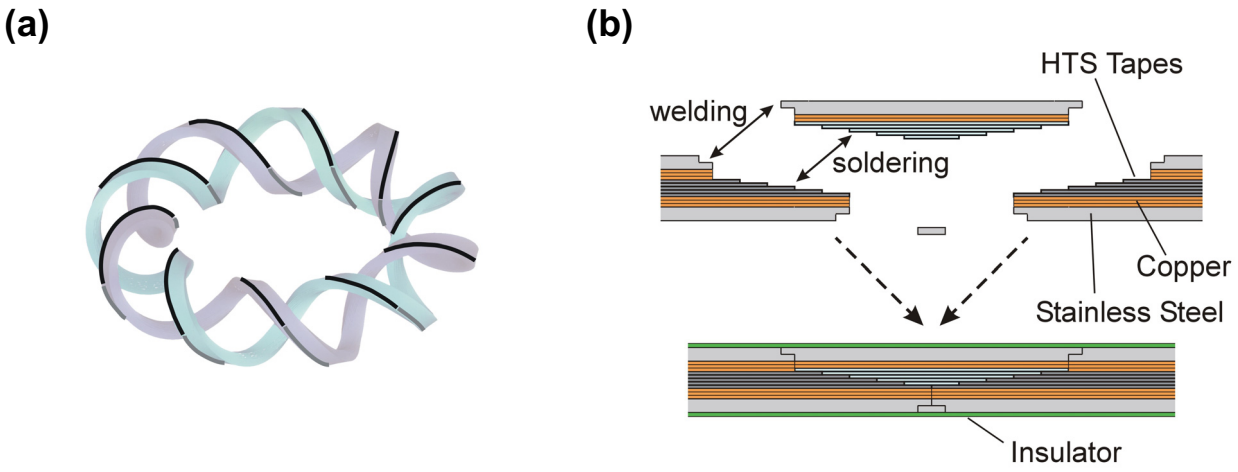

Fig. 2. Illustrative images of (a) segmented fabrication of helical coils with half-pitch conductor segments and (b) jointing method of YBCO conductors.

At the joint locations between half-pitch segments, the HTS conductors are cut in step-like structures, then overlapped and jointed with superconducting sides facing each other so that low-resistance joint can be formed, as shown in Fig. 2(b). We should note that a similar idea of having an intermediate jointing piece for connecting two conductors was incorporated in the LHD helical coils with NbTi superconductors [20]. For the HTS conductors, the stainless steel jacket should also be connected by welding to ensure the mechanical rigidity. The joint resistance was measured for single tapes, and we obtained ~6 nΩ for a 50 mm joint length. Using this value, the overall joint resistance of a 100-kA conductor is expected to be 0.3 nΩ, consisting of 2 connections at one joint location with 100 HTS tapes each having a 50 mm joint length. The entire helical coils

will have ~8000 joints (~400 turns of windings, 10 segments for each coil and 2 coils), and this requires ~1.5 MW increase of the refrigeration power for the entire cooling system operated at 20 K. This is still lower than 10% of the total power and should be accepted rather easily.

5. Invitation to collaboration on the development of HTS magnet technology for fusion reactors

At present, the research activity about the development of HTS magnet technology is still very limited. It needs to be further extended in order to apply the HTS to demo reactors in the near future. At NIFS, we have started discussions about the possible international collaborations for the development of HTS conductors and magnets especially with MIT in US and KIT in Germany. We also consider that this subject could be a good collaboration among Asian countries. We hereby propose a future international collaborative project of constructing and test large-scale HTS model coils having large-current capacity conductors. This could be a new version of the Large Coil Task (LCT) project conducted in 1980's for LTS [21].

6. Summary

The HTS magnet option is being investigated for the conceptual design studies of the heliotron-type fusion energy reactor FFHR. Segmented fabrication of the huge helical coils seems feasible by incorporating a new idea of having segmented conductor pieces and joint them on site. Development of HTS magnet technology could be a good international collaboration in the near future, especially among Asian countries.

Acknowledgements

The authors are grateful to the FFHR group for valuable discussion and support.

References

[1] O. Motojima, A. Komori, H. Yamada et al., "Extended steady-state and high-beta regimes of net-current free heliotron plasmas in the Large Helical Device", Nuclear Fusion, 47, S668 (2007).

[2] A. Komori, H. Yamada, S. Imagawa et al., "Goal and achievements of Large Helical Device project", Fusion Sci. Technol., 58, 1 (2010).

[3] A. Sagara, O. Mitarai, T. Tanaka et al., "Optimization activities on design studies of LHD-type reactor FFHR", Fus. Eng. Des., 83, 1690 (2008).

[4] S. Imagawa, A. Sagara, Y. Kozaki, "Conceptual design of magnets with CIC conductors for LHD-type reactors FFHR2m", Plasma Fus. Res., 3, S1050 (2008).

[5] K. Takahata, T. Mito, H. Tamura, S. Imagwa, A. Sagara, "Conceptual design of an indirect-cooled superconducting magnet for the LHD-type fusion reactor FFHR", Fus. Eng. Des., 82, 1487 (2007).

[6] F. Dahlgren, T. Brown, P. Heitzenroeder, L. Bromberg, ARIES team, "ARIES-AT magnet systems", Fus. Eng. Des., 80, 139 (160) 2006.

[7] P. Komarek, “Potential and desire for HTS application in thermonuclear fusion”, Fus. Eng. Des., 81, 2287 (2006).
[8] W.H. Fietz, S. Fink, R. Heller et al., “High temperature superconductors for the ITER magnets system and beyond”, Fus. Eng. Des., 75, 105 (2005).
[9] L. Bromberg, M. Tekula, L.A. El-Guebaly and R. Miller, “Options for the use of high temperature superconductor in tokamak fusion reactor designs”, Fus. Eng. Des., 54, 167 (2001).
[10] T. Ando, S. Nishio, H. Yoshimura, “Design of the high-Tc superconducting TF coil for the tight aspect ratio Tokamak power reactor (VECTOR)”, IEEE Trans. Appl. Supercond., 14, (1481) 2004.
[11] A. Ibi, H. Fukushima, R. Kuriki et al., “Development of long YBCO coated conductors by IBAD–PLD method”, Physica C, 445-448, 525 (2006).
[12] H. Fukushima, A. Ibi, H. Takahashi et al., “GdBCO and YBCO long coated conductors and coils”, Physica C, 463-465, 501 (2007).
[13] R. Champailler, N. Yanagi, G. Bansal et al., “Experiments of bending strain on reduced-scale HTS conductors for fusion energy reactors”, IEEE Trans. Appl. Supercond., 20, 1565 (2010).
[14] W Goldacker, A. Frank, A. Kudymow et al., “Status of high transport current ROEBEL assembled coated conductor cables”, Supercond. Sci. Technol., 22, 034003 (2009).
[15] G. Bansal, N. Yanagi, T. Hemmi, K. Takahata, T. Mito, “Experimental Results of Large-Current Capacity HTS Conductors”, IEEE Trans. Appl. Supercond., 18, 1151 (2008).
[16] G. Bansal, N. Yanagi, T. Hemmi, K. Takahata, T. Mito, A. Sagara, “High-temperature superconducting coil option for the LHD-type fusion energy reactor FFHR”, Plasma Fus. Res., 3, S1049 (2008).
[17] K. Uo, O. Motojima, T. Horiuchi et al., “Contact resistance of demountable multi-pin joint for superconducting helical coil”, Proc. 14th Symp. Fusion Techonol. , Avignon 1986, 2, 1727 (1986).
[18] H. Hashizume, S. Ito, K. Yagi, S. Kitajima, “Proposal of mechanically jointed superconducting magnet using high critical temperature superconductors”, Fus. Eng. Des.,, 63, 449 (2002).
[19] S. Ito, H. Hashizume, “Overview of fundamental study on remountable HTS magnet”, Fus. Eng. Des.,, 81, 2527 (2006).
[20] N. Yanagi, T. Mito, S. Imagawa et al., “Development, fabrication, testing and joints of aluminum stabilized superconductors for the helical coils of LHD”, in Proceedings of the 16th ICEC/ICM 751 (1997).
[21] L Dresner, W.A. Fietz, S. Gauss et al., “Results of the international Large Coil Task: a milestone for superconducting magnets in fusion power”, Cryogenics, 29, 875 (1989).

Recent experiments and future collaborations on QUEST

K.Hanada[a)], H.Zushi [a)], H.Idei [a)], K.Nakamura [a)], M.Ishiguro [b)], S.Tashima [b)], E.I.Kalinnikova[b)], M.Sakamoto [a)], M.Hasegawa [a)], A.Fujisawa [a)], A.Higashijima [a)], S.Kawasaki [a)], H.Nakashima [a)], H.Liu [b)], O.Mitarai [c)], T.Maekawa [d)], A.Fukuyama [e)], Y.Takase [f)], J. Qian[g)]

a): Research Institute for Applied Mechanics, Kyushu University, Japan,
b):Interdisciplinary Graduate School of Engineering Science, Kyushu University, Japan,
c): School of Industrial Engineering, Tokai University, Japan
d):Graduate School of Energy Science, Kyoto University, Japan
e): Graduate School of Technology, Kyoto University, Japan
f): Graduate School of Frontier Science, University of Tokyo, Japan
g): Institute of Plasma Physics, Chinese Academy of Sciences, China.

Keywards: Steady state operation of spherical tokamak, non-inductive current drive, QUEST
PACS: 52.55.-s, 52.50.-b, 52.40.Hf, 52.35.Hr, 52.35.Qz

QUEST (Q-shu University Experiment with Steady State Spherical Tokamak) [1] is a ST constructed in Kyushu University to aim steady state operation under controlled plasma wall interaction (PWI) and it has been running from 2008. The QUEST project has focused on the steady state operation of spherical tokamak (ST) which has a capability to attain high β rather than conventional tokamaks. A final target of the project is the steady state operation of ST with relatively high β under controlled plasma wall interaction (PWI). Present status of QUEST is introduced.

Introduction

A strategy of realization of fusion power generation is on the way that the appropriate size of integrated devices, such as JT-60SA, KSTER, EAST, and ITER. This way is promising, however too straightforward. When we stay on only the way, variety of achievable fusion power plants is not so wide. I think that an answer to the question what kinds of fusion power plant are needed is only coming from social request at that time. Recently strong request to production of electric power generation seems to focus on the cost of produced electricity, and also on the reduction of the impact to environment, and on the stable supply and safety. When the cost is highly valued, the impact to environment, and the stable supply and safety are marginalized and nuclear fission and hydraulic power generation is more preferable. When the impact of environment is selected as the most significant concern, renewable energy sources, such as photovoltaic and wind force power generations may have the preference. Generally it is difficult to decide only one concern, and people should aim at a well-balanced system. The goal of the balance is called as “Best Mixture”. Best Mixture strongly depends on geographical, economical, and political situation of nation. If we consider on that fusion power generation are set in Best Mixture, we had better prepare the wide-variety types of fusion power plants to adjust to Best Mixture at every situation. Therefore, it is important to obtain the academic basics to support high β, that is high economical potential, and steady state operation, that is high stability, approaches.

The QUEST (Q-shu University Experiment with Steady State Spherical Tokamak) project [1,2] focuses on the steady state operation of the spherical tokamak (ST) which has the capability to attain high β rather than conventional tokamaks. A final target of the project is the steady state operation of ST with relatively high β under well-controlled plasma wall interaction (PWI). The main difference between a pulsed operation and a steady one is the difficulties of handling of the heat and the particles loads. Although the transient huge heat load comes from plasma in the pulsed operation, the condition of the plasma facing components (PFCs) does not affect the performance of the plasma so much. While in the steady state operation, the erosion and the sputtering of the material make serious effect in the maintenance of the high performance plasmas via wall saturation and impurity accumulation [3,4]. The continuous heat load makes large damages to the material of PFCs. The particle handling is more complicate in steady state operation. Because the wall pumping works well

even on the divertor configuration, therefore the temperature and the number of absorbed particles of the PFCs should be controlled during discharges. Long duration discharges were sometimes terminated by the wall saturation phenomenon that the particles stored in the wall come back to the plasma abruptly. When the wall saturation phenomenon takes place, the in-flux of the particles increases and the particle handling could not work well [5]. As the behavior of Hydrogen from the wall significantly depends on the wall temperature [6], the control of the wall temperature and the number of the absorbed particles to the wall should be done.

The QUEST project will be developed in increment step such as, I. low β steady state operation in limiter configuration, II. low β steady state operation in divertor configuration, III relatively high β steady state operation in closed divertor configuration, where β means the ratio of plasma pressure to magnetic pressure [1]. The specific purpose in phase I is:

(1) To examine the steady state current drive and the generation of closed flux configuration by non-inductive current drive.

The purposes in Phase II are:

(1) To comprehensively establish recycling control based on control of wall temperature, and advanced wall control under high plasma performance.

(2) To improve diverter concepts and to establish the way of controlling particles and heat loads during long duration operation.

(3) To obtain relatively high β (10%) under high elongated plasma shape and additional heating power in short pulse discharge up to 1 s.

In this report, present status of the performance of QUEST is introduced.

Experimental Apparatus

The maximum toroidal field is 0.5T within 1sec and 0.25T in steady state at R=0.64m. Both the height and the diameter of the vacuum vessel is 2.8m. The schematic view of QUEST is shown in Fig. 1. QUEST has four pairs of poloidal field (PF) coils and three separated center solenoid (CS) coils, PF4-1/4-3, PF4-2, which is suitable to put in magnetic flux into the plasma via ohmic heating (OH). These have the capability to supply the magnetic flux by approximately 200 mVs. Vertical magnetic fields required to make an equilibrium can provide. The PF1/7 and the PF2/6 coils can provide the vertical magnetic field of 85 G and 145 G per 1kA at R=0.64m.

Two kinds of microwaves of 2.45GHz, 50kW and 8.2GHz, 400kW are available to drive plasma current and heat plasmas and they have the capability to operate in steady state. A system of 8.2GHz has the well-designed antenna to adjust injection mode, polarization, injection angle [7] as shown in Fig. 2. The dependence of the injection mode and angle on driving plasma current is studied using the antenna.

The inner part of the vacuum vessel is completely covered by stainless steel of 3mm in thickness coated by W. Moreover four fixed water-cooled limiters made of W are installed around only mid-plane on the inner part of the vessel. Lower flat-divertor is composed of W-coated 16 panels made of stainless steel and the upper one is composed of non W-coated 16 panels. Four fixed limiters which made of stainless steel are installed on the outer part of the vessel and they are not cooled-down actively.

61 flux loops are located on the inside surface of the vacuum chamber, and they are available as the instruments of magnetic measurement [8]. These loops are composed of vacuum-tight special cables. Center line of the cable is made of Cu and the line is isolated electrically by MgO. The most outer shell of the cable is made of SUS316 in the thickness of 0.25mm.

Hard X-ray (HXR) radiated via bremsstrahlung process from plasmas was monitored by two detectors (CdTe, CdZnTe), which can detect X-ray in the range of 3-200 keV [9]. Lower energy X-ray than 10keV can detect, however considerable correction is required because of the drastic variation of the detection efficiency. Detected X-ray was investigated using pulse-height analysis (PHA) to obtain energy spectrum.

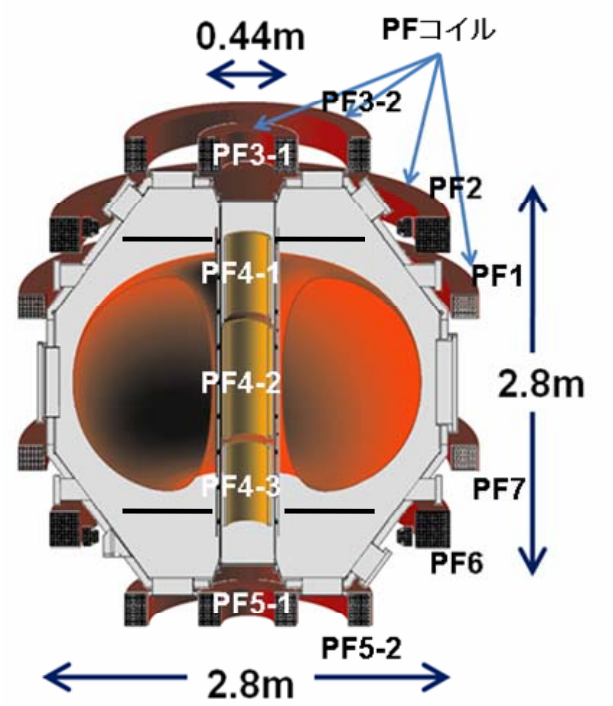

Fig. 1: Schematic view of QUEST is shown. Six pairs of PF coils (PF1/7, 2/6, 3-1/5-1, 3-2/5-2, 4-1/4-3, 4-2) are installed for double null configuration. Each coil can operate individually to form single null configuration. Flat divertor plates are installed in upper and lower side of the vacuum vessel (the positions are indicated by black lines on the figure.).

Present status of QUEST experiments.

Designed parameters and present status are summarized in table 1. As for the OH plasma, less experimental time is supplied, therefore we did not execute the OH plasma experiments in higher than B_T=0.14 T and the operation of PF coils was not optimized.

Non-inductive plasma current start-up and maintenance is one of a desired way to obtain cost-effective fusion power plants such as STs. Fully non-inductive plasma start-up and its maintenance up to 25kA were successfully done by using a well-controlled microwave of 8.2 GHz up to 120 kW. Magnetic surface reconstruction shows a plasma shape with the aspect ratio of less than 1.5, which means a ST-configuration could be obtained [2], and with the attachment of inner limiters located on a center stuck. Two pairs of poloidal field (PF) coils were used to keep the equilibrium on the limiter configuration. Plasma currents were almost proportional to magnitudes of vertical field at the plasma center.

	Designed	Achieved
R (m)	0.68	0.7
a (m)	0.4	0.48
A	1.6	1.47
I_P (kA) in OH plasma	300	110 (B_T=0.14T)
I_P (kA) in RF plasma	2~30 kA (0.45 MW) Phase I 100 kA (1MW) Phase II	25 kA (0.12MW)
P_{RF} (MW)	1	~0.12
B_T (T)	0.25 at R=0.64m	0.25 at R=0.64m
n_e (m^{-3})	0.4 x 10^{19}	~0.1 x 10^{19}
Discharge duration	Steady state	37 sec

Table 1: Designed parameters and present status of QUEST experiments

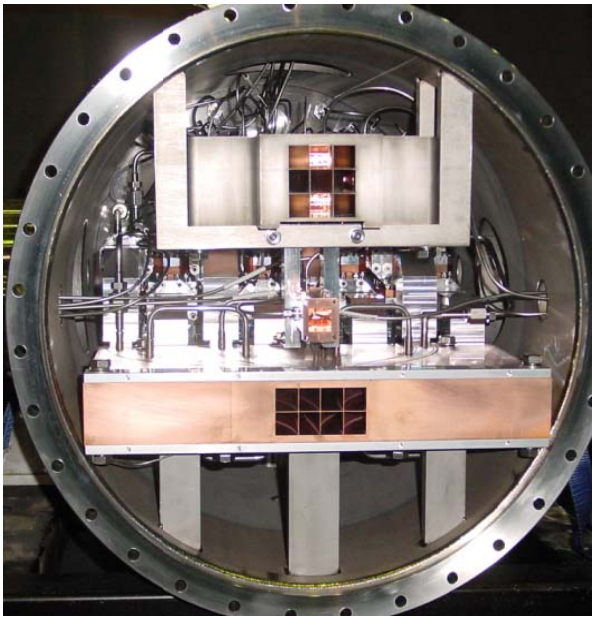

Fig. 2: A photo of newly constructed antenna for well-controlled microwave injection, which is cooled by water for steady state operation, is shown. This antenna has the structure of 4 x 2 stacked waveguide (See lower wave guide array.). Before installation to QUEST, these structures were covered by a thin panel made of stainless steel except the part of waveguides.

Experimental Results

Typical waveforms of plasma current, I_P, injected microwave power, P_{RF}, currents of the vertical field coil, PF1/7 and PF2/6, and H_α signal on non-inductive current drive experiment are shown in Fig. 3. Although no diagnostics for density was installed on QUEST at that time, a measurement of line-averaged density in a similar discharge with a microwave interferometer was indicated it was around several 10^{17} m^{-3}. The plasma current of 15kA could be achieved and it maintained for 1 s, significantly more than magnetic diffusion time of the vacuum vessel (approximately 10ms). As no loop voltage was supplied from PF coils during the maintenance on I_p of approximately 15kA shown in Fig. 3, the plasma current could be maintained by a fully non-inductive current drive. An example of magnetic surface reconstructed by EFIT is shown in Fig. 4 and the results show q_a~30, β_p~0.1, A=1.45, where q_a, β_p, and A mean safety factor at last closed flux surface, poloidal beta, and aspect ratio, respectively. The calculated aspect ratio is sufficiently low for a condition of spherical tokamak. These results represent that a spherical tokamak configuration can be maintained by full non-inductive current drive, and the possibility to steady-state operation of spherical tokamaks could be demonstrated.

Fueling was only done for the plasma production just before the discharge and no more fueling was done during the discharge. The plasma current was significantly reduced with a rise of H_α signal which can be worked on a good-monitor of out-gassing from the wall. Usually, several hot spots appeared mainly on the outer wall as shown in Fig. 5 and they are surely one of the strong sources of out-gassing. At present time, the longest discharge achieved on QUEST is shown in Fig.6. Out-gassing has been prevented from maintaining the plasma at any cases [10].

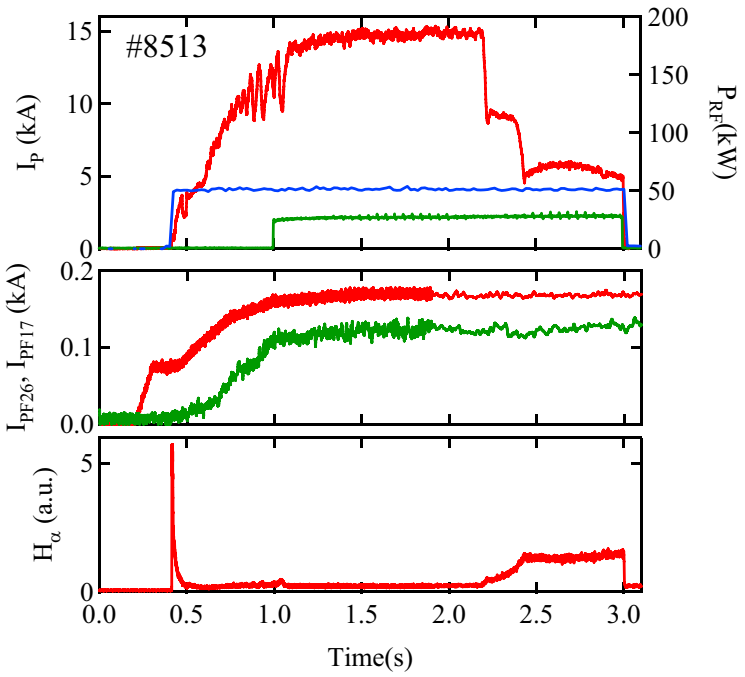

Fig. 3 Typical waveforms of plasma current, I_P, injected microwave power, P_{RF} (two systems were running in this shot) in top figure, currents of PF1/7 and PF2/6 in middle one, and H_α signal in bottom one on non-inductive current drive experiment are shown [2]. Sampling rate of PF1/7, PF2/6 coil currents for data acquisition was changed around 1.8 sec.

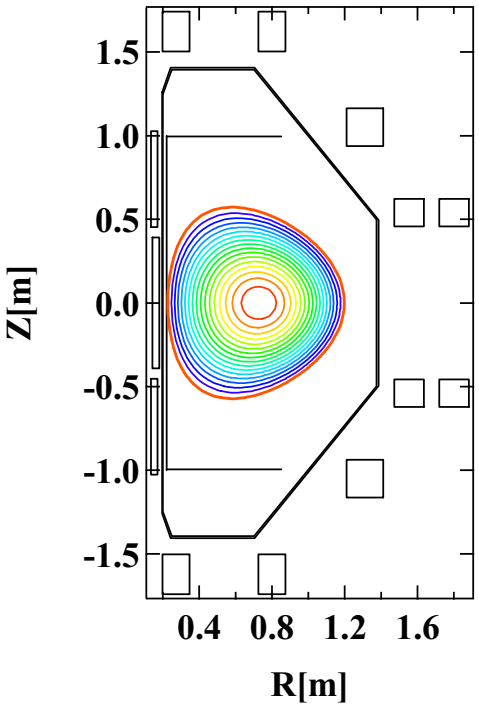

Fig. 4 Typical reconstructed magnetic surface using EFIT on full non-inductive current drive plasma (#9119) on QUEST. Calculated aspect ratio from this reconstructed magnetic surface is 1.47, which is sufficient for a spherical tokamak configuration [2].

Fig. 5 An example of a hot spot (left-middle side) on the outer wall during a long duration discharge is shown. Dark rectangle shadow around center part of the picture shows center stuck of QUEST. Round shape in peripheral region of the picture shows the edge of vacuum window for visible light [10].

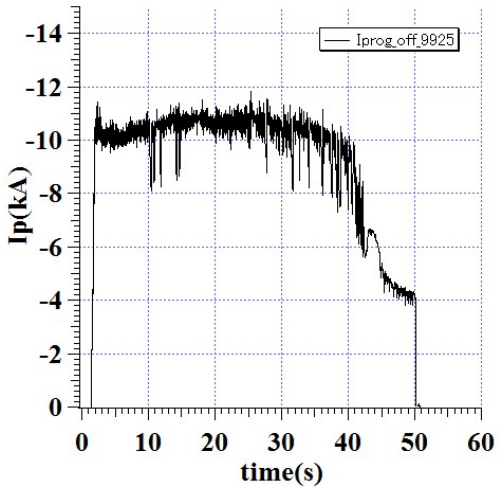

Fig. 6 The longest discharge achieved on QUEST is shown. The plasma current of more than 10kA could be sustained fro 37 s, and strong out-gassing as shown in a rise of H_α signal prevent from maintaining the plasma finally [10].

Detected X-ray was investigated using pulse-height analysis (PHA) to obtain energy spectrum and it was found that the plasma current was almost proportional to the number of photons in the range of 10-12keV [2]. This suggests that the non-inductive current may be driven by energetic electrons with around 10keV. The experimental results show the plasma current is almost proportional to the strength of the vertical magnetic field at R=0.64m where is the center of the vacuum vessel. The plasma current also increased with the injected power. While the excessive energetic electrons were observed as the plasma current grew up and they could directly attack to local vacuum wall on low field side and produced hot spots on the wall. Typical cases of electron orbit departing from electron cyclotron resonance (ECR) are illustrated on a poloidal cross-section in Fig. 7. Consequently, out-gassing from the hot spots prevent from maintaining plasmas.

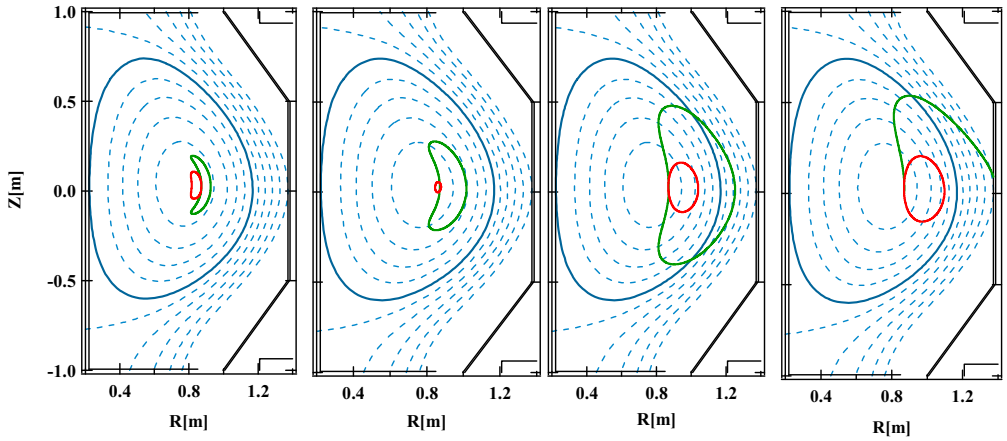

Fig. 7 Typical electron orbits with 1keV, 10keV, 100keV, 150keV are illustrated from left to right figures. Red line shows the orbit with pitch angle of -75 degree, and green one shows that of 75 degree, where minus means the direction to drive positive plasma current.

Two pairs of divertor coils PF3-1/5-1, and PF3-2/5-2 and a center solenoid coil (PF4-1/4-2/4-3) were applied, and finally several types of divertor configurations could be achieved using full non-inductive current drive technique.

Summary

Fully non-inductive plasma start-up and its maintenance were successfully done by using a well-controlled microwave of 8.2 GHz up to 80kW on the spherical tokamak, QUEST. Plasmas current of 10kA could be maintained for 37 s, which is longer than the typical current decay time multiplied by 100. Magnetic surface reconstruction shows a plasma shape with the aspect ratio of less than 1.5, which means a spherical tokamak configuration could be obtained. Hard x-ray (HXR) measurement showed the detected number of photons of 10-12 keV was almost proportional to the plasma current and this suggests that the energetic electrons accelerated by the microwave drive the current. The excessive energetic electrons were observed as the plasma current grew up and a part of them directly attacked to local vacuum wall on low field side and produced related hot spots. Consequently, out-gassing from the hot spot prevent from obtaining longer maintaining plasmas.

Acknowledgements

This work is performed with the support and under the auspices of the NIFS Collaboration Research Program (NIFS05KUTR014, NIFS08KUTR022). This work is partially supported by a Grant-in-aid for Scientific Research from Ministry of Education, Culture, Sports, Science and Technology of Japan. This work was also partially supported by the JSPS-CAS Core-University program in the field of ‘Plasma and Nuclear Fusion' and the Collaborative Research Program of Research Institute for Applied Mechanics, Kyushu University.

References

[1] K.Hanada *et al.*, (2010) Plasma Fusion Research **5**, S1007.
[2] K.Hanada *et al.*, Plasma science and technology, to be accepted.
[3] M.Chatelier *et al.*,, Nucl. Fusion **47**, S579-589 (2007).
[4] R.Bhattacharyay *et al.*, J. Nucl. Mater. **363-365**, 938-943 (2007).
[5] K.Hanada *et al.*, Nucl. Fusion **41**, 1539-1542 (2001).
[6] R.Bhattacharyay *et al.*,, Nucl. Fusion **47**, 864-874 (2007).
[7] H.Idei *et al.*, Proc. 32nd International Conf. on Infrared and Millimetre Waves, Cardiff, UK, 789-790 (2007).
[8] M.Ishiguro *et al.*, Plasma and Fusion Research Special Issue, to be published.

[9] S.Tashima *et al.*, Journal of Plasma and Fusion Research Series, Volume 9 (2010), pp.316-321.
[10] K.Hanada *et al.*, Proc. of 6th IAEA-TM on steady state operation of tokamaks, Vienna, Dec. 6-8, 2010, (2010)

A New Flame for Humanity

- An Innovation to the Heavy Industries using Green Electric Energy by Fusion Power

Motoyasu Sato, NIFS

Microwave technologies developed in the fusion experiment were applied for the material processing in the Inter University Exchange Program.

The Joint knowledge of Plasma Physics, Microwave and Material Science give us an innovation in the heavy industries suggesting the way to the independence from fire energy. The 10 years of our investigations has cleared the mechanism of microwave processing. The applications of microwave energy will extend to all the heavy industries for reducing the exhausting of carbon dioxide gases.

The microwave processing show the interesting behaviors so called microwave effects. It decreases the activation energy in the material processing. For example, the reduction energy from CuO to Cu_2O showed a drop from 320kJ/mol to 110 kJ/mol under the high power irradiation of microwave magnetic field. Another example is the generations of nano-crystallographic structures in powdery metallic oxide with unpaired spins on the 3d orbit.

Theoretical models were investigated on the bases of wave-solid plasma interactions. As the material contains boundaries of powders, magnetic domains and vacancies, the wave length of electromagnetic wave are modulated spatially by the non-uniformities, i.e., it is Fourier transformation mathematically. Microwave propagates with higher wave numbers in the material than in the vacuum. If the phase velocity is close to the components of thermal vibration at the neutral point in lattice, the Landau damping transfers fields energy to the electrons in the solid state plasma. If the binary collisions are low enough, the part of coherent momentum should be accumulated before it dissipates into the thermal energy. Finally, the energy transfers from the momentum to the material reactions. It can be solved with DFT(Density Functional Theory) method substituting to the Hamiltonians consisting of the momentums.

The theoretical investigations and industrial applications will be shown in the talk.

Agenda

JSPS-CAS Core University Program Seminar on "Summary of 10-year Collaborations in Plasma and Nuclear Fusion Research Area", 9 – 11 March 2011, Okinawa, Japan

==========9 March (Wed.), 2011==========

15:00-15:10: **Opening**

15:10-15:40: **Short summary of history and results of collaborations in the CUP from 2001 to 2005 [K.J. Wang, J.Y. Zhao, T. Watari, C. Namba]**

Session I: Magnetically confined core plasmas (11A & 11B) [Chair: K. Toi]

15:40-16:20: *"11A: Development of Advanced Plasma Heating for High Performance Plasma Confinement-Summary and Topical Talk"* (40 min) [R. Kumazawa (NIFS), X. Gao (ASIPP), L.W. Yan(SWIP)] (presented by R. Kumazawa)

16:20-17:00: "*Summary of Research Activities on 11B (Plasma Experiment and Diagnostics in MCF) During Past 5 Years and Future Prospect"* (40 min) [S. Morita(NIFS), X. Gao(ASIPP), L.W. Yan(SWIP)] (presented by S. Morita)

17:00-17:25: "*Recent results on EAST*" (25min) [X. Gao (ASIPP)]

17:25-17:50: "*The JT-60SA project and the plasma regimes*" (25min) [S. Ide (JAEA)]

Reception 18:45~

==========10 March (Thu.), 2011==========

Session II: Plasma wall interaction (12A) [Chair: K.J. Wang]

9:10~9:45: "*Overall activities on plasma wall interactions (12A) since 2006 and collaboration researches conducted at Hokkaido University*" (35 min) [T. Hino (Hokkaido Univ.), N. Ahikawa (NIFS) and N. Noda (NIFS)] (presented by T. Hino)

9:45-10:10: "*Program of plasma facing material and components for the steady state operation of EAST device*" (25min) [J.L. Chen (ASIPP)]

10:10-10:35: "*CUP collaborations on plasma wall interactions (12A)*" (25min) [N. Ashikawa (NIFS)]

Coffee break(10:35-10:55)

Session III: Atomic and Molecular Process in Plasmas (13A) [Chair: S. Morita]

10:55-11:30: *"Summary in 2006-2010 of 13 A: Research activities, exchanges and seminars of Atomic and Molecular Process in Plasmas"*(35 min) [D. Kato(NIFS), N. Nakamura (UEC) and T. Kato(NIFS)] (presented by D. Kato)

11:30-11:55: "*Atomic and Molecular process in plasmas*" (25min) [J.G. Wang (IAPCM, CAS),

B.G. Xiao (ASIPP)](presented by B.G. Xiao)

Lunch (11:55-13:30)

Session III: Atomic and Molecular Process in Plasmas (13A)(continued) [Chair: S. Morita]

13:30-13:55: *"Atomic Processes of Highly Charged Heavy Ions Relevant to Hot Plasmas"* (25min) [N. Nakamura(UEC)]

Session IV: Plasma industrial applications (14C) [Chair: B. J. Xiao]

13:55~14:30: *"Progress and Outlook of Plasma Industrial Application" (14C)"* (35 min) [R. Hatakeyama (Tohoku Univ.) & M. Sato (NIFS)] (presented by R. Hatakeyama)

14:30-14:55: "*PEMFCs Preparation by Plasma technique*" (25min) [Y.D. Meng (ASIPP)]

Coffee break(14:55-15:15)

Session V: Laser produced dense plasmas (15A, 15B) [Chair: Z. Gao]

15:15~15:45: "*Topical Summary of Japan-China CUP Program on Laser Plasma Theory for the Last Ten Years"*. (30 min) [K. Tanaka (Osaka Univ.) & H. Takabe (Osaka Univ.)] (presented by K. Takabe)

15:45-16:10: "*Some Progress on High Energy Density Physics under the China-Japan CUP Collaboration*" (25min) [Z.M. Sheng (Shanghai Jiatong Univ.)]

16:10-16:35: "*Laboratory Astorophysics Joint Research with China Group Lead by President Jie Zhang*" (25min) [H. Takabe (Osaka Univ.)]

Session VI: Fusion reactor technologies (20A, 20D, 20E, 20F) [Chair N. Yanagi]

16:35-17:10: "*Summary of CUP Collaborations and New Directions for Fusion Reactor Technologies*" (35 min) [T. Muroga (NIFS)]

17:10-17:35: "*Summarize on the researcher exchanges from FY2006-2011 from Chinese side (Basic Research of Nuclear Fusion Reactor Engineering) 20-A,D,E,F*" (25min) [Y. WU (ASIPP), Y. Song (ASIPP)] (presented by Y. Wu)

17:35-18:00: "*Hydrogen Fuel Society and Hybrid Energy Transfer Line of Hydrogen and Electricity*" (25min) [S. Yamada (NIFS)]

18:45 *Seminar Banquet*

==========11 March (Fri.), 2011==========

Session VI: Fusion reactor technologies (20A, 20D, 20E, 20F) (continued) [Chair L.Q. Hu]

9:10-9:35: "*In-situ Observation of Radiation Damage in Reduced Activation Ferritic Steels by means of HVEM-ion Accelerator Facility*" (25min) [S. Ohnuki (Hokkaido Univ.)]

9:35-10:00: "*Study of tritium behavior in solid breeder materials"* (25min) [Y. Oya (Shizuoka Univ.) and K.M. Feng (SWIP)] (presented by Y. Oya)

10:00-10:25: "Analysis on Tritium Management in FLiBe Blanket for Force-Free Helical Reactor FFHR2" [Y. Song (ASIPP), A. Sagara (NIFS)] (presented by A. Sagara)

Coffee break(10:25-10:45)

Session VII: Plasma theories (30A, 30B, 30C, 30D) [Chair H. Takabe]

10:45~11:10: "*Summary of 30A- Study on Theoretical Analysis of MHD and Microinstabilities in Plasmas* –" and "Summary of 30B- Study on transport Theory, Code Development of Numerical Analysis and Confinement Improved Mode in Torus Plasmas –" (25 min) [Y. Kishimoto (Kyoto Univ.), D. Li (USTC), Z. Gao (Tsinghua Univ.), Y. Tomita(NIFS)] (presented by Y. Kishimoto)

11:10-11:35: "*Summary of Physics of self-organization in Complex plasmas"(30C) and "Modeling of edge and divertor plasma and control of impurities and recycling particles(30D) since 2006*" (25 min) [R. Horiuchi (NIFS) & Y. Tomita(NIFS)] (presented by Y. Tomita)

11:35-12:00: "*Understanding for multi-scale interaction of fusion plasmas and future collaboration*" (25min) [Y. Kishimoto (Kyoto Univ.)]

Lunch(12:00-13:30)

Session VII: Plasma theories (30A, 30B, 30C, 30D)(continued) [Chair T. Watari]

13:30-13:55: "*Some points on rf physics in magnetic fusion plasmas"*(25min) [Z. GAO (Tsinghua University)]

13:55-14:20: "*Future Collaboration Researches on Peripheral Plasmas* "(25min) [Y. Tomita (NIFS)]

Coffee break(14:20-14:40)

Session VIII: Topical session (11A-B, 14A, 20A-F) [Chair X. Gao]

14:40-15:05**:** "*Invitation to collaboration on the development of HTS magnet technology for fusion reactors" (*25min) [N. Yanagi (NIFS)]

15:05-15:30: "*Recent experiments and future collaborations on QUEST*" (25min)
[K. Hanada (Kyusyu Univ.)]

15:30-15:55: *"A New Flame for Humanity - An Innovation to the Heavy Industries using Green Electric Energy by Fusion Power-"(*25min) [M. Sato (NIFS)]

15:55~16:20: **Session IX: Seminar summary [K.J. Wang, K. Toi]**

16:20-16:30 **Closing**

==========

List of participants

Name	Affiliation	E-mail address
LI Jiangang	Institute of Plasma Physics,CAS, Hefei, China	j_li@ipp.ac.cn
WANG Kongjia	Institute of Plasma Physics,CAS, Hefei, China	kjwang@ipp.ac.cn
HU Liqun	Institute of Plasma Physics,CAS, Hefei, China	lqhu@ipp.ac.cn
CHEN Weiping	Chinese Academy of Sciences, Beijing, China	wpchen@cashq.ac.cn
DONG Shaohua	Institute of Plasma Physics,CAS, Hefei, China	shdong@ipp.ac.cn
ZENG Gang	Chinese Academy of Sciences, Beijing, China	zenggang@cashq.ac.cn
ZHAO Junyu	Institute of Plasma Physics,CAS, Hefei, China	zhaoj@ipp.ac.cn
GAO Xiang	Institute of Plasma Physics,CAS, Hefei, China	xgao@ipp.ac.cn
CHEN Junling	Institute of Plasma Physics,CAS, Hefei, China	jlch@ipp.ac.cn
XIAO Bingjia	Institute of Plasma Physics,CAS, Hefei, China	bjxiao@ipp.ac.cn
MENG Yuedong	Institute of Plasma Physics,CAS, Hefei, China	ydmeng@ipp.ac.cn
SHENG Zhengming	Shanghai Jiaotong University, Shanghai, China	zmsheng@aphy.iphy.ac.cn
WU Yu	Institute of Plasma Physics,CAS, Hefei, China	wuyu@ipp.ac.cn
GAO Zhe	Tsinghua University, Beijing, China	gaozhe@tsinghua.edu.cn
KOMORI Akio	National Institute for Fusion Science, Toki, Japan	komori@LHD.nifs.ac.jp
TOI Kazuo	National Institute for Fusion Science, Toki, Japan	toi.kazuo@LHD.nifs.ac.jp
YAMADA Shuichi	National Institute for Fusion Science, Toki, Japan	yamada.shuichi@LHD.nifs.ac.jp
YOSHIZAWA Naomi	Japan Society for the Promotion of Science,Tokyo,Japan	yoshizawa@jsps.go.jp
KUMAZAWA Ryuhei	National Institute for Fusion Science, Toki, Japan	kumazawa.ryuhei@LHD.nifs.ac.jp
MORITA Shigeru	National Institute for Fusion Science, Toki, Japan	morita.shigeru@LHD.nifs.ac.jp
HANADA Kazuaki	Kyushu University, Fukuoka, Japan	hanada@triam.kyushu-u.ac.jp
IDE Shunsuke	Japan Atomic Energy Agency, Naka, Japan	ide.shunsuke@jaea.go.jp
HINO Tomoaki	Hokkaido University, Sapporo, Japan	tomhino@qe.eng.hokudai.ac.jp
ASHIKAWA Naoko	National Institute for Fusion Science, Toki, Japan	ashikawa.naoko@LHD.nifs.ac.jp
KATO Daiji	National Institute for Fusion Science, Toki, Japan	kato.daiji@LHD.nifs.ac.jp
NAKAMURA Nobuyuki	University of Electrocommunications, Tokyo, Japan	n_nakamu@ils.uec.ac.jp
HATAKEYAMA Rikizo	Tohoku University, Sendai, Japan	hatake@ecei.tohoku.ac.jp
SATO Motoyasu	National Institute for Fusion Science, Toki, Japan	sato.motoyasu@LHD.nifs.ac.jp
TAKABE Hideaki	Osaka University, Osaka, Japan	takabe@ile.osaka-u.ac.jp
OHNUKI Somei	Hokkaido University, Sapporo, Japan	ohnuki@eng.hokudai.ac.jp
MUROGA Takeo	National Institute for Fusion Science, Toki, Japan	muroga.takeo@nifs.ac.jp
OYA Yasuhisa	Shizuoka University, Shizuoka, Japan	syoya@ipc.shizuoka.ac.jp

Name	Affiliation	E-mail address
KISHIMOTO Yasuaki	Kyoto University, Kyoto, Japan	kishimoto@energy.kyoto-u.ac.jp
TOMITA Yukihiro	National Institute for Fusion Science, Toki, Japan	tomita@LHD.nifs.ac.jp
SAGARA Akio	National Institute for Fusion Science, Toki, Japan	sagara.akio@LHD.nifs.ac.jp
YANAGI Nagato	National Institute for Fusion Science, Toki, Japan	yanagi@LHD.nifs.ac.jp
WATARI Tetsuo	National Institute for Fusion Science, Toki, Japan	watari.tetsuo@toki-fs.jp
NAMBA Chusei	National Institute for Fusion Science, Toki, Japan	namba@nifs.ac.jp
OGAWA Kunihiro	Nagoya University, Nagoya, Japan	ogawa.kunihiro@LHD.nifs.ac.jp
KATO Naoki	Nagoya University, Nagoya, Japan	kato.naoki@LHD.nifs.ac.jp
OSHITANI Takanori	National Institute for Fusion Science, Toki, Japan	oshitani.takanori@nifs.ac.jp
YAMANAKA Makoto	National Institute for Fusion Science, Toki, Japan	yamanaka.makoto@nifs.ac.jp
TONOUCHI Noriaki	National Institute for Fusion Science, Toki, Japan	tonouchi.noriaki@nifs.ac.jp
KATO Mayumi	National Institute for Fusion Science, Toki, Japan	kato.mayumi@nifs.ac.jp